Investigating the effects of IFNγ signalling on transcriptional, epigenetic and enhancer landscapes

Anna Rita Lamstaes

St Hugh's College

University of Oxford

A thesis submitted for the degree of

Doctor of Philosophy

Hilary 2021

Abstract

IFNγ signalling can have contradictory roles in a tumour microenvironment. Predominantly, IFNγ has an anti-tumour function, activating the immune system against the cancer. However, pro-tumour activities of IFNγ have also been observed. Its choice between the two opposing outcomes appears to be context dependent and the mechanism instructing this choice isn't well understood. One prevailing determinant comes from the IFNγ-induced upregulation of PD-L1, an immunosuppressive ligand. Binding of PD-L1 to its receptor, PD-1, inhibits immune cells despite the presence of other activating signals, enabling cancer immune evasion. Increased knowledge of IFNγ-induced gene expression within cancer cells, including the regulation of PD-L1, would enable a more accurate prediction of IFNγ's behaviour in the tumour microenvironment.

This thesis examines the effect of IFNγ signalling on the transcriptional, epigenetic and enhancer landscape in a hepatocellular carcinoma cell line, Hep3B. Using a variety of genome-wide sequencing techniques, I find that IFNγ orchestrates differential gene expression and enhancer activity dynamically in at least three distinct phases within 24 hrs of treatment. IFNγ treatments were found to regulate more enhancers than genes, with a large proportion of these enhancers becoming primed but not fully activated. Capture-C, a 3C based technique, revealed that IFNγ treatments significantly increase promoter:enhancer interactions, adding a further level of gene regulation.

IFNγ treatments induced upregulation of PD-L1 in Hep3B cells. Capture-C revealed that the PD-L1 promoter interacts with the closest neighbouring promoter and a CTCF site downstream of the gene. Neither of these interactions appeared to regulate IFNγ-induced PD-L1 expression. Instead, this thesis proposes that the proximal promoter may be sufficient for IFNγ-induced upregulation of PD-L1. Altogether, this study increases our understanding of IFNγ-induced gene regulation.

"Let's get down to business"

(Shang Li, Mulan, 1998)

Word count: 49291

0.1 Acknowledgements

First and foremost I would like to thank Jane for her guidance, support and encouragement throughout my entire PhD. I have a boundless appreciation for the opportunity she has given me, it is one I will remember fondly. I also wish to thank her for finally remembering the name of my cell line.

I would like to thank Oxford BioDynamics, especially Alexandre Akoulitchev and Mehrnoush Dezfouli, whose initial work provided the foundations to my thesis project, and for providing fantastic advice throughout my time in Jane's lab.

I have a lot of gratitude towards members of the Hughes lab, including Damien Downes, Jelena Telenius and Jim Hughes himself, for their help with the Capture C experiment and their scripts and guidance towards analysing the data.

I have an enormous amount of thanks to Silvia, whose sassy comments kept me entertained for hours; Ülkü, whose 45 minute planks taught me how to speak confidently; Phil, whose low to medium skill set far exceeded everyone else's; Meredith, for being the life and soul of the lab (*party); Harry, for teaching me that Pol II is green and the rest of my lab, both past and present for providing the most enjoyable working atmosphere over the last four years. I would like to give a special shout out to Amanda, for making sequencing the highlight of my week.

I have a lot of thanks for my friends and family, who always pretended (badly) to understand what I was talking about, and feigning interest anyway. I thoroughly enjoyed saying the work 'RNA' and watching the blank faces staring back at me.

Finally, I would like to thank the boiling water tap in the biochemistry building for making me excited to go to work every day, without which, I probably would have spent 50% of my PhD waiting for the kettle to boil.

Contents

List of Figures

List of Tables

0.2 Abbreviations

2HG	2-Hydroxyglutarate
3'-UTR	3'-Untranslated Region
ALK	Anaplastic Lymphoma Kinase
APC	Antigen Presenting Cell
BET	Bromodomain and Extraterminal protein
BETi	BET inhibitors
CBP	CREB-binding protein
ChIP	Chromatin Immunoprecipitation
CTD	Carboxy-Terminal Domain
DNMT1	DNA Methyltransferase I
ER	Endoplasmic Reticulum
eRNA	Enhancer RNA
ERK	Extracellular-signal-Regulated Kinase
EMT	Epithelial-Mesenchymal Transition
GAS	Gamma interferon Activated Sites
GO	Gene Ontology

GTF	General Transcription Factors
HATs	Histone Acetyltransferases
HCC	Hepatocellular Carcinoma
HDAC	Histone Deacetylase
HIF	Hypoxia Inducible Factor
IDH	Isocitrate Dehydrogenase
IL-2	Interleukin-2
IFNγ	Interferonγ
IFNGR1/2	IFNγ Receptor 1/2
IRF1	Interferon Regulatory Factor 1
ISRE	Interferon Stimulated Response Element
ITIM	Immunoreceptor Tyrosine-based Inhibitory Motif
ITSM	Immunoreceptor Tyrosine-based Switch Motif
JAK1/2	Janus Kinase 1/2
KATs	Lysine acetyltransferases
K_d	Dissocition Constant
KO	Knock-Out
lncRNA	Long Non-Coding RNA

mAbs	Monoclonal Antibodies
MHC-I	Major Histocompatibility Complex class I
miR	micro RNA
mRNA	messenger RNA
ncRNA	Non-Coding RNA
NDR	Nucleosome Depleted Region
NSCLC	Non-Small Cell Lung Cancer
PD-1	Programmed Death 1 receptor
PD-L1	Programmed Death-Ligand 1
PD-L2	Programmed Death-Ligand 2
pSTAT1	Phosphorylated STAT1
PI3K	Phosphoinositide 3-Kinase
PIC	Pre-Initiation Complex
PLCγ	Phospholipase Cγ
Pol II	RNA polymerase II
PTMs	Post-Translational Modifications
RGMb	Repulsive Guidance Molecule b
RT-qPCR	Reverse-Transcription quantitative PCR

SHP2	Src Homology 2-domain containing tyrosine phosphatase 2
SNU-seq	Single-Nucleotide resolution 4sU-sequencing
sPD-1	soluble PD-1
sPD-L1	soluble PD-L1
sPD-L2	soluble PD-L2
SPR	Surface Plasmon Resonance
STAT1	Signal Transducer and Activator of Transcription 1
TAD	Topologically Associating Domain
TAFs	TBP-Associated Factors
TBP	TATA-box Binding Protein
TF	Transcription Factor
TNFα	Tumour Necrosis Factorα
TSS	Transcriptional Start Site
WT	Wild-Type

Chapter 1

Introduction

1.1 IFNγ in the innate and adaptive immune response

Having first been discovered for its antiviral effects, IFNγ is now known to be involved in both the innate and adaptive immune responses. It is an integral cytokine in a variety of processes including host defence against intracellular pathogens, tissue damage and immunosurveillance. It is pivotal in regulating immune and inflammatory responses, activating macrophages, NK cells and lymphocytes, as well as modulating chemokine production and upregulating antigen presentation pathways [Ivashkiv, 2018, Barrat et al., 2019].

Under physiological conditions, IFNγ is expressed at low basal levels to maintain tissue homeostasis and prime cells to fight infection. It is predominantly produced by NK cells, cytotoxic T lymphocytes and type I T helper cells. Its expression is heavily induced upon stimulation of antigen receptors as well as particular cytokines such as IL-12 and IL-18. Most cell types express the IFNγ receptor, IFNGR1/2, thus enabling a response in both immune and non-immune cells [Ivashkiv, 2018, Barrat et al., 2019].

1.2 IFNγ: cancer's double-edged sword

1.2.1 The anti-tumour activities of IFNγ

In addition to orchestrating the inflammatory and immune response, IFNγ also plays contradictory roles in tumour immunity (Fig:1.1). Upon recognition of transformed self by a T-lymphocyte, IFNγ is secreted into the tumour microenvironment. One can only assume that the consequences of this secretion are context dependent under different cellular and environmental conditions. Primarily, IFNγ has numerous anti-tumour capabilities, acting on tumour cells, immune cells, and other cells present in the tumour microenvironment (Fig:1.1).

IFNγ upregulates expression of MHC class I and II molecules in multiple cell types, increasing a cells antigenicity, promoting recognition and cytotoxic-mediated killing of the tumour [Street et al., 1997, Martini et al., 2010]. Beyond increasing antigen presentation, IFNγ induces several suppressive effects on tumour cells. It has been shown to inhibit proliferation in a range of tumour types, including hepatocellular carcinomas [Chin et al., 1996, Harvat et al., 1997, Li et al., 2012]. One mechanism used by IFNγ to achieve this anti-proliferative effect is upregulating the expression of cell cycle inhibitor proteins such as p27 and p21 [Chin et al., 1996, Harvat et al., 1997]. Furthermore, IFNγ can promote tumour cell apoptosis and RIP1-dependant necrosis in apoptosis-resistant cells [Li et al., 2012, Thapa et al., 2011, Cekay et al., 2017, Wang et al., 2018a].

With widespread effects on the tumours themselves, IFNγ can additionally steer the immune system against the tumours (Fig:1.1). It recruits immune cells to the tumour microenvironment and stimulates them to release a number of anti-tumour cytokines and chemokines such as IL-6 and CXCR3 [McLoughlin et al., 2003, Pak-Wittel et al., 2013]. Together with these signalling molecules, IFNγ promotes

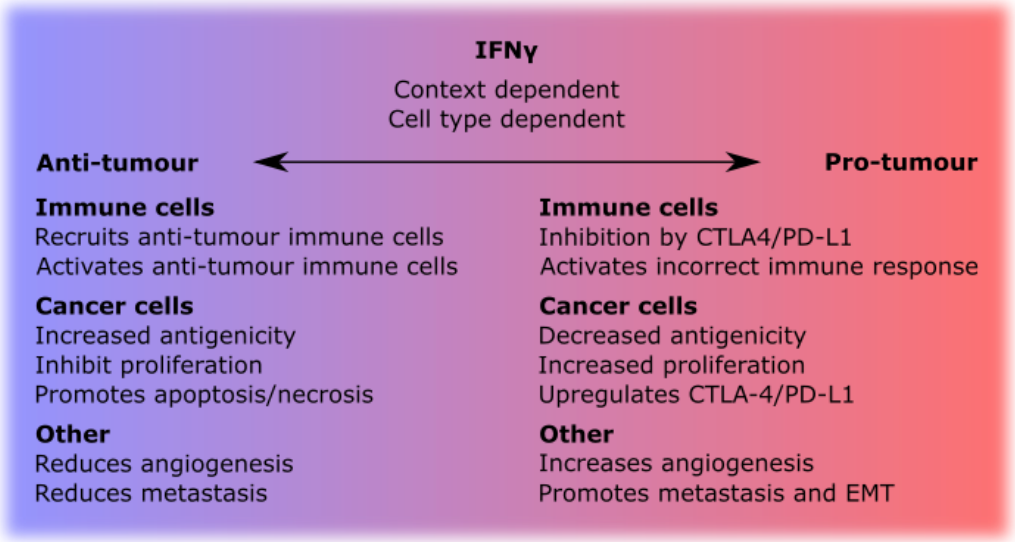

Figure 1.1: Contradictory roles of IFNγ in the tumour microenvironment. IFNγ can have either anti- or pro- activities within the tumour microenvironment. The overriding effect appears to be context dependent and cell-type specific.

T cell differentiation towards the type I phenotype and enhances T cell cytotoxicity [Gajewski and Fitch, 1988, Wang et al., 2006, Zaidi, 2019]. Similarly, it repolarises tumour-associated macrophages from a pro-tumour M2 state to an anti-tumour M1 state [Relation et al., 2018]. M2 macrophages stimulate expression of VEGF which promotes angiogenesis. Therefore switching tumour-associated macrophages away from an M2 polarisation may aid in reducing angiogenesis, thus depressing cancer growth [Wang et al., 2013]. Furthermore, IFNγ reduces immune inhibitory functions of other immune cells including regulatory type II T lymphocytes and myeloid-derived suppressor cells [Gajewski and Fitch, 1988, Medina-Echeverz et al., 2014, Overacre-Delgoffe et al., 2017]. All in all, this modulates the immune system for tumour destruction.

IFNγ can also repress tumour growth through its effects on other cells present in the tumour microenvironment (Fig:1.1). For instance, acting on endothelial cells, IFNγ disrupts the tumour vasculature, diminishing angiogenesis and resulting

in ischemia which, in turn, leads to tumour reduction [Coughlin et al., 1998, Rüegg et al., 1998, Kammertoens et al., 2017]. Reports have additionally found that IFNγ can modulate the extracellular matrix and tumour architecture to decrease metastasis formation [Glasner et al., 2018].

Further evidence of the anti-tumour role of IFNγ comes from mutation and deletion studies whereby mutational defects of vital IFNγ signalling molecules, such as IFNGR1/2 or JAK1/2, or IFNγ-induced genes, results in increased tumour survival. Indeed, defects in these proteins additionally lead to both innate and acquired resistance to cancer immunotherapies [Gao et al., 2016, Zaretsky et al., 2016, Manguso et al., 2017, Shin et al., 2017]. Efficacious treatment by radiotherapy was found to be dependent on IFNγ in mice [Gerber et al., 2013]. Thus, IFNγ appears to have an important role in anti-tumour immunity and cancer therapies.

1.2.2 The pro-tumour activities of IFNγ

Although IFNγ displays repressive tendencies against the growth of a tumour, it controversially also stimulates several pro-tumour effects which can counteract its negative impact (Fig:1.1). It does this through the complex and context dependent regulation of IFNγ-induced genes.

IFNγ has been shown to increase expression of IDO1, high expression of which is associated with a poor prognosis [Brody et al., 2009]. IDO1 expression can modulate local immune cells, enhancing Tregs and suppressing cytotoxic T cells, thus enabling immune escape [Prendergast, 2008]. Knock-down studies of IDO1 revealed that IFNγ induction of the IDO1/AhR pathway rescued tumour repopulating cells from IFNγ-induced apoptosis and tumour regression, instead directing the tumour into dormancy [Liu et al., 2017b]. Similarly, other IFNγ upregulated genes suppress the immune response. For instance, non-classical MHC genes, such as HLA-E,

upregulated by IFNγ reduced cytotoxic killing by T lymphocytes [Derré et al., 2006]. IFNγ upregulated iNOS enhanced immunosuppression by myeloid-derived suppressor cells, contradicting the previously discussed findings that IFNγ suppresses these cells (Section 1.2.1). MUC16, another IFNγ-induced gene, was found to suppress cytolysis of cancer cells by NK cells [Morgado et al., 2016, Shime et al., 2017, Aithal et al., 2018]. MUC16 also appears to promote metastasis and cancer cell signalling [Aithal et al., 2018]).

Furthermore, IFNγ has been linked to increasing angiogenesis by downregulating the anti-angiogenesis factor, TNFS15, and may also induce cancer EMT and metastasis [Lu et al., 2014, Lv et al., 2015]. These observations are antithetical to the previously discussed anti-tumour effects of IFNγ and thus are likely to depend on the conditions within the tumour microenvironment.

Chronic exposure of tumour cells to IFNγ can result in enhanced tumour growth by the process of immunoediting. Here, a selection pressure provided by IFNγ forces the cancer to evolve and adapt, leaving it resistant to the anti-tumour influence of IFNγ. This not only drives cancer progression but additionally results in resistance to therapies [Benci et al., 2016, Takeda et al., 2017]. Despite upregulating MHC molecules, IFNγ can reduce the processing and presentation of tumour specific antigens, reducing antigenicity and preventing recognition by the immune system [Beatty and Paterson, 2000, Le Poole et al., 2002, Takeda et al., 2017]. Long exposures to IFNγ have been found to increase genetic instability in tumours enabling cancer progression [Takeda et al., 2017]. It has additionally been shown to alter the epigenome of the cancer cell, modulating the expression of IFNγ-induced genes including inhibitory ligands facilitating immune evasion [Benci et al., 2016]. Understanding how the epigenetic and expression landscape within a cancer cell changes over the course of IFNγ exposure may further provide insights into the immunoediting process.

Despite increasing antigenicity of a cancer cell, IFNγ increases expression of immunosuppressive molecules, including CTLA-4 and PD-L1, on an assortment of cells within the tumour microenvironment [Garcia-Diaz et al., 2017, Mo et al., 2018]. Both of these proteins inhibit activation of T cells. These suppressive signals override activating signals preventing cytotoxic killing of the cancer and enabling immune evasion. Even with other anti-tumour activities present, PD-L1 expression can enable cancer immune evasion (discussed in section 1.3.4).

Altogether, IFNγ signalling within a tumour microenvironment can have different outcomes. Accurately predicting the specific outcome within individual tumour microenvironments is beyond current scientific capabilities. IFNγ-induced expression of the PD-L1 ligand, given its ability to inhibit the immune system, appears to be a prevailing feature that skews IFNγ signalling towards a pro-tumour response. Thus, gaining a better understanding of IFNγ-induced PD-L1 upregulation may help to develop therapies that restore the desired anti-tumour IFNγ response.

1.3 PD-L1 dampens the immune response

1.3.1 The PD-1 receptor and its ligands

The adaptive immune system is strictly controlled to prevent overactivation and consequent autoimmunity. One such immune checkpoint is the Programmed Death 1 receptor (PD-1) [Nishimura et al., 1999, Nishimura et al., 2001], expressed on a variety of immune cells, including T- and B-lymphocytes [Ishida et al., 1992, Keir et al., 2008]. PD-1, a 288 amino acid type I transmembrane protein is a member of the CD28 family of receptors [Agata et al., 1996]. Association of this receptor to one of its two ligands; Programmed Death-Ligand 1 (PD-L1, also known as B7-H1 or CD274) or PD-L2 (also known as B7-DC, PDCD1LG2 or CD273) provides an inhibitory signal, thus dampening the immune response (Fig:1.2). PD-L1 was first

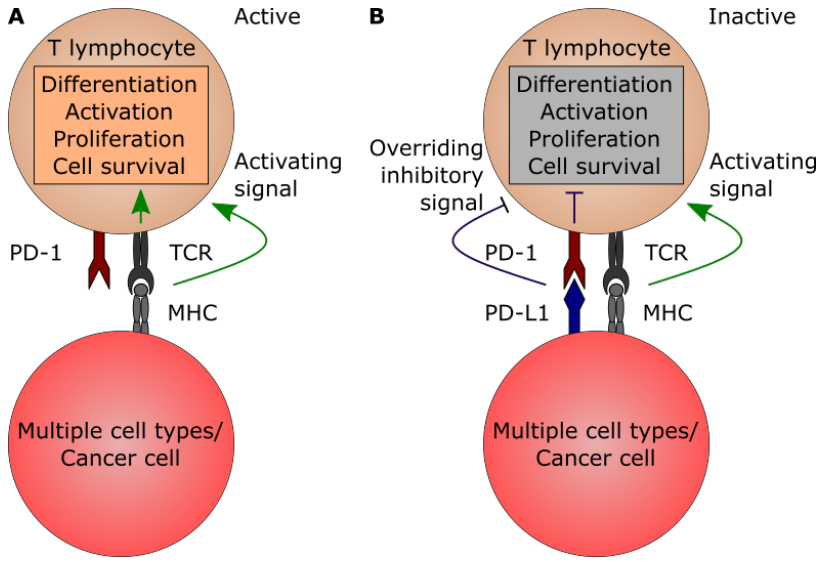

Figure 1.2: PD-L1 binding to its receptor, PD-1, produces an overriding inhibitory signal that prevents activation of a T lymphocyte.
A The T cell receptor recognises a harmful antigen presented on an MHC molecule, resulting in differentiation, activation, proliferation and cell survival of the T lymphocyte. **B** In addition to the TCR:MHC interaction, PD-L1 is recognised by PD-1. This produces an inhibitory signal that overrides activating signals, inhibiting differentiation, activation and proliferation of the T lymphocyte.

identified in 1999 due to its sequence similarity to the B7 family members and found to interact with PD-1 shortly after [Dong et al., 1999, Freeman et al., 2000]. PD-L2, with an amino acid identity of ∼40% to PD-L1, was identified as PD-1's second ligand the following year [Latchman et al., 2001].

Despite evidence suggesting a higher affinity of PD-1 to PD-L2, PD-L1's high abundance over PD-L2 favours it as the predominant ligand, making it the focus of PD-1 research [Youngnak et al., 2003, Butte et al., 2008]. PD-L1 is constitutively expressed on an assortment of lymphocytes and Antigen Presenting Cells (APCs), as well as being abundant in areas of immune privilege [Yamazaki et al., 2002, Wang et al., 2017b]. Expression has also been found in a variety of non-haematopoietic cells including in the lung and liver. Expression of PD-L2, in contrast, appears more limited, although expression in multiple cell types

has been observed [Tsuda et al., 2005, Mataki et al., 2007, Keir et al., 2008].

1.3.2 PD-1 signalling cascade

PD-1 signalling acts in synergy with other inhibitory molecules on the cells surface. Its signalling response is dependant on the combination of signals received as well as the intensity of these signals; sufficiently high levels of CD28 costimulation or exogenous Interleukin-2 (IL-2) can, at least partially, override the inhibitory signal [Freeman et al., 2000, Carter et al., 2002, Patsoukis et al., 2012]. Upon engagement with PD-L1/2, PD-1 is recruited to the immunological synapse between the lymphocyte and APC where it acts in *cis* to inhibit T cell activation (Fig:1.2) [Bennett et al., 2003, Pentcheva-Hoang et al., 2007, Yokosuka et al., 2012]. It functions by diminishing the PI3K/AKT and RAS/MEK/ERK pathways, massively altering the lymphocytes metabolism, downregulating glycolysis, increasing fatty acid oxidation and altering cytokine production [Okazaki et al., 2001, Parry et al., 2005, Yokosuka et al., 2012]. IL-2 production is inhibited, consolidating PD-1-mediated inhibition and promoting T cell anergy [Carter et al., 2002, Chikuma et al., 2009]. In turn, this impairs differentiation, activation, proliferation and cell survival of the lymphocyte, all in all, inhibiting the immune response (Fig:1.2) [Bardhan et al., 2016, Sharpe and Pauken, 2018].

1.3.3 PD-L1/2 signalling through derivative mechanisms

Evidence is surfacing that many immune checkpoints signal bidirectionally, not only causing orthodox receptor activation but also producing a reverse signal to the ligand expressing cell [Lecis et al., 2019]. Indeed, PD-L1/2 appear to play roles in both immune and tumour cells, dependently or independently of PD-1, affecting epithelial to mesenchymal transition (EMT), cell survival and proliferation, autophagy and the inflammatory response [Clark et al., 2016, Chen et al., 2017,

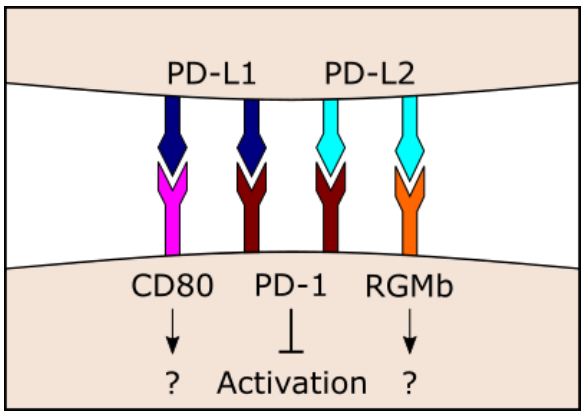

Figure 1.3: Binding partners of PD-L1 and PD-L2.
PD-L1 and PD-L2 interact with PD-1, their typical receptor, to inhibit activation of immune cells. PD-L1 and PD-L2 additionally interact with CD80 and RGMb respectively. The functions of these alternate interactions are unknown.

Gato-Canas et al., 2017, Hartley et al., 2018, Jalali et al., 2019].

To further complicate matters, PD-1 double Knock-Out (KO) experiments imply that PD-L1/2 inhibit T cell function via other receptors (Fig:1.3). Surface Plasmon Resonance (SPR) identified an association between human PD-L1 and CD80 (B7-1), another member of the B7 family, with a dissociation constant (K_d) of ∼1.4 µM. In comparison, PD-L1 and PD-L2 interacted with PD-1 with a K_d of ∼0.5 µM and ∼0.3 µM respectively, and CD80 had an affinity of K_d ∼0.4 µM and ∼4 µM to its two other known receptors; CTLA-4 and CD28, respectively [Butte et al., 2008]. Using various immunoreceptor KO cell lines and antibodies specific to just PD-1:PD-L1 or CD80:PD-L1 indicate that the CD80:PD-L1 interaction may produce a bidirectional inhibitory signal, decreasing T cell proliferation, cytokine production and inducing T cell anergy [Butte et al., 2007, Park et al., 2010]. No interaction between CD80 and PD-L2 was observed, however, PD-L2 was found to bind to Repulsive Guidance Molecule b (RGMb) with a K_d of 48.5 nM, similar to PD-L2:PD-1 [Xiao et al., 2014]. More research is required to determine whether these interactions are biologically active and what effects they may have (Fig:1.3).

1.3.4 Tumours hijack the PD-1:PD-L1 axis

1.3.4.1 Mechanisms of PD-1:PD-L1 immune escape

The robust inhibitory signals provided by PD-1 and its ligands play crucial roles in autoimmunity, central and peripheral tolerance, chronic viral infection, transplantation and more. Perhaps unsurprisingly, multiple tumours hijack this signalling pathway by overexpressing PD-L1, inhibiting immune cells and enabling immune evasion (Fig:1.2) [Iwai et al., 2002, Gordon et al., 2017, Lee et al., 2017]. As one of the major hallmarks of cancer, it is vital that tumorous cells avoid destruction by lymphocytes that recognise their tumour specific antigens [Hanahan and Weinberg, 2011]. They commonly achieve this by 'hiding' from the immune system, for example, by downregulating MHC expression, or, in the case of PD-L1 expression, inhibiting the immune response.

PD-L1 expression has been identified in a diverse range of both solid and haematologic cancers including Hepatocellular Carcinomas (HCCs), melanomas, Non-Small Cell Lung Cancers (NSCLC), pancreatic cancer, amongst many others [Konishi et al., 2004, Wu et al., 2006, Hamanishi et al., 2007, Nomi et al., 2007, Hino et al., 2010, Calderaro et al., 2016]. PD-L2 expression has also been detected in a variety of solid cancers although, in general, to a lesser extent than PD-L1 [Konishi et al., 2004, Hamanishi et al., 2007, Nomi et al., 2007], but is highly upregulated in certain B cell lymphomas, often due to chromosome amplification or translocation [Rosenwald et al., 2003, Steidl et al., 2011].

As previously described, PD-1:PD-L1 signalling inhibits T lymphocytes, reducing their cytotoxicity and promoting anergy. PD-L1 overexpression was first shown to enable tumour growth by inhibiting the cytolytic activity of CD8+ T cells in 2002, and this has since been verified in various experimental models [Iwai et al., 2002, Hirano et al., 2005, Juneja et al., 2017]. There is also evidence

that PD-L1 expression in the tumour microenvironment is associated with reduced lymphocyte infiltration, adding a further evasion mechanism through the PD-1:PD-L1 axis [Hamanishi et al., 2007, Nomi et al., 2007]. However, this is widely disputed and contradictory findings showing strong correlations between PD-L1 expression and lymphocyte infiltration have been observed [Taube et al., 2012, Hou et al., 2014]. The results are seemingly dependant on the cancer type and lymphocyte subset analysed.

Further to circumventing the immune system, PD-L1 expression correlates with genes involved in EMT, and PD-1 signalling was found to increase expression of slug (Snai2) and Twist, key drivers of EMT [Cao et al., 2011, Jiang and Zhan, 2020]. This suggests a potential role of this immune checkpoint in inducing metastatic cancers.

As expected, due to the cancer-promoting mechanisms described above, high PD-L1 expression correlates with a poor prognosis in multiple tumour types [Wu et al., 2006, Hamanishi et al., 2007, Nakanishi et al., 2007, Nomi et al., 2007, Hino et al., 2010]. Although, correlations between PD-L1 and unfavourable prognosis weren't always observed [Tsao et al., 2017]. Due to the increasing success of immunotherapies targeting this signalling pathway, it is now argued that PD-L1 expression results in an improved prognosis.

1.3.4.2 The tumour microenvironment establishes permissive PD-L1 expression

The tumour microenvironment is a mass of both malignant and non-malignant cells, blood vessels and extracellular matrix. The combination of cytokines and growth signals expressed by each cell type contributes to an environment enabling tumour growth. Large bodies of research have shown that PD-1/PD-L1/PD-L2 expression can be induced by the amalgamation of signals present in the tumour microenvironment. Key signals from cytokines such as Interferonγ (IFNγ),

Tumour Necrosis Factor α (TNFα), interleukins, etc. can regulate PD-L1 on both tumour and immune cells [Curiel et al., 2003, Hartley et al., 2017, Jiang et al., 2019]. Indeed, PD-L1 expression has been detected on multiple cells of the immune system including lymphocytes, tumour-associated macrophages and dendritic cells (Fig:1.4) [Tang et al., 2018, Lin et al., 2018]. Furthermore, a variety of CRISPR-Cas9 KO mice models have demonstrated that both tumour and immune cell PD-L1 expression can contribute to PD-L1 mediated immune evasion (Fig:1.4) [Juneja et al., 2017, Kleinovink et al., 2017, Lau et al., 2017, Noguchi et al., 2017]. T cell inhibition and tumour growth can also be established through PD-L1 positive exosomes (Fig:1.4) [Chen et al., 2018a, Kim et al., 2019]. Thus, even in PD-L1 negative tumours, PD-1:PD-L1 inhibitory signals can still be established within the tumour microenvironment, permitting immune escape (Fig:1.4).

Furthermore, soluble forms of PD-1, PD-L1 and PD-L2 (sPD-1, sPD-L1 and sPD-L2) are also expressed from both immune and tumour cell sources and still retain binding capacities [Frigola et al., 2011, Frigola et al., 2012, Gong et al., 2019]. The function of these soluble entities is not well understood (Fig:1.4). It has been hypothesised that sPD-1 may actually block PD-1:PD-L1/2 interactions by binding and thereby sequestering the PD ligands and has therefore been considered as an alternate therapy. Not only would this inhibit any potential PD-1 binding moiety, but it would also prevent binding of these moieties to other receptors, i.e. CD80:PD-L1. Indeed sPD-1 has been shown to activate T lymphocytes and reduce tumour growth [Yuan et al., 2004, Geng et al., 2006, Song et al., 2011]. Whether sPD-L1 acts in a similar manner, competing out functional PD-1:PD-L1 binding, or is able to stimulate PD-1 mediated inhibition remains debated. Correlations between high levels of sPD-L1 and a poor prognosis suggests the later, although this isn't conclusive [Zeng et al., 2011, Wang et al., 2015]. Moreover, experiments co-incubating sPD-L1 with T lymphocytes indicate that sPD-L1 can promote apoptosis, suggesting it

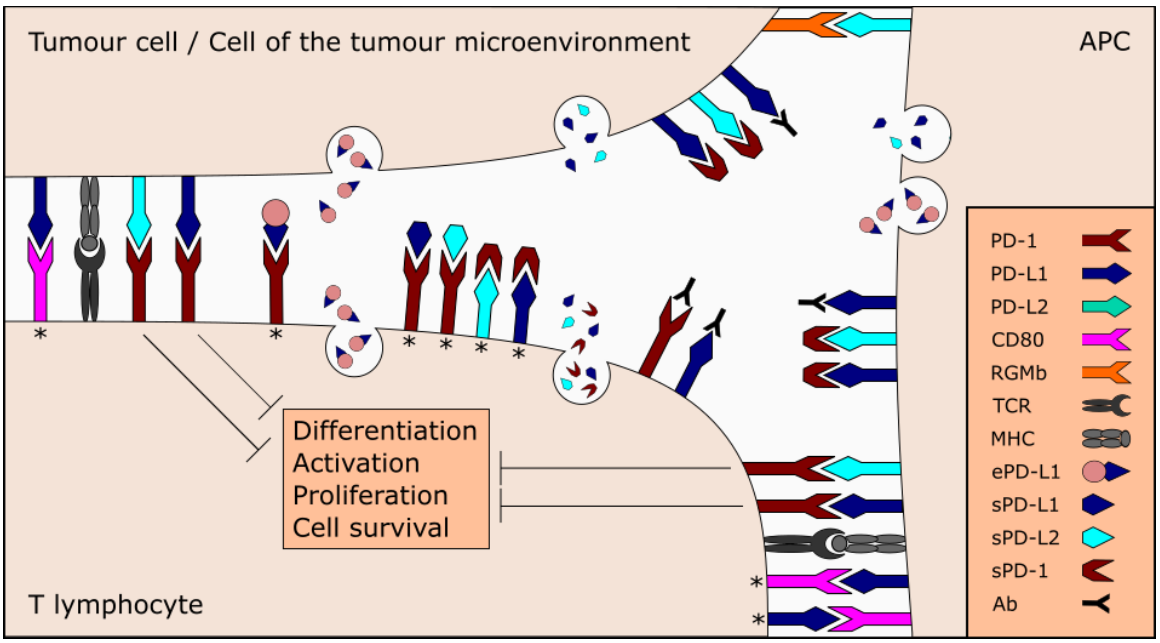

Figure 1.4: Potential binding partners of PD-1, PD-L1 and PD-L2 in the tumour microenvironment.
T lymphocytes can receive various signals from the PD-1 axis. Cell of the tumour microenvironment denotes any cell not excluding a second T lymphocyte. Signalling pairs whose function is not well characterised is denoted by *. TCR: T cell receptor, MHC: Major histocompatibility complex bound to peptide, ePD-L1: PD-L1 positive exosome, Ab: Monoclonal antibody against either PD-1 or PD-L1.

may aid immune evasion [Frigola et al., 2011, Frigola et al., 2012]. More research is required to understand the effect of soluble immune checkpoint proteins present in the tumour microenvironment.

1.3.5 Immunotherapies against PD-1:PD-L1

PD-1:PD-L1 immunotherapies impede this immune checkpoint interaction to overcome their suppressive signals, stimulating the immune system to destroy cancerous cells and providing sustained therapy against the tumour. Blocking the association of PD-1 to PD-L1 results in increased activation of T lymphocytes and alters the milieu of cytokines within the tumour microenvironment, including IFNγ, promoting elimination of the tumour (Fig:1.5)

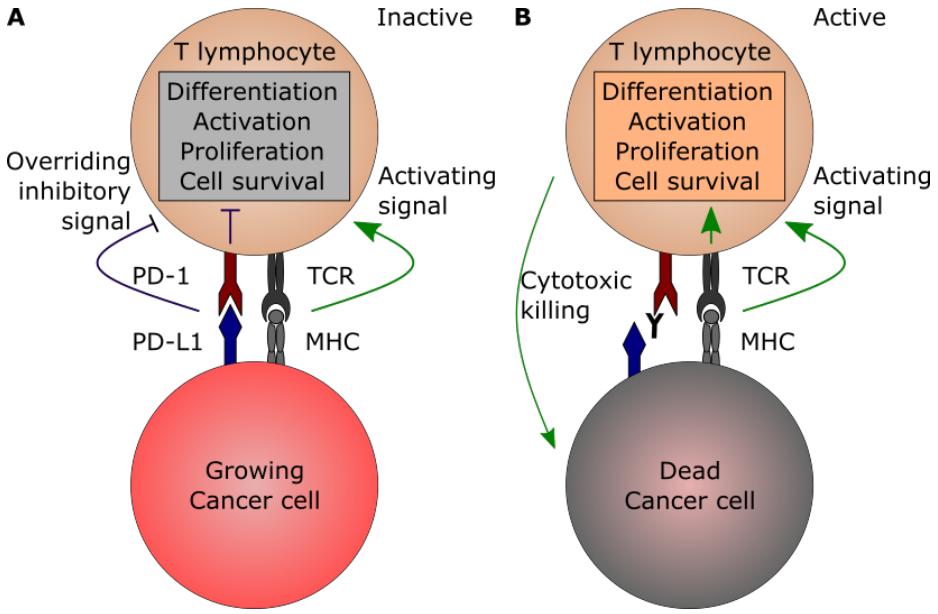

Figure 1.5: Anti-PD-1/PD-L1 immunotherapies activate the immune system against a cancer.
A PD-L1 interacts with PD-1, inhibiting activation of the T-lymphocyte. This allows immune evasion and consequent cancer growth. **B** PD-1:PD-L1 immunotherapies: an anti-PD-1 antibody binds to the PD-1 receptor preventing binding of the PD-L1 ligand. The inhibitory PD-1:PD-L1 signal is removed enabling activation of the T-lymphocyte and cytotoxic-mediated killing of the cancer.

[Curiel et al., 2003, Strome et al., 2003, Lin et al., 2018].

At the time of writing, there were six FDA approved inhibitory monoclonal antibodies (mAbs), used for treatment of 18 different types of cancer, including HCCs, melanomas and NSCLCs [Alsaab et al., 2017, Liu et al., 2017a]. Three of these, Pembrolizumab (Merck Co.), Nivolumab (Bristol-Myers Squibb), and Cemiplimab (Regenaron) target PD-1 whilst the others, Atezolizumab (Roche), Durvalumab (AstraZeneca) and Avelumab (Pfizer/Merck KGaA) target PD-L1. They all disrupt the PD-1:PD-L1 interaction, and additionally PD-1:PD-L2 or CD80:PD-L1 depending on the antibody's target. As of September 2019, nearly 3000 clinical trials involving PD-1:PD-L1 mAbs were active. 75% of these were in combination with other therapies, including other immunotherapies, chemotherapies, radiotherapies or targeted therapies [Xin Yu et al., 2019].

1.3.6 Innate and acquired resistance to PD-1:PD-L1 immunotherapies

Despite the success of PD-1:PD-L1 immunotherapies, only approximately 30% of patients respond, although this varies massively depending on cancer type [Borghaei et al., 2015, Robert et al., 2015]. Hodgkin's lymphomas, for example, which frequently contain genetic alterations leading to constitutive overexpression of PD-L1/2, have response rates of up to 87% [Ansell et al., 2015], compared to gastric cancer with a response rate of 22% [Muro et al., 2016]. The cost of treatment is high (>£30,000 per patient) and the therapy has been implicated with adverse effects, including autoimmune diseases [Hu et al., 2017, O'Neil et al., 2017, Wang et al., 2017c], hence emphasizing the requirement for an improved stratification method predicting patients that will respond to the therapy.

Currently, PD-L1 expression serves as the only FDA approved biomarker for PD-1:PD-L1 immunotherapies. Despite increasing response rates to approximately 50%, some patients not expressing PD-L1 still respond to the therapies [Sunshine and Taube, 2015]. As mentioned previously, both PD-1 and PD-L1 have additional binding partners, and PD-L1 in the tumour microenvironment from multiple sources can contribute to the inhibitory signal. As these biomarkers measure PD-L1 expressed either on immune cells or tumour samples, they could omit PD-L1 present in the tumour microenvironment. In addition, tumours tend to be heterogeneous in PD-L1 expression, and the thresholds defining PD-L1 positive tumours vary between biomarker assays, again resulting in falsely classified PD-L1 negative tumours. Thus these biomarkers are limited in their prediction abilities [Taube et al., 2018].

A high proportion of patients expressing PD-L1 have an innate (no response) or acquired (relapse after initial tumour regression) resistance to the therapies.

An increased understanding of these resistance mechanisms could enable improved stratification of patients into responders and non-responders as well as developing more efficacious immunotherapies. IFNγ has a reported involvement in both innate and acquired resistance and can have either a favourable or pernicious effect. Plainly, expression of PD-L1 is crucial, although not necessary (due to PD-1's alternate binding partners), for response to PD-1:PD-L1 immunotherapies. Some research has shown that inducing IFNγ mediated PD-L1 expression can increase sensitivity to PD-1:PD-L1 blockade [Samson et al., 2018].

Mutations in genes involved in the IFNγ signalling pathway, such as IFNγ Receptor 1/2 (IFNGR1/2), Janus Kinase 1/2 (JAK1/2) and Interferon Regulatory Factor 1 (IRF1), result in defects in IFNγ signalling, reduce PD-L1 expression and show innate resistance to immune checkpoint blockade [Gao et al., 2016, Shin et al., 2017, Bullock et al., 2019]. Indirect genes involved in IFNγ signalling have also been related to desensitisation to immunotherapies: Loss-of-function mutations in the apelin receptor, which interacts with JAK1 to modulate IFNγ signalling, and amplifications of IFNγ signalling inhibitors SOCS1 and PIAS4, were all linked to non-responders [Gao et al., 2016, Patel et al., 2017, Bullock et al., 2019].

Mutations in this pathway, including in JAK1/2, stemming after immune checkpoint blockade treatment, were identified in patients and mouse models with acquired resistance [Zaretsky et al., 2016, Manguso et al., 2017]. Although decreased IFNγ signalling should, in theory, attenuate PD-L1 expression and hence render the cancer susceptible to T cell cytotoxicity independently of PD-1:PD-L1 mAbs, IFNγ tends to have anti-tumour effects, extensively discussed in section 1.2.1. IFNγ signalling promotes antigen presentation and chemotaxis of immune cells to the tumour microenvironment. In support of this, defective IFNγ pathways failed to upregulate antigen presentation by Major Histocompatibility Complex class I (MHCI)

[Manguso et al., 2017].

Conversely, prolonged IFNγ exposure results in immunoediting, the process by which cancers are first eliminated, reach an equilibrium and then escape from the immune system, facilitating acquired resistance [Benci et al., 2016, Takeda et al., 2017]. Indeed, sustained IFNγ exposure in mouse models seemingly altered the epigenome of the tumour, augmenting expression of IFNγ driven inhibitory ligands. In turn, this desensitised tumours to immune checkpoint blockade independently of PD-L1 expression [Benci et al., 2016]. Inhibiting PD-1:PD-L1 interactions activates T lymphocytes, stimulating the secretion of IFNγ. Thus, the treatment of patients could inadvertently encourage the IFNγ immunoediting process. Taken together, IFNγ appears to have a complex role in determining response to PD-1:PD-L1 immunotherapies. An improved knowledge of IFNγ signalling in cancer cells would, therefore, help to elucidate its niche in immune evasion.

1.4 Regulation of PD-L1 expression in cancer cells

1.4.1 The CD274 and PDCD1LG2 loci

A better understanding of the regulatory mechanisms behind PD-L1/2 expression is required to overcome resistance to PD-1 based immunotherapies. As the predominant ligand to PD-1, most research has focused on the expression of PD-L1. PD-L1 and PD-L2 are expressed from the CD274 and PDCD1LG2 genes respectively. These two neighbouring genes are found on the plus strand of the 9p24.1 cytogenetic band and are approximately 40kb apart, with PDCD1LG2 downstream of CD274. PDCD1LG2 is triple the length of CD274 ($\sim$60kb over $\sim$20kb) despite their similar protein size. Both genes are comprised of seven exons. For simplicity, the genes will hereafter be referred to as PD-L1 and PD-L2.

1.4.2 IFNγ induces expression of PD-L1

Expression of PD-L1 has distinct mechanisms depending on whether expression is constitutive or inducible. Some cell types with constitutive expression can further upregulate PD-L1 through inducible pathways. Cancer cell PD-L1 expression has been reportedly induced by many pro-inflammatory cytokines such as IFNα, IFNβ, IFNγ, TNFα, IL-6 etc. (Fig:1.7) [Wintterle et al., 2003, Lienlaf et al., 2016, Garcia-Diaz et al., 2017, Wang et al., 2017e]. Of these, IFNγ appears to be emerging as a crucial factor upregulating PD-L1 expression to promote tumour growth.

Binding of IFNγ, a type II interferon, to its receptor, IFNGR1/2, results in the dimerisation of receptor subunits leading to autophosphorylation, and subsequent activation, of receptor-associated JAK1/2 (Fig:1.6) [Silvennoinen et al., 1993, Platanias, 2005]. These active kinases, in turn, phosphorylate (p) Signal Transducer and Activator of Transcription (STAT) transcription factors (TFs) on tyrosine residues, causing the pSTAT proteins to form homo- or hetero- dimers and translocate into the nucleus. Serine residues on their carboxy-terminal domain are also phosphorylated, enabling full transcriptional activation [Wen et al., 1995]. STAT1 is the main effector in the IFNγ pathway. Dimerised pSTAT1 binds to gamma interferon activated sites (GAS elements) where they activate the expression of early induced interferon-stimulated genes, such as IRF1 [Platanias, 2005]. Many of these early stimulated genes are TFs that work in conjunction, together and with STATs, to transcribe the collation of IFNγ stimulated genes.

IFNγ is expressed by T lymphocytes upon recognition of tumour-associated antigens. Subsequently, this secreted IFNγ potently induces PD-L1 expression within the tumour microenvironment enabling immune escape (Fig:1.6) [Yan et al., 2020]. Indeed, IFNγ has been shown to reduce T lymphocyte cytotoxicity towards cancerous

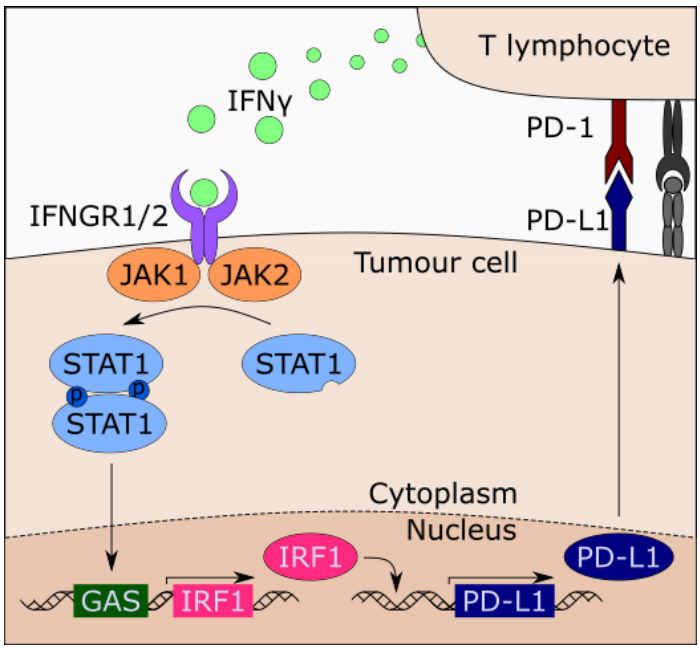

Figure 1.6: IFNγ induces PD-L1 expression.
Upon recognition of a tumour cell, T lymphocytes secrete IFNγ into the tumour microenvironment. Recognition of IFNγ by the IFNγ receptor chains (IFNGR1/2) activates JAK1/2. These activated kinases phosphorylate STAT1 which dimerises and translocates to the nucleus where it binds to GAS elements, inducing expression of the associated genes including IRF1. IRF1 binds to the PD-L1 promoter, stimulating its expression.

cells, which in turn can be rescued by addition of PD-1:PD-L1 immunotherapies [Mimura et al., 2018]. There is increasing evidence that IFNγ mediated upregulation of PD-L1 appears to be dependent on the JAK/pSTAT1/IRF1 pathway [Garcia-Diaz et al., 2017, Li et al., 2017, Moon et al., 2017, Mimura et al., 2018, Yan et al., 2020]. The PD-L1 promoter contains putative binding sites for the STAT1/3 dimer, STAT2/5 dimer and IRF1. Chromatin Immunoprecipitation (ChIP) experiments have found IRF1 bound to the PD-L1 promoter in IFNγ treated cells. Deleting the IRF1 binding site attenuates expression of PD-L1 upon IFNγ treatment [Garcia-Diaz et al., 2017, Moon et al., 2017, Yan et al., 2020]. However, a study deleting the STAT1/3 putative binding site led to a huge increase in PD-L1 expression, both with and without IFNγ stimulation, suggesting further regulation at this locus [Garcia-Diaz et al., 2017]. Inhibition or KO of JAK proteins or IRF1

diminishes PD-L1 expression *in vivo* [Pitroda et al., 2018, Shao et al., 2019]. Despite the TFs involved in the IFNγ signalling pathway being fairly well characterised, how binding of IRF1 results in activation of PD-L1 is not fully understood.

1.4.3 Alternate extrinsic regulation

Besides IFNγ, other proinflammatory cytokines present in the tumour microenvironment can upregulate PD-L1 expression (Fig:1.7). Type I interferons can induce increased PD-L1 protein levels, most likely through JAK/STAT signalling, albeit not to the same extent as IFNγ [Garcia-Diaz et al., 2017, Bazhin et al., 2018]. Multiple publications demonstrated that TNFα could synergistically enhance IFNγ-mediated upregulation of PD-L1, although these studies could not find evidence that TNFα could upregulate transcription of PD-L1 independently [Kondo et al., 2010, Li et al., 2017]. A hypoxic environment, as is commonly found in tumours, reprogrammes gene expression namely through the expression of Hypoxia Inducible Factors (HIFs). A ChIP experiment found that HIF-1α could bind to a hypoxia response element at the PD-L1 promoter and was shown to induce PD-L1 expression in both tumour and immune cells, promoting resistance to T lymphocyte cytotoxicity [Barsoum et al., 2014, Noman et al., 2014]. Results indicate HIF-2α is also involved in PD-L1 regulation in certain cell types [Messai et al., 2016]. Altogether, this demonstrates that the combination of signals present in the tumour microenvironment can fine-tune PD-L1 expression.

1.4.4 Multiple TFs regulate PD-L1 expression

PD-L1 has been extensively studied and so it is unsurprising that a number of variables have been related directly or indirectly to its expression. In addition to IRF1 and HIF-1/2α, other TFs are thought to directly act at PD-L1's promoter region to stimulate transcription of the gene (Fig:1.7). Continuing

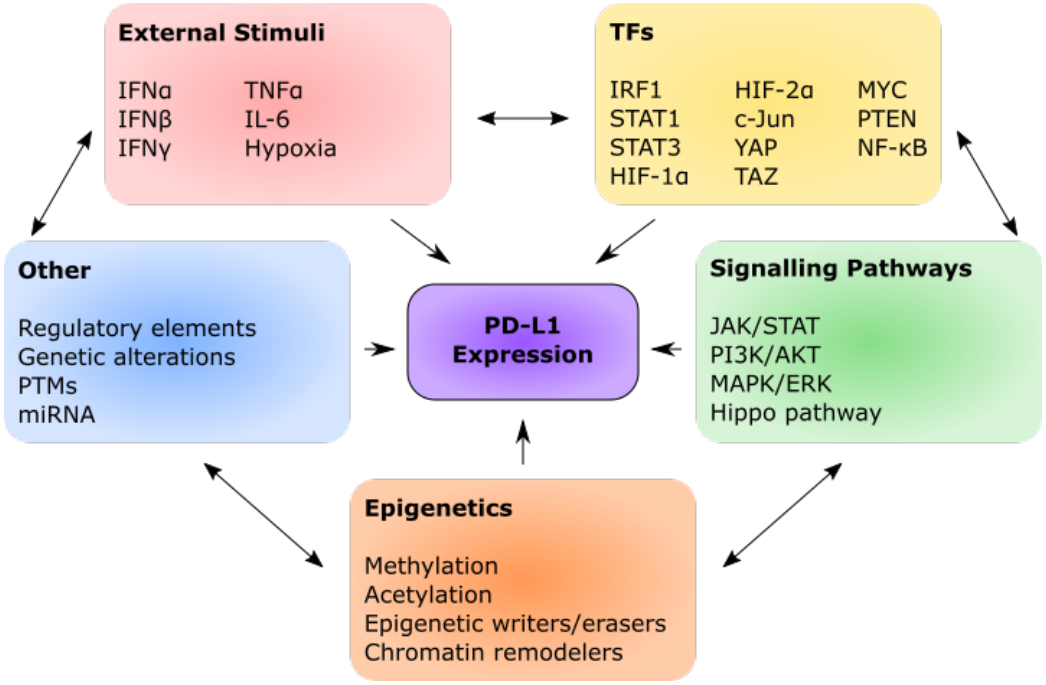

Figure 1.7: Regulation of PD-L1 expression.
Examples of external stimuli, TFs, signalling pathways, epigenetics and other modes of PD-L1 expression regulation. PTMs: post-transcriptional/translational modifications. miRNA: microRNA.

with JAK/STAT signalling, STAT3 seems to be an important regulator of PD-L1 expression. STAT3 can be activated through both type I and II interferon signalling, although STAT1 activation is preferential in the latter. Furthermore, STAT3 can be activated through alternate mechanisms. STAT3, activated by the anaplastic lymphoma kinase (ALK) through JAK3, was able to bind the PD-L1 promoter and induce its expression [Marzec et al., 2008]. Conversely, STAT3 modulated PD-L1 expression in ALK negative cancers, demonstrating further mechanisms of regulation [Atsaves et al., 2017]. In line with this, deletion of STAT3 in other cancer types reduced PD-L1 expression [Bu et al., 2017, Jiang et al., 2013]. These results are in sharp contrast with the finding by Garcia-Diaz [Garcia-Diaz et al., 2017], that mutating or deleting the STAT3 binding site at the PD-L1 promoter increased PD-L1 expression. Although this could be due to differential regulation in the different

cell types studied.

Transcription of PD-L1 can be further augmented by co-activation of STAT3 with c-Jun [Schaefer et al., 1995, Jiang et al., 2013], a component of the AP-1 complex. ChIP experiments illustrate that c-Jun is able to bind within the first intron of PD-L1, and depletion of this TF significantly impedes PD-L1 expression [Green et al., 2012]. Similarly, other TFs commonly involved in oncogenesis such as the hippo pathway effectors (YAP and TAZ), MYC, PTEN and NF-κB have also demonstrated modulation of PD-L1 expression, many of which have demonstrated PD-L1 promoter binding [Song et al., 2013, Casey et al., 2016, Atsaves et al., 2017, Asgarova et al., 2018, Janse van Rensburg et al., 2018, Kim et al., 2018].

However, due to the promiscuous nature of the aforementioned TFs, indirect mechanisms of PD-L1 regulation elicited by the altered expression landscapes can't be ruled out. This could explain contradicting data such as the hypothesis put forward by Zou et al. that silencing of MYC upregulates PD-L1 due to elevated STAT1 levels [Zou et al., 2018]. Other TFs such as the tumour suppressor p53 have also been implicated in PD-L1 regulation, although there is no evidence of binding of this TF to the PD-L1 promoter [Gowrishankar et al., 2015, Shen et al., 2019].

1.4.5 Signalling pathways involved in PD-L1 regulation

Many signalling pathways, including JAK/STAT, PI3K/AKT, MAPK/ERK and the hippo pathway, have all demonstrated regulation of PD-L1 (Fig:1.7) [Parsa et al., 2007, Jiang et al., 2013, Sumimoto et al., 2016, Janse van Rensburg et al., 2018]. These pathways are major regulators of gene expression and therefore are likely to alter PD-L1 abundance through a variety of mechanisms, including through activation/inactivation of the forenamed TFs. Nonetheless, how they exert their effects on PD-L1 is not well characterised, and contradictory results in the literature indicate

that their roles, if any, appear to be dependant on conditions and cellular context [Gowrishankar et al., 2015, Sumimoto et al., 2016, Zerdes et al., 2018]. Indeed, IFNγ induced upregulation in numerous cell types was predominantly independent of PI3K/AKT, MAPK/ERK and YAP/TAZ signalling [Gowrishankar et al., 2015, Kim et al., 2018, Mimura et al., 2018]. Thus there are multiple distinct regulatory mechanisms involved in PD-L1 expression, complicating the elucidation of how each individual pathway operates.

1.4.6 Epigenetic regulation of PD-L1 expression

DNA and histone modifications are becoming increasingly popular drug targets due to their ability to create permissive or repressive environments. Epigenetic landscapes can predispose a gene to domineering repression or activation, or prime it for induced regulation. A variety of histone and DNA modifications are present throughout the genome, and different marks often correlate to particular elements. Whether this is causative or correlative remains debated for many modifications. Preventing or reversing these histone marks can alter transcription, hence the ever-increasing interest in their regulation.

1.4.6.1 Methylation

One fundamental epigenetic factor is DNA methylation, which in general suppresses gene expression. The PD-L1 promoter contains regions of high CpG dinucleotide content, known as a CpG island, which can be differentially methylated. Indeed, increased methylation of the PD-L1 promoter correlated with attenuated expression (Fig:1.7) [Goltz et al., 2017, Micevic et al., 2019]. 5-azacytidine, a hypomethylating agent, reduced methylation of PD-L1, resulting in increased expression [Wrangle et al., 2013, Micevic et al., 2019]. Furthermore, comparing Isocitrate Dehydrogenase (IDH) mutant gliomas to IDH wild-

type (WT) gliomas found increased PD-L1 expression in the WT tumours [Berghoff et al., 2017, Mu et al., 2018]. Mutations in IDH alter cell metabolism to produce more 2-Hydroxyglutarate (2HG). This inhibits histone and DNA demethylases which, in turn, results in increased epigenetic methylation. This suggests that IDH mutant cancers may increase methylation of the PD-L1 promoter, reducing expression. Supporting this, addition of 2HG to glioma cells lead to upregulated PD-L1 promoter methylation and reduced expression [Mu et al., 2018].

Alongside DNA methylation, correlations between histone methylation, particularly H3K4me3, at the PD-L1 promoter and PD-L1 expression have been found. Silencing or inhibition of the histone methyltransferase, MLL1, which was found to bind to the promoter region, reduced this trimethylation and suppressed expression of PD-L1 [Lu et al., 2017]. In contrast, another study found no effect of MLL1 knock-down on PD-L1 messenger RNA (mRNA) or protein levels [Xiong et al., 2019]. Instead, they identified MLL3 as a modulator of PD-L1 transcription and established a positive correlation between MLL3 and PD-L1 in tumour samples. They demonstrated MLL3 binding to a putative enhancer region at the 3'-end of PD-L1. Knocking-down the MLL3 protein reduced H3K4me1 at this site, corresponding to attenuated transcription of PD-L1 [Xiong et al., 2019]. However, as suppressing methyltransferases can have pleiotropic downstream effects, the upregulation of PD-L1 could be through indirect mechanisms, thus further investigation is warranted to validate these results.

1.4.6.2 Acetylation

Histone acetylation neutralises the positive charge on histones, reducing their DNA binding affinity, thus relaxing chromatin to allow increased gene expression. Histone deacetylases (HDACs) erase these marks, suppressing genes, and inhibitors against HDACs are being evaluated for use as anti-cancer drugs. Indeed, HDAC inhibitors

alter PD-L1 levels in multiple cell types. Different HDACs have shown differential roles in regulating PD-L1, with HDACs 1, 2, 3 and 6 linked to upregulation of PD-L1 and HDAC8 linked to its downregulation [Woods et al., 2015, Lienlaf et al., 2016, Booth et al., 2017, Bae et al., 2018, Wang et al., 2018b]. ChIP experiments have identified binding of both HDAC6 and 8 upstream of the PD-L1 promoter, and both have been associated with STAT3 at these sites [Lienlaf et al., 2016, Wang et al., 2018b]. However, discrepancies exist within the literature, with negative correlations between HDAC3 and PD-L1, or no correlation between HDAC6/8 and PD-L1, being described [Woods et al., 2015, Booth et al., 2017, Wang et al., 2020]. This suggests their effects are orchestrated through a number of mechanisms. Altered acetylation coordinated by these HDACs likely reshapes the expression landscape within a cell, with the corresponding genes modulating the expression of PD-L1.

Recent experiments suggest that IRF1 and STAT1 interact with the acetylation writers p300 and CREB-binding protein (CBP). These lysine acetyltransferases (KATs) were found at the PD-L1 promoter in prostate cancer cell lines. Moreover, shRNA knockdown of IRF1 reduced binding of p300/CBP as well as BRD4, an acetyl lysine binding protein, reduced H3 acetylation and attenuated PD-L1 expression. This implies that IRF1 increases acetylation of PD-L1 to enable its expression by recruiting p300/CBP to the PD-L1 promoter [Liu et al., 2020].

1.4.6.3 Chromatin modifiers

A second family of inhibitors, the Bromodomain and Extraterminal (BET) protein inhibitors (BETi), are also under examination as anti-cancer therapies. BET proteins are 'readers' of chromatin. They bind to acetylated lysine residues in nucleosomes and recruit chromatin modifiers to promoters and enhancers which stimulate or repress gene expression depending on the context [Belkina and Denis, 2012]. Treatments with multiple different BET inhibitors, including JQ1, suppresses PD-L1 mRNA and

protein levels in both tumour and immune cells. JQ1 treatments reduced occupancy of the BET protein BRD4 at the PD-L1 loci and prevented IFNγ induced association of BRD4 to this locus [Zhu et al., 2016, Hogg et al., 2017, Ebine et al., 2018]. BRD4 knockdown, but not BRD2 or BRD3, depleted both constitutive and IFNγ induced PD-L1 expression. BETi attenuation of PD-L1 appeared independent of MYC and IRF1, prominent targets of BRD4, which showed minimal expression changes throughout BETi treatments, ruling out some indirect mechanisms of PD-L1 regulation [Hogg et al., 2017, Ebine et al., 2018].

Hogg et al. found that IFNγ induced loading of IRF1 was not affected by JQ1 treatments [Hogg et al., 2017]. On the other hand, knockdown of IRF1 reduced BRD4 binding in prostate cancer cells [Liu et al., 2020]. Additionally, experiments inducing PD-L1 expression by inhibiting HDACs and consequently increasing acetylation of the PD-L1 promoter found increased binding of BRD4 to the promoter. Knockdown of BRD4 attenuated this induced upregulation of PD-L1 suggesting BRD4 is a key reader of H3 acetylation at the PD-L1 promoter, driving PD-L1 transcription [Liu et al., 2020]. One proposed model is that binding of IRF1 to the PD-L1 promoter recruits KATs, increasing acetylation. This, in turn, recruits the acetylation reader, BRD4, which stimulates transcription of PD-L1 [Hogg et al., 2017, Liu et al., 2020]. In sharp contrast, Ebine et. al demonstrated stunted IFNγ-induced IRF1 binding to the PD-L1 promoter upon JQ1 treatments and suggested that BRD4 is required for IRF1 association [Ebine et al., 2018]. Therefore, further analysis is required to determine the exact role of BET proteins in PD-L1 constitutive and induced expression.

Thus, despite identifying correlations between certain epigenetic modifications and PD-L1 expression, how IFNγ induces epigenetic changes to the PD-L1 locus and how these consequently produce a permissive environment for expression of the gene is only just beginning to be untangled.

1.4.7 PD-L1's regulatory elements

In addition to the promoter sequence, activation of transcription often requires regulatory elements to upregulate gene expression. A number of potential regulatory elements for PD-L1 have been identified, including regions ∼8kb upstream of the gene, in the first intron, between the PD-L1 and PD-L2 loci, and downstream of PD-L2 (Fig:1.8). These enhancers were identified in different cell types thus indicating that different environmental and epigenetic cues may regulate which regulatory elements are active. These enhancers were characterised by TF binding and correlations between promoter and enhancer transcription levels [Green et al., 2012, Sumimoto et al., 2016, Chen et al., 2018b, Hsu et al., 2018b, Zhu et al., 2018b, Xu et al., 2019]. In one case a gene loop between the promoter and enhancer was identified by Hi-C analysis [Chen et al., 2018b]. However, each of the cell types investigated expressed PD-L1 constitutively and hence lack evidence determining whether they are required for IFNγ induced PD-L1 expression. Chen et al. produced a CRISPR-Cas9 KO of the active enhancer at chr9:5580709-5581016. Despite this causing ∼90% retardation of constitutive PD-L1 expression, its expression could still be largely induced by IFNγ [Chen et al., 2018b]. Thus any regulatory elements involved in IFNγ induction of PD-L1 have yet to be discovered.

1.4.8 Genetic alterations at the PD-L1 locus

Genomic instability is a common feature for multiple cancer types. Genomic rearrangements of the 9q24.1 locus, containing the PD-L1 gene, have been identified in over 20 cancer types. Copy number gains, amplifications and translocations have all been associated with PD-L1 overexpression [Twa et al., 2014, Budczies et al., 2016, Roemer et al., 2016]. PD-L2 and JAK2 expression, genes also present in 9q24.1, additionally correlate with copy numbers [Green et al., 2010]. As JAK2 can stimulate

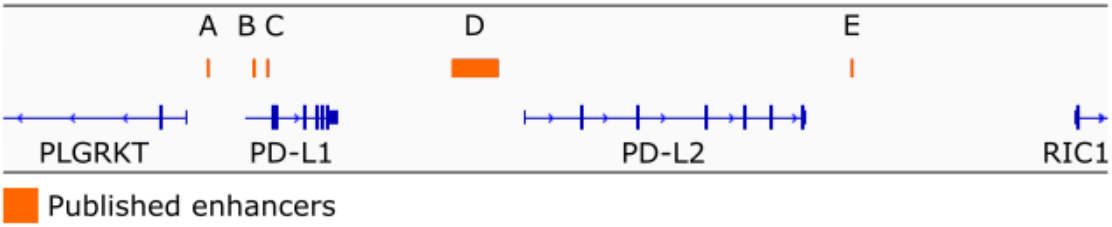

	Cell type	Experimental evidence	Reference
A	Human malignant pleural mesothelioma	TF binding (YAP)	[Hsu et al., 2018b]
B	Melanomas	TF binding (NRF2), Luciferase assay	[Zhu et al., 2018b]
C	Hodgkin's Lymphoma, Adenocarcinoma	TF binding (c-Jun), Luciferase assay	[Green et al., 2012] [Sumimoto et al., 2016]
D	Breast Cancer	H3K27ac ChIP data, TF binding (BRD4, Med1), CRISPR-Cas9 KO	[Xu et al., 2019]
E	Multiple cancer cells, Adenocarcinoma	Hi-C interaction, mRNA coexpression, CRISPR-Cas9 KO	[Chen et al., 2018b]

Figure 1.8: Published enhancers involved in the regulation of PD-L1 expression.
Table describing experimental evidence and cell lines used to identify published constitutive PD-L1 enhancers. The figure above depicts the location of each enhancer relative to the PD-L1 gene.

the STAT1/IRF1/PD-L1 axis, overexpression of this protein may further augment PD-L1's expression.

Furthermore, mutations or structural variants in PD-L1's 3'-untranslated region (3'-UTR) have been identified in patient cancer samples. Disruption or truncation of the 3'-UTR has been shown to increase PD-L1 transcript levels through increased stability [Wang et al., 2012, Kataoka et al., 2016]. Mutations have also been identified in the promoter region, altering PD-L1 expression [Tao et al., 2017].

1.4.9 Post-transcriptional and post-translational regulation

In addition to the amalgamation of signals controlling transcription of PD-L1, layers of post-transcriptional regulation also exists controlling expression of functional PD-L1. Signals stemming from epigenetic marks and the transcriptional machinery can recruit components required to aid or repress nuclear export, translation, correct folding and translocation of a protein.

1.4.9.1 ncRNA

Continuing from the previous section, perturbing the PD-L1 3'-UTR led to increased expression. This increased transcript stability is likely to be, at least partially, dictated by microRNAs (miRs). miRs are single-stranded ncRNAs of approximately 22 nucleotides and have been implicated in cancer progression, altering gene expression either by promoting transcription, destabilising transcripts or repressing translation. Multiple miRs have been identified as having a direct or indirect role in PD-L1 expression. Most of those directly binding to PD-L1 transcripts bind to its 3'-UTR region, destabilising the mRNA [Wang et al., 2017d, Ji et al., 2018]. miRs also indirectly modulate PD-L1 expression by targeting TFs, such as STAT1 and PTEN, involved in its regulation [Zhu et al., 2014, Xi et al., 2018]. Moreover, the long ncRNA (lncRNA), lncMX1–215, was recently identified as an indirect inhibitor

of IFNα induced PD-L1 expression by interfering with GCN5/H3K27ac binding at the PD-L1 promoter [Ma et al., 2020], thus suggesting multiple ncRNA types play a role.

1.4.9.2 Spliced variants

Numerous isoforms of PD-L1 arising from post-transcriptional alternative splicing have been detected in different normal and cancerous tissues. These alternatively spliced variants have altered cellular fates. Whilst canonical PD-L1 enriches to the plasma membrane, an isoform excluding exon 2, which encodes an IgV-like domain, is preferentially localised to intracellular membranes [HE et al., 2005]. Other variants lack the transmembrane domain, encoded by exon 5 in the WT protein, and are conversely secreted. There is evidence that these secreted isoforms can dimerise and retain PD-1 binding affinity. Indeed, they were able to negatively regulate T cells [Gong et al., 2019, Hassounah et al., 2019, Mahoney et al., 2019]. The exact role of each splice variant in a biological setting is not well defined.

1.4.9.3 N-glycosylation

Once translated, PD-L1 undergoes a variety of post-translational modifications which determine the proteins fate. PD-L1 can be extensively N-glycosylated on four asparagine residues; N35, N192, N200 and N219, with the latter three having a role in stabilising the protein [Li et al., 2016]. Corroborating this, knocking down the glycosylases STT3 or B3GNT3 results in reduced glycosylation and stability of PD-L1 [Hsu et al., 2018a, Li et al., 2018]. Removing PD-L1 glycosylation weakened its affinity for PD-1 and increased T cell-mediated tumour cell killing [Li et al., 2016, Li et al., 2018], highlighting the importance of this post-translational modification.

1.4.9.4 Phosphorylation

A second post-translational modification, phosphorylation, is reported to regulate the stability of PD-L1, with phosphorylation, in general, decreasing PD-L1's stability. Both tyrosine and serine phosphorylation of PD-L1 have been reported [Horita et al., 2017, Cha et al., 2018]. GSK-3β binds to and phosphorylates non-glycosylated PD-L1, targeting it for ubiquitination and subsequent degradation. Glycosylation of PD-L1 buries the binding site for GSK-3β, thus partially explaining the stabilising role of PD-L1 glycosylation [Li et al., 2016]. Also linking to glycosylation, phosphorylation of PD-L1 S195 by AMPK, a metabolite sensor, results in abnormal glycosylation of PD-L1 in the endoplasmic reticulum (ER). Evidence strongly suggests this increases degradation of PD-L1 via the ER-associated protein degradation pathway [Cha et al., 2018].

1.4.9.5 Ubiquitination

Typically, ubiquitination targets proteins for degradation via the proteasome. E3 ubiquitin ligases, SPOP, β-TrCP and STUB1, have all been implicated in PD-L1 ubiquitination and subsequent destabilisation of the protein [Li et al., 2016, Mezzadra et al., 2017, Zhang et al., 2018]. Enzymes promoting deubiquitination of PD-L1, such as CSN5, a subunit of the COP9 signalosome, and CMTM6, increase PD-L1 stability [Lim et al., 2016, Burr et al., 2017, Mezzadra et al., 2017]. CMTM6, present at the plasma membrane and recycling endosomes, reduces ubiquitination of PD-L1 and subsequent lysosome-mediated degradation, thus maintaining PD-L1 expression at the plasma membrane. CMTM4 may have a similar role [Burr et al., 2017, Mezzadra et al., 2017]. In contrast, mono and multi-ubiquitination of PD-L1, stimulated upon EGF treatments, appeared to stabilise the protein [Horita et al., 2017].

1.4.9.6 Other post-translational modifications

PD-L1 has also been shown to undergo palmitoylation on C272, once again increasing stability of the protein. This palmitoylation was mediated by the palmitoyltransferase ZDHHC9 [Yang et al., 2019]. Additionally, there is evidence showing PD-L1 acetylation upon EGF treatments [Horita et al., 2017]. However, the role or regulation of these modifications are poorly understood.

1.4.10 PD-L2 regulation

Regulation of PD-L2 expression is poorly characterised in comparison to PD-L1, perhaps due to its less ubiquitous expression. However, it appears to have multiple layers of regulation, comparative to PD-L1. Similarly to PD-L1, PD-L2 induction has been shown upon both type I and type II IFN signalling, with the JAK/STAT pathway appearing to play a key role [Garcia-Diaz et al., 2017, Mimura et al., 2018, Shibahara et al., 2018]. Both IRF1 and STAT3 have been found to bind to the PD-L2 promoter and deletion of their binding sites stunts IFN induced PD-L2 expression [Garcia-Diaz et al., 2017]. STAT1, c-Fos and activated YAP are among other TFs implicated in modulating its expression [Janse van Rensburg et al., 2018, Shibahara et al., 2018].

Additionally, PD-L2 can be regulated at the genetic and epigenetic level. 9q24.1 copy number gains or amplifications correlate with both increased PD-L1 and PD-L2 expression in cancers [Green et al., 2010]. Knock-down or inhibition of HDACs have been linked with upregulation and downregulation of PD-L2, suggesting histone acetylation is involved in its modulation [Woods et al., 2015, Booth et al., 2017].

Like PD-L1, PD-L2 has alternate splice variants which alter its cellular location [He et al., 2004]. Furthermore, evidence suggests that the PD-L2 protein is glycosylated, although the mediators or role of this glycosylation were not evaluated

[Wang et al., 2017a]. Therefore, many similarities exist between the control of PD-L1 and PD-L2 expression, with both having multiple factors fine-tuning their regulation. However, the two ligands must have distinct mechanisms of regulation given that their expression does not always coincide.

1.5 Requirements for transcriptional activation

1.5.1 Initiation of transcription

As described above, IFNγ induces the transcription of PD-L1. Despite having evidence of the key TFs involved (JAK/STAT1/IRF1), how these TFs drive the formation of permissive chromatin to enable PD-L1 expression is not well understood, and minimal research exists on regulatory elements required for this inducible expression. In general, how IFNγ alters higher-order chromatin structure and the enhancer landscape to reprogramme gene expression is yet to be elucidated. To further resolve the mechanisms behind IFNγ induced gene expression, one must first consider the basic requirements of transcription initiation. Transcription describes the process of converting the genetic information encoded in DNA into molecules of RNA. This RNA may be functional, as is the case of ncRNA, or must be translated into a protein to become functional as is the case of mRNA. RNA polymerases are the vital enzymes involved in transcription. Eukaryotic cells express three RNA polymerases, with RNA polymerase II (Pol II) involved in the synthesis of mRNA and a large proportion of ncRNA. In order to initiate, elongate and terminate transcription, Pol II requires a wealth of signals from a large plethora of proteins, over 100 in humans, adding layers of regulation at each step.

One requirement for gene transcription is the core promoter which encompasses the transcriptional start site (TSS) and spans roughly 50bp upstream and downstream of this site. The core promoter is composed of numerous promoter

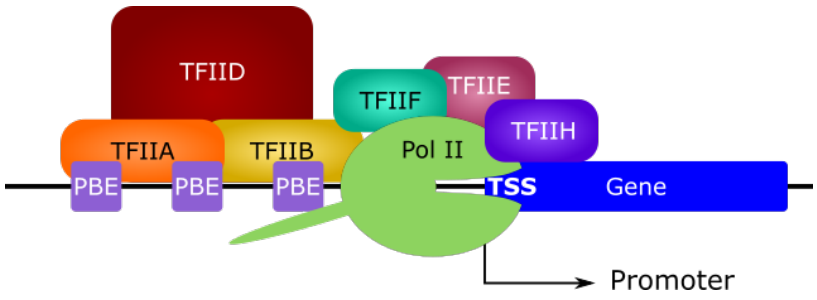

Figure 1.9: The Pre-Initiation Complex.
TFIID binds to promoter binding elements (PBE). This recruits TFIIA and TFIIB. Pol II bound to TFIIF is recruited, followed by TFIIE and TFIIH, completing the formation of the PIC.

elements. Many promoter elements have been identified including the TATA-box, Inr, DPE and more [Smale and Baltimore, 1989, Burke and Kadonaga, 1996, Lagrange et al., 1998, Lim et al., 2004]. Additionally, certain nucleotide compositions, such as CpG dinucleotide rich regions are commonly found at core promoters [Haberle and Stark, 2018]. None of these elements are essential in themselves, but a combination of multiple elements is required. Together these elements act as the docking site for the general transcription factors (GTFs), such as the TATA-box binding protein (TBP), a subunit of GTF IID (TFIID) (Fig:1.9) [Pugh and Tjian, 1991, Burke and Kadonaga, 1996].

The binding of TFIID, whether via TBP or the TBP-associated factor (TAF) subunits, recruits the remaining GTFs (TFIIA, TFIIB, TFIIE, TFIIF and TFIIH) along with Pol II to form the pre-initiation complex (PIC) (Fig:1.9). In the classical model, TFIIA and TFIIB bind both upstream and downstream of TBP, stabilising the association of TFIID. This recruits a Pol II-TFIIF complex, followed by TFIIE and TFIIH, forming the complete PIC [Buratowski et al., 1989, Sainsbury et al., 2015].

TFIIH is a large protein complex formed of two subcomplexes; the core and the CAK subcomplex, both of which are important for transcription initiation. The core complex comprises ATP-dependent DNA helicases which unwinds the DNA to form an

open complex [Fishburn et al., 2015]. This enables positioning of the open template into Pol II ready for transcription [Cheung et al., 2011, Grünberg et al., 2012]. The CAK subcomplex contains kinase activity which phosphorylates a number of substrates including Ser5 and Ser7 in the Pol II carboxy-terminal domain (CTD) [Akhtar et al., 2009]. This causes conformational changes that releases Pol II from the GTFs and enables promoter escape [Wong et al., 2014]. Pol II, at a number of genes, pauses after transcribing a short transcript of ∼20-60bp, a phenomenon known as promoter-proximal pausing [Core et al., 2008]. Further transcriptional control is added by the requirement of additional factors needed to overcome this pause and for the complete production of the transcript.

1.5.2 TFs and cofactors in transcription regulation

The PIC alone, although sufficient for transcription initiation, results in extremely low basal activity of Pol II. Numerous signals from TFs, cofactors, ncRNAs and epigenetic marks are required to further activate or silence transcription. They mediate this by altering PIC assembly and the recruitment and activation of Pol II. TFs recognise sequence-specific DNA motifs typically found at regulatory elements such as regions proximal to promoters or enhancers. Promoters and enhancers contain multiple TF motifs enabling a vast number of TF combinations that provide stringent regulation of gene expression.

TFs function by recruiting cofactors. One example of a cofactor is mediator, a 1.2 MDa multi-subunit complex that wraps around the PIC [Borggrefe and Yue, 2011, Plaschka et al., 2015]. Mediator integrates signals from activators and repressors to the transcriptional machinery. It can act as a bridge between the promoter and distal regulatory elements, enabling DNA looping and bringing several signalling molecules close together in 3D space. In addition, it possesses a kinase activity that can phosphorylate a number of substrates adding further layers of regulation

[Borggrefe and Yue, 2011]. Many cofactors, similarly, have enzymatic activity that regulates post-translational modifications (PTMs) of the transcriptional machinery and the epigenetic landscape. Chromatin remodelers or histone modifiers, for example, function to create a more permissive/repressive chromatin environment.

1.5.3 Epigenetics in transcriptional regulation

Most TFs can only bind to exposed regions of DNA, as highly compact nucleosomes occlude their DNA binding sites [Thurman et al., 2012, Klemm et al., 2019]. Chromatin remodelers and histone modifiers can dynamically alter DNA accessibility enabling binding of TFs and the PIC. This can be achieved by increasing turnover, repositioning or modifying the nucleosome [Cairns, 2009, Hughes and Rando, 2014]. A high proportion of promoters have two nucleosomes well-positioned upstream and downstream of the TSS, termed the -1 and +1 nucleosome respectively, with a nucleosome depleted region (NDR) in-between (Fig:1.10) [Lee et al., 2004, Cairns, 2009]. Altering the positions of these +/-1 nucleosomes can expose/occlude core promoter elements in addition to TF motifs, thereby regulating gene expression [Schones et al., 2008].

In addition, histone globular domains and tails within the nucleosomes can be dynamically modified by acetylation, methylation, etc. Novel modification sites and types continue to emerge, expanding our knowledge of the complex epigenetic landscape [Kebede et al., 2017, Viéitez et al., 2020]. These modifications can relax/compact nucleosomes due to alterations in histone charge and/or structure, and can also act as platforms to recruit TFs and cofactors [Bannister and Kouzarides, 2011, Lawrence et al., 2016]. Some modifications may exert their functions simply by preventing other modifications, for example, acetylation or methylation of the same lysine residue is mutually exclusive.

Different combinations of modifications can recruit particular factors and

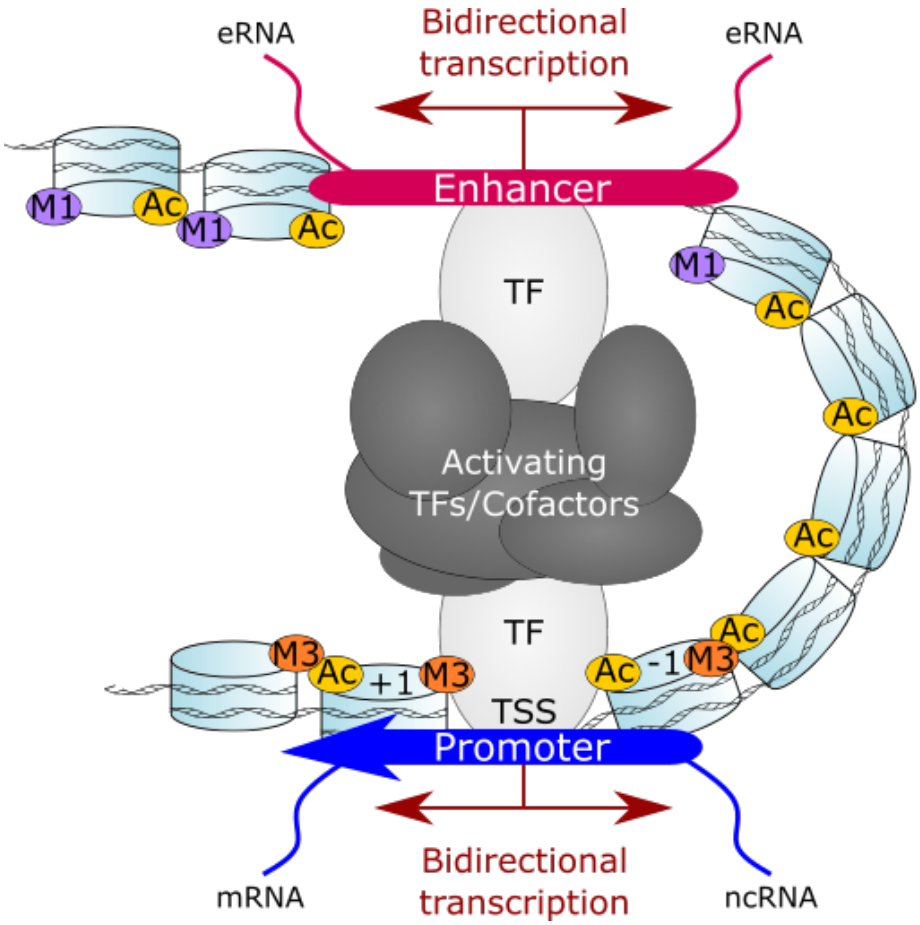

Figure 1.10: Typical features of a promoter and enhancer element.
A typical active promoter and enhancer. The promoter has an accessible region exposing the TSS. +1 and -1 histones are found downstream and upstream of the accessible site respectively. Coding and non-coding bidirectional transcription stem from the accessible site. The promoter is bound by numerous TFs and cofactors. TFs and cofactors bridge the promoter to the enhancer. The active enhancer is also characterised by an accessible region of DNA. This accessibility is maintained through the binding of TFs to these sites. The chromatin surrounding both the active promoter and enhancer is commonly acetylated. Histones surrounding enhancers are typically associated with H3K4me1, as opposed to promoters, which are thought to correlate with H3K4me3. Bidirectional transcription from the enhancer element produces eRNAs.

certain modifications/chromatin states correlate with silenced or active promoters (Fig:1.10) [Bannister and Kouzarides, 2011]. Silenced promoters generally have compact nucleosomes with minimal DNA accessibility, and correlate with silencing modifications such as H3K9me3, H3K27me3 and DNA methylation [Barski et al., 2007, Hansen et al., 2008]. Poised promoters are characterised by an accessible NDR. These promoters can often become activated by different environmental cues. Histone acetylation, by removing the positive charge on histone tails, weakens contacts between the histone and DNA, reducing nucleosome stability [Di Cerbo et al., 2014]. It is therefore typically associated with active promoters, a key example being H3K27ac which has strong correlations with expressed genes (Fig:1.10) [Wang et al., 2008]. H3K4me3 and H3K36me3, in addition to the histone variants H2A.Z and H3.3, also correlate well with active promoters [Barski et al., 2007, Jin et al., 2009, Hu et al., 2013]. It is thought that these histone variants increase nucleosome turnover, thus making the promoter more accessible. For many histone modifications, it is unclear whether their correlations are causative or consequential [Howe et al., 2017]. All in all, it is the amalgamation of signals from TFs, cofactors and epigenetic marks that fine-tune gene expression.

1.5.4 Regulatory elements in transcription

Regulatory elements such as enhancers or insulators can upregulate or downregulate transcription respectively. Enhancers function independently of orientation and genomic distance. They contact promoters by coming within spatial proximity, mediated by the 3D higher-order chromatin structure within the nucleus (Fig:1.10) [Sanyal et al., 2012, Rao et al., 2014]. Architectural proteins and cofactors, such as cohesin and mediator, are involved in bridging promoters and enhancers together [Kagey et al., 2010, Phillips-Cremins et al., 2013]. Transcription may be induced by increased contact between the promoter and enhancer, or by recruitment of

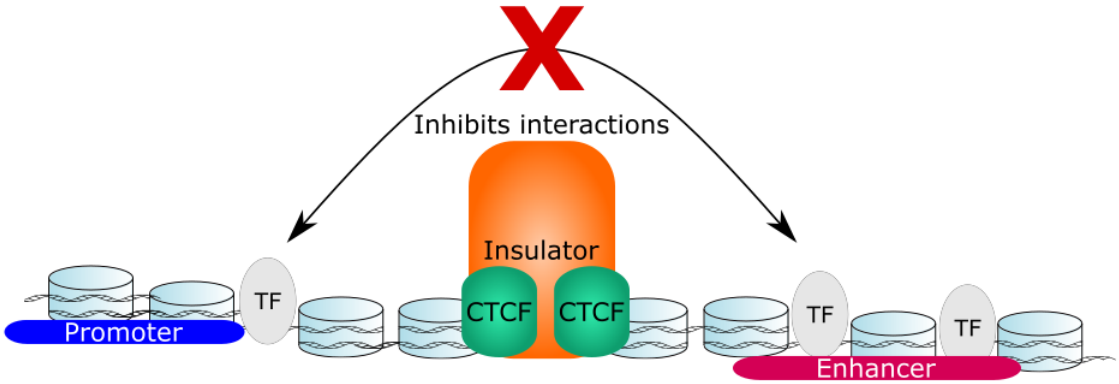

Figure 1.11: Insulator elements inhibit interactions between promoters and enhancers.
An insulator element found between promoters and enhancers prevents looping between these elements. This prevents aberrant activation of promoters. Insulators are typically bound by CTCF TFs.

TFs/cofactors to a pre-existing loop. Insulators function by preventing these loop formation and are vital to gene regulation (Fig:1.11). Loss of insulators can result in aberrant gene expression leading to disease phenotypes.

A single regulatory element can contact multiple promoters and vice versa [Sanyal et al., 2012]. There is evidence of 100,000s enhancer like elements within the human genome, hugely exceeding the ∼20,000 genes. Thus it is likely that the combination of active enhancers and the contacts made, i.e. the higher-order chromatin structure within the cell, dictates gene expression. Indeed, different cell types show diverse enhancer landscapes and alterations of the enhancer landscape is commonly found in disease [Sakabe et al., 2012, Sanyal et al., 2012].

Enhancers have characteristic promoter properties and, in many ways, can function as a promoter. Enhancer elements contain multiple TF motifs enabling recruitment of TFs, chromatin remodelers, histone modifiers and cofactors [Koch et al., 2011, Calo and Wysocka, 2013, Haberle and Stark, 2018]. They can also initiate bidirectional transcription (Fig:1.10). However, unlike a promoter, enhancer transcription usually results in the formation of short, unstable, non-

polyadenylated enhancer RNA (eRNA) [Kim et al., 2010, Core et al., 2014]. Whether active transcription or eRNA transcripts are required for enhancer function remains debated. Some argue that enhancer transcription is coincidental due to the high concentration of transcription machinery present. Indeed levels of eRNA transcripts correlate with target mRNA transcription [Kim et al., 2010]. However, there are reports that eRNAs associate and stimulate coactivators such as CBP and BRD4 [Bose et al., 2017, Rahnamoun et al., 2018]. Additionally, shRNA studies have identified reduced looping and target mRNA expression upon eRNA KD suggesting a key role in enhancer function [Pnueli et al., 2015, Liang et al., 2016].

eRNAs are used to identify enhancers, along with accessible regions of DNA, high H3K4me1:H3K4me3 ratios and high levels of H3K27ac (Fig:1.10) [Creyghton et al., 2010, Calo and Wysocka, 2013]. Promoter contact with an enhancer essentially increases the milieu of TFs, ncRNAs and cofactors associated with the promoter, thus enhancing transcription.

Studies have identified gene and lncRNA promoters displaying enhancer activity independently of their conventional transcriptional product, termed ePromoters. CRISPR-Cas9 mediated KO of these ePromoters results in downregulation of distal genes [Engreitz et al., 2016, Dao et al., 2017, Diao et al., 2017]. Although many of these ePromoters were associated with housekeeping genes, a subset appeared to be involved in stress responses, including the type I and II IFN response. This provides a model where pre-formed promoter loops can enable rapid activation of distal promoters upon stress [Dao et al., 2017].

1.6 Targeting epigenetic marks and regulatory elements for cancer therapy

Aberrant chromatin and enhancer landscapes can promote oncogenesis through altered gene expression [Waldmann and Schneider, 2013]. Epigenetic modifiers are being targeted in a growing number of clinical trials for use as cancer therapies. Inhibitors of the epigenetic machinery, including inhibitors of DNA methyltransferase I (DNMT1), HDACs and the histone methyltransferase EZH2, have been FDA approved for use against certain cancer types [Kelly and Issa, 2017, Zhao et al., 2019, Mullard, 2020]. They work by enhancing the expression of tumour suppressors and other immune-related genes, including IFN signalling pathways, and are being widely tested for use in combination with immunotherapies [Terracina et al., 2016, Briere et al., 2018, Lai et al., 2018]. Indeed, combination therapies using anti-PD-1/PD-L1 immunotherapies with inhibitors of epigenetic modifiers are currently being investigated in animal models and clinical trials [Hogg et al., 2017, Lai et al., 2018, Xin Yu et al., 2019].

Additionally, a number of studies are analysing ways to alter the oncogenic enhancer landscape as potential cancer therapies. Currently, certain approved therapeutic elements, for instance, cyclosporine and thiazolidinediones achieve this by targeting particular TFs; NFAT via calcineurin, and PPARG respectively. Alternatively, targeting BET or CDK proteins have shown potential as cancer treatments by inhibiting enhancer driven oncogene expression [Hamdan and Johnsen, 2019, Tang et al., 2020]. However, as these proteins regulate transcription, they could have many off-target effects.

Therefore, further characterisation of the epigenetic changes and regulatory elements involved in induced PD-L1 expression will assist in the development of improved anti-PD-1:PD-L1 immunotherapies.

1.7 Aims

This thesis aims to investigate how IFNγ signalling alters the transcriptional, epigenetic and enhancer landscape within the HCC cell line, Hep3B. To this end, multiple -omics sequencing techniques are performed examining transcript levels, nascent transcription, DNA accessibility, H3K27ac, H3K4me3 and CTCF binding, enabling promoter and enhancer activity to be investigated. Additionally, Capture-C is performed to access promoter interactions.

The first half of this work focuses on the IFNγ-induced expression of PD-L1. PD-L1 expression is examined upon IFNγ treatments in a variety of cell lines to assess cell-type specific responses to IFNγ. PD-L1 promoter interactions coupled with transcriptional and epigenetic changes in Hep3B cells will be used to investigate any potential regulatory elements involved in inducible PD-L1 expression. The latter half of this thesis analyses the effects of IFNγ signalling genome-wide, investigating the dynamics of IFNγ-stimulated gene and enhancer activation throughout 24 hrs of treatment. Taken together, the overall objective is to improve our understanding of IFNγ-induced gene regulation in cancer cells.

Chapter 2

Materials and Methods

2.1 Cell strains and cell culture

Hep3B (ATTC), HeLa and Hek-293 (local sources) were cultured in DMEM high glucose supplemented with 10% (v/v) FBS and 1x (v/v) Penicillin/Streptomycin. GM12878 (Coriell institute) were cultured in RPMI 1640 supplemented with 15% (v/v) FBS. All cells were grown at 37^{o}C, 5% CO_2. Cells were left untreated or treated with 10 ng/ml of IFNγ for 0.5, 2 or 24 hrs unless stated otherwise. Cells were counted on a Nexcelom Biosciences Auto 2000 Cell Counter.

2.2 Western blots

Cells were lysed in RIPA buffer (10 mM Tris-HCl pH 8, 1 mM EDTA, 1% Triton X-100, 0.1% Na-deoxycholate, 0.1% SDS, 140 mM NaCl, Roche mini-EDTA free Complete tablets, 1 mM AEBSF). Samples were run on a 12% SDS-PAGE gel and transferred at 15V to a nitrocellulose membrane. The membrane was blocked in BSA and incubated with primary antibody overnight at 4^{o}C. The membranes were washed and incubated with the corresponding HRP secondary antibody. After additional washes, the membrane was incubated with ECL reagent (ThermoFisher Scientific),

exposed to an x-ray film for varying times which were then developed. Primary antibodies used: mouse anti-actin (abcam, ab14128), rabbit anti-IRF1 (CST, 8478S), rabbit anti-STAT1 (CST, 9172S), rabbit anti-pSTAT1 (CST, 7649S), mouse anti-STAT3 (Santa Cruz, sc-8019), mouse anti-pSTAT3 (Santa Cruz, sc-8059). Secondary antibodies used: anti-mouse IgG peroxidase (abcam, A9044) and anti-rabbit IgG peroxidase (abcam, A6154).

2.3 RNA extraction and reverse-transcription

2x10^6 cells were washed in PBS and lysed in Qiazol. Chloroform was added and the samples vortexed thoroughly. Following a 3 min incubation at room temperature (RT), samples were centrifuged for 15 min, 13000g, 4^{o}C. RNA, from the upper phase, was precipitated with isopropanol and centrifuged as before to obtain an RNA pellet, which was washed in 75% ethanol, dried and resuspended in RNase-free H_2O. RNA was DNase treated by addition of 1x DNase I buffer, 1U DNase I (Roche) and 40U RNaseOUT (ThermoFisher Scientific), incubating at 37^{o}C for 1 hr. The reaction was stopped by a 10 min incubation at 75^{o}C.

5 µg of DNase treated RNA was reverse transcribed as follows: Random primers and dNTPs (ThermoFisher Scientific) were incubated with the RNA for 5 min at 65^{o}C. 1x First strand buffer, 5 mM DTT (final concentrations), 40U RNaseOUT and 200U SuperScript III (ThermoFisher Scientific) were added to the RNA mix and incubated at 50^{o}C for 1 hour followed by 15 min at 70^{o}C. A negative control was prepared in the same way excluding the SuperScript III reverse transcriptase.

Reverse transcribed samples were analysed by qPCR (Section 2.4) using the ACTB, IRF1, PD-L1, PD-L2 and PLGRKT mRNA primers (Table: 2.1). The results were normalised using the Comparative Ct method [Schmittgen and Livak, 2008]:

$$2^{(-\Delta\Delta Ct)}$$

where

$-\Delta\Delta$ Ct = (Average Ct for each sample - Average Ct for respective actin sample) - (Average Ct nRT - Average Ct nRT for respective actin sample)

Where RT and nRT correspond to the reverse transcribed sample and its negative control equivalent respectively. Unpaired T-tests with 99% confidence levels were performed on the results using GraphPad Prism 7.

2.4 qPCR

qPCRs were performed on a Corbett Rotor-Gene Q using SensiMix^{TM} SYBR Hi-ROX Kit (Bioline), holding at 95^{o}C for 10 min before 45 cycles of 95^{o}C (7 s), 58^{o}C (12 s) and 72^{o}C (12 s). Ct values, extrapolated using the Second Derivative Maximum Method, and the specificity of the amplified product, assessed by melting curve analysis, was determined using Q-rex Software. Primers used can be found in table 2.1.

2.5 Flow cytometry

Cells were treated with or without 10 ng/ml of IFNγ for 6 hours. Cells were washed in PBS and resuspended in cell staining buffer (Biolegend). The cells were incubated with Human TruStain FcX (Biolegend) prior to an incubation with PE conjugated PD-L1 antibody (Biolegend, 329705) or PE Mouse IgG2b, Isotype Ctrl Antibody (Biolegend, 400313). These were incubated in the dark, on ice, for 45 min. Cells were washed in cell staining buffer before analysis on a FACScalibur. Gating was used to remove debris. 10000 cells were counted using FL2 filters.

2.6 ATAC-seq

ATAC-seq was performed based on methods previously described [Buenrostro et al., 2015]: $5x10^4$ Hep3B cells were treated with 10 ng/ml IFNγ for 0, 0.5, 2 or 24 hrs. Cells were washed in cold PBS (containing IFNγ for treated groups) and resuspended in lysis buffer (10 mM Tris-HCl pH 7.4, 10 mM NaCl, 3 mM $MgCl_2$, 0.1% IGEPAL). The nuclei were pelleted and resuspended in 1x TD with 2.5 µl TDE1 (Nextera DNA library prep kit, Illumina). These were incubated for 30 min at 37^{o}C. The tagmented DNA was purified using the MinElute PCR purification kit (Qiagen, 28004).

Each sample was amplified using the Nextera DNA library prep kit and Nextera index kit (Illumina) with the following thermocycler programme: hold at 72^{o}C (5 min), 98^{o}C (30 s), 9 cycles of 98^{o}C (10 s), 63^{o}C (30 s), 72^{o}C (30 s) with a final 72^{o}C extension for 1 min.

The libraries were purified by adding 1.8 x volume of RT AxyPrep beads (Appleton Woods AxyPrep Mag PCR clean up) to each reaction. They were then size selected with a ratio of 0.6:1 beads to remove fragments larger than 600bp. Libraries were run on the Agilent Bioanalyzer with a DNA-High Sensitivity chip to assess quality.

2.6.1 ATAC-seq sequencing and analysis

Paired-end sequencing was performed on a NextSeq 500 with the 75 cycles NextSeq 500/550 High Output v2 kit (Illumina). FastQCs were performed on each dataset to ensure good quality of the run. The adapter sequences were trimmed and paired using Trimmomatic, removing reads with a quality score below 20 in a 5bp sliding window and reads below a minimum length of 30bp [Bolger et al., 2014]. Trimmed reads were aligned to the hg38 genome if un-spiked, or to a combined hg38-dm6 genome if spiked, using Bowtie2 [Langmead and Salzberg, 2012]. SAMtools were

used to remove duplicates and filter out reads with a MAPQ quality score <30 as well as mitochondrial reads [Li et al., 2009]. MACS2 was used to call peaks with a minimum FDR (q-value) of 0.01 [Zhang et al., 2008]. Following this, ENCODE blacklisted regions were removed. For visualisation of tracts, reads were normalised based on sequencing depth. Filtered BAM files were converted to bedgraphs using BEDtools [Quinlan and Hall, 2010]. Bedgraphs were further converted to BigWig files using the UCSCtools (UCSC genome browser).

2.7 Single-Nucleotide resolution 4sU (SNU)-seq

$6x10^6$ Hep3B cells were treated with 10 ng/ml IFNγ for 0, 0.5, 2 or 24 hrs. During the final 12 min of IFNγ treatment, 500 µM 4sU was additionally added. Following treatments, cells were washed with cold PBS before lysing in Qiazol on ice. Samples were spiked with *Saccharomyces cerevisiae* RNA (∼0.01%). RNA was purified by addition of chloroform, vortexing and centrifuging for 15 min, 4^{o}C, 13000g. RNA was precipitated with isopropanol, washing three times in 75% ethanol, drying at RT and resuspending in RNase-free H_2O.

300 µg RNA was biotinylated by incubation in 1x biotinylation buffer (10 mM Tris-HCl pH 7.5, 1mM EDTA), 10% dimethylformamide and 400 µg EZ-link HPDH biotin (ThermoFisher Scientific) for 2 hrs in the dark, shaking at 800 rpm. Biotinylated RNA was extracted by addition of chloroform in a phase-lock tube, centrifuging at 21000g for 5 min at RT. Salt and isopropanol were added to precipitate the RNA, centrifuging for 30 min, 21000g at 4^{o}C. The pellet was washed in 75% ethanol and resuspended in RNase-free H_2O.

µMACs streptavidin beads (Miltenyi Biotec) were used to capture biotinylated RNA, using µMACs Separators and magnetic stand enable washing of the beads three times with 65^{o}C wash buffer (100 mM Tris-HCl pH 7.5. 10 mM EDTA pH 8, 1 M

NaCl, 0.1% Tween-20) and three times with RT wash buffer, eluting in 100 mM DTT. The RNA was purified using the miRNeasy Mini Kit (Qiagen) as per manufacturers instructions, treating RNA bound columns with 25U DNase I (Qiagen) in 1x RDD buffer for 15 min at RT before washing and eluting the column in RNase-free H_2O.

RNA was poly(A) tailed in 1x Poly(A) reaction buffer, 1 mM ATP, 2.5U *E.coli* Poly(A) Polymerase (NEB) and 10U Superase In^{TM} RNase Inhibitor (ThermoFisher Scientific), incubating for 20 min at 37^{o}C. The RNA was precipitated in salt and isopropanol before washing in 80% isopropanol and resuspending in RNase-free H_2O.

Libraries were prepared using the QuantSeq 3' mRNA-seq library prep kit for ion torrent (Lexogen), following the manufacturers protocol. Libraries were run on the Agilent Bioanalyzer with a DNA-High Sensitivity chip to assess quality.

2.7.1 SNU-seq sequencing and data analysis

The libraries were loaded onto an Ion PITM Chip (ThermoFisher) using the Ion Torrent Chef (ThermoFisher) snd sequenced using the Ion PI Hi-Q sequencing 200 Kit on the Ion Proton Sequencer (ThermoFisher). Fastq files were downloaded and quality checked with FastQC. Files were trimmed with trimmomatic, removing reads with a quality score below 20 in a 5bp sliding window and clipping the poly(A) stretches [Bolger et al., 2014]. Trimmed reads were aligned to hg38 using hisat2 including the –no-mixed and the -no-discordant flags [Kim et al., 2015]. SAMtools were used to filter and sort aligned files [Li et al., 2009]. Scaling factors were calculated based on spike-in counts between samples. Scaled 3'end bedgraph files were generated using BEDtools with the -scale, -bg and -3 flags [Quinlan and Hall, 2010].

2.8 3'-end RNA-seq

After treating cells for 0, 0.5, 2 or 24 hrs with 10 ng/ml IFNγ, 10^6 cells were washed with cold PBS and lysed in Qiazol. 2% of *drosophila* sg4 cells were added. RNA was extracted with chloroform, vortexing and centrifuging for 15 min, 4^{o}C, 13000g. RNA was precipitated with isopropanol and the pellet resuspended in 1x DNase buffer and 7.5 U DNase (Qiagen). The pellet was DNase treated for 30 min at 37^{o}C. Again this was precipitated with isopropanol, washing three times in 75% ethanol, drying at RT and resuspending in RNase-free H_2O.

Each sample was reverse transcribed, amplified and purified to form a library using the QuantSeq 3' mRNA-seq library prep kit for ion torrent (Lexogen) following the manufacturers protocol exactly. Libraries were run on the Agilent Bioanalyzer with a DNA-High Sensitivity chip to assess quality.

2.8.1 3'-end RNA-seq sequencing and data analysis

The libraries were loaded onto an Ion PITM Chip (ThermoFisher) using the Ion Torrent Chef (ThermoFisher) and sequenced using the Ion PI Hi-Q sequencing 200 Kit on the Ion Proton Sequencer (ThermoFisher). Fastq files were downloaded and quality checked with FastQC. Files were trimmed with trimmomatic, removing reads with a quality score below 20 in a 5bp sliding window and reads below a minimum length of 30bp [Bolger et al., 2014]. A combined human hg38 and *drosophila* dm6 genome was prepared, filtering highly repetitive regions. Hisat2 was used to align the reads to the hg38-dm6 genome [Kim et al., 2015] followed by filtering and sorting using SAMtools [Li et al., 2009]. Number of reads per gene (Ensembl Homo Sapiens GRCh38 release 92) were counted. Scaling factors were calculated based on spike-in counts between samples and used when converting the filtered BAM files to bedgraphs using BEDtools [Quinlan and Hall, 2010]. Bedgraphs were further converted to BigWig files using the

UCSCtools (UCSC genome browser).

2.9 ChIPmentation

The ChIPmentation protocol used is largely based on the protocol published by Schmidl et al. [Schmidl et al., 2015]. 10^6 cells were treated with 10 ng/ml IFNγ for 0, 0.5, 2 or 24 hrs. Cells were washed and collected in cold PBS (containing IFNγ for treated groups). The cell pellet was resuspended in RT PBS and fixed for 5 min with 1% formaldehyde before quenching with 0.125 M Glycine. 5000 fixed *drosophila* sg4 cells (0.05%) were added as a spike-in control. The cell pellet was obtained, washed in cold PBS and incubated on ice in cold swelling buffer (10 mM Tris-HCl pH 8, 10 mM NaCl, 0.2% NP-40, 1 mM AEBSF and 1x complete mini EDTA-free proteasome inhibitor, Roche) for 10 min. The subsequent nuclear pellet was resuspended in cold lysis buffer (10 mM Tris-HCl pH 8, 1% NP-40, 0.5% Na-deoxycholate, 0.1% SDS, 1 mM AEBSF and 1x complete mini EDTA-free proteasome inhibitor, Roche) and sonicated for 90 min, 30 s on/30 s off at 4^oC(Bioruptor, Diagenode).

One tenth of the sample was taken as input control. The remaining sample was incubated overnight, rotating at 4^oC with the required antibody (see end of section), 5 µl of H2AV *drosophila* Ab and blocked Protein A dynabeads (Invitrogen). Protein A dynabeads were blocked rotating overnight with 200 µg/ml BSA, 200 µg/ml yeast tRNA, 200 µg/ml glycogen in lysis buffer. Additionally, a negative (NO) control was prepared using an equivalent amount of non-specific antibody.

The IPs and NOs were washed with the following; TSE-150 (1% Triton X-100, 0.1% SDS, 2 mM EDTA, 20 mM Tris-HCl pH 8, 150 mM NaCl) rotating for 3 min, TSE-500 (TSE-150 except with 500 mM NaCl) rotating for 3 min, LiCl wash (0.2 M LiCl, 1% NP-40, 1% dioxycholate, 1 mM EDTA, 10 mM Tris-HCl pH 8)

rotating for 15 min and twice in 10 mM Tris-HCl pH 8, transferring the beads to a fresh tube.

The beads were resuspended in 1x tagmentation buffer (10 mM Tris-HCl pH 8, 5 mM $MgCl_2$, 10% dimethylformamide) with 1 µl Tagment DNA enzyme (Nextera DNA Library Prep Kit), incubating for 10 min at 37^{o}C. The tagmentation reaction was stopped by addition of cold TSE-150 buffer. Beads were washed twice in cold TSE-150 buffer and twice in cold TE (10 mM Tris-HCl pH 8, 1 mM EDTA). Tagmented DNA was eluted off the beads with pre-heated elution buffer (10 mM Tris-HCl pH 8, 1 mM EDTA), incubating at 65^{o}C for 30 min.

The eluted IPs, NOs and Input controls were decrosslinked by addition of 330 mM NaCl for 3 hrs at 65^{o}C. Samples were treated with 1U RNase A (Roche) for 1 hr at 37^{o}C followed by a protein digestion overnight at 65^{o}C using Proteinase K (MERCK).

The samples were purified using the MinElute PCR purification kit (Qiagen) as per manufacturers instructions, eluting in H_2O. The input controls were tagmented for 10 min at 37^{o}C with 0.5 µl 1:5 diluted tagment enzyme in 1x tagment buffer.

Library preparations of all samples were made using the Nextera XT Index Kit and NPM from the Nextera DNA Library Prep Kit according to manufacturers instructions. The libraries were purified by addition of 1.8 x volume of room temperature AxyPrep beads (Appleton Woods AxyPrep Mag PCR clean up), washing beads twice in 80% ethanol before elution in H_2O. A size selection using a 0.65:1 bead:sample ratio followed by a 1:1 bead:sample ratio was performed to obtain fragments mostly between 200-400 bps. Libraries were run on the Agilent Bioanalyzer with a DNA-High Sensitivity chip to assess quality.

Primary antibodies used: anti-H3K4me3 (MERCK, 05-745R), anti-H3K27ac (Millipore, 07-360), anti-CTCF (CST, 3418S), anti-H2AV *drosophila* Ab (Active Motif, 39715) and PE Mouse IgG2b, Isotype Ctrl Antibody (Biolegend, 400313) was

used for the non-specific isotype control.

2.9.1 ChIPmentation sequencing and analysis

Sequencing and analysis were performed as in section 2.6.1. Scaling factors were calculated based on spike-in counts between samples, or based on sequencing depth for CTCF ChIP, and used when converting the filtered BAM files to bedgraphs using BEDtools [Quinlan and Hall, 2010]. Bedgraphs were further converted to BigWig files using the UCSCtools (UCSC genome browser).

2.10 NG Capture-C

The method used is based on the methods published from the Hughes lab [Hughes et al., 2014, Davies et al., 2015]. For each condition $2x10^7$ cells were harvested in cold PBS (containing IFNγ for treated samples). The cells were fixed in 1% formaldehyde for 10 min followed by quenching with 0.125 M glycine. Fixed cells were resuspended in lysis buffer (10 mM Tris-HCl pH 8, 10 mM NaCl, 0.2% Igepal, Roche cOmplete Protease Inhibitor Cocktail), incubating for 20 min on ice. Cells were resuspended in PBS and snap-frozen in liquid nitrogen.

Thawed cells were pelleted and resuspended in 1x cutsmart buffer and 0.28% SDS, shaking intermittently at 500 rpm, 30 s on/ 30 s off for 1 hr at 37^{o}C. 1.67% Triton X-100 was added and the samples incubated as before. 10U of NlaIII (NEB) was added to each sample, incubating as before for $\sim$6 hrs before addition of another 10U overnight, and an extra 10U the following morning, incubating for a further 6 hrs. The enzyme was inactivated by heating to 65^{o}C for 20 min. Samples were cooled and ligated with 240U T4 DNA ligase (ThermoFisher Scientific) in 1x ligase buffer for $\sim$22 hrs, shaking intermittently at 500 rpm, 30 s on/ 30 s off at 16^{o}C.

The nuclear pellet was collected, resuspended in TE buffer and treated with 3U

of Proteinase K (ThermoFisher Scientific) overnight at 65^{o}C. Reactions were cooled and the RNA digested with 7.5mU RNase A (MERCK) for 30 min at 37^{o}C shaking intermittently 30 s on/30 s off at 500rpm. The ligated 3C library was purified by a phenol:chloroform extraction and resuspended in H_2O.

Two lots of 6 µg 3C library per condition were sonicated using a Bioruptor (Diagenode) for 75 min, 30 s on/30 s off at 4^{o}C. Sonicated samples were purified using AxyPrep beads (Appleton Woods AxyPrep Mag PCR clean up), eluting with H_2O. The sonicated material underwent end-repair, dA-tailing, adapter ligation and PCR addition of indices using the NEBNext DNA library Prep Reagent Set and NEBNext Multiplex Oligos for Illumina as per manufacturers instructions, purifying with AxyPrep beads after each step.

For the first round of hybridisation, ordered biotinylated probes (Section 2.14) were diluted and pooled to a concentration of 2.9 nM per probe. 2 µg of each indexed library was mixed with 5 µg human COT DNA (ThermoFisher Scientific) per library, 1 nmol TS-HE universal oligo per library and 1 nmol of the corresponding TS-HE Index oligo (Nimblegen SeqCap EZ HE-oligo kit). This DNA was dried in a heated vacuum centrifuge and resuspended in 1x hybridisation buffer and hybridisation component A (Nimblegen SeqCap EZ Hybridisation and wash kit). This DNA-hybridisation mix was denatured by heating to 95^{o}C for 10 min before addition to the pre-heated pooled biotinylated probes. This hybridisation reaction was incubated at 47^{o}C for 72 hrs.

The hybridised samples were washed using the Nimblegen SeqCap EZ Hybridisation and wash kit and then amplified using the Nimblegen SeqCap EZ Accessory kit v2 as per manufacturers instructions. The captured sample was purified with AxyPrep beads. A second round of hybridisation, washes and amplification was carried out as before, shortening the hybridisation reaction to 24 hrs. Libraries were run on the Agilent Bioanalyzer with a DNA-High Sensitivity

chip to assess quality.

2.10.1 Capture-C sequencing and analysis

Paired-end sequencing was performed on a NextSeq 500 with the 150 cycles NextSeq 500/550 High Output v2 kit (Illumina). Reads were mapped using the Capture-C published scripts found at https://github.com/telenius/captureC/releases [Davies et al., 2015, Telenius et al., 2020]. Following mapping, reads were normalised and comparisons between conditions were made using the published scripts found at https://github.com/djdownes/CaptureCompare/ [Telenius et al., 2020].

2.11 Downstream analysis of sequencing data

2.11.1 Differential analysis

Differential analysis between two datasets was performed on unnormalised data using a custom R script employing the DESeq2 package [Love et al., 2014]. In order to identify differential peaks rather than differential gene expression, peak files for each repeat/sample were merged into a single file in which reads were counted using FeatureCounts and differentially accessed [Liao et al., 2014]. A cut-off threshold of FDR<0.05 was used to define statistical significance.

2.11.2 Gene and enhancer annotations

Peaks were annotated with their corresponding genes or enhancers using ensembl hg38 genes and FANTOM permissive hg38 enhancers using BEDtools [Quinlan and Hall, 2010]. A custom R script using the ChIPseeker package [Yu et al., 2015] was used to annotate genomic regions of peaks.

2.11.3 Gene ontology analysis

Gene ontology (GO) analysis was performed using the online **GO**RILLA tool [Eden et al., 2009]. The ranked gene outputs resulting from the DESeq2 analysis (Section 2.11.1) were used as input for the analysis.

2.11.4 Motif screening and enrichment analysis

Motif scanning was performed using FIMO on MEME-suite (http://meme-suite.org/index.html) [Bailey et al., 2009, Grant et al., 2011]. Motif sequences for pSTAT1 and IRF1 were taken from the JASPAR and HOMER databases [Sandelin, 2004, Heinz et al., 2010].

HOMER software [Heinz et al., 2010] was used to screen for enriched motifs identifying both known and *de novo* motifs. For genes, this involved screening sequences in a 2 kb window surrounding the TSS. For peaks, sequences within each peak were analysed.

2.11.5 Correlation analysis

When correlating two datasets, genes/peaks common to both datasets and showing significant differential signals in either dataset at any IFNγ timepoint analysed were chosen. Correlations of these genes/peaks were performed using the ggplot2 package on R [Wickham, 2016].

2.12 CRISPR-Cas9 KO cell lines

Guide RNAs were designed using the benchling online tool (https://www.benchling.com/) to knock out potential enhancer regions as discussed in section 3.2.10. These were cloned into plasmid pSpCas9(BB)-2A-Puro (Addgene), containing the double cutting

form of Cas9. The cloned plasmids were transfected into Hep3B using Lipofectamine 3000 overnight. Cells were split and allowed to grow for 72 hrs before adding 5 µg/ml puromycin for 48 hrs. Puromycin selected cells were serially diluted and grown from single cells. Homozygous KOs were tested by performing a PCR amplification of genomic DNA, followed by visualisation on a 2% agarose gel. Shorter or longer extension times were used (from 30 s to 8 min) where appropriate to amplify DNA of differing length. Amplified fragments of the correct size were excised from the gel, purified with the Zymogen gel extraction kit and sequenced to confirm the correct DNA deletion.

2.13 Using published data

Published macrophage ChIP-seq and ATAC-seq raw data were downloaded as fastq files (GSE43036, GSE98367 and GSE98365). The data was processed as described in section 2.6.1.

2.14 Primers and Probes

Biotinylated probes, length 70 nucleotides, for Capture C were designed with the CapSequm web tool (http://apps.molbiol.ox.ac.uk/CaptureC/cgi-bin/CapSequm.cgi) [Hughes et al., 2014, Telenius et al., 2020] and pooled to a final concentration of 2.9 nM.

RT-qPCR primers were designed against the coding sequence of the gene of interest using the online primer blast tool (https://www.ncbi.nlm.nih.gov/tools/primer-blast/).

For Reverse-Transcription qPCR		
Name	**Forward sequence**	**Reverse sequence**
ACTB mRNA	GACTACCTCATGAAGATCC TCACC	TCTCCTTAATGTCACGCAC GATT
IRF1 mRNA	ACCCTGGCTAGAGATGCAG	TGCTTTGTATCGGCCTGTG
PD-L1 mRNA	ACTACCTCTGGCACATCCT C	ACGGAAGATGAATGTCAGT GC
PD-L2 mRNA	ACAGTGCTATCTGAACCTG TGG	GCAAGTTTCATGGCCAGGT G
PLGRKT mRNA	AGTTCATGCTTATGAATGC TCGAC	ATGGAACAATCGGGACCAG G
Biotinylated Capture Probes		
Name	**Left Probe**	**Right Probe**
CD274 Pr	CATGTTTCACTTTCTGTTT CATTTCTATACACAGCTTTA TTCCTAGGACACCAACACT AGATACCTAAAC	TAGCTCTGATGCTAGGCTG GAGGTCTGGACACGGGTCC AAGTCCACCGCCAGCTGCT TGCTAGTAACTG
IRF1 Pr	CATGCAAGTGATGGCTTCA GGATTCATATGCAGGAAAA GAGACAAAATGCACAGATA CCCTAATTTCAGA	TCCGCAATGGAAGCATTGC TGTCATCTCTGAGTCCCCA GGGCTTGGCCCAGAGAGGT TCTGGGCAGCATG
MYC Pr	CATGCGGCTCTCTTACTCT GTTTACATCCTAGAGCTAG AGTGCTCGGCTGCCCGGCT GAGTCTCCTCCCC	CGGCGGTGGCGGGAGCTTC TCCACGGCCGACCAGCTGG AGATGGTGACCGAGCTGCT GGGAGGAGACATG
STAT1 Pr	CATGAACATTTACTGACCT GCCACCTTGTGCCCCAACA AGGGCCTGGGGATTCAACC AAAGGAGCAGCTA	ACCTCCGTGTTGCTAAACC CAGGGAACGCTTTTCTGTT TTTCTCACTTTACTTGACA GCTCGGAAGCATG

Table 2.1: Primers and probes used

Chapter 3

IFNγ upregulates PD-L1 in a hepatocellular carcinoma cell line

3.1 Introduction

3.1.1 Immunotherapies for treatment of hepatocellular carcinoma

Liver cancer is one of the most common cancers worldwide with the third highest mortality rate, resulting in 781,631 deaths in 2018 [Bray et al., 2018]. Hepatocellular carcinomas (HCC) account for the majority of these cases. Despite improvements to these figures in certain global areas due to vaccines against viral hepatitis B, the difficulties in diagnosis of HCC means that over 80% of patients are diagnosed too late to receive curative treatments [Zongyi and Xiaowu, 2020]. With a severe lack of efficacious treatments for advanced HCC, the number of deaths is not far off the number of HCC cases. Thus, improved therapies for HCCs are urgently required.

The liver is highly exposed to neoantigens and, as a consequence, must strictly modulate the immune system to prevent its over-activation [Jenne and Kubes, 2013].

Without this tight regulation, chronic inflammation and cirrhosis may ensue. HCCs take advantage of these pathways, creating an immunosuppressed environment enabling its growth. Both PD-1 and PD-L1 are commonly detected on a variety of cell types in HCC patients tumour microenvironment and are likely to be involved in cancer immune evasion [Zhou et al., 2017, Chang et al., 2017]. Indeed, antibodies against the PD-1:PD-L1 interaction resulted in increased activation of T lymphocytes [Zhou et al., 2017].

Two anti-PD-1:PD-L1 immunotherapies, Nivolumab and Pembrolizumab, have received accelerated FDA approval as second-line therapies of advanced HCCs following their successful Phase II trials [El-Khoueiry et al., 2017, Zhu et al., 2018a]. However, two follow up trials examining the use of Nivolumab over Sorafenib, the current approved first-line HCC therapy, and Pembrolizumab as a second-line therapy did not reach statistical significance for their criteria, despite demonstrating improved median overall survival and progression-free survival [Yau et al., 2019, Finn et al., 2020]. The overall response rates from these trials were under 20%, and hence, due to their initially promising results, multiple combination trials using these mAbs are underway.

3.1.2 IFNγ induces PD-L1 expression in HCC

An increased understanding of PD-L1 expression in HCC may enable development of combination therapies with higher response rates. HCC is usually associated with an inflammatory environment. IFNγ, a pro-inflammatory cytokine, can induce the expression of PD-L1 from undetectable to highly expressed in multiple HCC cell types [Xie et al., 2016, Li et al., 2017, Zou et al., 2018, Yan et al., 2020]. In addition, significant positive correlations between PD-L1 and IFNγ expression have been identified in patient HCC tumour tissues, thus suggesting PD-L1 expression in HCCs is induced by IFNγ as oppose to being expressed constitutively [Xie et al., 2016].

Silencing of STAT1 or IRF1 largely diminishes IFNγ induction of PD-L1, suggesting that JAK/STAT1/IRF1 is the primary pathway involved in IFNγ upregulated PD-L1 expression (Fig:1.6) [Li et al., 2017, Yan et al., 2020]. Overexpression of IRF1 upregulated PD-L1 expression in both mouse and human cells lines and mutating the two interferon-stimulated response elements (ISREs, the binding motifs of IRF1), diminished the PD-L1 promoter activity suggesting IRF1 was directly involved in regulating PD-L1 [Yan et al., 2020].

Despite having an understanding of the TFs involved in IFNγ mediated upregulation of PD-L1, the mechanisms by which they initiate transcription have not been established. As extensively discussed in section 1.5, TFs, cofactors, epigenetic modifications, ncRNA and regulatory elements function in combination to create a permissive chromatin environment on which the PIC is recruited and transcription initiated in a tightly regulated manner. pSTAT1 and IRF1, as the key modulators of IFNγ mediated expression, likely dictate this amalgamation of epigenetic and transcriptional signals upon association with the IRF1 and PD-L1 promoters respectively.

3.1.3 Aims

This chapter uses ChIP-seq, ATAC-seq, transcriptional techniques and Capture-C to examine the transcriptional and epigenetic changes associated with the IRF1 and PD-L1 promoters in a HCC cell line, Hep3B. Both promoters show large increases in active epigenetic marks corresponding to transcriptional upregulation. A region $\sim$5kb upstream of the IRF1 TSS becomes heavily acetylated, initiates bidirectional ncRNA transcription and increases DNA accessibility, indicative of an enhancer element. This putative enhancer element is further confirmed by a gene loop between the promoter and enhancer region. The promoter shows over 2 fold increased association with the enhancer after just 30 min of IFNγ treatment.

Unlike IRF1, no obvious putative enhancer element can be visualised for PD-L1. Instead, PD-L1 is found to loop to the nearest promoter, PLGRKT. Small interactions can also be seen to a downstream site bound by CTCF. No differential higher-order chromatin structure is observed throughout IFNγ treatments, and deleting these regions do not appear to affect IFNγ-induced PD-L1 expression. Although three possible unorthodox regulatory mechanisms controlling PD-L1 expression are proposed, evidence indicates that the PD-L1 proximal promoter may be sufficient for IFNγ-dependent upregulation of PD-L1.

3.2 Results

3.2.1 IFNγ induces PD-L1 expression in Hep3B cells

3.2.1.1 The pSTAT1-IRF1 signalling cascade is rapidly activated in Hep3B cells

High levels of PD-L1 expression have previously been observed in the HCC cell line, Hep3B, upon treatments with IFNγ [Li et al., 2017, Zou et al., 2018]. Thus analysing the mechanisms by which IFNγ induces PD-L1 expression in Hep3B cells may help to elucidate modes of PD-L1 regulation occurring in cancer patients. To first confirm the sensitivity of Hep3B cells to IFNγ, cells were treated with increasing lengths or concentrations of the cytokine. Western blots of these treatments were performed analysing STAT1 and IRF1 expression, the major TFs thought to be involved in IFNγ mediated upregulation of PD-L1 (Fig:3.1A & B) [Garcia-Diaz et al., 2017, Li et al., 2017, Yan et al., 2020]. In accordance with other published IFNγ signalling kinetics, pSTAT1 becomes upregulated at the earliest timepoint taken upon IFNγ treatment and IRF1 protein upregulation occurs after approximately 2 hrs (Fig:3.1A), thus confirming activation of the canonical downstream IFNγ signalling pathway in Hep3B cells. Unphosphorylated STAT1 was expressed even in untreated Hep3B cells, thus enabling a rapid response to IFNγ. Expression of STAT1 increased after longer exposures to IFNγ despite levels of pSTAT1 falling slightly at this latest timepoint. Increasing concentrations of IFNγ did not result in a significant increase in pSTAT1 or IRF1 expression (Fig:3.1B).

pSTAT3 has additionally been linked to PD-L1 expression and thus levels of STAT3 in both its phosphorylated or unphosphorylated form were additionally assessed (Fig:3.1A) [Bu et al., 2017, Jiang et al., 2013]. Both were present in untreated cells and levels remained fairly stable throughout the treatment timecourse,

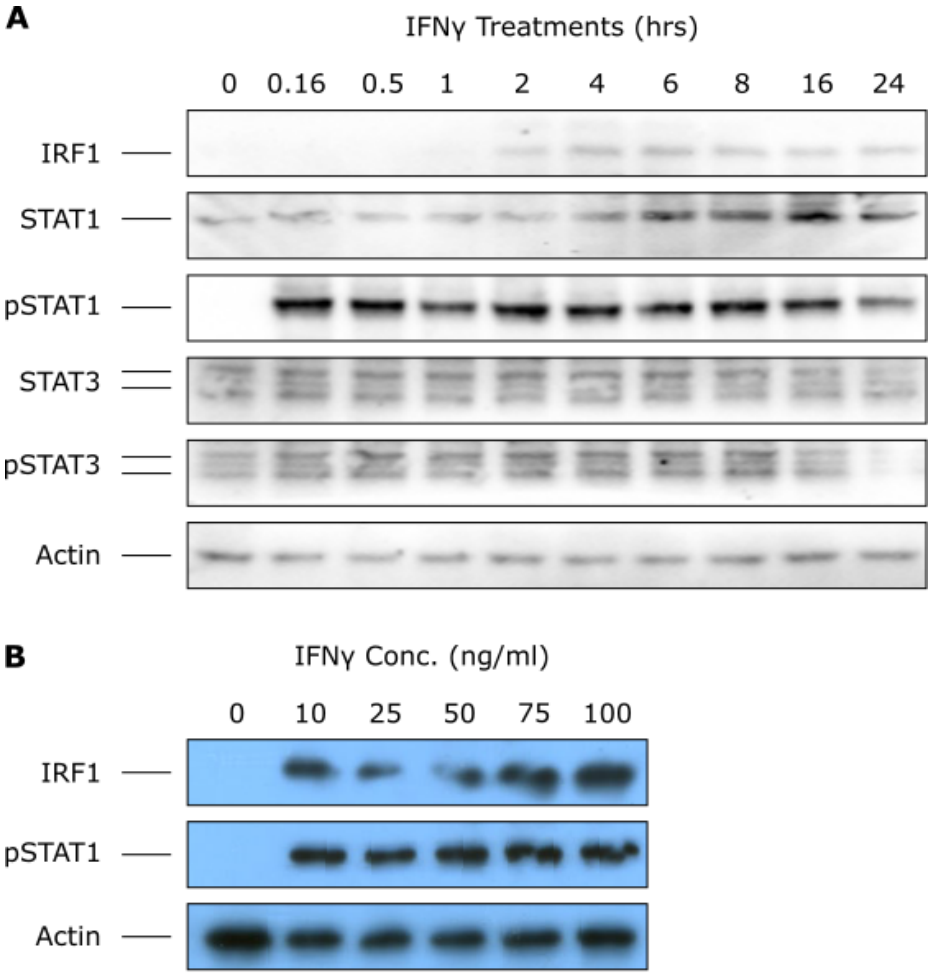

Figure 3.1: IFNγ upregulates pSTAT1 and IRF1 in Hep3B cells.
A & B Representative western blots showing expression of IRF1, STAT1, pSTAT1, STAT3 and pSTAT3 with increasing times (**A**) or concentrations (**B**) of IFNγ treatments (n=3). All timecourse experiments are treated with 50 ng/ml IFNγ and dosage experiments are treated for 6 hrs.

with pSTAT3 quantities falling by 24 hrs of IFNγ treatment. The presence of pSTAT3 in untreated cells makes it unlikely to independently drive IFNγ-induced modulation of genes. This is in agreement with published results suggesting STAT1/IRF1 over STAT3 are the drivers of IFNγ-mediated upregulation of PD-L1 [Garcia-Diaz et al., 2017].

3.2.1.2 PD-L1 mRNA is significantly upregulated after 2 hrs of IFNγ treatment

As changes in chromatin architecture are likely to correlate more strongly with changes in transcriptional expression over protein expression, IRF1 and PD-L1 mRNA expression were analysed by reverse-transcription quantitative PCR (RT-qPCR) with increasing IFNγ concentrations and treatment lengths (Fig:3.2A-C). Both genes showed extremely low to no expression in untreated Hep3B cells. Upon addition of IFNγ, both IRF1 and PD-L1 mRNA were massively upregulated. As with pSTAT1 and IRF1 protein expression, IFNγ dosage did not appear to affect mRNA expression (Fig:3.2B). IRF1 mRNA upregulation occurs significantly within just 30 min of IFNγ treatment, demonstrating a highly rapid cellular response, reminiscent of an early response gene (Fig:3.2C). PD-L1 mRNA upregulation can be seen at 2 hrs of treatment, the time at which IRF1 protein is first detected by the western blot analysis and, therefore, likely represents a late response gene (Fig:3.1A & 3.2A). The induction of both genes is maintained throughout the 24 hr timecourse. Given that levels of pSTAT3 do not increase upon IFNγ treatment whilst PD-L1 transcription becomes induced suggests that pSTAT3 isn't the principle TF involved in IFNγ-inducible PD-L1 expression (Fig:3.1A & 3.2A). Flow cytometry was used to verify that PD-L1 mRNA expression resulted in upregulation of PD-L1 protein at the plasma membrane, its site of function (Fig:3.2D). Indeed, IFNγ treatments increased PD-L1 protein expression on the cell surface.

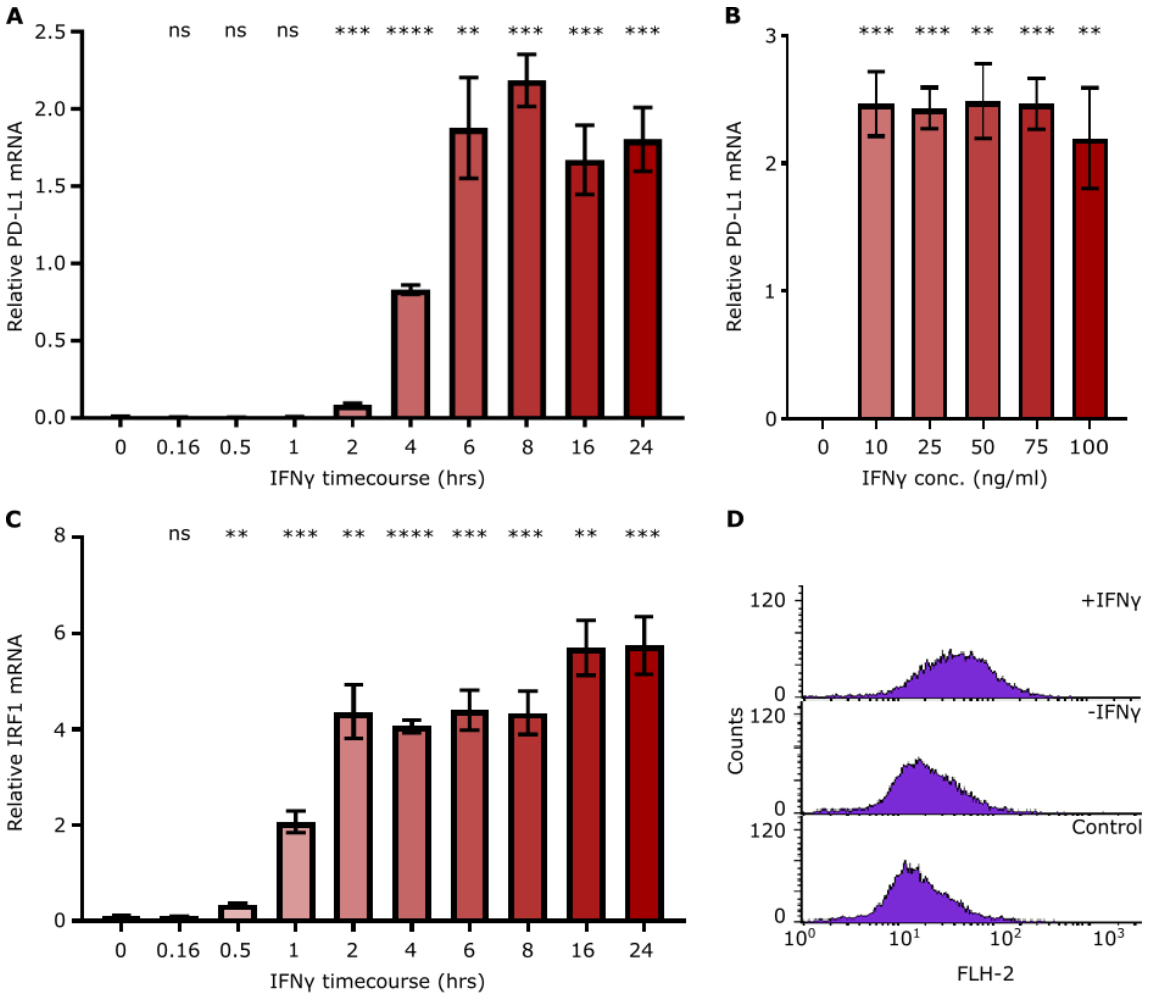

Figure 3.2: IFNγ upregulates PD-L1 and IRF1 mRNA in Hep3B cells. **A-C** RT-qPCRs showing upregulation of PD-L1 (**A** & **B**) or IRF1 (**C**) with increasing times (**A** & **C**) or concentrations (**B**) of IFNγ treatments, normalised to β-actin mRNA (n=3). Relative expression is measured using the $2^{-\Delta\Delta Ct}$ method. All timecourse experiments are treated with 50 ng/ml IFNγ and dosage experiments are treated for 6 hrs. Significance was calculated against the untreated sample: ns P>0.05, * P$\leq$0.05, ** P$\leq$0.01, ***P$\leq$0.001, ****P$\leq$0.0001. **D** Representative flow cytometry analysis of PD-L1 protein expression (n=3). The bottom control lane uses a non-specific antibody. The upper two lanes analyse PD-L1 expression at the plasma membrane with (top lane) or without (middle lane) 6 hrs of IFNγ treatment.

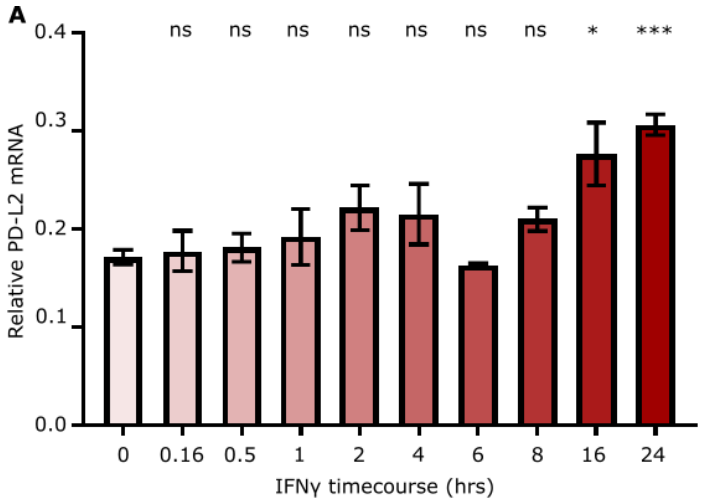

Figure 3.3: IFNγ does not induce PD-L2 expression in Hep3B cells.
A RT-qPCR showing minimal PD-L2 expression in Hep3B cells normalised to β-actin mRNA (n=3). Relative expression is measured using the $2^{-\Delta\Delta Ct}$ method. Significance was calculated against the untreated sample: ns P>0.05, * P≤0.05, ** P≤0.01, ***P≤0.001, ****P≤0.0001

As PD-L2 is also known to bind to the PD-1 receptor, inhibiting immune responses, PD-L2 expression was also examined by RT-qPCR. To this end, PD-L2 mRNA expression remained minimal regardless of IFNγ treatment, although a slight but significant increase in expression was observed after lengthy IFNγ treatments (Fig:3.3A). This could be due to increases in transcription or stabilisation of the transcript. However, RNA-seq and SNU-seq data, shown later in Figure 3.19, reveal a lack of both transcripts and transcription of PD-L2 after 24 hrs of IFNγ treatment. Therefore this significant increase seen here is likely due to the high variability of the RT-qPCR technique when trying to quantify negligible RNA levels.

3.2.2 IRF1 is not sufficient to stimulate PD-L1 expression

To examine whether PD-L1 expression was common to any IRF1 expressing cell line, a variety of cell lines were treated with IFNγ. Hek293, HeLa and GM12878, a non-cancerous, cancerous and lymphocyte cell line respectively, all showed upregulation

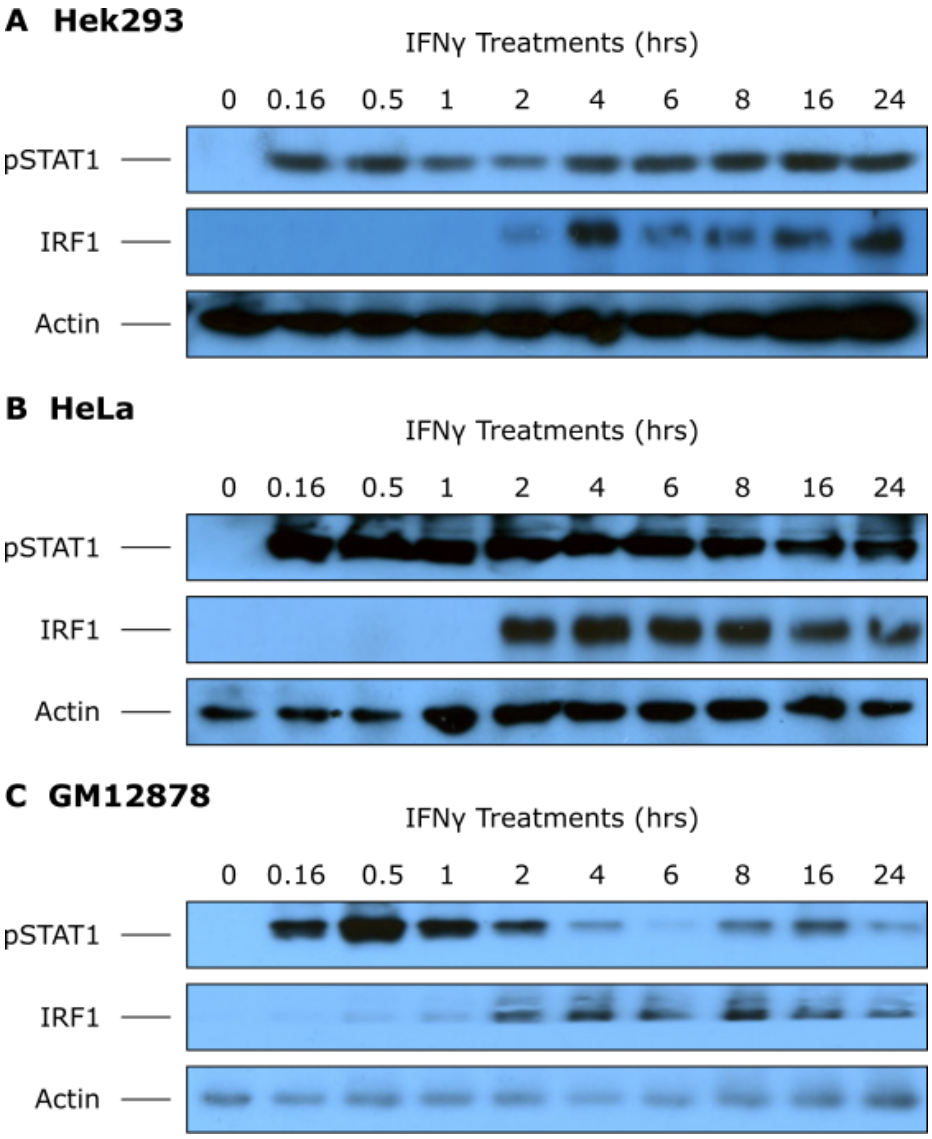

Figure 3.4: IFNγ upregulates the pSTAT1/IRF1 pathway in all cell types analysed.
A-C Representative western blots showing upregulation of IRF1 and pSTAT1 with increasing lengths of IFNγ treatments in Hek293 (**A**), HeLa (**B**) and GM12878 (**C**) cells (n=3).

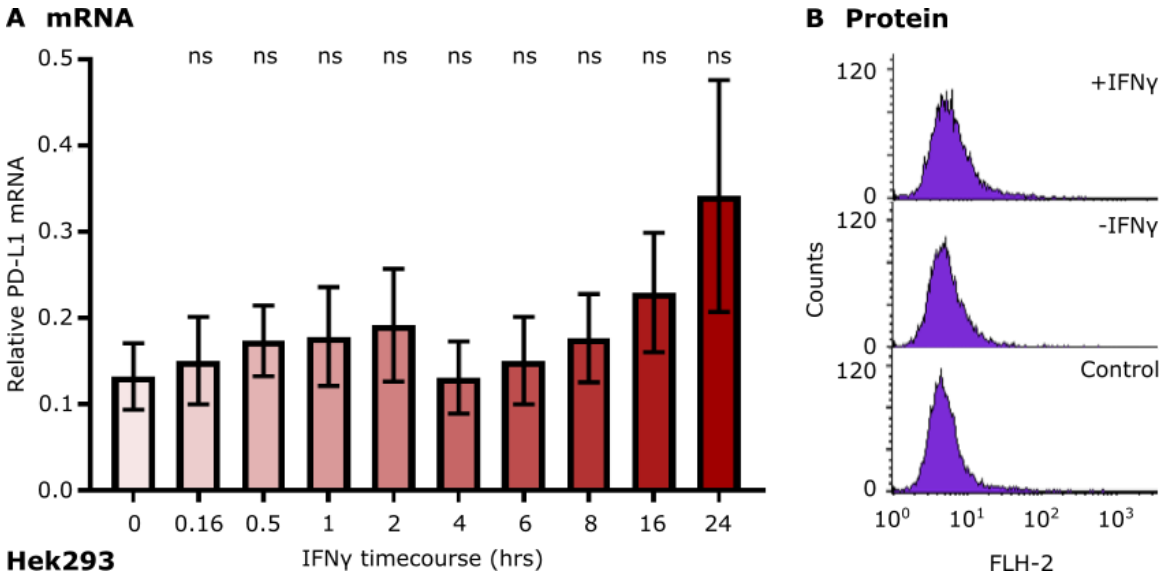

Figure 3.5: IFNγ does not upregulate PD-L1 in Hek293.
A RT-qPCR analysing PD-L1 expression upon IFNγ treatments in Hek293 cells. RT-qPCRs are normalised to β-actin mRNA (n=3). Relative expression is measured using the $2^{-\Delta\Delta Ct}$ method. Significance was calculated against the untreated sample: ns P>0.05, * P≤0.05, ** P≤0.01, ***P≤0.001. **B** Flow cytometry analysing PD-L1 expression upon IFNγ treatments in Hek293 cells. The bottom control lane uses a non-specific antibody. The upper two lanes analyse PD-L1 expression at the plasma membrane with (top lane) or without (middle lane) 6 hrs of IFNγ treatment. The graphs shown are representative plots (n=3).

of IRF1 protein by 2 hr IFNγ treatments, comparably to Hep3B cells (Fig:3.4).

Despite this upregulation of IRF1, extremely low or no expression of PD-L1 at either the protein or mRNA level could be detected in Hek293 cells under these conditions (Fig:3.5). The presence of IRF1 alone, therefore, cannot be sufficient for PD-L1 expression. Hence, additional forms of regulation must exist in Hep3B cells to enable the production of the transcript.

HeLa cells show a significant increase in PD-L1 transcript by 4 hrs of treatment that is maintained throughout the timecourse, albeit to a lesser extent than Hep3B cells (Fig:3.6A). Interestingly, this increase in transcript levels did not lead to detectable PD-L1 protein at the plasma membrane (Fig:3.6B). This indicates that HeLa cells possess an inhibitory process between transcribing the gene and displaying

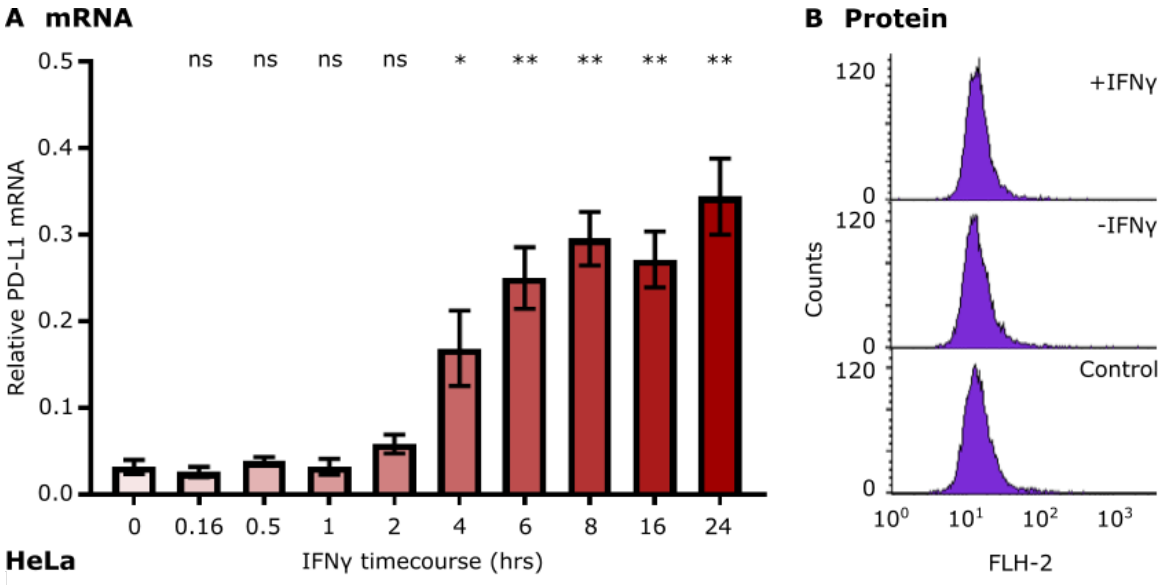

Figure 3.6: IFNγ upregulates PD-L1 mRNA but not protein in HeLa.
A RT-qPCR analysing PD-L1 expression upon IFNγ treatments in HeLa cells. RT-qPCRs are normalised to β-actin mRNA (n=3). Relative expression is measured using the $2^{-\Delta\Delta Ct}$ method. Significance was calculated against the untreated sample: ns P>0.05, * P≤0.05, ** P≤0.01, ***P≤0.001. **B** Flow cytometry analysing PD-L1 expression upon IFNγ treatments in HeLa cells. The bottom control lane uses a non-specific antibody. The upper two lanes analyse PD-L1 expression at the plasma membrane with (top lane) or without (middle lane) 6 hrs of IFNγ treatment. The graphs shown are representative plots (n=3).

the functional protein at the plasma membrane. This downregulation could manifest in various regulatory mechanisms including destabilising the RNA or incorrect RNA or protein processing.

Not all cancer cells, therefore, can upregulate PD-L1 protein at the plasma membrane under the conditions tested here. More research should be performed to understand how certain cancers cells behave differently in the presence of IFNγ signalling. The results from HeLa and Hek293 affirm that tight regulations are usually in place to prevent the expression of the potentially detrimental PD-L1 protein.

Finally, the B lymphocyte GM12878 cell line constitutively expresses PD-L1, as can be seen in the flow cytometry analysis (Fig:3.7B). IFNγ marginally upregulates PD-L1 mRNA with borderline significance, although no increased protein expression

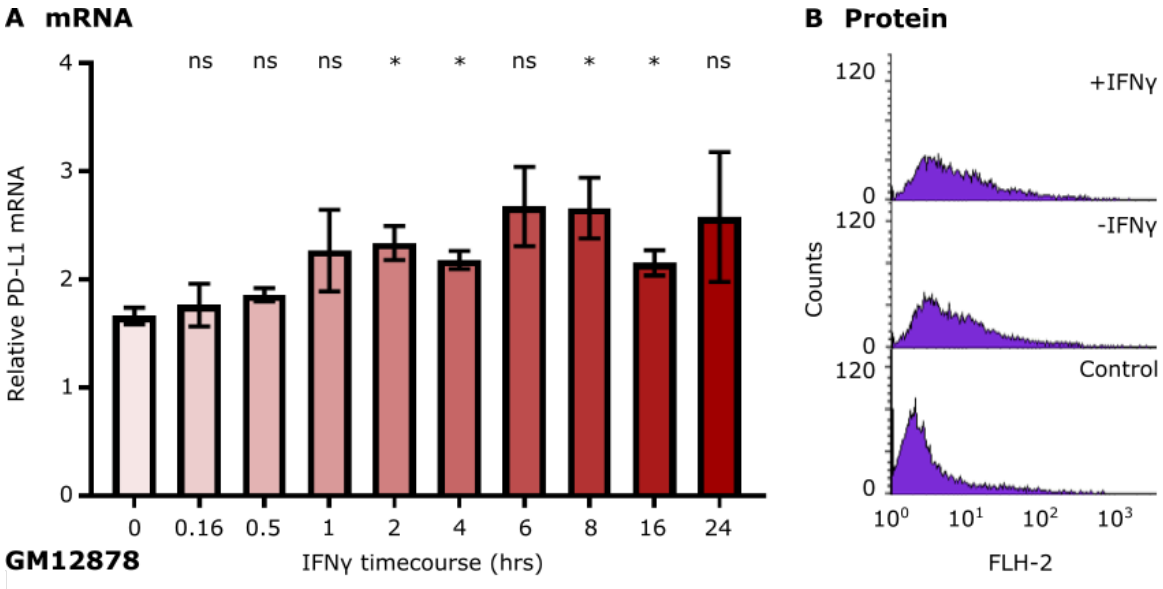

Figure 3.7: IFNγ marginally upregulates PD-L1 over constitutive levels in GM12878.
A RT-qPCR analysing PD-L1 expression upon IFNγ treatments in GM12878 cells. RT-qPCRs are normalised to β-actin mRNA (n=3). Relative expression is measured using the $2^{-\Delta\Delta Ct}$ method. Significance was calculated against the untreated sample: ns P>0.05, * P≤0.05, ** P≤0.01, ***P≤0.001. **B** Flow cytometry analysing PD-L1 expression upon IFNγ treatments in GM12878 cells. The bottom control lane uses a non-specific antibody. The upper two lanes analyse PD-L1 expression at the plasma membrane with (top lane) or without (middle lane) 6 hrs of IFNγ treatment. The graphs shown are representative plots (n=3).

was detected (Fig:3.7). It is possible that an induced increase in expression is masked by the already high expression levels.

Together, the distinct responses demonstrated by each cell line emphasises the complexity of PD-L1 regulation. Each cell line tested induces IRF1 and pSTAT1 protein expression within 2 hrs of IFNγ signalling. Despite the presence of these TFs, PD-L1 isn't expressed in all cell lines and, therefore, IRF1 and pSTAT1 alone cannot be sufficient for induced expression of PD-L1. Understanding how these differences arise could help explain the inconsistent responses observed in patients to PD-1/PD-L1 immunotherapies.

3.2.3 IFNγ induces an immense and rapid change in chromatin architecture at the IRF1 locus

3.2.3.1 Highly accessible DNA at the IRF1 locus

Like most stress responses, cells must respond quickly to IFNγ. As a major cytokine in both innate and adaptive immunity, a swift reaction to the presence of IFNγ is vital to fight pathogens, induce inflammation and protect the host from damage. The highly conserved nature of this signalling molecule, traced back over 450 million years, demonstrates its functional importance [Savan et al., 2009]. Cells express inactive forms of the type II interferon signalling modulators, JAK1/2 and STAT1, so that, upon association with the IFNGR, the kinase activities of JAK1/2 rapidly phosphorylate and consequently activate STAT1 within 10 min (Fig:3.1A). This leads to transcriptional upregulation of IRF1 within just 30 min. Due to the phenomenal speed at which IRF1 is induced, we hypothesised that the IRF1 promoter has accessible pSTAT1 binding sites, priming it for activation. It additionally seemed likely that any promoter:enhancer loops necessary for transcription would be preformed to ensure minimal changes were required to swiftly initiate IRF1 expression.

To test these hypotheses, DNA accessibility was assessed using ATAC-seq (protocol outlined in Fig:3.8A). Further to analysing untreated Hep3B cells, ATAC-seq was performed on cells treated with 0.5 and 2 hrs of IFNγ, the lengths of treatment required for significant IRF1 and PD-L1 mRNA upregulation respectively (Fig:3.2A & C). 24 hrs of treatment was additionally tested to identify any long term changes to the chromatin environment. In the untreated sample, a sharp peak of open chromatin can be seen at the IRF1 promoter, accompanied by a broad region of accessible DNA approximately 5kb upstream of the TSS (Fig:3.8B). As predicted, both of these accessible regions contain GAS elements (putative pSTAT1 binding

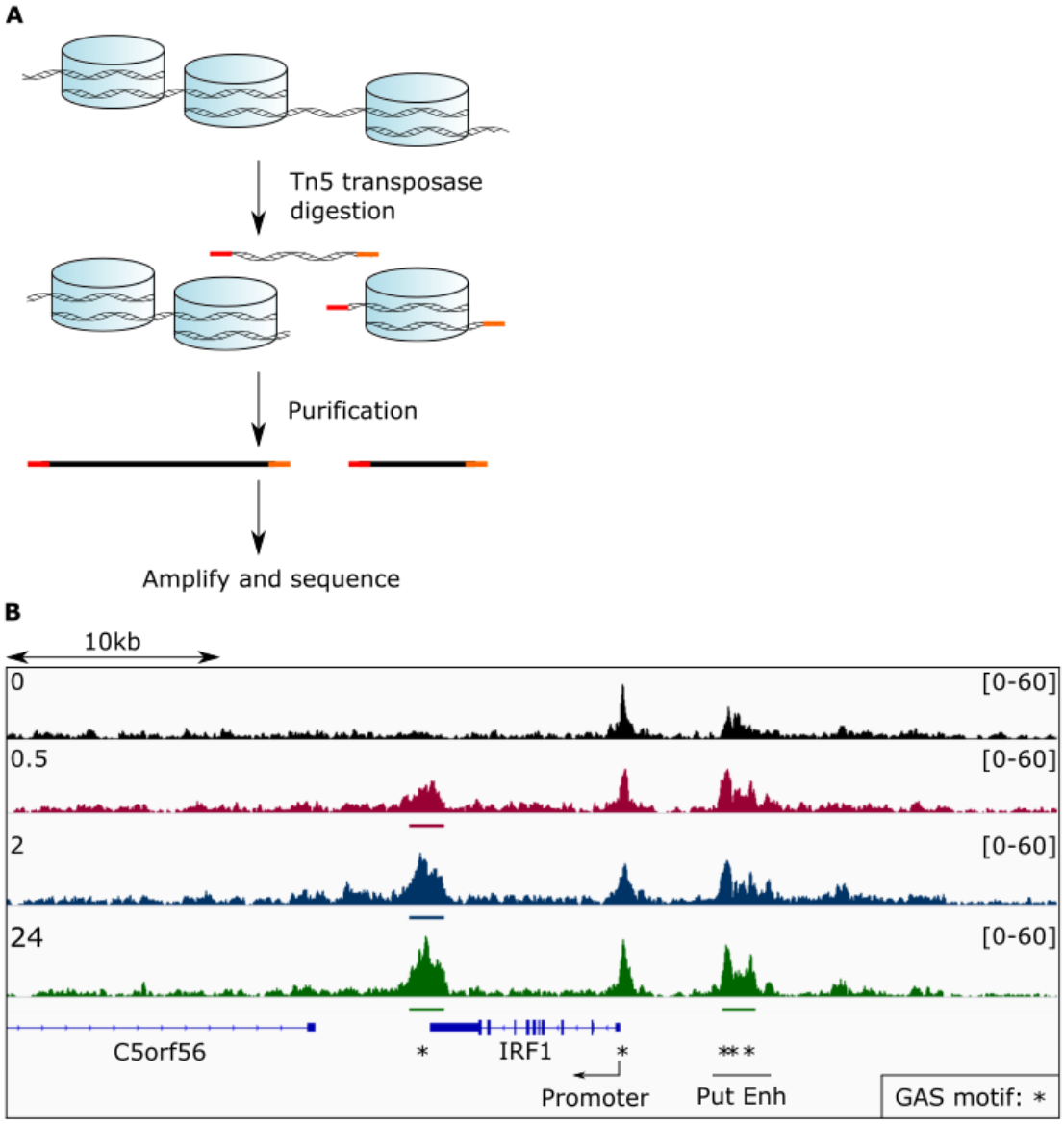

Figure 3.8: DNA accessibility at the IRF1 locus increases upon IFNγ treatment.
A The ATAC-seq protocol: Chromatin is purified and digested with Tn5 transposase. This transposase digests open chromatin and adds specific adapter sequences to the DNA. This DNA is then purified, amplified and sequenced. **B** 50kb stretch around the IRF1 locus showing DNA accessibility in untreated or treated Hep3B cells. IRF1 is expressed on the reverse strand. The three ATAC-seq repeats were merged and normalised based on sequencing depth. The track in black displays open DNA in untreated cells. In pink, navy and green are cells treated with 0.5, 2 or 24 hrs IFNγ respectively. Bars below tracks show significant ($q<0.05$) differential peaks compared to the untreated samples, calculated by DESeq2. * represents GAS elements (putative STAT1 binding motifs). The promoter and putative enhancer (Put Enh) are annotated.

motifs) thus priming the gene for rapid activation by pSTAT1. Enhancer elements are characterised by regions of nucleosome depletion and these usually correspond to the loop anchors between promoter:enhancer contacts (Fig:1.10, section 1.5.3). Given the proximity of this accessible region to the IRF1 promoter, it seems likely that this represents the enhancer element for IRF1. Assuredly, this region lies within a GeneHancer predicted enhancer element for IRF1 (GeneHancer identifier: GH05J132484) [Fishilevich et al., 2017]. This predicted element was granted an elite enhancer status given its identification in both the FANTOM and ENCODE enhancer datasets, with a good correlation between mRNA and eRNA expression. As far as I'm aware, no physical gene looping between this region and the IRF1 promoter has been identified. These two nucleosome depleted regions persist throughout the treatments.

By 24 hrs of IFNγ signalling, the putative enhancer site upstream of the promoter shows a significant increase in signal (Fig:3.8B). These differences appear to be at the extremities of the peak and seem to begin increasing from 0.5 hrs, despite significance only being reached at the end of the timecourse. The enhancer also aligns with putative GAS motifs indicating that pSTAT1 could be the cause of this increased accessibility.

Additionally, at 0.5 hrs a *de novo* peak of open chromatin appears at the 3'-end of the gene (Fig:3.8B). This significant increase in ATAC-seq signal could represent a second regulatory element, or could simply be due to the high levels of terminating Pol II. As accessible chromatin is a common feature of loop anchors, this could represent a *de novo* gene loop forming between IRF1's promoter and terminator. Juxtaposition between promoters and terminators have been observed, primarily in yeast [O'Sullivan et al., 2004, Ansari and Hampsey, 2005], a phenomenon which may potentially be involved in recycling Pol II back to the promoter after transcribing the gene. A putative pSTAT1 binding motif present within this region suggests this accessibility could be driven by pSTAT1. By 2 hrs the signal increased further to a

level that is maintained until at least 24 hrs.

3.2.3.2 Transcriptional changes at the IRF1 locus

Enhancer elements often transcribe eRNA bidirectionally (Fig:1.10), levels of which correlate strongly with mRNA expression of the genes they regulate [Kim et al., 2010]. Therefore, we sought to quantify levels of eRNA, if present, at this locus. The transient nature of eRNAs makes their detection challenging and so multiple sequencing techniques analysing nascent RNA have been developed. Techniques such as 4sU-seq and TT-seq incorporate a nucleoside analogue into actively transcribing RNA. These actively transcribed transcripts can be captured and sequenced thus facilitating highly sensitive detection of eRNA [Cleary et al., 2005, Schwalb et al., 2016, Michel et al., 2017]. However, these techniques lack high resolution and long pre-existing 5'-regions of RNA add bias into the data. Our lab have evolved these techniques to remove this 5'-bias and obtained nascent transcript data at single-nucleotide resolution. This new method, **S**ingle-**N**ucleotide resolution 4s**U**-sequencing (SNU-seq), similarly to 4sU-seq and TT-seq, involves a short pulse labelling with 4sU followed by biotinylation and streptavidin pull-down to purify the nascent RNA. A poly(A)-tail is synthetically added to the 3'-end enabling identification of the last transcribed nucleotide within the pulse labelling window and hence providing near single-nucleotide resolution (Fig:3.9).

SNU-seq was used to measure transcription in untreated and IFNγ treated Hep3B cells. In untreated cells, transcription of the gene is minimal but is detected on both DNA strands within the gene body and upstream of the gene (Fig:3.10). By just 30 min of treatment, a huge increase in transcription of the IRF1 gene can be seen on the negative DNA strand. This increase is significant and is the most significant change in transcription genome-wide at 30 min (q value = $4.26\text{x}10^{-26}$). Transcription is spread over the entire gene and can be seen in both exons and introns, as is

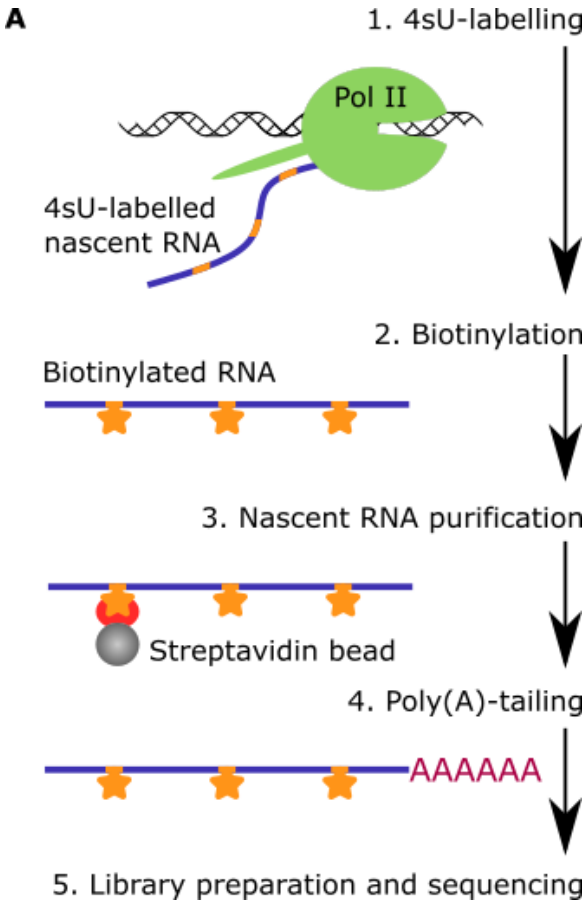

Figure 3.9: Diagram of the SNU-seq protocol.
A SNU-seq protocol: Cells are pulse labelled with 4-thiouridine for 12 min. 4sU-labelled nascent RNA is biotinylated and purified on streptavidin beads. A poly(A)-tail is added to the 3'-end of the purified RNA. After library preparation and sequencing the poly(A)-tail is removed *in silico* and the position of the aligned 3'-nucleotide is used to provide single-nucleotide resolution.

characteristic of SNU-seq output. Although displaying near full gene coverage, peaks of transcription can still be seen along the gene body and at the terminating region of the transcript. These peaks likely signify pauses along the transcript, whereby increasing time spent by Pol II at a specific position increases the likelihood of identifying that nucleotide as the last transcribed nucleotide in the sequencing library (Fig:3.10).

IRF1 continues to be highly expressed at least until 24 hrs of treatment. When analysing SNU-seq changes genome-wide in section 4.2.1.2, IRF1 remains one of the

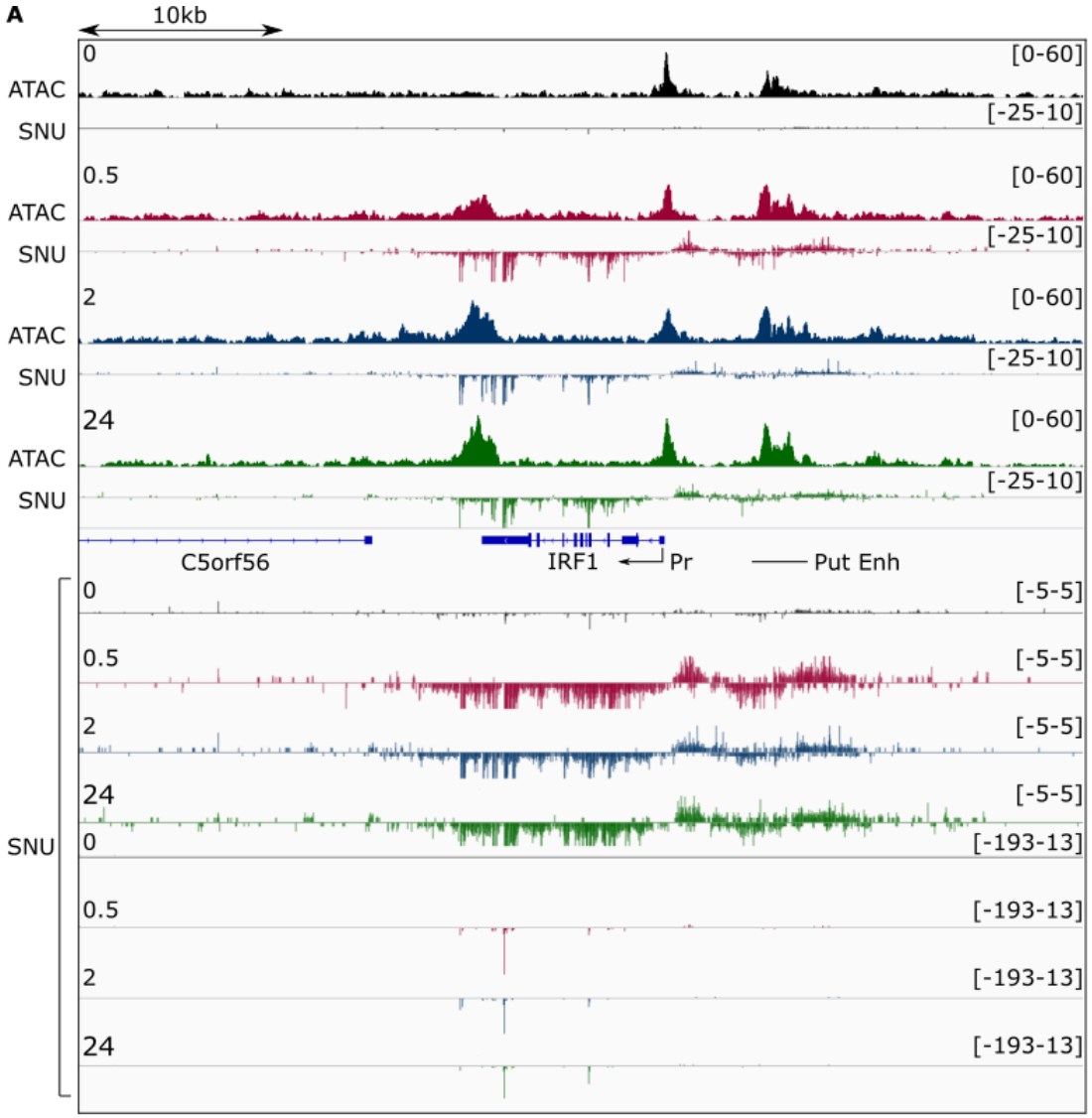

Figure 3.10: SNU-seq identifies induced bidirectional transcription at IRF1.

A A 50kb stretch around the IRF1 locus showing DNA accessibility alongside strand specific transcription in untreated or treated Hep3B cells (n=3). SNU-seq tracks are spike-in normalised. Untreated, 0.5, 2 and 24 hrs treated tracks are shown in black, pink, navy and green respectively. The promoter (Pr) and putative enhancer (Put Enh) are annotated. The SNU-seq tracks on the top half of the figure have a data range from -25 to +10. The same data is shown on the bottom half of the figure with a data range of -5 to +5, and -193 to +13. This is to enable visualisation of the complete transcriptional coverage of the gene and enhancer, as well as visualising the predominant poly(A) and alternative poly(A) sites.

most significantly upregulated genes for each IFNγ treated sample when compared to untreated cells.

In addition to sense transcription, anti-sense ncRNA transcription stemming from the IRF1 promoter can also be observed. Furthermore, bidirectional transcription is induced at the region ∼5kb upstream of the promoter and appears to derive from within the ATAC-seq signal. All of this ncRNA appears to correlate with the pre-mRNA transcription: It is heavily upregulated by 30 min IFNγ treatment and is maintained throughout the timecourse. This further cements evidence suggesting this upstream region is indeed an enhancer of IRF1 involved in its IFNγ induced expression.

No bidirectional transcription is detected within the accessible region at the 3'-end of the gene. Although this region may still represent a regulatory element of IRF1, it seems more likely that this open chromatin is a result of the extremely high transcription termination occurring. Transcription continues downstream of the gene. This transcriptional read-through may engage Pol II resulting in the nucleosome depletion witnessed in IFNγ treated Hep3B cells.

3.2.3.3 Active histone marks are written within 30 min of IFNγ treatment at IRF1

Different regulatory elements are commonly associated with particular modifications: An actively transcribing promoter tends to be modified with both H3K4me3 and H3K27ac. H3K4 at enhancer elements are more often mono-methylated rather than tri-methylated and enhancer activation strongly correlates with H3K27ac (Fig:1.10) [Catarino and Stark, 2018]. Insulator elements are usually bound by CTCF [Phillips-Cremins and Corces, 2013]. To test for each of these elements, ChIPmentation was used to analyse the distribution of H3K4me3, H3K27ac and CTCF. ChIPmentation is an adaptation of the standard ChIP-seq protocol,

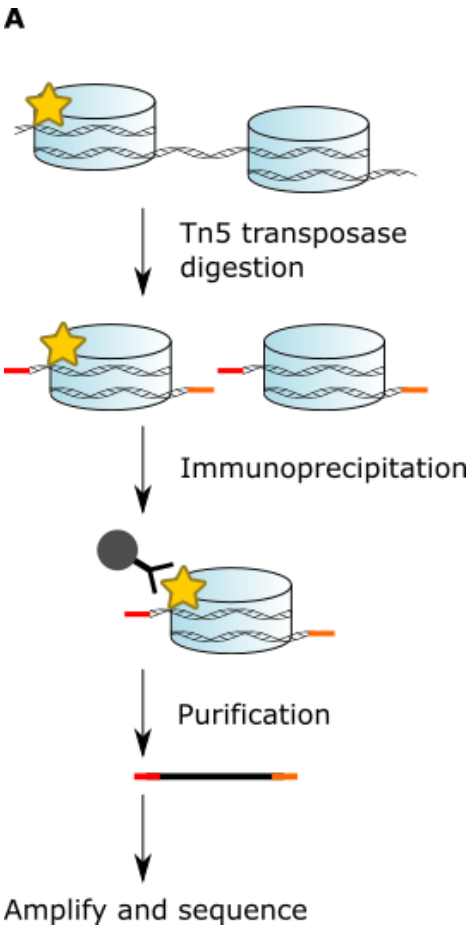

Figure 3.11: Diagram of the ChIPmentation protocol.
A The ChIPmentation protocol: Chromatin is purified and digested with Tn5 transposase. This transposase digests open chromatin and adds specific adapter sequences to the DNA. Modified chromatin is captured using an antibody against the histone modification/TF of interest. This captured material is then purified, amplified and sequenced.

combining it with the ATAC-seq protocol to simplify and increase the efficiency of the library preparation, shortening the protocol and allowing fewer cells and materials to be used (Fig:3.11) [Schmidl et al., 2015].

3.2.3.3.1 The IRF1 promoter

Data from this technique show that the IRF1 locus becomes flooded with histone modifications associated with active genes at just 0.5 hrs of IFNγ treatment (Fig:3.12). Downstream of the promoter, a significant increase in H3K27ac can immediately be

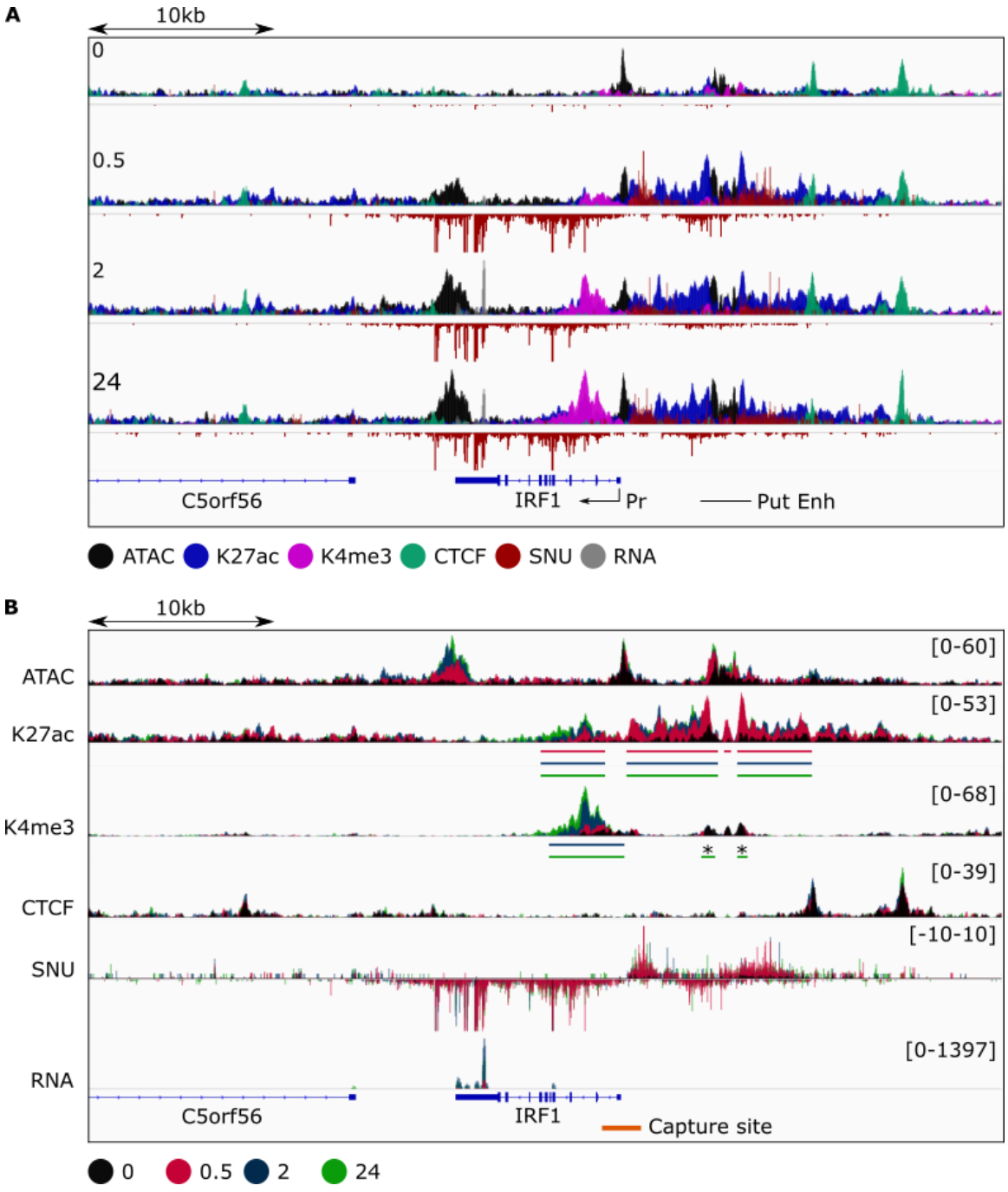

Figure 3.12: The chromatin environment at the IRF1 locus.
See [1] on next page

seen from 0.5 hrs of treatment. The peak of this modification is broad, spreading over approximately half of the gene body. The acetylation signal continues to increase marginally over the treatment timecourse. This acetylation downstream of the promoter is accompanied by an increase in H3K4me3. Although a slight increase in tri-methylation can be observed by 30 min of IFNγ treatment, the majority of the H3K4me3 deposition occurs between the 0.5 and 2 hr timepoints, with the increase in signal becoming significant at 2 hrs. As the IFNγ treatment lengthens, the H3K4me3 ChIP signal becomes more intense and spreads further into the gene body.

3.2.3.3.2 The putative enhancer element

Additionally, by 30 min H3K27ac has increased broadly from the -1 nucleosome to approximately 10kb upstream of the gene, covering the putative enhancer site and the sites of ncRNA transcription (Fig:3.12). The signal dips at the site of high DNA accessibility, perhaps due to the lower occupancy of histones at this region. The bulk of the signal is already present in the 0.5 hr sample and minimal increases can be seen in longer treatments. The acetylation signal of this upstream region reaches double the intensity of that within the gene body. Small peaks of both H3K27ac and H3K4me3 can be seen in untreated cells directly adjacent to the upstream

[1]**Fig3.12: The chromatin environment at the IRF1 locus.**
A A 50kb stretch of the IRF1 locus showing DNA accessibility (black), ChIP profiles of H3K27ac (blue), H3K4me3 (purple) and CTCF (turquoise), strand-specific SNU-seq data (red) and 3'-RNA-seq (grey) data for each treatment sample (n=2-3). All tracks are spike-in normalised except ATAC-seq and CTCF which are normalised based on sequencing depth. The promoter (Pr) and putative enhancer (Put Enh) are annotated. **B** Shows exactly the same data as in A, except now each track shows a specific data set for each timecourse sample, with the untreated sample in black, and 0.5, 2 and 24 hrs of IFNγ treatment in pink, navy and green respectively. Significant changes ($q<0.05$) for H3K4me3, H3K27ac and CTCF are represented by bars below the corresponding track. The colour of the bar denotes which timepoint shows a significant difference compared to the untreated sample, with pink, navy and green representing 0.5, 2 and 24 hrs respectively. * denotes a significant decrease in the modification compared to the untreated sample, otherwise bars can be assumed to represent increases in signal.

nucleosome depleted regions. Unlike acetylation, tri-methylation does not increase in this region and instead shows a significant decrease by 24 hrs. Whether this is due to demethylation of these histones converting the tri-methylation into a mono-methylation mark, to the lower occupancy of histones at this region or due to higher histone turnover cannot be determined from this data.

Together, the highly transcribed, nucleosome depleted region accompanied by heavy H3K27ac generally marks an active enhancer element (Fig:3.12). As both the upregulation of transcription and acetylation signal correspond to the upregulation of IRF1 transcription, it is highly likely that this enhancer is directly involved in the regulation of IRF1.

3.2.3.3.3 Other regions within this locus

Binding of the TF, CTCF, remains constant throughout the timecourse at this locus, with no significant changes detected. The first CTCF peak upstream of the IRF1 promoter (∼10kb upstream) coincides with the 3'-end of the significant H3K27ac increase (Fig:3.12). Furthermore, virtually no H3K27ac and ncRNA transcription can be seen beyond the second upstream CTCF peak (∼15kb upstream of IRF1). Therefore it is possible that these two CTCF sites insulate genes upstream of IRF1 from being aberrantly upregulated.

In contrast to the upstream accessible site, there is very little H3K27ac at the downstream accessible site in all samples, again supporting that this region is not an enhancer element of IRF1.

3.2.4 Expression of IRF1 corresponds with increased looping to its enhancer element

Enhancers activate transcription by interacting with a promoter, providing it with a plethora of activating signals from TFs and coactivators. Enhancers are often

found in nearby genomic sequence to the promoter, but have also been identified several hundreds of kb away, or even in *trans* [Bateman et al., 2012]. They are dynamic in nature, with the enhancer landscape of a cell changing significantly during development and differentiation [Rubin et al., 2017]. The human genome is packed full of enhancers, with estimated numbers far exceeding the number of genes. These enhancers can exist in three major states; inactive, primed for activation or active. The enhancer states vary massively in different cell types. Primed enhancers may already be in proximity to promoters within 3D space or enhancer activation may promote loop formation to a promoter. Certainly, differentiation of a cell massively alters its higher-order chromatin structure and can change interactions between enhancers and promoters [Simon et al., 2017]. Whether loop formation/dissolution can be induced by external stresses on a fully differentiated cell isn't well understood.

Given the upregulation of IRF1 within 30 min of IFNγ, it seemed probable that an enhancer element was constitutively juxtaposed to the IRF1 promoter. This would, in turn, reduce the amount of change to the chromatin required, thus, in theory, enabling a more rapid response to IFNγ treatments. In line with this, nucleosome depleted regions were present at both the promoter and the putative enhancer and may serve as the loop anchor sites, bridging the two together in proximal space (Fig:3.8B). This hypothesis was tested using Capture-C. Capture-C is a one to all 3C method [Hughes et al., 2014]. Here, following a basic 3C protocol, chromatin is cross-linked to regions that are proximal in 3D space. The DNA is digested and religated all within intact nuclei (Fig:3.13A). The ligation step joins digested ends that are in close 3D proximity and results in a DNA library containing NlaIII digested fragments joined together out of sequence and based instead on their spatial distance. Capture-C takes this 3C library and captures only regions of interest, in this case, the IRF1 promoter, pulling down sequences of interacting DNA with it. By sequencing this captured library, one can identify any region of DNA that is in close spatial proximity to the

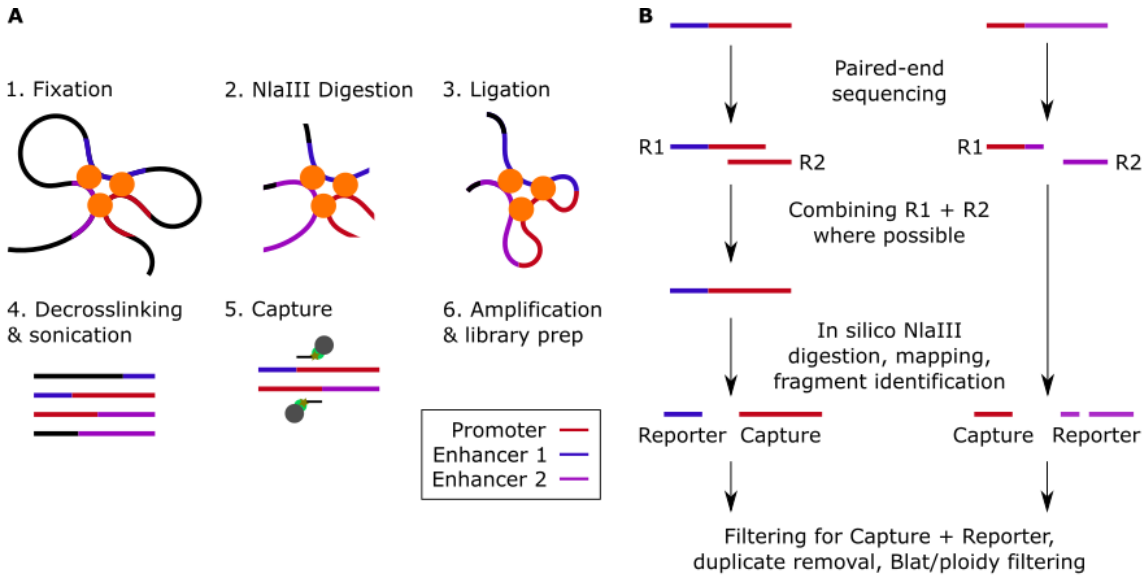

Figure 3.13: Diagram of the Capture-C protocol.
A The Capture-C protocol: Chromatin is fixed, NlaIII digested and religated within intact nuclei. This ligated chromatin is decrosslinked and the DNA is purified and sonicated. DNA containing the capture site is captured using biotinylated hybridization probes. This captured material is amplified and sequenced. **B** Capture-C data processing and alignment: If paired-end sequencing reads overlap they are flash combined, otherwise the separate non-flashed paired reads are taken forward. The flashed and unflashed reads undergo *in silico* NlaIII digestion. Any flashed reads not containing an NlaIII restriction enzyme site are discarded. Digested fragments are aligned to the hg38 genome and sorted into capture and reporter fragments. Aligned fragments are filtered; reads must contain a capture site plus a reporter site, PCR duplicates are removed, as are reads with low-quality alignment scores. The script also checks for regions of the genome that may be non-specifically captured by the probes and removes all reads containing these regions.

region of interest (Fig:3.13A & B).

Biotinylated Capture-C probes were designed to capture an NlaIII restriction enzyme fragment spanning the IRF1 promoter (Fig:3.12B, orange bar denotes capture site). Figure 3.14 A-E reveals that the predominant interactions to the IRF1 promoter are all within approximately 10kb upstream and downstream of the promoter. No interactions can be seen in *trans* (Fig:3.15). Contradictory to the hypothesis, in the untreated Hep3B cells, the IRF1 promoter shows very low-frequency or weak interactions with any regions of DNA (Fig:3.14A). The majority of these low-frequency interactions present are in the gene body or slightly downstream of the

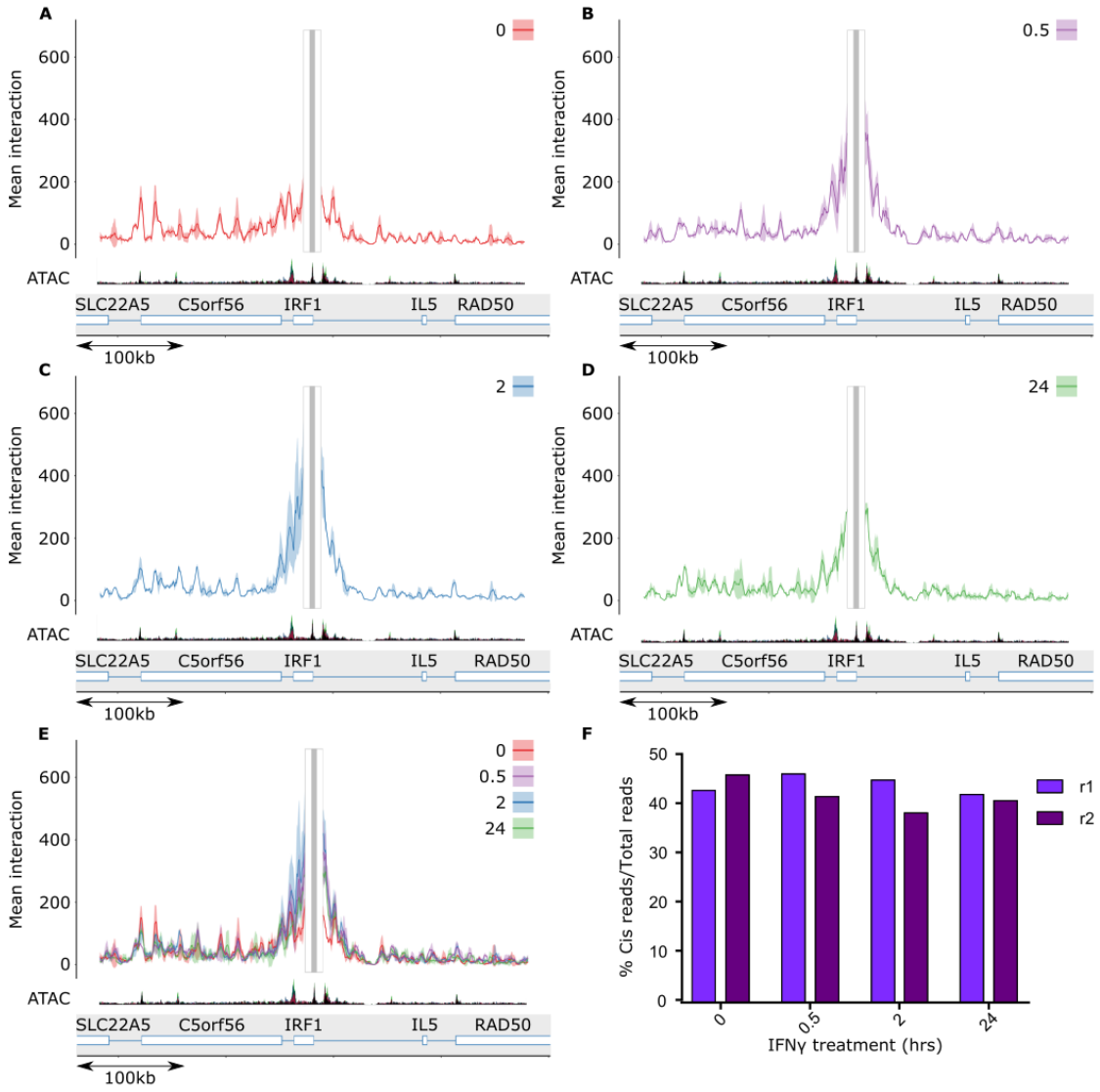

Figure 3.14: Capture-C identifies differential interactions between the IRF1 promoter and enhancer.

A-E Normalised Capture-C data showing mean and standard deviation of reads for the IRF1 promoter for untreated (**A**), 0.5 hrs (**B**), 2 hrs (**C**), 24 hrs (**D**) IFNγ treated or all samples (**E**) (n=2). Reads were normalised based on number of *cis* reads per 100,000 reads. The data is smoothed based on mean reads within a 2000bp window. ATAC-seq data is shown below the Capture-C data. **F** Bar chart showing the percent of *cis* reads over the total reads for each Capture-C sample and repeat for IRF1. Similar ratios indicate similar library qualities.

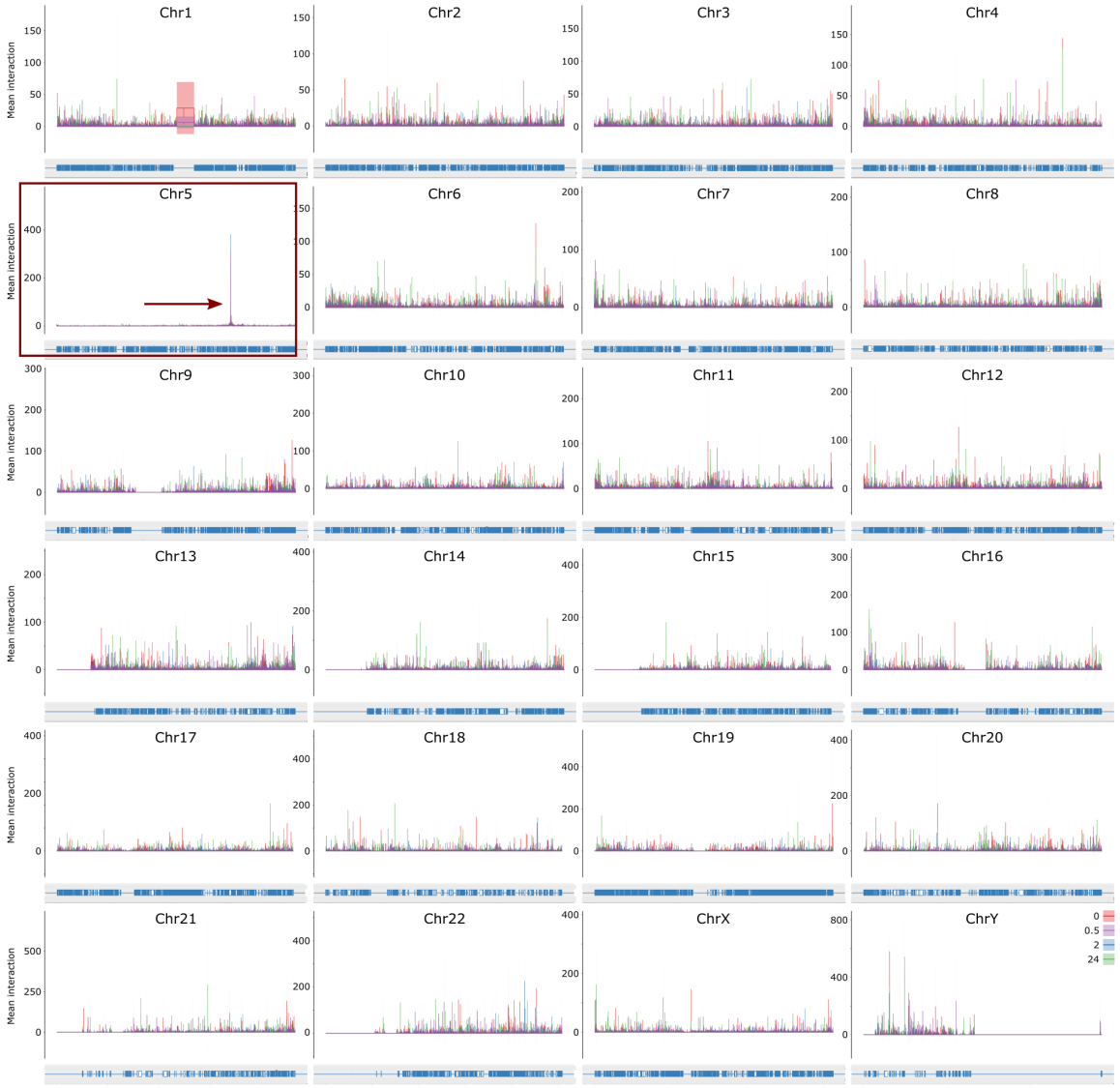

Figure 3.15: IRF1 only forms detectable loops in cis
Normalised Capture C data showing the mean and standard deviation of reads for the IRF1 promoter for each sample (n=2) on each chromosome. Reads were normalised based on the number of chromosome reads per 100,000 reads. The data is smoothed based on mean reads within a 6000bp window. The IRF1 locus is situated on chromosome 5, where a sharp peak of interaction can be seen. A red box and red arrow highlight this chromosome and interaction. Data from other chromosomes show noisy background due to the lack of interactions from these chromosomes to the capture site. Artefacts over centromere regions can sometimes be seen, as is the case on chromosome 1.

gene. Some low-level interactions can also be seen just upstream of the gene, peaking upstream of the putative enhancer, as well as at the C5orf56 promoter (also known as IRF1-AS1). C5orf56 is a lncRNA with an unknown function.

As with many other marks tested at this locus, by just 30 min of IFNγ treatment, a large change occurs in the local chromatin environment (Fig:3.14A-E & 3.16). An increase in interaction can be seen within the gene body and at the putative enhancer site 5kb upstream of the promoter. The library quality appears to be very similar between each repeat of each sample, as denoted by the ratio of *cis* reads over total (*cis* + *trans*) reads (Fig:3.14F), thus this increase appears to be real. The comparable background mean interactions shown by each sample additionally supports the validity of the increase in signal seen. Indeed, significant increases at the putative enhancer and within the gene body can be seen at both 0.5 and 2 hrs compared to the untreated sample (Fig:3.16A & B). The significant increase at the putative enhancer overlaps the ATAC-seq signal and putative pSTAT1 binding sites. This interaction between the two loci fully supports this element as an enhancer of IRF1. These data show that, unexpectedly, the IRF1 promoter dynamically and rapidly forms interactions in 3D space to the enhancer element upstream of the gene upon short treatments of IFNγ. Although a large increase in mean interaction can be seen after 24 hrs of treatment over the untreated sample (Fig:3.14A, D & E), none of these increases are significant. This will be further discussed in section 4.3.4.

Virtually all interactions with the promoter are lost beyond the second upstream CTCF site in all samples tested, again supporting that this CTCF site functions as an insulator preventing aberrant upregulation of nearby genes (Fig:3.16 & 3.15).

3.2.5 Combining all data at the IRF1 locus

Combining the data from both Fig 3.12 and 3.14, IFNγ induces dramatic changes at the IRF1 locus. At the promoter, huge increases in transcription, H3K27ac

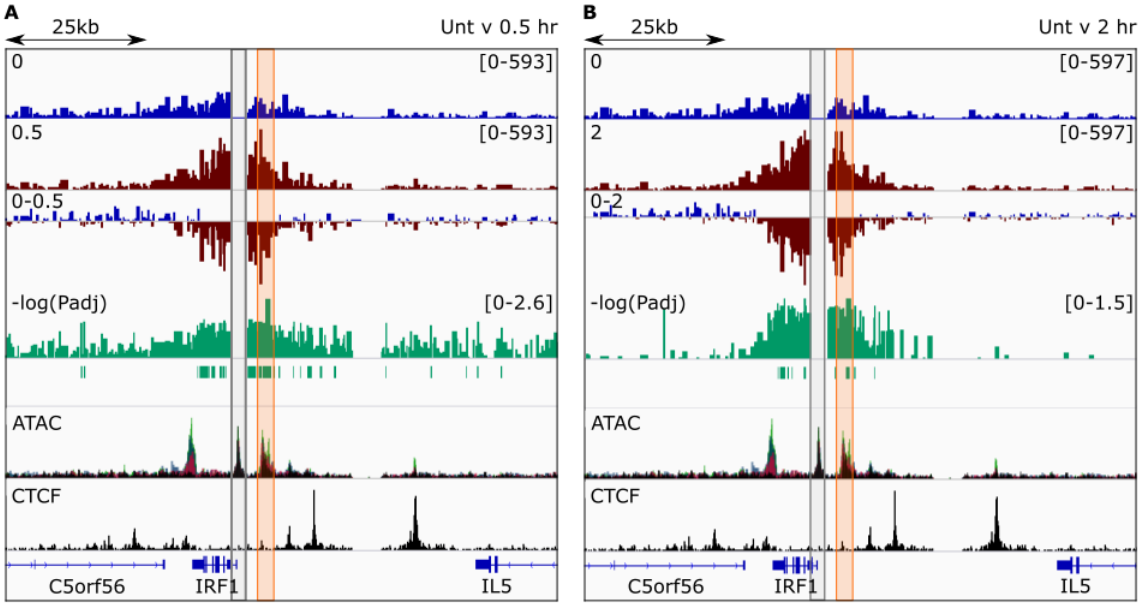

Figure 3.16: Differential interactions between the IRF1 promoter and enhancer are significant.
A-B Untreated vs treated Capture-C data for the IRF1 promoter. 0 vs 0.5 hrs and 0 vs 2 hrs treatments are shown in **A** and **B** respectively. Reads are counted per NlaIII digested fragment. The top two tracks show *cis*-normalised mean data for the untreated and treated samples in blue and red respectively. The 3^{rd} track is subtracted treated sample from untreated sample, with blue and red corresponding to more signal in the untreated or treated sample respectively. In green is the -$\log_{10}$(Padj) value from the DESeq2 results, with bars below showing significant (Padj<0.05) differential reads between the untreated and treated NlaIII digested fragment. Normalised ATAC and CTCF tracks are shown. The position of the IRF1 probe is highlighted in grey and the putative IRF1 enhancer element highlighted in orange.

and H3K4me3 are observed from 30 min of treatment. Correspondingly, significant increases in transcription, H3K27ac, ATAC-seq signal and chromatin loops were found at the upstream enhancer region. Given the known role of pSTAT1 in IFNγ induced IRF1 upregulation, along with the identification of putative GAS motifs at both loop anchors (promoter and enhancer), it is likely that pSTAT1 binding induces the changes seen and may even stimulate bridging between the two loci (Fig:3.17). Finally, IFNγ treatments rapidly induce a *de novo* highly accessible region at the 3'-end of IRF1. No other marks tested could be seen near this region, apart from transcription

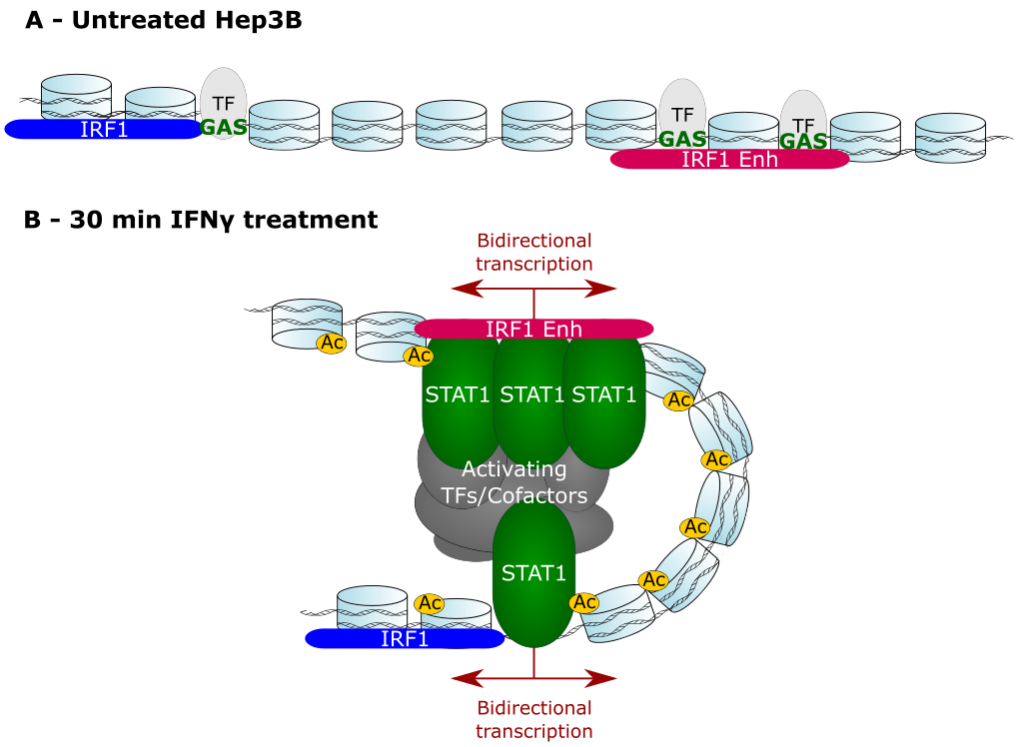

Figure 3.17: Model: IFNγ-induced activation of IRF1
A The IRF1 locus is inactive in untreated Hep3B cells. Unknown TFs maintain accessible DNA at the IRF1 promoter and enhancer region, exposing GAS binding motifs. **B** After 30 min of IFNγ treatments, the IRF1 locus dramatically changes. pSTAT1 binds to accessible GAS binding motifs. STAT1 recruits activating TFs and cofactors. This results in the deposition of acetylation, looping between the promoter and enhancer, and activation of bidirectional transcription at both elements.

of the gene and only weak interaction between this site and the promoter were seen. The function of this induced change, if any, is yet to be determined.

3.2.6 The PD-L1 promoter shows activating chromatin marks within 2 hrs of IFNγ treatment

Understanding the tight regulation of inducible PD-L1 expression may aid in the development of improved PD-1:PD-L1 immunotherapies. Unlike IRF1, whose induction occurs within 30 min of IFNγ treatment, PD-L1 is a late gene whose

expression becomes induced within 2 hrs of IFNγ signalling (Fig:3.2A). Several labs have shown IRF1 to have a major role in PD-L1's induced expression. Although IRF1 is transcribed within 30 min of treatment, its protein expression isn't observed until 2 hrs (Fig:3.1A). However, the sensitivity of a western blot makes it difficult to know exactly when IRF1 is first translated into protein and, therefore, makes it difficult to know how quickly PD-L1 is induced upon IRF1 protein expression. Still, given the rapid dynamic changes occurring at the IRF1 loci within just 30 min, one might hypothesise that similar changes occur at the PD-L1 loci upon IRF1 protein expression.

To test this, we examined the ATAC-seq, ChIP-seq, RNA-seq and SNU-seq datasets at a 50kb locus spanning the PD-L1 gene (Fig:3.18). Both untreated and 30 min treated samples look highly similar, with an accessible site present at the PD-L1 promoter. A peak of H3K4me3 is present at the -1 nucleosome and a very small amount at the +1 nucleosome. Virtually no RNA, transcription or H3K27ac can be detected at the PD-L1 promoter. A sharp peak of CTCF can be seen approximately 8kb upstream of the promoter.

3.2.6.1 Transcriptional changes at PD-L1

By 2 hrs of IRFγ signalling the chromatin environment begins to change (Fig:3.18). In line with the RT-qPCR, RNA transcripts begin emerging from 2 hrs treatment. Transcription over the entire gene body significantly increases in the 2 hr sample. Unlike IRF1 which showed peaks of SNU-seq signal, PD-L1 maintains fairly even coverage across the gene. Both transcription levels and full transcripts are further induced by 24 hrs of IFNγ exposure. Looking at the RNA-seq data, three alternative poly(A) sites can be observed, with the two longest transcripts being the most predominant. Exon 5 of PD-L1 encodes the transmembrane domain and so it is possible that use of the poly(A) site producing the shortest transcript, if functional,

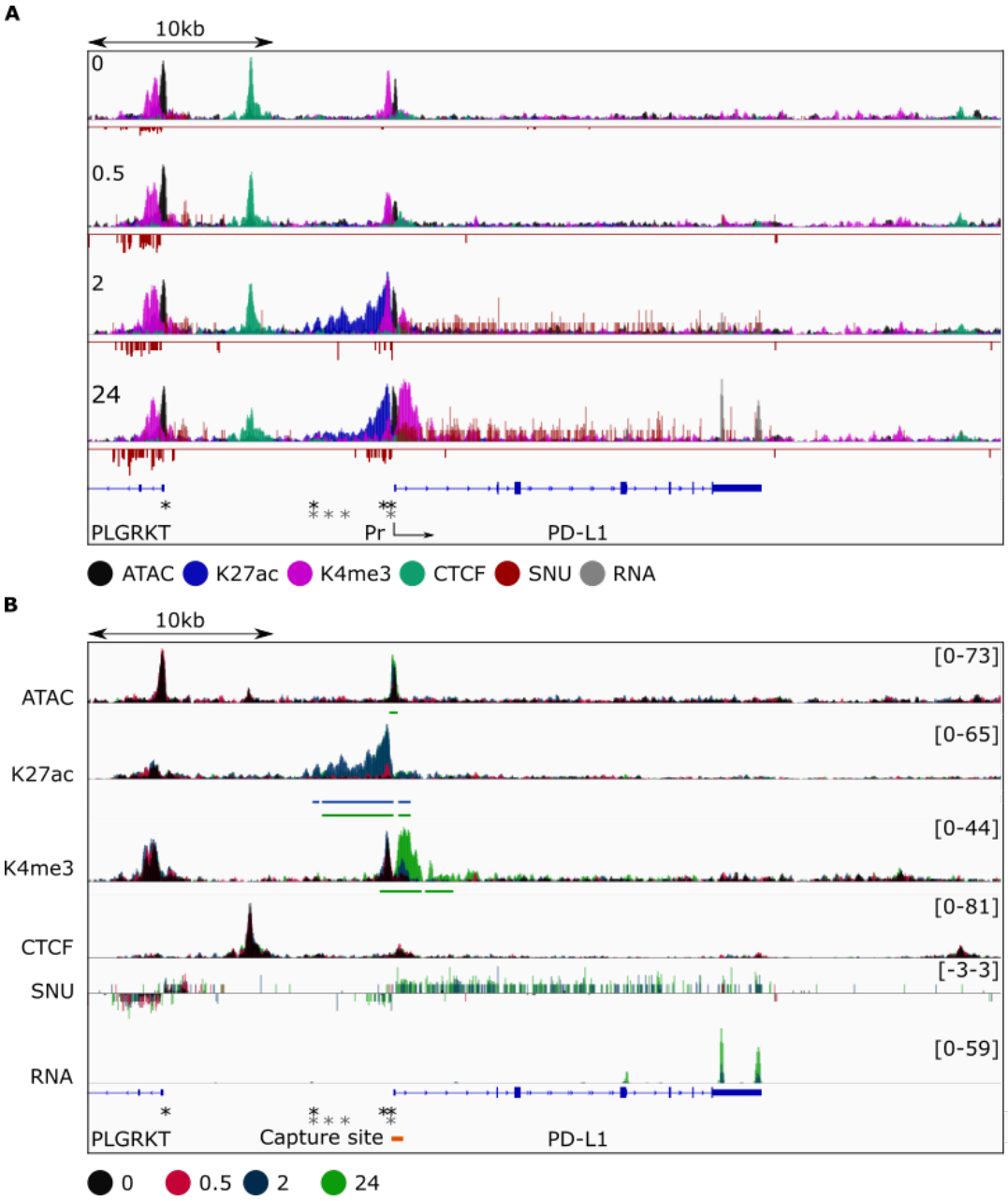

Figure 3.18: The chromatin environment at the PD-L1 locus.
A A 50kb stretch of the PD-L1 locus showing DNA accessibility (black), ChIP profiles of H3K27ac (blue), H3K4me3 (purple) and CTCF (turquoise), strand-specific SNU-seq data (red) and 3'-RNA-seq (grey) data for each treatment sample (n=2-3). All tracks are spike-in normalised except ATAC-seq and CTCF which are normalised based on sequencing depth. * in black denotes a putative IRF1 binding motif and * in grey denotes a STAT1 binding motif. **B** Shows exactly the same data as in A, except now each track shows a specific data set for each timecourse sample, with the untreated sample in black, and 0.5, 2 and 24 hrs of IFNγ treatment in pink, navy and green respectively. Significant changes ($q<0.05$) for ATAC-seq, H3K4me3, H3K27ac and CTCF are represented by bars below the corresponding track. The colour of the bar denotes which timepoint shows a significant difference compared to the untreated sample, with pink, navy and green representing 0.5, 2 and 24 hrs respectively. The capture site for Capture-C is represented by the orange bar.

may lead to the expression of sPD-L1. Only a small fraction of transcripts were detected at this truncated site and so it is unclear how significant this transcript could be in a cell.

3.2.6.2 Changes in histone modifications at PD-L1

Additionally, by 2 hrs H3K4me3 at the +1 nucleosome has increased, however, this increase is not significant (Fig:3.18). Significance is obtained by 24 hrs with the H3K4me3 signal both increasing and beginning to spread into the gene, as is typical with an active gene. The peak at the -1 nucleosome decreases slightly by 24 hrs but this is not significant.

Unexpectedly H3K27ac signal begins increasing at the -1 nucleosome from just 30 min, the timepoint at which IRF1 transcripts were first significantly upregulated (Fig:3.18). This increase is not significant, but the huge significant increase at this region by 2 hrs suggests that the increase at 30 min is real and represents the initial stages of deposited acetylation. It seems unlikely, but not impossible, that IRF1 has already been expressed as a protein and is beginning to change the chromatin environment by 30 min. Both STAT1 and IRF1 have been shown to associate with CBP/p300 and correlate with increased H3K27ac at their binding sites [Ramsauer et al., 2007, Qiao et al., 2013]. Putative binding motifs for both STAT1 and IRF1 were found just upstream of the TSS (Fig:3.18). It is possible that pSTAT1 could be driving this induced change in the chromatin environment. However, given that expression of the PD-L1 transcript isn't induced by 30 min, additional factors, such as IRF1, are probably required.

A massive, significant increase in acetylation is observed by 2 hrs of IFNγ signalling (Fig:3.18). By 24 hrs this signal has decreased marginally at the upstream edges of the peak but still remains significantly upregulated when compared to the untreated sample. Bizarrely, nearly all of this modification is deposited upstream of

the promoter, with very low levels of acetylation at the +1 and +2 nucleosomes. In contrast, upstream of the promoter the acetylation signal is broad, spanning approximately 5kb. This region contains multiple putative STAT1 and IRF1 binding motifs that could dictate writing of this mark.

3.2.6.3 CTCF binding at PD-L1

The CTCF peak roughly 8kb upstream of the promoter remains fairly constant throughout the timecourse (Fig:3.18). This could signify an insulator element at this site. The other modification peaks that can be seen within this 50kb locus are present at the nearest upstream promoter; the PLGRKT promoter. A putative IRF1 binding motif was found at this promoter, however, the lack of significant change in H3K27ac or other mark analysed suggests IRF1 is not binding to this site or, atypically, isn't conferring change to the chromatin environment upon binding.

3.2.7 No obvious IFNγ-dependant enhancer element is observed at the PD-L1 locus

Contrary to the IRF1 locus, there is no obvious nearby enhancer element at the PD-L1 locus. As enhancers are not always situated in close proximity to the gene it regulates, chromatin modifications within a 500kb locus surrounding the PD-L1 gene were examined (Fig:3.19). Again, activation of the PD-L1 promoter can be seen 2 hrs after the addition of IFNγ. Only one other significant change is observed in the locus: There is a small increase in ATAC-seq signal just upstream of the RIC1 promoter after 24 hrs IFNγ treatment compared to the untreated sample. Zooming in on this locus (Fig:3.20) reveals that this very small peak of accessibility is accompanied by a similarly small peak of H3K27ac. There is a slight increase in acetylation by 24 hrs of IFNγ treatment, however, this is not significant according to its q-value, but is significant (<0.05) with respect to its p-value. It is possible that with further

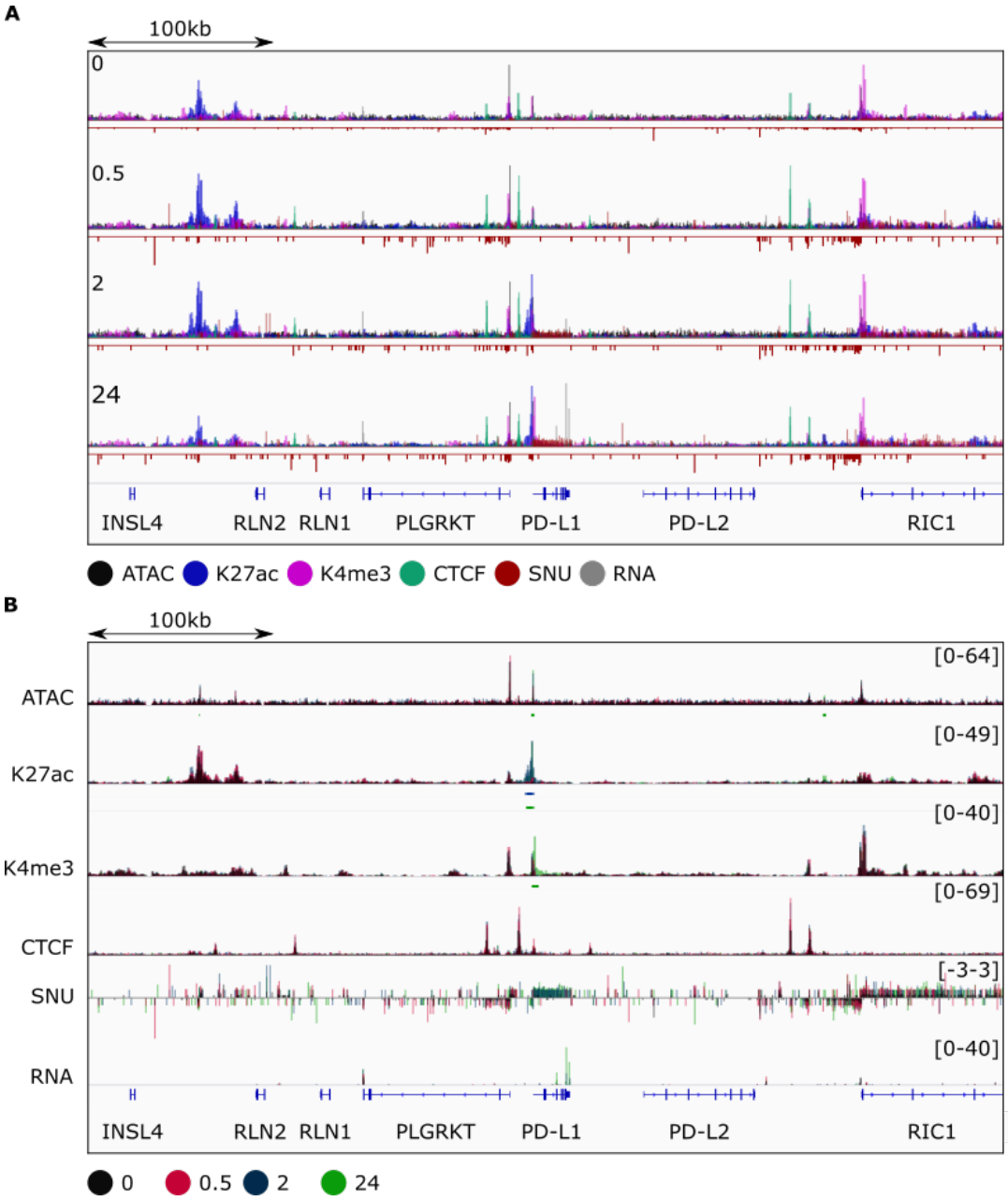

Figure 3.19: Zoomed out chromatin environment at the PD-L1 locus.
A A 500kb stretch of the PD-L1 locus showing DNA accessibility (black), ChIP profiles of H3K27ac (blue), H3K4me3 (purple) and CTCF (turquoise), strand-specific SNU-seq data (red) and 3'-RNA-seq (grey) data for each treatment sample (n=2-3). All tracks are spike-in normalised except ATAC-seq and CTCF which are normalised based on sequencing depth. **B** Shows exactly the same data as in A, except now each track shows a specific data set for each timecourse sample, with the untreated sample in black, and 0.5, 2 and 24 hrs of IFNγ treatment in pink, navy and green respectively. Significant changes ($q<0.05$) for ATAC-seq, H3K4me3, H3K27ac and CTCF are represented by bars below the corresponding track. The colour of the bar denotes which timepoint shows a significant difference compared to the untreated sample, with pink, navy and green representing 0.5, 2 and 24 hrs respectively.

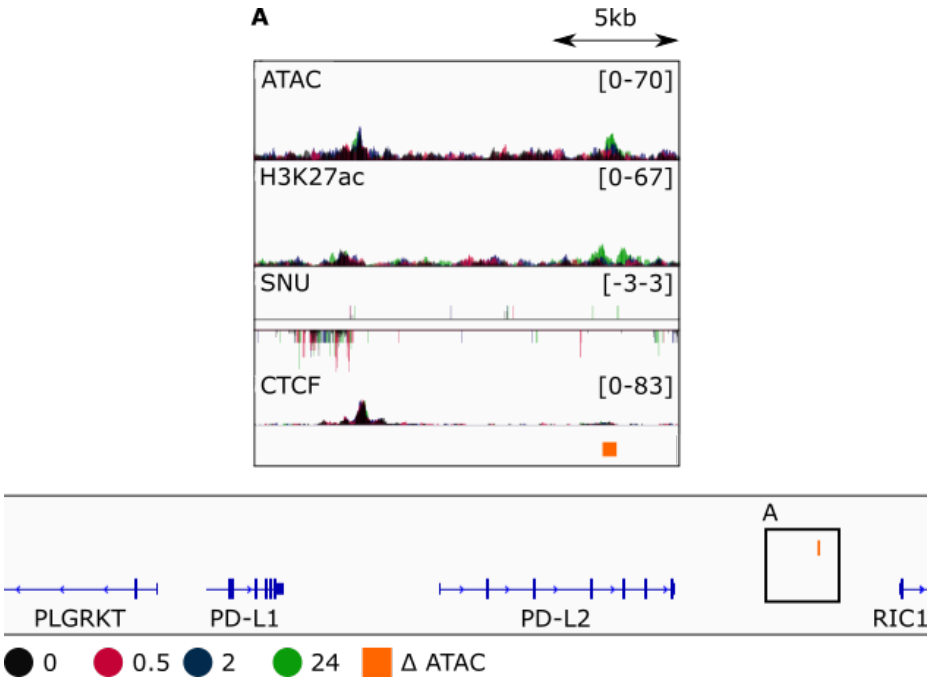

Figure 3.20: A peak of differential DNA accessibility.
A Tracks of ATAC-seq, H3K27ac, SNU-seq and CTCF normalised data (n=2-3) with the untreated sample in black, and 0.5, 2 and 24 hrs of IFNγ treatment in pink, navy and green respectively. The location relative to PD-L1 is shown at the bottom. The orange bar shows the significant increase in ATAC-seq signal after 24 hrs of IFNγ treatment compared to untreated cells.

repeats this increase would become significant. The minimal acetylation and lack of transcription makes it unlikely to be an enhancer element.

Oddly, the CTCF peak approximately 10kb upstream is associated with unidirectional ncRNA transcription (Fig:3.20). The lack of bidirectionality could indicate that CTCF is functioning as an insulator at this site. Alternatively, cases of unidirectional transcription at enhancers have been observed [Catarino and Stark, 2018]. Published CTCF orientations identify convergent CTCF binding between the PD-L1 promoter and the downstream CTCF sites (Fig:3.21) [Nanni et al., 2020]. As gene loop anchors predominantly bind CTCF in convergent orientations, this suggests that these two regions may interact in 3D space [Rao et al., 2014]. Interaction between these loci would support these downstream

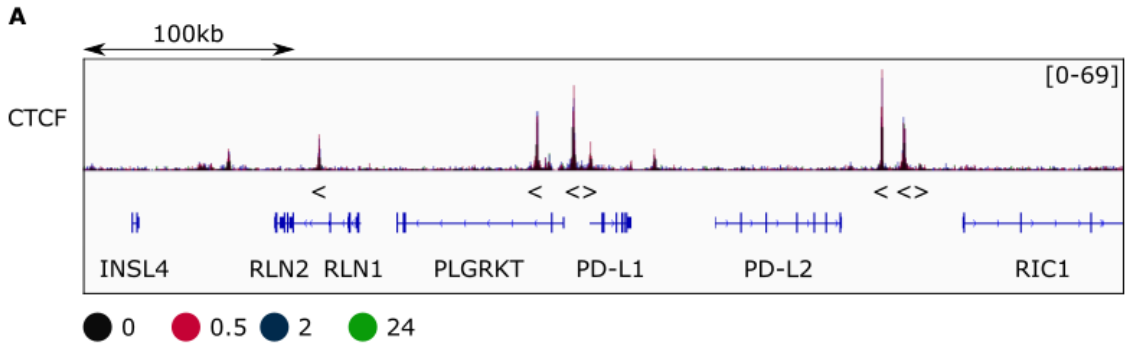

Figure 3.21: CTCF binding orientation at the PD-L1 locus.
A Tracks of CTCF binding in Hep3B cells upon differential treatment of IFNγ, with the untreated sample in black, and 0.5, 2 and 24 hrs of IFNγ treatment in pink, navy and green respectively. Published CTCF orientations from [Nanni et al., 2020] are shown below CTCF peaks.

CTCF binding sites as an enhancer or insulator of PD-L1. However, the minute levels of H3K27ac and accessibility, as well as the lack of change after 2 hrs of IFNγ treatment again make it an unlikely candidate as an enhancer of PD-L1.

In addition to PD-L1, two other genes within this region are actively transcribed; PLGRKT and RIC1 (Fig:3.19). These genes are both constitutively expressed with no significant changes in transcript/transcription levels between treated and untreated samples. The DNA accessibility and chromatin modifications studied remain constant at these promoters throughout the treatment timecourse. Thus, none of these nearby genes appear to be coupled to PD-L1 inducible expression. However, it is possible that upon IFNγ exposure, the PD-L1 promoter may loop to these constitutively active promoters, subsequently leading to upregulation of PD-L1. The remaining genes found within this locus, including PD-L2, remain mostly inactive under the conditions studied. The inactivity of PD-L2 here supports the previous RT-qPCR experimental data showing virtually no PD-L2 expression (Fig:3.3).

One potential enhancer element is present between the INSL4 and RLN2 genes (Fig:3.19). There are two peaks of ATAC-seq signal both associated with high levels of H3K27ac. There is a very low level of bidirectional transcription stemming from

these ATAC-seq peaks, perhaps indicating low activity of this putative enhancer. However, as neither acetylation nor SNU-seq signal correlate with PD-L1 expression (i.e. increase after 2 hrs IFNγ signalling), it seems unlikely that this putative enhancer regulates interferon-inducible PD-L1 expression. Its presence in the untreated cells suggests that this putative enhancer is likely involved in the constitutive expression of other genes. Despite this, IFNγ-induced spatial contact between this enhancer and the PD-L1 promoter could provide a mechanism of PD-L1 activation and, therefore, will be further investigated.

Thus, looking at the chromatin environment surrounding the PD-L1 gene did not reveal an obvious enhancer element regulating PD-L1 expression. This prompted a number of questions; where are PD-L1's IFNγ-dependent regulatory elements and is an enhancer element even required for interferon-inducible expression?

3.2.7.1 Searching the literature for PD-L1's enhancer element

To further explore the whereabouts of potential regulatory elements, the literature was revisited. Previously, a number of putative enhancers regulating constitutive PD-L1 expression have been identified. The putative enhancer found by *Hsu et al.* upstream of the PD-L1 gene coincides with a sharp peak of CTCF (Fig:3.22A) [Hsu et al., 2018b]. However, it lacks both H3K27ac and transcription under these conditions and thus does not appear to be involved in interferon-inducible PD-L1 activation.

The remaining identified enhancers present in the first intron, between the PD-L1 and PD-L2 gene loci and downstream of PD-L2, do not correlate with any marks examined in Hep3B cells under the studied conditions (Fig:3.22A-C) [Green et al., 2012, Sumimoto et al., 2016, Chen et al., 2018b, Zhu et al., 2018b, Xu et al., 2019]. The putative enhancer between PD-L1 and PD-L2 genes was observed in cells with high PD-L1/2 expression and corresponded with high levels of

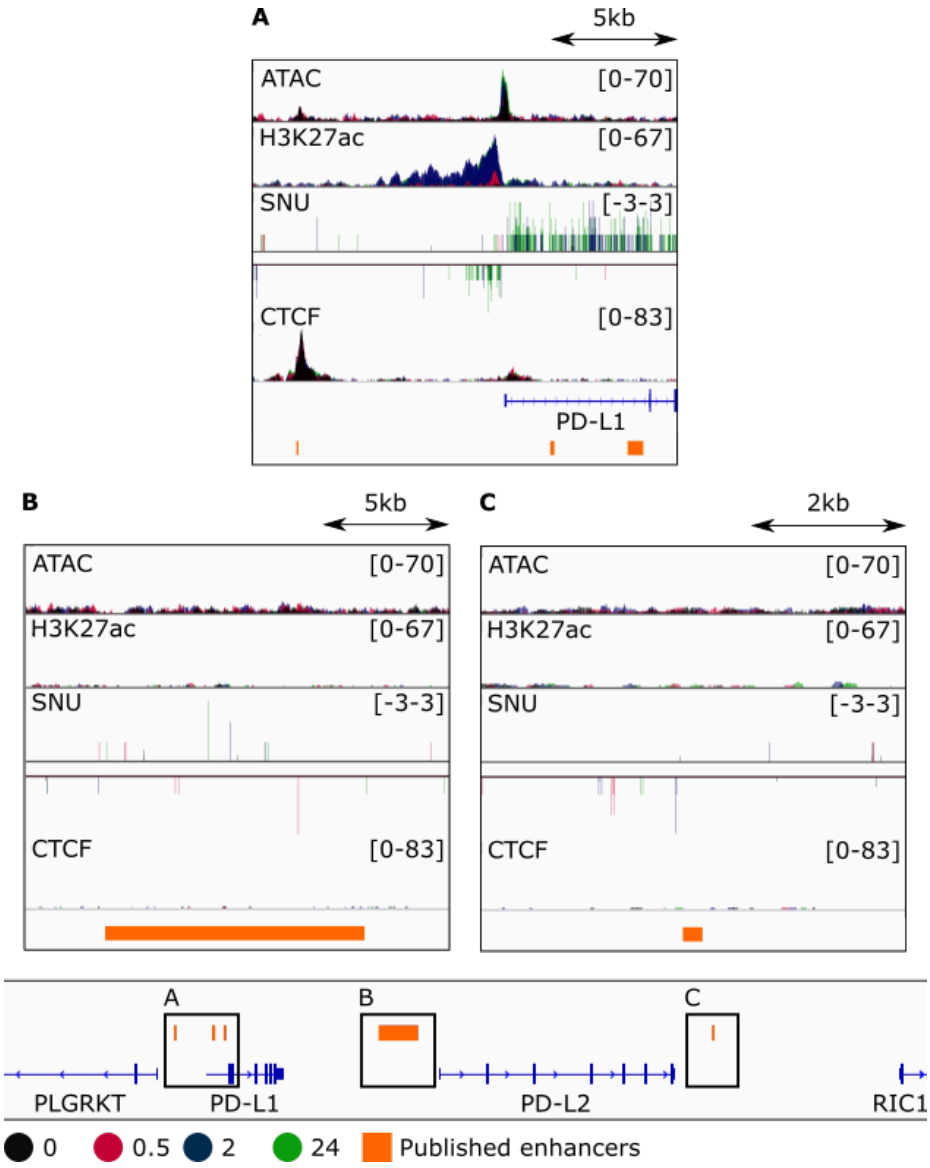

Figure 3.22: Searching for PD-L1's regulatory elements.
A-C Tracks of ATAC-seq, H3K27ac, SNU-seq and CTCF normalised data (n=2-3) with the untreated sample in black, and 0.5, 2 and 24 hrs of IFNγ treatment in pink, navy and green respectively. The position of each box relative to PD-L1 is shown at the bottom. Orange bars show locations of published putative enhancer elements involved in regulating constitutive PD-L1 expression [Green et al., 2012, Sumimoto et al., 2016, Chen et al., 2018b, Hsu et al., 2018b, Zhu et al., 2018b, Xu et al., 2019].

H3K27ac [Xu et al., 2019]. Thus the lack of H3K27ac at this locus within Hep3B cells further supports the inactivity of this enhancer. Altogether it seems that none of the enhancers involved in constitutive PD-L1 expression are necessary for IFNγ-induced upregulation of PD-L1. Inducible upregulation of this protein is likely achieved through alternative mechanisms.

3.2.8 The PD-L1 promoter loops to the nearest active promoter

Having found no conclusive evidence as to the location of PD-L1's interferon-dependent enhancer elements, if they exist, from the previous datasets, Capture-C against the PD-L1 promoter was performed. Biotinylated probes against an NlaIII fragment containing the PD-L1 promoter element were designed and used to identify regions of DNA contacting this locus using Capture-C (Fig:3.18B, orange bar). Given the rapidly dynamic nature of the IRF1 enhancer element observed upon IFNγ treatments, one might expect a similar scenario occurring at other IFNγ-inducible genes such as PD-L1, whereby alterations of higher-order chromatin structure concurrently occur with transcriptional upregulation. However, this does not appear to be the case. Instead of looping to a conventional enhancer element, a peak of interaction can be seen to the nearest gene promoter; PLGRKT, a plasminogen receptor protein (Fig:3.23A-E). This peak can be seen in both the treated and untreated samples. Each sample and repeat contain similar percentages of *cis* reads over total reads demonstrating fairly even library qualities (Fig:3.23F). Thus, the lack of change in mean interactions at the PLGRKT promoter is likely real (Fig:3.23E).

As seen previously, PLGRKT is constitutively expressed, with transcription and full mRNA transcripts of the gene identified in every sample tested (Fig:3.19). No significant changes were observed in either 3'-RNA-seq or SNU-seq using DESeq2

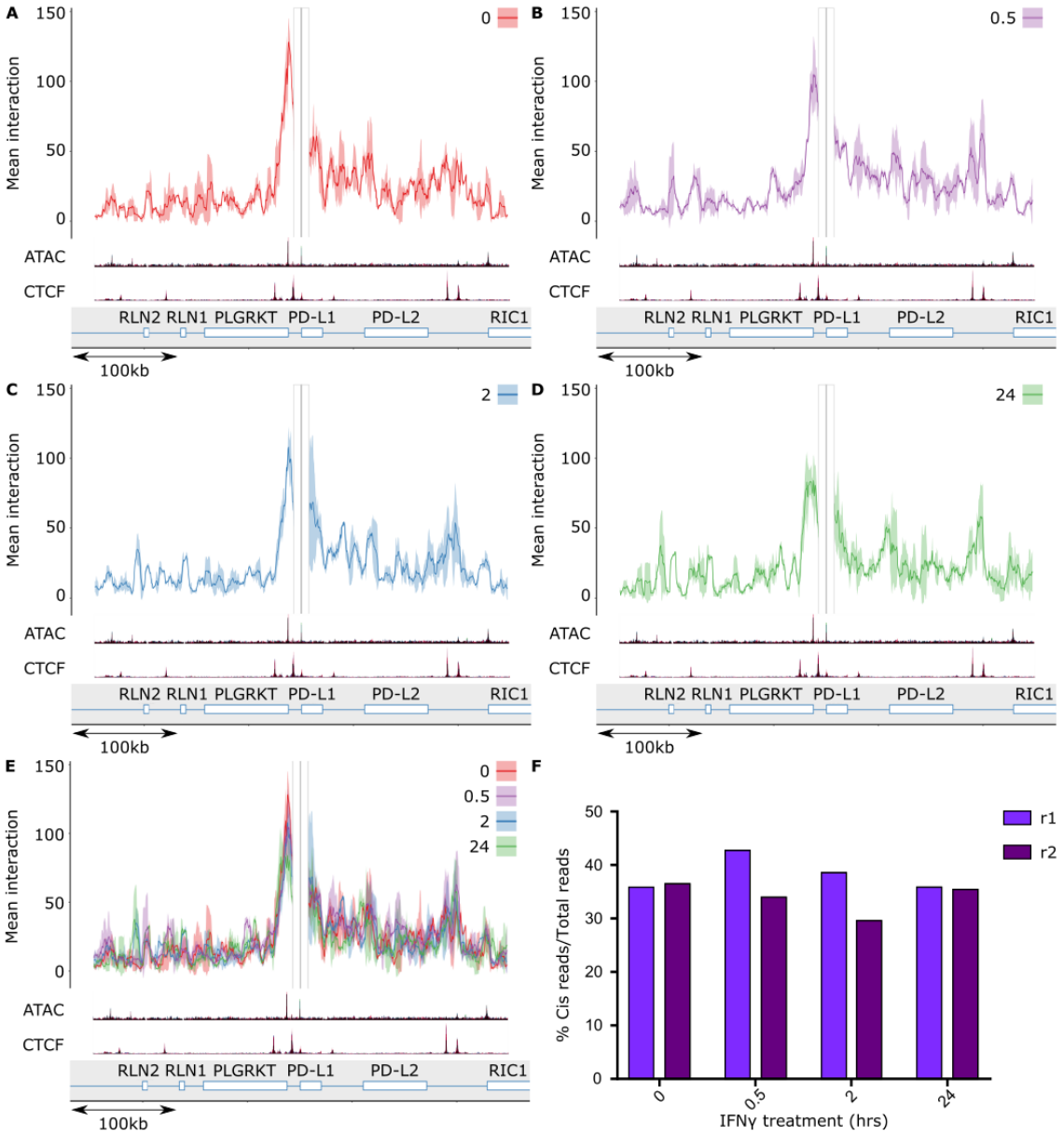

Figure 3.23: Capture-C data analysing interactions to the PD-L1 promoter.
A-E Normalised Capture-C data showing the mean and standard deviation of reads for the PD-L1 promoter for untreated (**A**), 0.5 hrs (**B**), 2 hrs (**C**) or 24 hrs (**D**) IFNγ treated samples or all samples (**E**) (n=2). Reads were normalised based on number of *cis* reads per 100,000 reads. The data is smoothed based on mean reads within a 6000bp window. ATAC-seq and CTCF binding data are shown below the Capture-C data. **F** Bar chart showing the percent of *cis* reads over the total reads for each Capture-C sample and repeat for PD-L1. Similar ratios indicate similar library qualities.

analysis. The promoter itself contains active chromatin marks; accessibility, H3K27ac and H3K4me3 (Fig:3.18 & 3.19). Enhancers share multiple characteristics with promoters, including their ability to recruit TFs and cofactors as well as a capability to initiate transcription [Koch et al., 2011]. Furthermore, a number of mammalian promoters act as enhancers (termed ePromoters), looping to other promoters and regulating neighbouring genes in *cis* [Engreitz et al., 2016, Dao et al., 2017, Diao et al., 2017]. Thus a preformed promoter:promoter loop may enable rapid induction of PD-L1 upon IFNγ treatments. However, the lack of cooperativity between PLGRKT and PD-L1 suggests that this may not be the case. In untreated Hep3B cells, the PD-L1 promoter interacts with the active PLGRKT promoter and yet PD-L1 is not expressed (Fig:3.18 & 3.23). As there is no change in this higher-order chromatin structure and no change in any studied dataset at the PLGRKT promoter, it seems unlikely that this contact enables IFNγ-induced PD-L1 expression.

Zooming out further reveals very little interaction with any other loci, including regions in *trans* (Fig:3.24). All samples show low interactions to the region between PD-L2 and RIC1 (Fig:3.23A-E). Interestingly, this peak does not incorporate the significant differential ATAC-seq peak found between these two genes but instead overlaps with the CTCF peak approximately 10kb upstream of the differential ATAC-seq peak (Fig:3.23A-E). This CTCF peak is present in a convergent orientation to CTCF bound at the PD-L1 promoter, as is common to loop anchors (Fig:3.21) [Rao et al., 2014, Nanni et al., 2020]. However, this low interaction either indicates a weak interaction of this locus to the promoter, or an interaction in a small proportion of cell numbers. A much stronger mean interaction would be assumed for a key regulatory element. No interaction can be seen to the potential constitutive enhancer element identified in Hep3B cells between INSL4 and RLN2 indicating that this likely regulates other loci within the genome (Fig:3.19, 3.23E & 3.25).

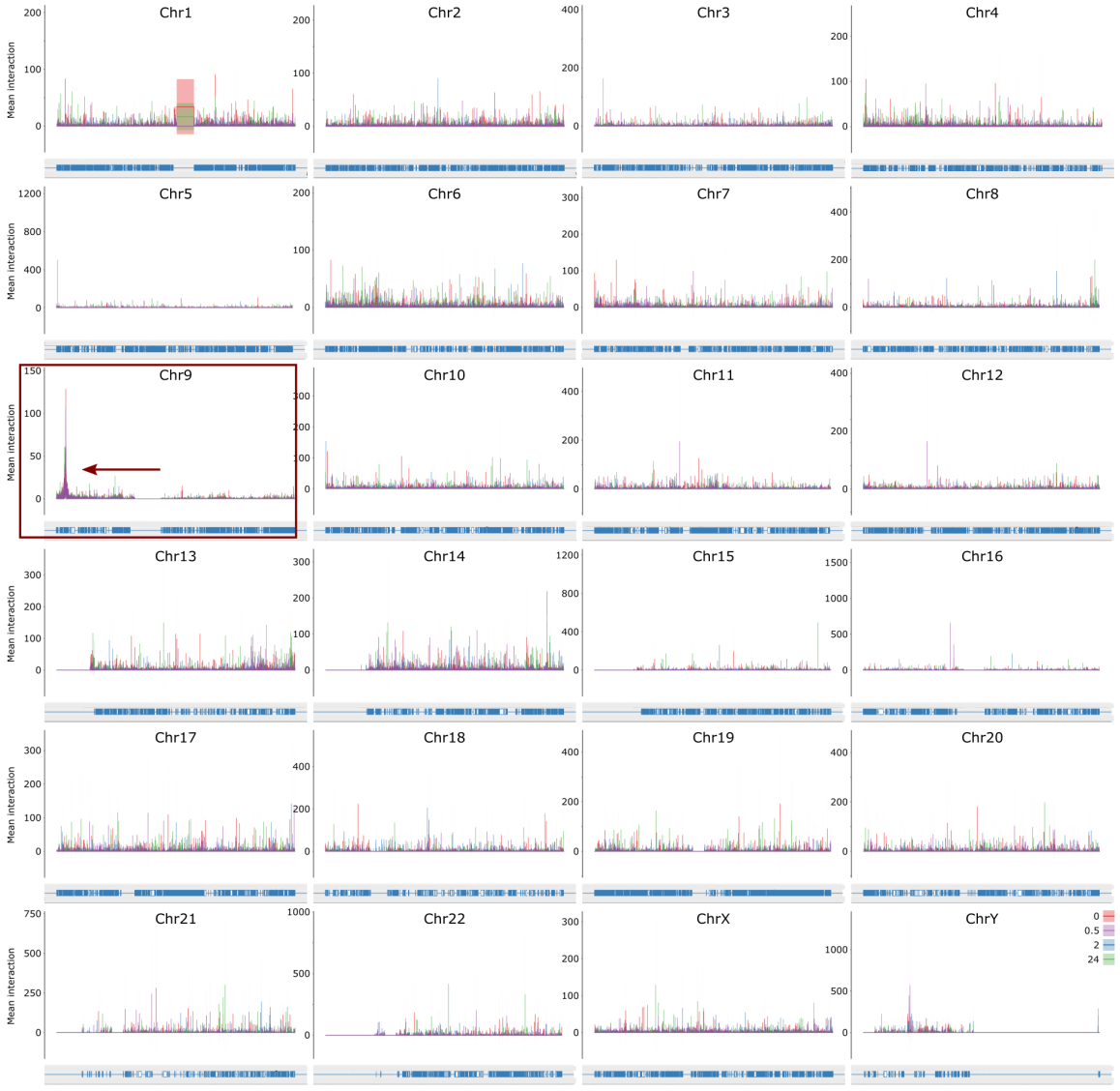

Figure 3.24: The PD-L1 promoter only forms detectable loops in cis
Normalised Capture C data showing mean and standard deviation of reads for the PD-L1 promoter for each sample (n=2) on each chromosome. Reads were normalised based on number of chromosome reads per 100,000 reads. The data is smoothed based on mean reads within a 6000bp window. The PD-L1 locus is situated on chromosome 9, where a sharp peak of interaction can be seen. A red box and red arrow highlights this chromosome and interaction. Data from other chromosomes show noisy background due to the lack of interactions from these chromosomes to the capture site. Artefacts over centromere regions can sometimes be seen, as is the case on chromosome 1.

3.2.8.1 No significant changes in interactions are observed to PD-L1's promoter

Given the change in higher-order chromatin structure at the IRF1 locus corresponding to the upregulation in IRF1 expression, one may have expected to see a similar change at the PD-L1 locus by 2 hrs IFNγ treatment. However, differential analysis revealed no significant changes in interactions between untreated and treated samples (Fig:3.25A). Thus any loops required for IFNγ-induced PD-L1 expression, if any are required, already constitutively exist, perhaps enabling rapid induction of transcription. Indeed, inactive pre-formed promoter:enhancer loops have been identified, whereby activation of each element did not involve changes in higher-order chromatin structure [Simon et al., 2017].

3.2.9 Analysing published STAT1 and IRF1 ChIP-seq libraries reveals clues towards PD-L1's regulatory elements

Capture-C was unable to confidently identify regulatory elements for PD-L1. Further evidence was therefore sought to elucidate the location of PD-L1's IFNγ-inducible enhancers, provided they exist. To this end, I sought published STAT1 and IRF1 ChIP-seq datasets on IFNγ treated cells. These TFs, especially IRF1, have been identified as key regulators of IFNγ-induced PD-L1 expression [Garcia-Diaz et al., 2017]. Discovering their IFNγ-induced binding sites may provide further evidence as to the location of PD-L1's regulatory elements. Given that TF binding may vary between cell types, ChIP-seq data in hepatocytes was preferable, however, I was unable to locate data from these cells. Most research to date on the effects of IFNγ treatments to a cell's enhancer landscape has been performed in monocytes/macrophages. STAT1 and IRF1 ChIP-seq datasets in macrophages

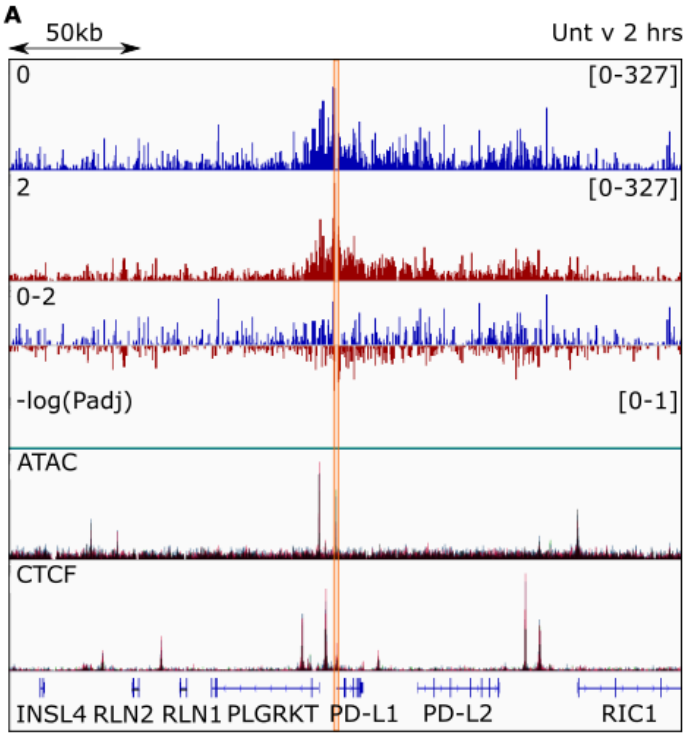

Figure 3.25: Interactions to the PD-L1 promoter do not change with IFNγ treatments.
A Untreated vs 2 hrs treated Capture-C data for the PD-L1 promoter. Reads are counted per NlaIII digested fragment. The top two tracks show *cis*-normalised mean data for the untreated and treated samples in blue and red respectively. The 3^{rd} track substitutes the treated sample from the untreated sample, with blue and red corresponding to more signal in the untreated or treated sample respectively. The 4^{th} track is the -$\log_{10}$(Padj) value from the DESeq2 results. Normalised ATAC and CTCF tracks are shown. The position of the PD-L1 probe is highlighted in orange.

from the Ivashkiv lab, either untreated or treated with 24 hrs of IFNγ, were processed using the ChIPmentation pipeline (GSE43036) [Qiao et al., 2013]. Pol II ChIP-seq and ATAC-seq data published from the same lab at a later date was also analysed to estimate gene expression levels in these cell lines and compare accessible regions between macrophages and Hep3B cells (GSE98367 and GSE98365) [Kang et al., 2017].

3.2.9.1 STAT1 binds to the promoter and enhancer element of IRF1 upon IFNγ treatments

3.2.9.1.1 IFNγ induces expression of IRF1 in macrophages

Initially the IRF1 locus was analysed and compared between macrophages and Hep3B cells, highlighting both similarities and differences. In macrophages, highly accessible regions of DNA were found both at the IRF1 promoter and enhancer region, similarly to that seen in Hep3B cells (Fig:3.26A). The peak summits of these ATAC-seq signals aligned between the two cell types, with multiple distinguishable peaks of open or highly dynamic chromatin at the enhancer element. Unlike in Hep3B cells, the enhancer region is already accessible in the untreated macrophage cells, with little or no increase after IFNγ treatments. Upon treatment with IFNγ there is a slight increase in ATAC-seq signal at the 3'-end of IRF1 in macrophages, however, the extent of this is extremely minor when compared to the increase seen at the same region in Hep3B cells. The macrophage dataset additionally shows small peaks of accessibility upstream of the enhancer site and within the neighbouring C5orf56 gene that are not identified in Hep3B cells. These peaks are present in both IFNγ treated and untreated macrophages. They are likely to be cell-type specific and not involved in IFNγ upregulation of IRF1 in Hep3B cells.

Pol II signal dramatically increases and spreads across IRF1 upon treatment with IFNγ, signifying upregulation of IRF1 transcription in macrophages, akin to that seen in Hep3B cells (Fig:3.26A). Interestingly, Pol II signal is enriched at and downstream of the 3'-end of IRF1. The high levels of Pol II at this loci could cause reduced nucleosome occupancy witnessed in Hep3B cells. Indeed, nucleosome occupancy at poly(A) sites was found to be inversely correlated to Pol II levels [Huang et al., 2013].

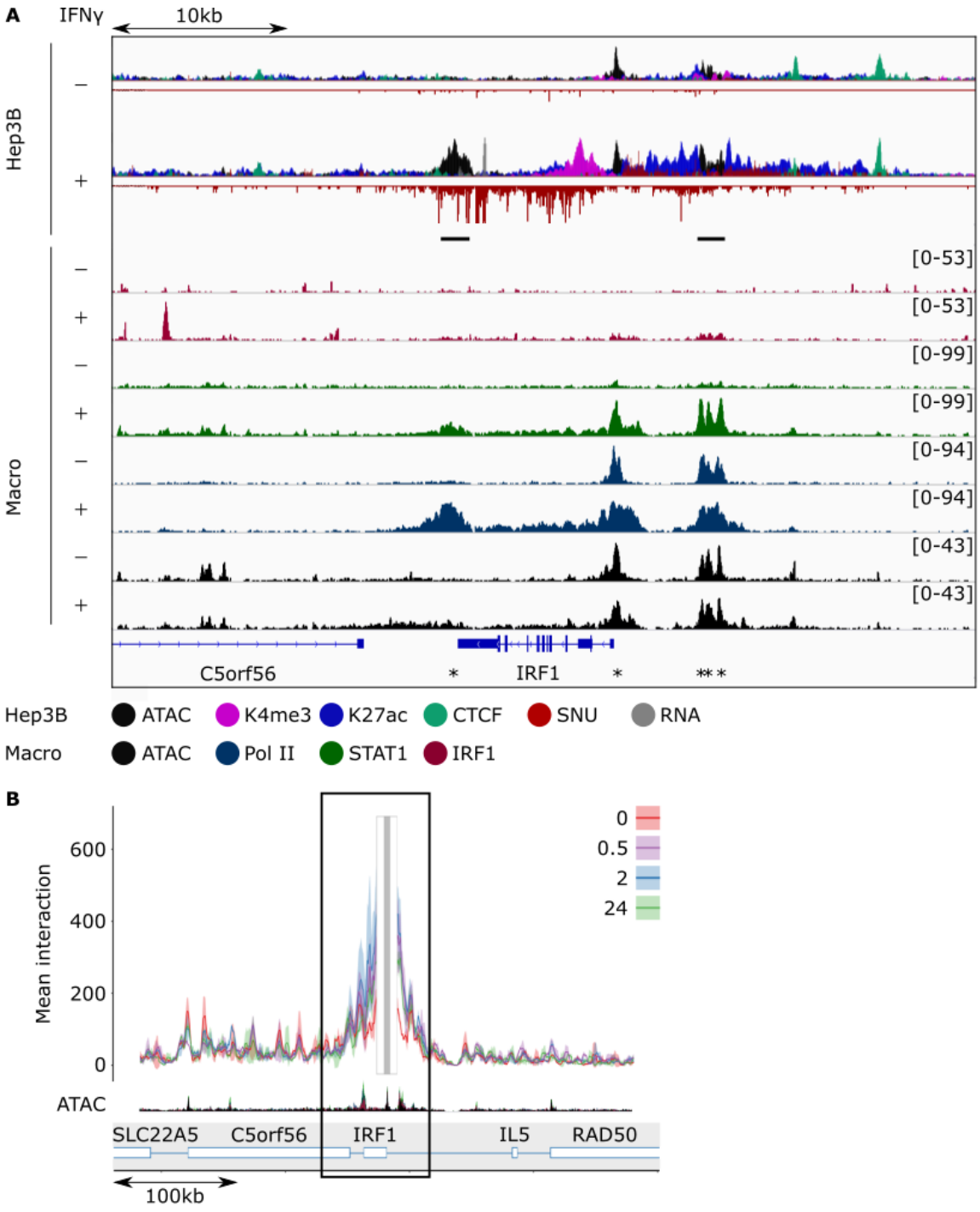

Figure 3.26: Analysing STAT1 binding at the IRF1 locus.
See [2] on next page

3.2.9.1.2 IFNγ induces STAT1 binding at IRF1's promoter and enhancer

In untreated macrophage cells virtually no binding of STAT1 or IRF1 can be observed (Fig:3.26A). As expected, upon addition of IFNγ, STAT1 binds to both the promoter and enhancer region of IRF1, overlapping the identified STAT1 binding motifs and, once more, validating the upstream accessible region as IRF1's enhancer. This supports previously published data that STAT1 is a vital TF for IFNγ-induced IRF1 expression [Platanias, 2005]. Its binding sites strongly overlap the accessible regions in both macrophages and Hep3B cells, making it likely that STAT1 binds to the same regions in Hep3B cells when treated with IFNγ. The increase in accessibility in Hep3B cells seen at the enhancer element could be explained by binding of STAT1 to these sites, displacing bound histones. STAT1 can also be seen at the 3'-end of IRF1, albeit with a much lower signal than that seen at the enhancer or promoter.

Very small IFNγ-induced increases in IRF1 can be visualised at the promoter and enhancer region in macrophages (Fig:3.26A). Although self-regulation of IRF1 is possible, the low signal is more likely off-target effects seen due to interactions between STAT1 and IRF1. IRF1 binding could be important to sustain upregulation of IRF1 after long exposures to IFNγ. As no repeats were made for the IRF1 ChIP-seq dataset, one can not say with certainty whether these increases are real. A sharp peak of IRF1 is present in IFNγ-treated macrophages approximately 10kb from the 3'-end of C5orf56. A lack of other marks analysed in Hep3B cells or macrophages make it difficult to speculate the role of this bound IRF1.

[2]**Fig3.26: Analysing STAT1 binding at the IRF1 locus. A** A 50kb stretch of the IRF1 locus showing Hep3B cells and published macrophage data. The top two tracks show Hep3B DNA accessibility (black), ChIP profiles of H3K27ac (blue), H3K4me3 (purple) and CTCF (turquoise), strand-specific SNU-seq data (red) and 3'-end RNA-seq (grey) data for untreated and 24 hr IFNγ treated cells (n=2-3). Black bars represent significant increases in DNA accessibility. The following tracks (top to bottom) show published macrophage ChIP-seq profiles of IRF1 (pink), STAT1 (green) and Pol II (dark blue) as well as ATAC-seq data (black). * denotes putative STAT1 binding motifs. **B** Shows the location of data in **A** relative to the Capture-C results, signified by the black box.

IFNγ was shown to increase looping from the enhancer element to the IRF1 promoter in section 3.2.4. These increased interactions to the IRF1 promoter in Hep3B cells overlap with the IFNγ-induced STAT1 binding in macrophages (Fig:3.26). It is likely that STAT1 binding directly or indirectly increases interactions between IRF1's promoter and enhancer element (Modelled in Fig:3.17).

3.2.9.2 STAT1 and IRF1 have multiple binding sites surrounding the PD-L1 locus

3.2.9.2.1 Pol II at PD-L1 is upregulated in macrophages by IFNγ

Having identified numerous potential regulatory elements involved in IFNγ-induced upregulation of PD-L1 in Hep3B cells using Capture-C, all without conclusive evidence, I was intrigued to equate the data from both cell types. First I analysed a 50kb locus surrounding PD-L1 in which a high proportion of interactions to the PD-L1 promoter occurred, as quantified using Capture-C (Fig:3.27B). Pol II signal in macrophages dramatically increases from virtually no signal when treated with IFNγ (Fig:3.27A). Thus strongly suggesting, analogously to Hep3B cells, expression of PD-L1 in macrophages is induced by IFNγ.

Regions of high accessibility are present at both the PD-L1 and PLGRKT promoters in both cell types (Fig:3.27A). There are some very small additional peaks of accessibility between these two genes in macrophages, all of which are present with or without IFNγ. These cell-type specific accessible regions are unlikely to be necessary for IFNγ-inducible upregulation of PD-L1 in Hep3B cells.

3.2.9.2.2 IFNγ induces STAT1 and IRF1 binding at and in-between the PD-L1 and PLGRKT promoters

Neither STAT1 or IRF1 bind to the PD-L1 locus in the untreated macrophages (Fig:3.27A). After treatment with IFNγ, both of these TFs bind strongly to the

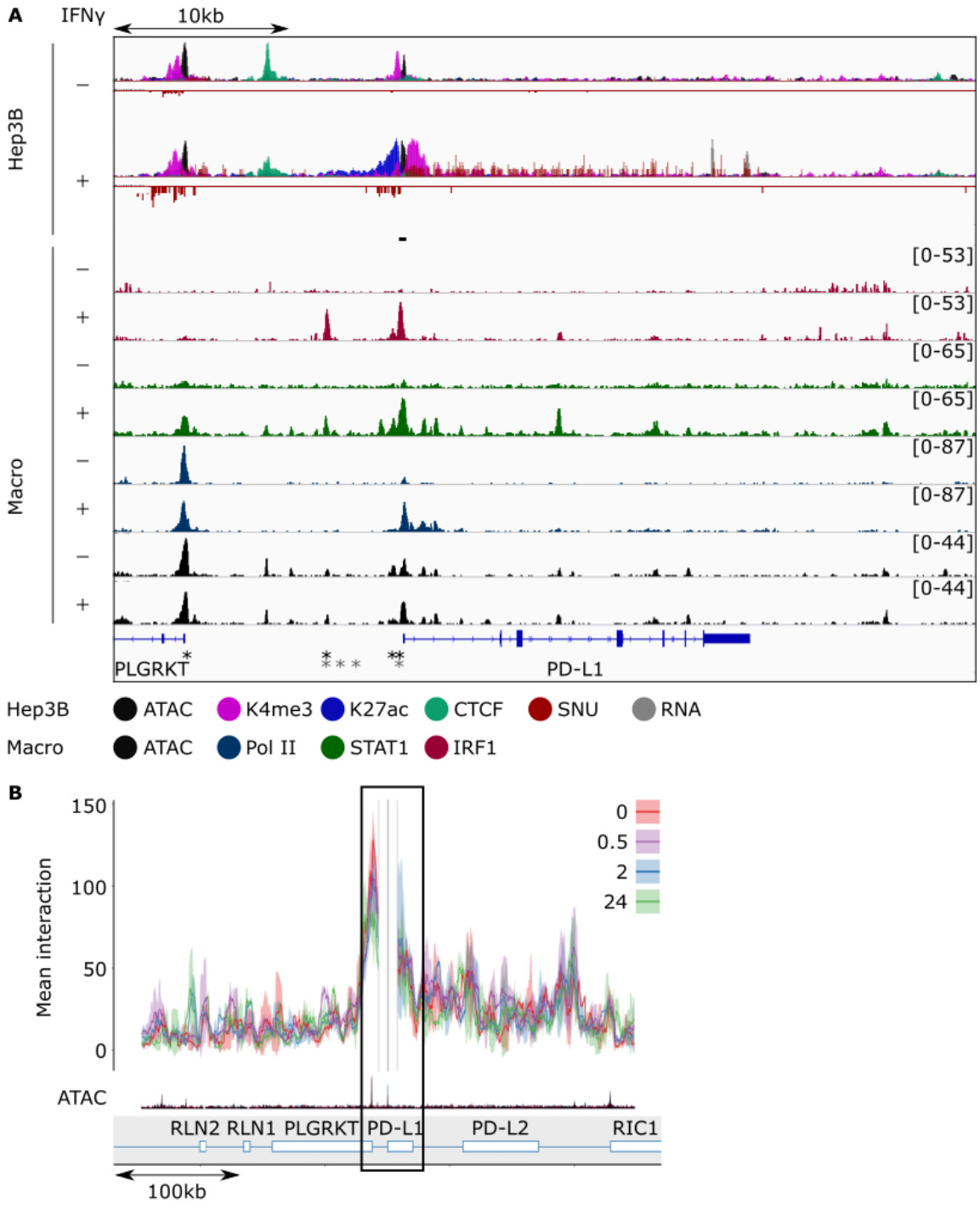

Figure 3.27: Analysing IRF1 and STAT1 binding at the PD-L1 locus.
See [3] on next page

PD-L1 promoter in macrophages, coinciding with their binding motifs. This further supports these TFs as modulators of IFNγ-induced upregulation of PD-L1. A peak of IRF1 and, to a smaller extent, STAT1 is present approximately 4kb upstream of the promoter. If IRF1 also bound to this upstream region in Hep3B cells one might expect a corresponding peak of accessibility which is not present in any condition in this cell line. However, the peak of ATAC-seq signal overlapping the IRF1 peak in macrophages is extremely small, especially considering the large IRF1 signal. It is therefore possible that open DNA isn't required for IRF1 to associate to this region. IRF1 binding just 4kb from PD-L1 may help recruit TFs and other activating factors to the PD-L1 promoter to stimulate transcription, despite relatively weak interactions to this locus as determined by Capture-C (Fig:3.28).

The highest interaction signal to the PD-L1 promoter identified by Capture-C in Hep3B cells comes from the PLGRKT promoter (Fig:3.27B). In Hep3B cells this plasminogen receptor is constitutively expressed, with no significant changes to any analysed modification (Fig:3.27A). The presence of invariable ATAC-seq signal as well as Pol II in untreated or IFNγ-treated macrophages likewise suggests constitutive expression of this gene. A binding motif for IRF1 but not STAT1 was identified at the PLGRKT promoter. Unexpectedly, IRF1 was not observed at this region in any condition, whilst a small peak of STAT1 signal is seen in the treated sample. STAT1 is known to interact with other TFs, including other TFs in the STAT and IRF family, and these can redirect its DNA binding properties

[3]**Fig3.27: Analysing IRF1 and STAT1 binding at the PD-L1 locus. A** A 50kb stretch of the PD-L1 locus showing Hep3B cells and published macrophage data. The top two tracks show Hep3B DNA accessibility (black), ChIP profiles of H3K27ac (blue), H3K4me3 (purple) and CTCF (turquoise), strand-specific SNU-seq data (red) and 3'-end RNA-seq (grey) data for untreated and 24 hr IFNγ treated cells (n=2-3). Black bars represent significant increases in DNA accessibility. The following tracks (top to bottom) show published macrophage ChIP-seq profiles of IRF1 (pink), STAT1 (green) and Pol II (dark blue) as well as ATAC-seq data (black). * in black and grey denotes putative IRF1 and STAT1 binding motifs respectively. **B** Shows the location of data in **A** relative to the Capture-C results, signified by the black box.

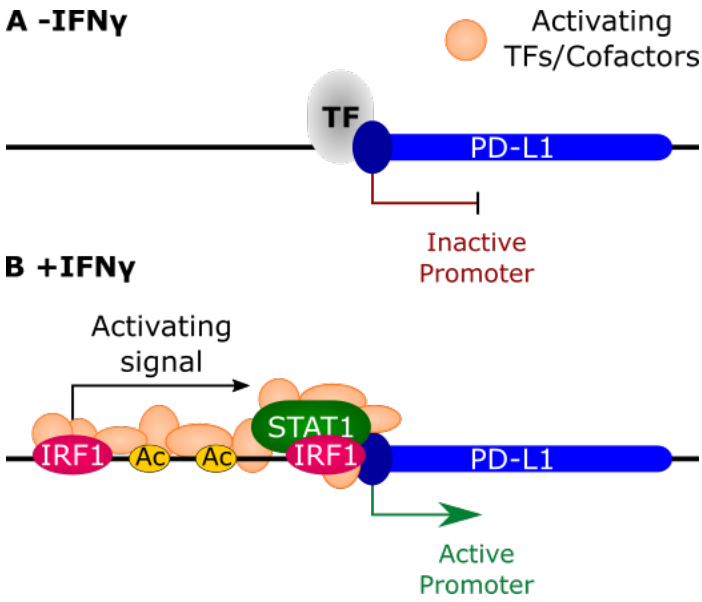

Figure 3.28: Model: The proximal PD-L1 promoter is sufficient for IFNγ upregulation of PD-L1.
A In untreated Hep3B cells, PD-L1 is unexpressed. Unknown TFs maintain DNA accessibility at the PD-L1 promoter. **B** Treatment with IFNγ results in binding of IRF1 and STAT1 to the PD-L1 promoter and a region upstream of the promoter. This proximal region spreads activating signals, i.e. histone acetylation, and activating TFs and cofactors to the promoter, upregulating PD-L1 expression.

[Ostuni et al., 2013, Langlais et al., 2016, Abou El Hassan et al., 2017]. This could explain binding of STAT1 to the PLGRKT promoter despite not identifying a GAS motif. The lack of IRF1 ChIP-seq signal would indicate that this protein isn't redirecting STAT1 to this site. IRF8, another TF commonly induced by IFNγ, whose expression is significantly induced in Hep3B cells, could modulate binding of STAT1 to this site. A second possibility is that the loop between the PD-L1 and PLGRKT promoters brings STAT1, present at the PD-L1 promoter, in close proximity to the PLGRKT promoter. This could produce off-target signal seen in the ChIP-seq data, despite STAT1 not actually binding to the PLGRKT promoter.

Despite no significant change in interaction between the PD-L1 and PLGRKT promoter, it is possible that binding of STAT1 to both promoters provides a bridge enabling recruitment of essential factors to stimulate transcription of PD-L1. Thus,

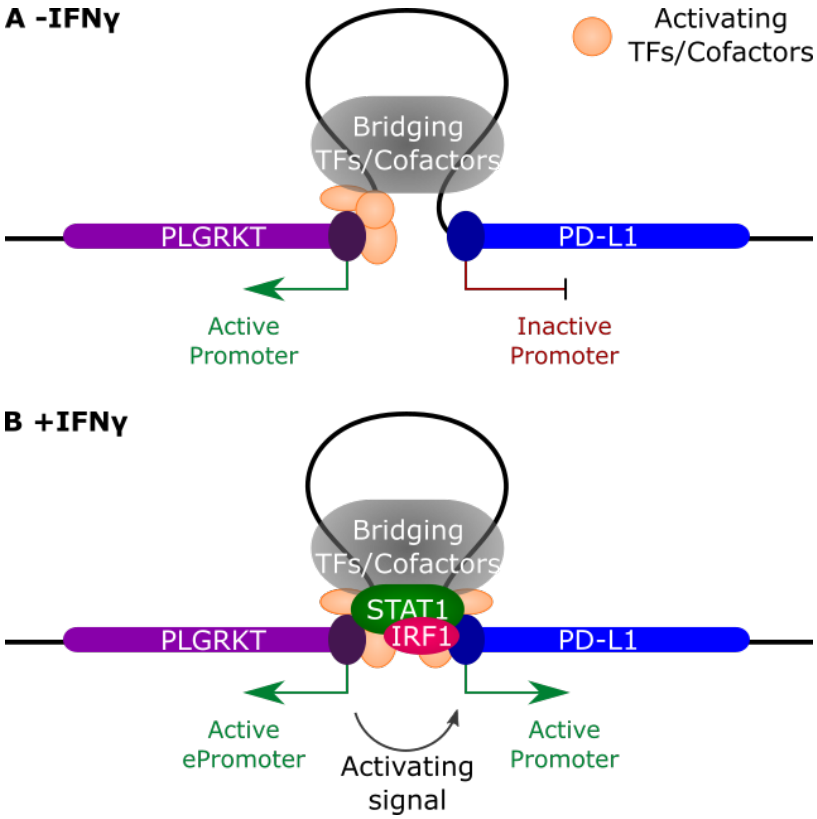

Figure 3.29: Model: The PLGRKT ePromoter activity regulates IFNγ-induced PD-L1 expression.
A In untreated Hep3B cells, the PD-L1 promoter interacts with the PLGRKT promoter. PLGRKT is constitutively expressed, with activating TFs and cofactors bound to its promoter. These activating signals are not relayed to PD-L1, despite the interaction. **B** Treatment with IFNγ results in binding of IRF1 and STAT1 to the PD-L1 promoter and the latter additionally interacts with the PLGRKT promoter. This activates ePromoter activity of PLGRKT, enabling it to fully activate the PD-L1 promoter, initiating transcription of the gene.

STAT1, potentially in combination with IRF1, may promote enhancer activity from the PLGRKT promoter (Fig:3.29).

3.2.9.2.3 IRF1 binds to the putative regulatory element between PD-L2 and RIC1

A second potential enhancer at the differential ATAC-seq site in-between PD-L2 and RIC1 was next examined (Fig:3.30B). Capture-C revealed some interaction between the PD-L1 promoter and the CTCF sites adjacent to the differential ATAC-seq peak under all conditions analysed. Further to the increase in accessibility, some enhancer-like features can be found at this locus; non-coding transcription and acetylation (Fig:3.20).

In both untreated and IFNγ treated macrophages, small peaks of ATAC-seq signal can be visualised overlapping with the two CTCF peaks present in Hep3B cells (Fig:3.30A). Very little amounts of open DNA is seen in either macrophage condition at the differential ATAC-seq peak in Hep3B cells, although a peak was identified though MACS2 peak calling, suggesting presence of accessible DNA. Another region of accessibility is observed further towards RIC1 in macrophages, but is not present in Hep3B cells (Fig:3.30).

Although non-coding transcription is present within this locus in Hep3B cells, only background levels of Pol II is present in macrophages (Fig:3.30A). This could signify a lack of transcription in the latter cell type, however, due to the highly transient nature of ncRNA transcription, it is likely that ChIP-seq is not sensitive enough to detect Pol II at these locations. It is also possible that a different RNA polymerase is involved in this transcription.

No STAT1 or IRF1 binding is detected in untreated macrophages (Fig:3.30). After exposure to IFNγ, a peak of IRF1 appears overlapping the differential ATAC-seq peak in Hep3B cells and aligning to the IRF1 binding motif. Binding of IRF1 to this locus in

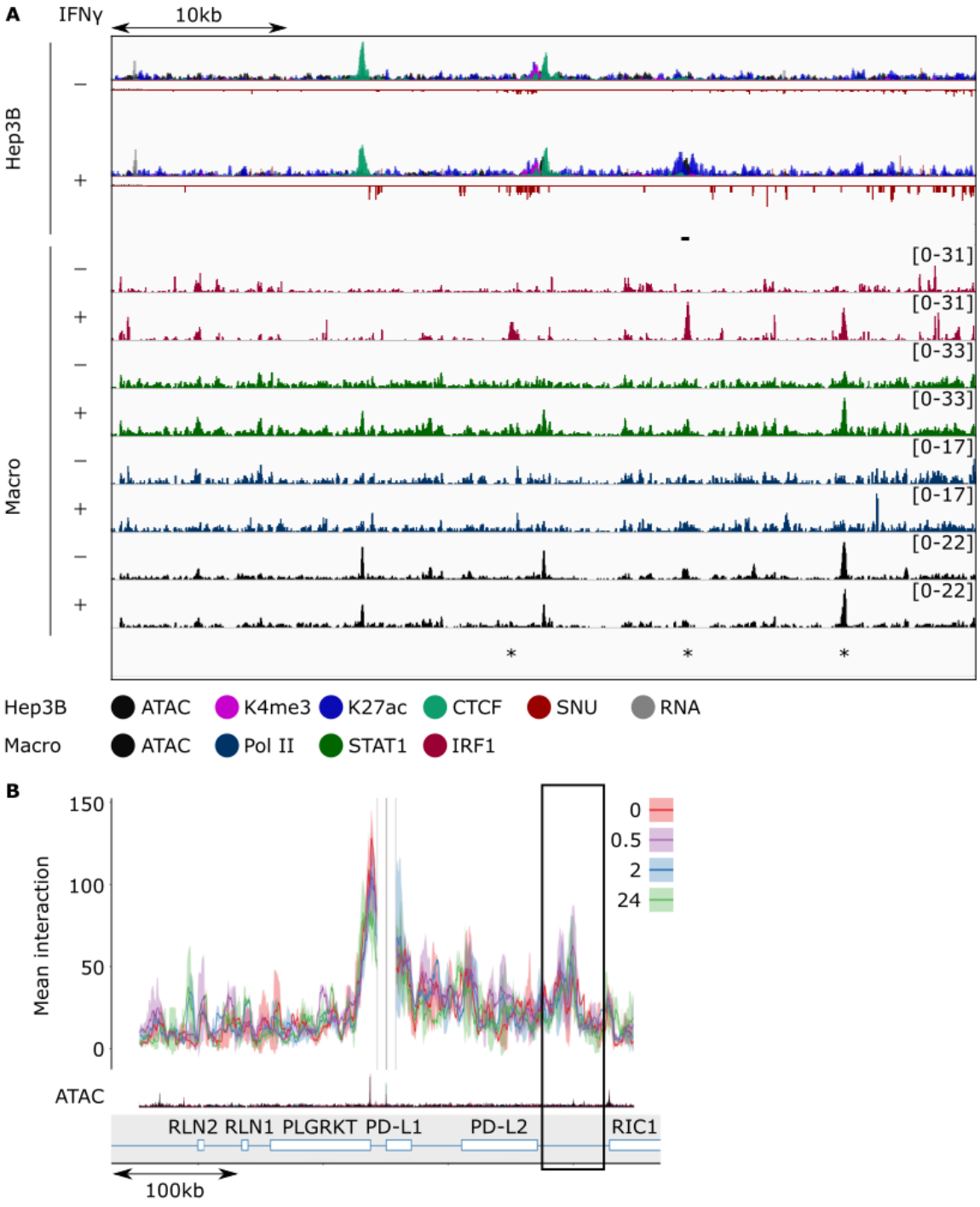

Figure 3.30: Analysing IRF1 and STAT1 binding at putative regulatory elements.

See [4] on next page

Hep3B cells could explain the increase in both accessibility and histone acetylation. This supports this region as a putative enhancer of PD-L1, despite the relatively weak interaction to the PD-L1 promoter (Modelled in Fig:3.31). Other IRF1 peaks are present on either side of the differential ATAC-seq signal, both corresponding to an IRF1 binding motif. The lack of other features analysed in Hep3B cells at both of these peaks makes it difficult to determine whether IRF1 binds and has a function at these locations.

STAT1 does not appear to bind anywhere within this 50kb locus except at an accessible peak nearest to RIC1. As this peak of accessibility is not identified in Hep3B cells, binding of IRF1 and STAT1 to this region seems less likely.

3.2.9.2.4 The three models of PD-L1's IFNγ-dependent regulatory elements

All in all, upon IFNγ-treatments, IRF1 and STAT1 bind to multiple sites surrounding PD-L1 in macrophages. Given the similarities in accessible regions and gene expression between macrophages and Hep3B cells at many of these IRF1/STAT1 binding sites, it is likely that they bind at least some of these regions in Hep3B cells. Localisation of these TFs to the PD-L1 promoter, ∼4kb upstream of the promoter, the PLGRKT promoter and to the region between PD-L2/RIC1, indicates that these loci, either alone or in combination, may be the key regulatory factors involved in IFNγ-induced upregulation of PD-L1 (Fig:3.28, 3.29 & 3.31).

[4]**Fig3.30: Analysing IRF1 and STAT1 binding at putative regulatory elements. A** A 50kb stretch of the putative regulatory element between PD-L2 and RIC1, approximately 150kb downstream of the PD-L1 promoter, showing Hep3B and published macrophage data. The top two tracks show Hep3B DNA accessibility (black), ChIP profiles of H3K27ac (blue), H3K4me3 (purple) and CTCF (turquoise), strand-specific SNU-seq data (red) and 3'-end RNA-seq (grey) data for untreated and 24 hr IFNγ treated cells (n=2-3). Black bars represent significant increases in DNA accessibility. The following tracks (top to bottom) show published macrophage ChIP-seq profiles of IRF1 (pink), STAT1 (green) and Pol II (dark blue) as well as ATAC-seq data (black). * in black and grey denotes putative IRF1 and STAT1 binding motifs respectively. **B** Shows the location of data in **A** relative to the Capture-C results, signified by the black box.

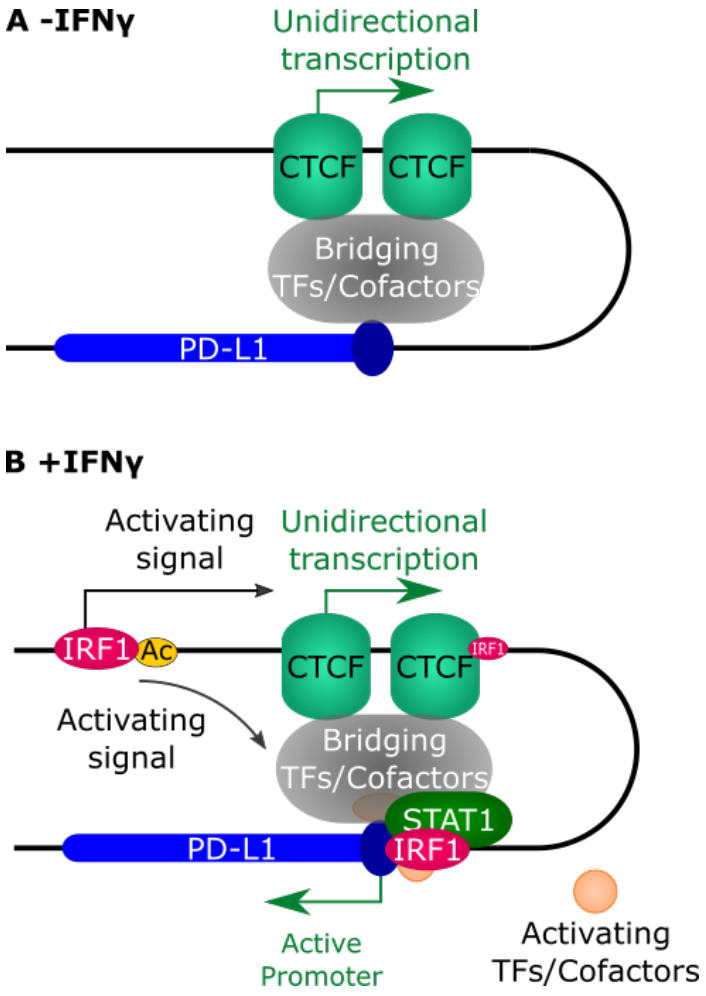

Figure 3.31: Model: A distal regulatory element regulates IFNγ upregulation of PD-L1.
A In untreated Hep3B cells, the PD-L1 promoter interacts with downstream CTCF binding sites. PD-L1 is unexpressed. **B** Treatment with IFNγ results in binding of IRF1 and STAT1 to the PD-L1 promoter and IRF1 to a regions nearby the interacting CTCF sites. This binding spreads activating signals, i.e. histone acetylation, and activating TFs and cofactors to the promoter, upregulating PD-L1 expression.

3.2.10 CRISPR-Cas9 KOs of potential IFNγ-inducible PD-L1 regulatory elements

Combining transcriptional, epigenetic, higher-order chromatin structure and STAT1/IRF1 TF binding data presented multiple possible regulatory elements controlling IFNγ-induced PD-L1 expression. To obtain more conclusive data, CRISPR-Cas9 KO experiments were designed to delete these putative enhancer elements to access their effect on IFNγ-induced upregulation of PD-L1 mRNA expression. To this end, five loci were selected for deletion; the PLGRKT promoter, the IRF1 binding site upstream of the PD-L1 promoter, the CTCF binding site showing interactions to the PD-L1 promoter, the IRF1 binding site adjacent to this CTCF site, and the differential ATAC-seq peak upstream of RIC1 (1, 2, 4, 3 and 5 respectively in Fig:3.32). Additionally, combinations of the aforementioned regions were targeted, deleting larger regions of DNA (6 and 7 in Fig:3.32). These cell lines will be named Del1-7 for the remainder of this thesis.

In my experience, Hep3B cells have a doubling time of approximately 48 hrs. The process of growing puromycin-selected transfected cells, serially diluting them and growing them from a single cell required 4 months of uninterrupted care. Due to the coronavirus pandemic, departmental closure and constant risk of the requirement to self isolate, being in the laboratory continuously for this length of time was extremely challenging.

Del1-3, 5 and 7 were all grown from a single puromycin-selected cell. PCR primers were designed to amplify the target region of DNA. Following PCR amplification, DNA containing the desired deletion produced a short PCR product, whilst WT DNA produced a long PCR product, each of known length specific to the target. PCR tests revealed that, unfortunately, a homozygous population of any target was not obtained (Fig:3.33 & 3.34). Both WT and a deleted DNA product was identified

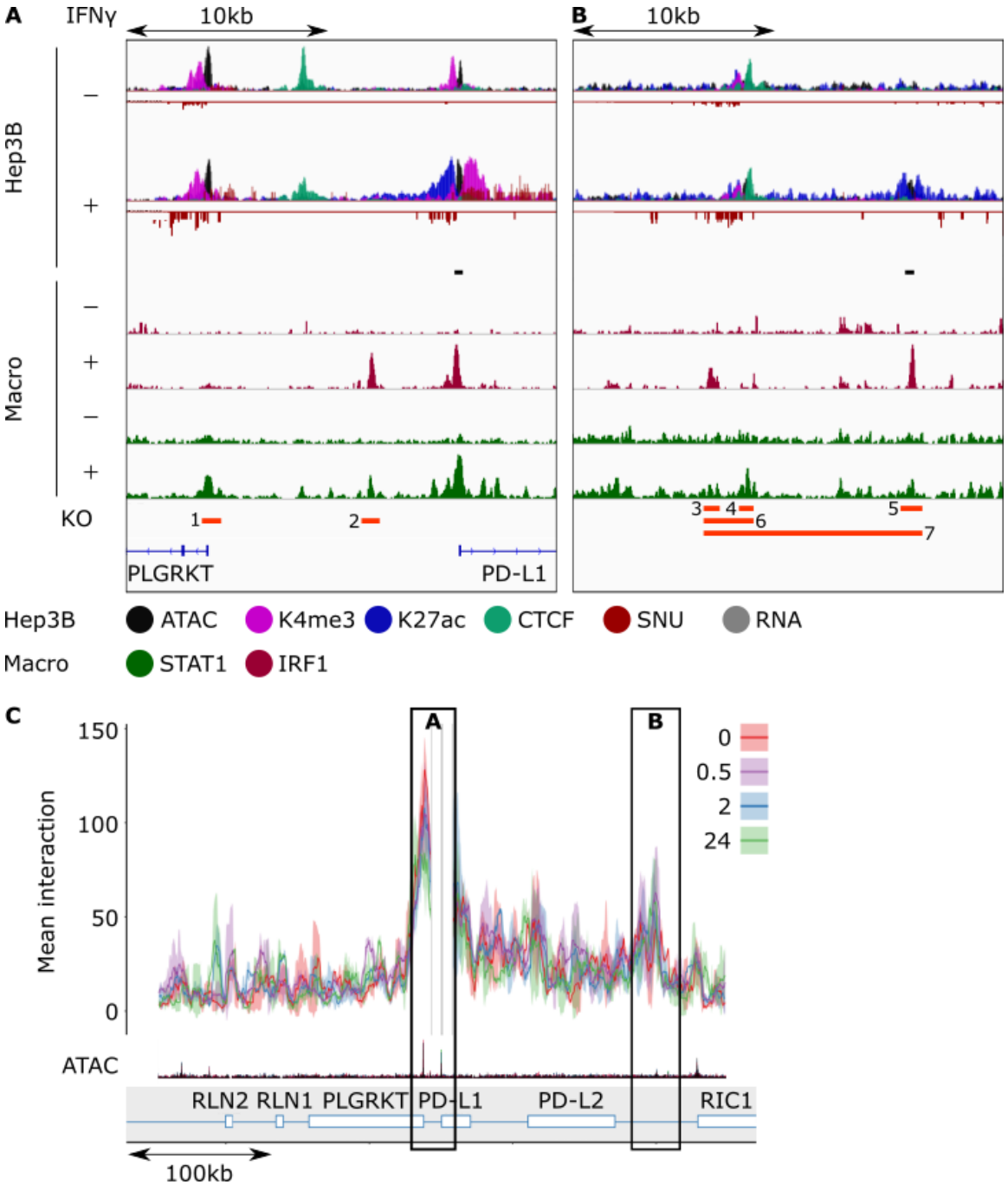

Figure 3.32: CRISPR-Cas9 KO design.
A & B Hep3B cells and published macrophage data. The top two tracks show Hep3B DNA accessibility (black), ChIP profiles of H3K27ac (blue), H3K4me3 (purple) and CTCF (turquoise), strand-specific SNU-seq data (red) and 3'-end RNA-seq (grey) data for untreated and 24 hr IFNγ treated cells (n=2-3). Black bars represent significant increases in DNA accessibility. The following tracks (top to bottom) show published macrophage ChIP-seq profiles of IRF1 (pink) and STAT1 (green). Orange bars numbered 1-7 represent regions of interest to be deleted. **C** Shows the location of data in **A & B** relative to the Capture-C results, signified by the black boxes.

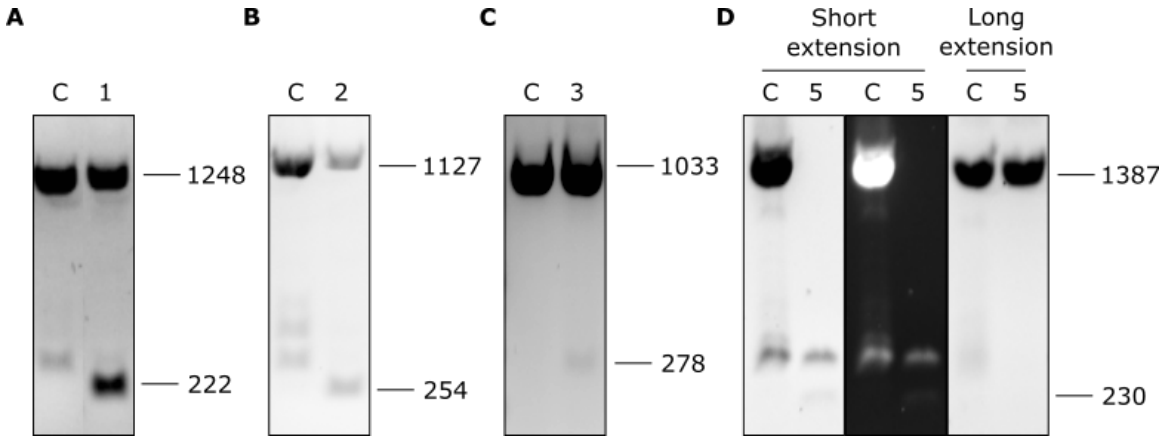

Figure 3.33: CRISPR-Cas9 KO PCR test reveals heterozygous populations.
A - D PCR tests amplifying long WT fragments of DNA and short deleted DNA sequences in Del1 (**A**), Del2 (**B**), Del3 (**C**) and Del5 (**D**). The left lane of each gel is amplified WT control gDNA, the right lane is amplified gDNA from each CRISPR-Cas9 KO cell line. Short fragments present in the right lane but not present in the left control lane represent the desired delete. Long fragments corresponding to that seen in WT cells represent undesired WT DNA still present in the CRISPR-Cas9 KO population. Longer extensions in **D** were required to amplify the WT DNA sequence in Del5. An inverted gel in (**D**) is shown to see the shorter fragment more clearly. Each cell line tested is heterozygous for WT and CRISPR-Cas9 deleted DNA.

for each, meaning either a population of both WT and KO cells were present, or cells were heterozygous for the deletion. Del1, Del2 and Del7 showed a good enrichment for the desired KO, whilst in Del3 and Del5 a deleted fragment could only just be visualised. All transformations should be repeated in the future in order to obtain a homozygous population.

As Del7 deleted a region of approximately 11kb, three different primer pairs were used to test for WT DNA (Fig:3.34). Using primers to amplify the full 11kb of WT DNA did not identify this non-deleted region in Del7. A band at 11kb in the control suggests that the PCR reaction worked. Given the difficulty of amplifying a long DNA sequence, primers amplifying shorter regions of WT DNA were used (Fig:3.34D). Primers 2 amplified the WT DNA sequence, albeit to a lesser extent than in the control (Fig:3.34B). Bizarrely, Primers 3 amplified the WT DNA to a

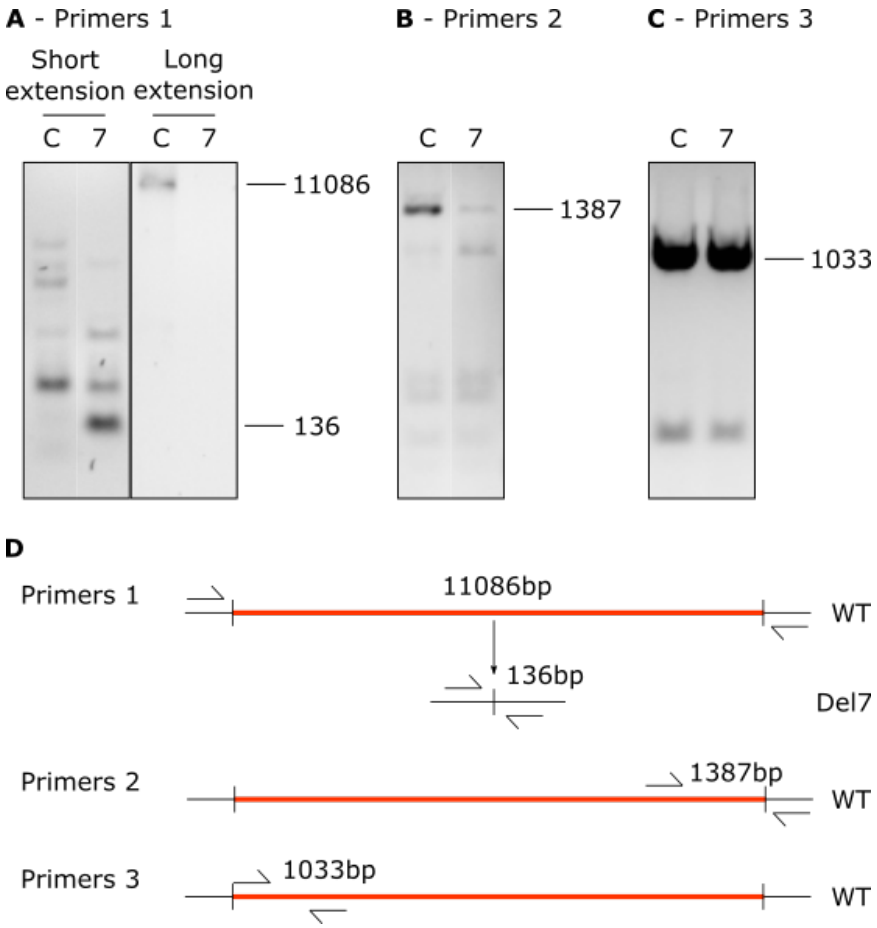

Figure 3.34: CRISPR-Cas9 KO PCR test reveals a heterozygous population in Del7.
A - C PCR tests amplifying long WT fragments of DNA and short deleted DNA sequences in Del7 using three different sets of primers, depicted in (**D**). The left lane of each gel is amplified WT control gDNA, the right lane is amplified gDNA from Del7. Short fragments present in the right lane but not present in the left control lane represent the desired delete. Only Primers 1 (**A**), test for this short fragment. Long fragments corresponding to that seen in WT cells represent undesired WT DNA still present in the CRISPR-Cas9 KO population. Longer extensions in (**A**) were required to amplify the WT DNA sequence in Del5. The desired deleted fragment can be seen in (**A**) with short PCR extensions. WT DNA was not observed with Primers 1 (**A**), was visualised at a lower concentration than the control using Primers 2 (**B**), or was observed at similar concentrations to the control using Primers 3 (**C**).

similar extent in both the control and Del7 (Fig:3.34C). These amplified fragments should be extracted and sequenced to confirm that the correct sequence of DNA has been amplified, rather than a non-specific product. Given the prominent amplification of the desired 136bp deleted fragment using Primers 1 and the minimal amplification of WT DNA using Primers 1 and 2, Del7 cells seem to have a good enrichment for the deletion.

The short deleted fragments were excised from each gel and sequenced. Unfortunately this did not yield enough DNA for Del2, Del3 and Del5. This control should, therefore, be repeated for these cell lines. The fragments present in Del1 and Del7 were confirmed as containing the correct CRISPR-Cas9 deleted sequence.

Although no cell line was homozygous for a deletion, some cell lines had a different phenotype to WT cells; some cells were larger, and others more elongated. Due to their altered phenotype, I decided to continue with a RT-qPCR to analyse any affect on IFNγ-induced PD-L1 expression, despite the cells heterozygous nature. To this end, WT and Del cell lines were left untreated, or treated with 2 hrs and 24 hrs of IFNγ. As seen at the beginning of this chapter, 2 hrs of IFNγ treatment was the first timepoint at which PD-L1 was significantly upregulated in WT Hep3B cells (Fig:3.2A). 24 hrs was additionally chosen to analyse the increased upregulation visualised after longer treatments (Fig:3.2A).

Del1, Del2 and Del7 were assessed due to their good enrichment for a deleted fragment. As in figure 3.2A, WT cells showed significant upregulation of PD-L1 after 2 hrs and 24 hrs of IFNγ treatments (Fig:3.35). Similarly, the three Del cell lines tested also showed significant increases in expression following IFNγ treatments. This suggests that deletion of these regions do not affect IFNγ-induced upregulation of PD-L1.

Del2 cells investigate the role of a region $\sim$4kb upstream of PD-L1's promoter (Fig:3.32). IRF1 was found to bind to this region in macrophages treated with IFNγ

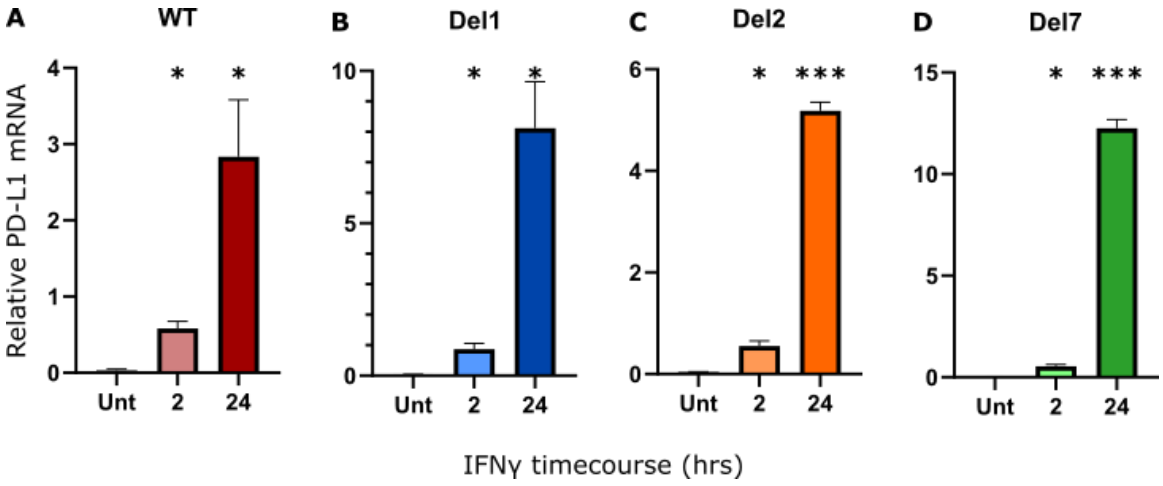

Figure 3.35: RT-qPCR analysing IFNγ-induced PD-L1 mRNA upregulation in different CRISPR-Cas9 KO cell lines
A-C RT-qPCRs showing upregulation of PD-L1 after 2 hrs or 24 hrs of IFNγ treatments, in WT (**A**), Del1 (**B**), Del2 (**C**) and Del7 cells (**D**). Relative expression is normalised to β-actin mRNA (n=3) and measured using the $2^{-\Delta\Delta Ct}$ method. Significance was calculated against the untreated sample: * P≤0.05, ***P≤0.001. All cell lines significantly upregulated PD-L1 expression when treated with 2 hrs and 24 hrs of IFNγ.

(Fig:3.27). In Hep3B, this locus lacks a peak of accessibility and H3K27ac at this site, so it is possible that IRF1 does not bind to this region in Hep3B cells. This would explain why deleting this region had no effect on IFNγ-induced PD-L1 expression (Fig:3.35).

The PD-L1 promoter interacts with a downstream locus between PD-L2 and RIC1. Del7 cells were produced to access whether this region was acting as an enhancer element involved in IFNγ-dependent PD-L1 expression (Fig:3.32). Again, cells containing this delete were still able to significantly upregulate PD-L1 mRNA expression from 2 hrs of IFNγ treatments, indicating that this site does not regulate PD-L1 in Hep3B cells (Fig:3.35).

Finally, Del1 cells were used to examine whether the PLGRKT promoter, which interacts with the PD-L1 promoter (Fig:3.32), used ePromoter activity to induce PD-L1 expression upon IFNγ treatments. IFNγ treatment significantly upregulated PD-L1 expression in Del1 cells, suggesting that PLGRKT is not an ePromoter for

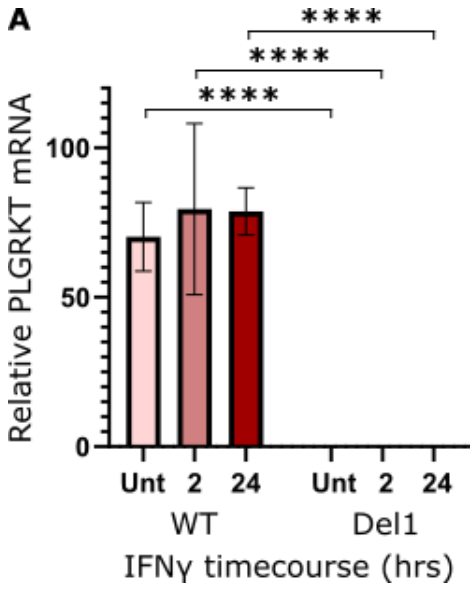

Figure 3.36: RT-qPCR analysing PLGRKT mRNA expression in WT or Del1 cells.
A-C RT-qPCRs showing mRNA expression of PLGRKT in WT or Del1 cells, with or without IFNγ treatments. Relative expression is normalised to β-actin mRNA (n=3) and measured using the $2^{-\Delta\Delta Ct}$ method. Significance was calculated between Del1 and corresponding WT cells: ****P$\leq$0.0001. Expression of PLGRKT mRNA was not observed in Del1 cells.

PD-L1 (Fig:3.35).

Given that none of these cell lines were homozygous for the deletion, it is possible that the WT DNA present is still able to significantly upregulate PD-L1 expression after treatment with IFNγ (Fig:3.33 & 3.34). Thus one cannot conclusively rule out these regions as IFNγ-dependent regulatory elements of PD-L1. The experiment should therefore be repeated on homozygous populations of each repeat.

However, one additional control was performed for Del1; a RT-qPCR analysing the expression of PLGRKT mRNA in WT Hep3B and Del1 cells. PLGRKT is constitutively transcribed in WT Hep3B cells (Fig:3.18). Del1 deletes the PLGRKT promoter, additionally deleting exon 1 and parts of exon 2. In theory, fully deleting this region should obliterate expression of PLGRKT. qPCR primers were designed to amplify the PLGRKT CDS within exons 3-6. In WT Hep3B cells, PLGRKT

was constitutively expressed under any condition tested (Fig:3.36). Remarkably, no PLGRKT mRNA expression was detected in Del1 cells indicating that this KO fully inactivates the PLGRKT promoter. Combining these results, that PD-L1 expression is significantly induced whilst PLGRKT is unexpressed, one can more confidentially argue that the PLGRKT promoter is not an ePromoter involved in regulating IFNγ-dependent PD-L1 expression (Fig:3.35 & 3.36).

Taken together, the results from this section demonstrate that IFNγ-induced PD-L1 expression may not require an enhancer but, instead, the proximal promoter region may be sufficient to induce PD-L1 expression.

3.3 Discussion

3.3.1 Using Hep3B cells to examine IFNγ-inducibility of PD-L1

IFNγ in the tumour microenvironment has been found to upregulate PD-L1, an immunoinhibitory ligand, resulting in cancer immune evasion [Yan et al., 2020]. Positive correlations between PD-L1 and IFNγ expression have been identified suggesting a role for induced, contrary to constitutive, upregulation of PD-L1 in cancers [Xie et al., 2016]. Aberrant PD-L1 signalling has additionally been implicated in other disease states including autoimmune disease, chronic infection, and more recently, severe Covid-19 [Qin et al., 2019, Vivarelli et al., 2021]. An improved understanding of IFNγ-induced PD-L1 upregulation is highly desired to advance therapies towards these diseases.

To this end, I sought a human cell line in which to study the IFNγ-inducibility of PD-L1. The perfect cell line would be of cancerous origin and show a large and significant IFNγ-induced upregulation of PD-L1 at both the transcriptional and protein level. In untreated cells PD-L1 should be unexpressed to prevent constitutive activating signals from masking inducible signals.

Multiple publications have found Hep3B, a human HCC cell line, to massively upregulate PD-L1 expression in response to IFNγ treatments [Li et al., 2017, Zou et al., 2018], as discovered in this study. HCCs are frequently diagnosed too late for curative treatment and thus improved therapies are required for this cancer type. PD-L1 is commonly detected in the tumour microenvironment of a HCC patient, highlighting the importance of understanding PD-L1 expression within hepatocytes [Zhou et al., 2017, Chang et al., 2017]. Hence, Hep3B cells were chosen for the analysis of IFNγ-induced PD-L1 expression in this thesis. My results confirmed

the sensitivity of this cell line to IFNγ, strongly inducing pSTAT1, IRF1 and PD-L1 transcription and protein levels. Furthermore, PD-L1 was not transcribed in untreated cells, and known enhancers involved in constitutive PD-L1 expression showed no activity in both untreated and IFNγ treated cells.

3.3.2 Assessing necessary and sufficient signals required for IFNγ-induced PD-L1 expression

Large bodies of evidence suggest that the JAK/STAT1/IRF1 pathway is vital for IFNγ-induced PD-L1 expression [Garcia-Diaz et al., 2017, Li et al., 2017, Moon et al., 2017, Mimura et al., 2018, Yan et al., 2020]. IRF1 has been found to bind to the PD-L1 promoter upon treatment with IFNγ. Overexpression of IRF1 upregulates PD-L1, whilst deletion of the IRF1 binding motifs at the promoter diminishes IFNγ-induced PD-L1 expression in multiple cell types [Li et al., 2017, Yan et al., 2020]. Altogether, literature has highlighted IRF1 as the major TF directly driving PD-L1 upregulation by IFNγ.

Four diverse cell lines were subjected to IFNγ treatments; Hep3B, GM12878, HeLa and Hek293, a HCC, B-lymphocyte, cervical cancer and a non-cancerous cell line respectively. IFNγ treatments upregulated pSTAT1 and IRF1 in each cell line, with similar kinetics. Despite all cell lines showing sensitivity towards IFNγ, each displayed a different response in regards to the expression of PD-L1 (Fig:3.37).

GM12878 constitutively expressed PD-L1 and IRF1 protein (a very faint band of IRF1 was present in the WB in the untreated sample). When treated, PD-L1 mRNA levels were marginally increased from 2 hrs, whilst PD-L1 protein levels remained stable with or without IFNγ treatments. It is possible that high constitutive quantities of PD-L1 masked IFNγ-induced increases.

HeLa cells significantly upregulated PD-L1 mRNA from 4 hrs of IFNγ treatment. Surprisingly, this did not equate to upregulated PD-L1 protein at the plasma

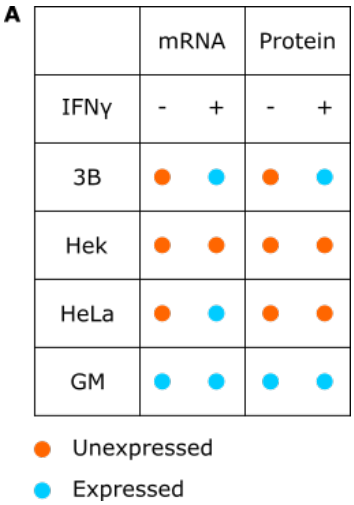

Figure 3.37: IFNγ-induced PD-L1 mRNA and protein expression in different cell lines.
A An overview of PD-L1 mRNA and protein expression at the plasma membrane, with or without IFNγ treatment in four different cell lines; Hep3B (3B), Hek293 (Hek), HeLa and GM12878 (GM).

membrane, as determined by flow cytometry analysis, revealing additional layers of regulation between mRNA and protein (Fig:3.37). Unpublished data from our lab reveals an unexpected lack of correlation between mRNA and protein levels within yeast. It is possible that similar mechanisms exist in mammalian cells, preventing increased protein synthesis from corresponding increased mRNA levels. Due to its role in autoimmunity and disease, PD-L1 expression must be tightly controlled, thus signifying the importance of multiple regulatory processes. An alternative possibility is that HeLa expresses a truncated form of PD-L1 resulting in soluble expression, rather than expression on the plasma membrane. Regardless, it reveals that not all cancer cell lines express PD-L1 at the plasma membrane in the presence of IFNγ signalling.

Interestingly, Hek293 cells did not express PD-L1 mRNA or protein under any condition tested (Fig:3.37). IRF1 protein was observed following 2 hrs of IFNγ treatment. The presence of IRF1 in Hek293 exemplifies that IRF1 is not sufficient to

upregulate PD-L1. Additional experiments would be required to determine if IRF1 was necessary for IFNγ-induced PD-L1 expression in Hep3B cells.

This poses a key question: What is necessary and sufficient for IFNγ-induced PD-L1 upregulation? Several possibilities exist; particular TFs required, certain epigenetic states, activity of regulatory elements, specific higher-order chromatin structure. Visualising publicly available ENCODE data on the UCSC genome browser (http://genome.ucsc.edu) showed a peak of accessibility, H3K4me3 and H3K27ac at the PD-L1 promoter in each cell line (GM12878, HeLa and Hek293), similar to that seen in untreated Hep3B cells [Dunham et al., 2012]. Thus, these features are unlikely to determine the IFNγ-inducibility of PD-L1.

As well as activating features, many inhibitory mechanisms may be in place within Hek293. Insulators and silencing epigenetic modifications are known to inhibit activation of a gene. Certain TFs may repress activation, for example, the transcriptional repressor BLIMP1 was suggested to antagonise IRF1-dependent activation of genes [Mould et al., 2015]. Further research should be performed to discover which features prevent/enable induction of PD-L1 by IFNγ signalling. Identifying the necessary and sufficient properties required would shed light on how a cancer cell evolves to enable PD-L1 induced expression and may provide targets for cancer therapies.

3.3.3 How does IFNγ signalling upregulate IRF1 expression

Treating Hep3B cells with IFNγ led to significant and substantial transcriptional upregulation of IRF1 within 30 min. This gene activation was accompanied by transcriptional activation of the upstream putative enhancer element. STAT1 binding motifs were identified within peaks of accessible DNA at the promoter and enhancer elements. ChIP-seq performed in macrophages found bound STAT1 overlapping these regions upon stimulation with IFNγ. STAT1 is widely accepted to drive IFNγ-induced

upregulation of IRF1 [Castro et al., 2018]. Taken together, it is extremely likely that STAT1 binds to both the promoter and enhancer in Hep3B cells upon IFNγ treatments, stimulating transcription of both elements.

STAT1 has been shown to interact with and recruit acetylation writers, CBP and p300 [Zhang et al., 1996, Ramsauer et al., 2007, Qiao et al., 2013]. Indeed, a notable increase in H3K27ac was seen at both the IRF1 promoter and putative enhancer region. Histone acetylation weakens histone:DNA contacts resulting in more open and transcriptionally permissive chromatin. This provides a mechanism by which STAT1 induces bidirectional transcription at these loci.

Further, the STAT1 binding sites overlap with the peak of promoter:enhancer interaction observed within the Capture-C data, suggesting its potential involvement in bridging this interaction. The interaction between the IRF1 promoter and putative enhancer provides extremely strong evidence that this region is indeed the enhancer involved in IFNγ-induced upregulation of IRF1.

Within 30 min of IFNγ treatment, STAT1 likely binds accessible sites at the promoter and enhancer, histone acetylation occurs, interactions between the two elements are increased and bidirectional transcription at both elements are activated (Modelled in Fig:3.17). The order in which these events occur and the causality, if any, of each in upregulating gene transcription requires further research. The effect of IFNγ signalling on higher-order chromatin structure will further be discussed in section 4.3.4.

3.3.4 How does IFNγ signalling upregulate PD-L1 expression

Transcription of PD-L1 was initially observed after 2 hrs of IFNγ treatments in Hep3B cells. This corresponds to the earliest time point at which IRF1 protein expression was witnessed. Together with evidence from the literature, this suggests that IRF1 is a major driver of IFNγ-induced PD-L1 expression [Garcia-Diaz et al., 2017,

Li et al., 2017, Moon et al., 2017, Yan et al., 2020]. However, IFNγ-induced Hek293 cells expressed IRF1 but did not result in PD-L1 expression, as discussed in section 3.3.2. Therefore, additional features must be required for PD-L1's induced expression. Possibilities include that IRF1 is unable to bind to the PD-L1 promoter in Hek293 cells, or that IRF1 binds but other factors, such as particular TFs, epigenetic modifications or regulatory elements required are not present. Alternatively, inhibitory mechanisms such as silencing chromatin modifications or insulator elements could prevent activation of this gene in Hek293 cells. In this thesis I was interested in investigating whether particular enhancer elements were required for IFNγ-induced upregulation of PD-L1.

Unlike in Hek293 cells, Hep3B cells treated with IFNγ resulted in the upregulation of PD-L1 expression. Correspondingly, the PD-L1 promoter showed increased DNA accessibility, H3K27ac and bidirectional transcription. Unlike IRF1, no obvious enhancer element for PD-L1 could be identified. Capture-C assessing interactions to the PD-L1 promoter revealed strong interactions to the nearest gene promoter; PLGRKT. A low level of interaction could additionally be seen to a downstream region between PD-L2 and RIC1. Virtually no interactions were found elsewhere in the genome. Thus these loci were examined as potential regulatory elements to PD-L1. Poised promoter:enhancer contacts may undergo rapid activation following environmental cues, such as pSTAT1 and IRF1 binding.

Firstly, the PD-L1 promoter constitutively loops to the PLGRKT promoter. Promoters share many traits with enhancers; they both provide factors and chromatin features that create a transcriptionally permissive environment [Koch et al., 2011]. Indeed, promoters have been found to act as enhancers (termed ePromoters) whereby they regulate activity of neighbouring genes [Engreitz et al., 2016, Dao et al., 2017, Diao et al., 2017]. A subset of ePromoters has been implicated in stress responses, including interferon signalling [Dao et al., 2017]. The PLGRKT promoter was active

and possessed numerous features common to both promoters and enhancers; a peak of accessible DNA, H3K27ac and bidirectional transcription. However, these features, and its interaction with the PD-L1 promoter, is present in untreated cells. The lack of cooperativity between the two promoters contradicts the role of PLGRKT as an ePromoter for IFNγ-induced PD-L1 upregulation. ChIP-seq data within macrophages identified binding of both IRF1 and STAT1 to the PD-L1 promoter upon addition of IFNγ treatments. A small peak of STAT1 also bound to the PLGRKT promoter after the treatment. Binding of these TFs may complete the link between the two promoters, enabling communication of transcriptionally facilitative features and activating expression of PD-L1 (Fig:3.29). However, a Hep3B cell line containing a delete of the PLGRKT promoter was still able to significantly upregulate PD-L1 following IFNγ treatments, despite complete loss of PLGRKT expression. This indicates that the PLGRKT promoter has no role in IFNγ-induced PD-L1 upregulation. Alternatively, the interaction between the two promoters could simply be a consequence of PD-L1 looping to the nearest open region of DNA, without any causality.

The PD-L1 promoter additionally interacts, albeit less intensely, to a region approximately 150kb downstream of the promoter, between PD-L2 and RIC1. A second alternative is that this region forms a regulatory element targeting PD-L1 (Fig:3.31). The interacting region overlaps two adjacent CTCF peaks. Unidirectional transcription stemmed from the 3'-CTCF peak and was accompanied by a small peak of H3K4me3. CTCF is often associated with TAD boundaries and insulator elements [Szabo et al., 2019, Klein and Hainer, 2020]. However, CTCF has also been found at promoters and enhancers and has been suggested to aid loop formation between the two [Melgar et al., 2011, Ren et al., 2017]. Additionally, cases of unidirectional transcription at enhancers have been demonstrated, thus raising the possibility that this region may act as an enhancer for PD-L1 expression [Catarino and Stark, 2018].

As with the PLGRKT promoter, this CTCF region does not show IFNγ-induced changes for any feature analysed, including no increased interaction to the PD-L1 promoter.

A region approximately 8kb downstream of this CTCF site significantly increased in DNA accessibility after 24 hrs IFNγ treatments. An increase in H3K27ac was visualised at this site but was not significant. The macrophage IRF1 ChIP-seq data identified peaks of IRF1 bound to sites overlapping the differential ATAC-seq peak, and within 2kb of the CTCF site, upon treatment with IFNγ. Binding of IRF1 to these sites, in addition to the PD-L1 promoter, may provide the necessary signals to express the gene (Fig:3.31). If validated to regulate PD-L1, this regulatory element would be unorthodox, with little acetylation and no bidirectional transcription. Although H3K27ac is a common feature of enhancers, other sites for histone acetylation exist and have been linked to enhancer activation. Furthermore, active enhancers lacking H3K27ac have been identified [Pradeepa et al., 2016, Catarino and Stark, 2018]. Modified cells deleting this differential accessibility peak in addition to the upstream CTCF did not hamper IFNγ-induced expression of PD-L1. This suggests that this region does not regulate IFNγ-dependent PD-L1 upregulation, although this should be reassessed in a homologous KO cell line.

Virtually no other interactions genome-wide were identified to the PD-L1 promoter. It is possible that the Capture-C experiment is biased to capturing regions of DNA in close sequence proximity, as opposed to spatial proximity. In theory, this should not be the case, however, not enough research has been performed to validate this.

With minimal gene loops identified, the final proposed possibility is that no disparate regulatory element is required for IFNγ-induced upregulation of PD-L1 (Fig:3.28). In this scenario, all factors required for permissive transcription would be

present within the proximal promoter of PD-L1. Indeed, IRF1 was found to bind in an IFNγ-dependent manner to both the PD-L1 promoter and to a proximal region approximately 4kb upstream. Hundreds of TF binding sites are present within the proximal promoter site which, hypothetically, may provide enough activating signal to induce PD-L1 expression. This would explain a lack of differential interactions to the PD-L1 promoter, the lack of altered activity at the interaction loci, or the significant induction of PD-L1 in the CRISPR-Cas9 cell lines produced in this thesis.

Research into constitutive expression of PD-L1 identified numerous cell-type specific PD-L1 enhancers, none of which were active in treated or untreated Hep3B cells [Green et al., 2012, Sumimoto et al., 2016, Chen et al., 2018b, Hsu et al., 2018b, Zhu et al., 2018b, Xu et al., 2019]. Particular cell types in which PD-L1 is constitutively expressed may, therefore, constantly form interactions with these enhancer elements. IFNγ treatments were found to upregulate PD-L1 expression despite constitutive expression in GM12878 cells (this study) and other cell lines [Chen et al., 2018b]. Thus, removing the necessity of a promoter:enhancer loop for IFNγ-induced expression may enable this signal to upregulate PD-L1 beyond its constitutive expression, without disrupting previously established interactions. This may enable numerous cell types to respond to IFNγ in diverse scenarios.

As with a lot of science, proving a negative, in this case a lack of enhancer element, is extremely challenging. Repeating the CRISPR-Cas9 experiment to obtain homozygous KOs of each potential enhancer region would help elucidate which, if any, of these postulations are correct. All three theorems hint at an unorthodox mechanism of PD-L1 regulation. An improved understanding of which may identify novel mechanisms of gene induction, in addition to helping develop PD-L1 cancer therapies.

Chapter 4

IFNγ signalling causes large scale global changes to the transcriptional, epigenetic and enhancer landscape in Hep3B cells

4.1 Introduction

4.1.1 The IFNγ paradox in the tumour microenvironment

IFNγ, a type II interferon, has an important role in regulating the innate and adaptive immune system to maintain a healthy cellular state. Its primary function is to activate the immune system to fight infected, damaged or cancerous cells. Its expression is restricted almost exclusively to immune cells, such as T lymphocytes, NK cells and macrophages. Despite this, its receptor proteins, IFNGR1/IFNGR2, are expressed by most cell types, enabling response to IFNγ signalling in a diverse range of cells [Ivashkiv, 2018, Barrat et al., 2019]. Recognition of IFNγ results in a

cell-type specific response.

As extensively discussed in section 1.2, IFNγ signalling can have both anti- and pro-tumour effects in a tumour microenvironment (Fig:1.1, Section 1.2). Upon immune recognition of a tumour, IFNγ is expressed. Principally, IFNγ signalling promotes the destruction of a cancer, increasing antigenicity and decreasing proliferation of tumour cells, recruiting immune cells and activating the correct immune response [Street et al., 1997, Li et al., 2012, Zaidi, 2019]. However, many scenarios have been observed whereby IFNγ signalling has opposing effects, encouraging tumour growth [Zaidi, 2019]. The outcome of IFNγ signalling appears to be context dependent, with the amalgamation of signals present in the tumour microenvironment acting in synergy to define the response. Mechanisms by which IFNγ stimulates varying responses is not well understood and further research is required to accurately predict the specific outcome of IFNγ signalling in a cancer patient.

4.1.2 IFNγ as a cancer therapy

Unsurprisingly, with its cancer stunting capabilities, IFNγ administration has been assessed as a cancer therapy in multiple clinical trials. Initial results were promising, showing positive clinical responses in multiple cancer types [Windbichler et al., 2000, Zaidi, 2019]. However, further trials found insignificant or negative responses and adverse effects, perhaps due to the conflicting roles of IFNγ [Zaidi, 2019]. Multiple clinical trials using IFNγ as a therapeutic agent either alone or in combination are still ongoing. A more complete knowledge of IFNγ signalling in the tumour microenvironment under certain contexts may elucidate when IFNγ will favour an anti- or pro- tumour response, and thus aid in the development of IFNγ based cancer therapies.

4.1.3 IFNγ induces widespread cellular changes

To better comprehend the effects of IFNγ within the tumour environment one must first consider the direct effects of interferon signalling on specific cell types. IFNγ causes large transcriptional, epigenetic and enhancer landscape changes. Some of these changes are rapid and short lived, becoming reversed even upon continuous IFNγ exposure. Other changes are more permanent, lasting despite withdrawal of the type II interferon [Ostuni et al., 2013, Kang et al., 2017]. These long-lived changes provide a transcriptional memory and can enable a stronger and faster response to second stimulation [Ostuni et al., 2013, Siwek et al., 2020]. This allows rapid protection against infection but can also result in hyper inflammation and subsequent tissue damage. An in-depth understanding of these differential landscapes is becoming a focus of research due to the role of IFNγ in cancer therapies. Most research focuses on the effects of IFNγ on immune cells, predominantly macrophages. Whether these mechanisms are transferable to non-haematopoietic cells isn't well understood.

IFNγ causes large changes in accessibility and acetylation on histones H3 and H4, both at gene promoters and intergenic elements [Qiao et al., 2013]. Many of these changes occur at loci poised with open chromatin. Certainly in macrophages, differential chromatin modifications overlap with regions prebound by the lineage-determining TF, PU.1, and the C/EBP family of proteins [Qiao et al., 2013, Mancino et al., 2015, Ivashkiv, 2018]. This open chromatin allows rapid binding of IFNγ-upregulated TFs. Numerous rapidly induced *de novo* alterations on chromatin have been observed [Ostuni et al., 2013].

IFNγ signalling leads to the recruitment of KATs and chromatin remodelers, such as CBP and BRG1, which create more transcriptionally permissive epigenetic states and result in the activation of IFNγ-stimulated genes

[Ni et al., 2008, Chen and Ivashkiv, 2010, Qiao et al., 2013, Kang et al., 2017]. Not all chromatin modifications observed by IFNγ treatments result in alterations of gene transcription and are essentially 'silent' changes. Instead these differential regions prime the cells for activation by other stimuli, such as TLR4, perhaps explaining the cooperativity often seen between IFNγ and other signalling molecules. These primed regions enable a larger and more rapid response to environmental changes [Qiao et al., 2013]. They may also factor as to why IFNγ can warrant different outcomes based on the cellular context.

IFNγ additionally represses multiple genes and can make them refractory to activation from other stimuli [Qiao et al., 2016, Piccolo et al., 2017]. In macrophages, IFNγ was found to target MAF bound enhancers for repression [Kang et al., 2017]. It can also induce H3K27me3 deposition, a well characterised silencing mark, via the recruitment of components of the PRC2 complex [Qiao et al., 2016]. Many anti-inflammatory genes are downregulated by this mechanism. Overall, exposure to IFNγ results in a differential transcription programme within the cell.

4.1.4 The role of pSTAT1 and IRF1 in IFNγ signalling

Binding of IFNγ to its receptor activates the JAK/STAT pathway, predominantly phosphorylating and subsequently activating STAT1 over other STATs. pSTAT1 dimerises and translocates to the nucleus where it binds to GAS motifs and modifies both the chromatin and enhancer landscape to alter the cells transcriptional programme. It upregulates a small number of genes including TFs such as IRF1 and IRF8. These IRF family members are amongst multiple TFs that bind to STAT1 and redirect its DNA binding properties, increasing its binding repertoire [Ostuni et al., 2013, Langlais et al., 2016, Abou El Hassan et al., 2017]. Indeed, motifs associated with bound STAT1 shift from GAS elements under short IFNγ-stimulations towards motifs associated with IRF protein binding after long

IFNγ exposures. The IRF proteins themselves can additionally bind regions of DNA independently of STAT1 [Abou El Hassan et al., 2017]. It is the combination of STAT and IRF proteins working independently or together that account for the majority of the IFNγ-induced differential epigenetic, enhancer and transcriptional milieu.

Mechanistically, both STAT and IRF proteins recruit chromatin remodellers, TFs and cofactors to regions of DNA thus varying gene expression. STAT1 binding shows good correlations to IFNγ-induced acetylation changes and has been found to recruit the KATs CBP and p300 in numerous cell types [Zhang et al., 1996, Ramsauer et al., 2007, Qiao et al., 2013]. Correlations have been identified between histone acetylation changes and IRF1/8 and IRF1 was found to coimmunoprecipitate with CBP and p300, as well as Pol II [Ramsauer et al., 2007, Langlais et al., 2016, Leung et al., 2019]. However, this could be due to their ability to recruit STAT1. Only approximately 25% of identified IRF1 binding peaks lacking concomitant STAT1 binding induced writing of acetylation [Abou El Hassan et al., 2018]. This suggests that particular environmental cues were required for IRF1-associated deposition of acetylation. Mutational studies found STAT1 was required for chromatin remodelling by BRG1, a catalytic subunit of the SWI/SNF complex [Christova et al., 2007]. Together this exemplifies the means by which these TFs drive IFNγ-mediated signalling.

4.1.5 Aims

Although initial studies have been performed in monocytes/macrophages, little information is known about IFNγ-induced transcriptional, epigenetic and enhancer landscapes within cancer cells. By gaining an increased understanding of the effects of IFNγ on the tumour microenvironment population, one might better predict whether IFNγ is likely to have a positive or undesirable effect in cancer. This chapter analyses the genome wide effects of IFNγ on the HCC cell line, Hep3B.

To this end, several -omics techniques examining DNA accessibility, transcript levels, active transcription, histone modifications, binding of CTCF, and higher-order chromatin structure are performed. I find that IFNγ induces the expression of hundreds of genes. Remarkably thousands of intergenic elements are regulated, indicating that substantially more enhancers than genes are modulated by IFNγ. Furthermore, IFNγ treatments are shown to rapidly increase promoter:enhancer contacts, demonstrating higher-order chromatin structure as another regulatory layer.

I show that IFNγ treatments affect both gene expression and enhancer modification in distinct and dynamic phases over the course of 24 hrs, showing a shift from the enrichment of STAT1 binding motifs to IRF1. The shift not only regulates a new faction of IFNγ-stimulated elements but rapidly curtails early changes made.

Finally, I find an uncoupling between transcription and histone modifications; H3K4me3 and H3K27ac. This suggests that these relationships are not as clear-cut as currently thought, with either modification not necessarily resulting in increased transcription or vice versa. Therefore multiple layers of regulation must operate to obtain the coordinated expression of IFNγ-induced gene expression.

4.2 Results

4.2.1 IFNγ induces widespread gene transcriptional changes in Hep3B cells

The presence of the inflammatory cytokine, IFNγ, in the tumour microenvironment induces expression of a host of IFNγ stimulated genes in multiple cell types. It acts on both the immune system and other cell types to maintain cell fitness. It does this by upregulating and downregulating multiple cellular pathways through differential gene expression, modulating the immune response. Despite most cells expressing the IFNγ receptor, different cell types show different responses to IFNγ, as demonstrated in Figure 3.5, 3.6 & 3.7 (Section 3.2.2). To gain a better understanding of the direct effects of IFNγ on cancer cells, IFNγ treatments on Hep3B cells were studied. IFNγ signalling in Hep3B cells results in phosphorylation of STAT1 and consequent expression of IRF1 (Fig: 3.1, Section 3.2.1.1). Together these TFs drive the majority of the IFNγ response.

4.2.1.1 3'-end RNA-seq identifies IFNγ-stimulated genes in Hep3B cells

4.2.1.1.1 IFNγ treatments upregulate over 100 genes

Firstly, genome-wide gene expression changes were analysed using 3'-end RNA-seq. Cells treated with IFNγ for 0.5 hrs, 2 hrs or 24 hrs were compared to untreated cells to examine the early, intermediate and late responses. IFNγ significantly altered the expression of 132 genes in Hep3B cells under the conditions tested (Fig:4.1A). Only one gene, IRF1, is significantly upregulated by IFNγ after 30 min. This increases to 23 IFNγ-induced genes by 2 hrs. A further 109 genes are differentially expressed by 24 hrs of IFNγ treatment. This nicely demonstrates an early response resulting in the upregulation of a handful of genes, followed by a larger late response. Approximately

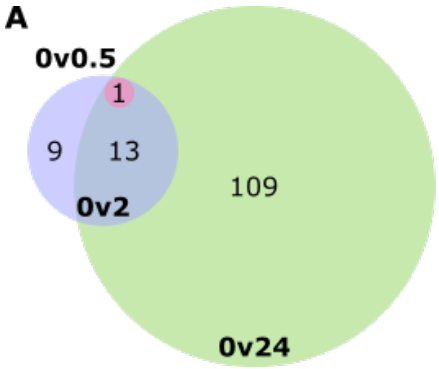

B

	# of genes	
	↑	↓
0v0.5	1	0
0v2	23	0
0v24	117	6

Figure 4.1: RNA-seq identifies over 100 differentially expressed genes in Hep3B cells upon IFNγ treatments.
A Venn diagram showing overlaps between significant changes in gene expression as measured by RNA-seq (n=3) for each condition; untreated vs 0.5 hrs (pink), 2 hrs (blue) or 24 hrs (green) of IFNγ treatments. **B** Summary of the number of upregulated or downregulated genes per condition; untreated vs 0.5 hrs, 2 hrs or 24 hrs of IFNγ treatment.

60% of the early genes (defined here as significantly different by 2 hrs treatment) are sustained throughout the 24 hr period. Nine genes significantly upregulated by 2 hrs lose significance upon longer treatments, demonstrating bursts of gene expression caused by IFNγ. This may signify negative feedback loops within IFNγ signalling.

Of the 132 differential genes, only six genes were downregulated (Fig:4.1B). Three of these genes are cell receptors and four are involved in activating either the EGRF or TNF pathways. Thus it appears IFNγ may impede particular signalling pathways in this cell line. However, it is clear that, in Hep3B cells, IFNγ predominantly acts by upregulating a number of genes.

4.2.1.1.2 Gene Ontology analysis of differentially induced genes

Unsurprisingly, gene ontology (GO) analysis on 0v24 hrs IFNγ-induced differential gene expression found the biological process - Interferon-gamma-mediated signalling pathway - to be significant (Table: 4.1A). Other significant biological processes identified are related to an immune response as expected. GO analysis of molecular functions (Table: 4.1B) and cellular components (Table: 4.1C) found that 24 hrs of

GO term	Description	q value
A - Biological processes		
GO:0006952	Defence response	$5.51e^{-29}$
GO:0051707	Response to other organism	$2.82e^{-23}$
GO:0006955	Immune response	$2.89e^{-23}$
GO:0060333	IFNγ-mediated signalling pathway	$1.02e^{-14}$
B - Molecular functions		
GO:0030545	Receptor regulator activity	$5.01e^{-7}$
GO:0048018	Receptor ligand activity	$4.21e^{-6}$
GO:0005102	Signalling receptor binding	$1.96e^{-5}$
GO:0005539	Cytokine activity	$5.55e^{-5}$
C - Cellular components		
GO:0005615	Extracellular space	$6.57e^{-17}$
GO:0005576	Extracellular region	$4.87e^{-12}$
GO:0031012	Extracellular matrix	$7.45e^{-9}$
GO:0005886	Plasma membrane	$1.14e^{-7}$

Table 4.1: GO analysis of untreated versus 24 hrs IFNγ treated RNA-seq data.
A-C Gene ontology (GO) analysis of DESeq2 ranked genes comparing 24 hrs IFNγ treated to untreated Hep3B cells analysing biological processes (**A**), molecular functions (**B**) or cellular components (**C**). The top four results (**B & C**) or the top three results and IFNγ-mediated signalling pathway (**A**) are shown.

IFNγ treatment predominantly altered the expression of genes located at the plasma membrane or extracellularly such as receptors or cytokines. Highly upregulated genes include those involved in antigen presentation, such as MHCI subunits and TAP1/2, as well as genes involved in the complement pathway, i.e. C1S, C1R, C2. Given the location and types of genes expressed, these data suggest that a key role of IFNγ in this cancerous cell line is adjusting cell-to-cell signalling. Most genes upregulated, including those listed above, should prime the cell for recognition by the immune system. However, immunosuppressive genes such as PD-L1 are also upregulated and may nullify immune activation even in the presence of immune-activating signals.

4.2.1.2 SNU-seq reveals multiple subsets of differential gene expression upon IFNγ treatments

4.2.1.2.1 IFNγ treatments differentially regulates transcription of hundreds of genes

Although 3'-end RNA-seq provides a good indication of RNA levels in the cell population, it can't distinguish changes in transcription. Cell RNA concentrations are regulated by numerous processes including splicing, export, modifications and degradation, and hence RNA levels don't always correlate with transcriptional changes. SNU-seq is a highly sensitive technique measuring transcription at single-nucleotide resolution (Fig:3.9, Section 3.2.3.2). Due to the short incubations with 4-thiouridine (12 min), transient RNA such as ncRNA is also captured. Where IFNγ treatments induce a burst of gene expression, it is likely that negative feedback loops switch off transcription and additionally result in degradation of the transcript. Thus the ability to sensitively capture active transcription as opposed to full transcripts may better capture ephemeral gene expression. In the previous section, RT-qPCR found that, despite being significant, only very slight upregulations of IRF1 and PD-L1 were seen after 30 min or 2 hrs of IFNγ treatments respectively (Fig:3.2A

& C, Section 3.2.1.1). These timings were therefore chosen to represent early and intermediate responses. As it takes time to express the full transcript captured by 3'-end RNA-seq, many genes, especially longer genes, may not be fully transcribed at the timepoints taken. This could explain why the majority of differential transcript expression is only seen at 24 hrs of IFNγ treatment (Fig:4.1). On the other hand, increases in transcription can almost immediately be detected by SNU-seq. Thus I expected SNU-seq to provide more in-depth information on differential transcription upon IFNγ treatments.

Accordingly, a higher number of significant transcriptional changes were identified by SNU-seq. After addition of IFNγ to Hep3B cells for just 30 min, 94 genes showed significant differential transcription (Fig:4.2). IRF1 was the most significantly upregulated gene at this timepoint with a q-value of $4.26e^{-26}$. Other significantly upregulated early genes include TFs such as NLRC5, a regulator of MHC class I genes [Kobayashi and Van Den Elsen, 2012] as well as negative regulators of the JAK/STAT pathways i.e. SOCS3 [Carow and Rottenberg, 2014]. An additional 104 and 138 genes are differentially transcribed by 2 and 24 hrs of IFNγ treatments respectively when comparing to untreated cells. When comparing, instead, between treatment groups (0.5v2 hrs, 2v24 hrs), fewer changes can be seen (49 and 86 gene changes respectively) (Fig:4.2B). This suggests that IFNγ may begin upregulating a gene at an earlier timepoint, but the change only becomes significant at a later timepoint. As seen in the 3'-end RNA-seq data, the majority of genes are upregulated as opposed to downregulated upon IFNγ signalling (Fig:4.2B). Out of the 336 differential genes, only 56 of these are downregulated. GO analysis of only the downregulated genes did not find any significant processes, likely due to the small number of genes. GO analysis of ranked genes at each timepoint compared to untreated cells identified similar significantly upregulated processes as found in 3'-end RNA-seq, i.e. defence response and IFNγ-mediated signalling pathway.

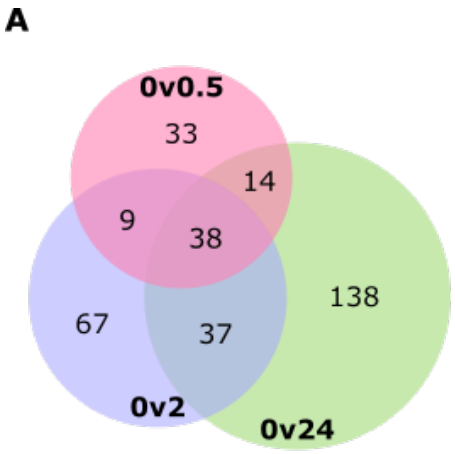

B

	# of genes	
	↑	↓
0v0.5	86	8
0v2	119	32
0v24	205	22
0.5v2	33	16
2v24	80	6

Figure 4.2: SNU-seq identifies subsets of differentially transcribed genes in Hep3B cells upon IFNγ treatments.
A Venn diagram showing overlaps between significant changes in gene expression as measured by SNU-seq (n=3) for each condition; untreated vs 0.5 hrs (pink), 2 hrs (blue) or 24 hrs (green) of IFNγ treatments. **C** Summary of the number of upregulated or downregulated genes per condition; untreated vs 0.5 hrs, 2 hrs or 24 hrs, 0.5 hrs vs 2 hrs and 2 hrs vs 24 hrs of IFNγ treatment.

4.2.1.2.2 Correlation analysis of SNU-seq and RNA-seq results

To further compare the RNA-seq and SNU-seq data, correlation analysis was performed. Here, $\log_2$(fold change) of significant differentially expressed genes upon 24 hr IFNγ treatments in 3'-end RNA-seq compared to SNU-seq show a significant positive correlation as expected (Fig:4.3A). However, there remains some genes that show increases in transcription with no increase or slight decreases in transcript levels or vice versa. Out of the 132 genes with differential transcript levels, only approximately two-thirds were differentially transcribed (Fig:4.3B). Conversely, only 26% of genes differentially transcribed resulted in significant increases/decreases in transcript levels. Not all transcription within a gene is involved in producing a transcript: Many regulatory elements reside within genes. This could explain the increases in transcription within some genes without a change in the RNA transcript. Additionally, other mechanisms of RNA maintenance tightly regulate transcripts and

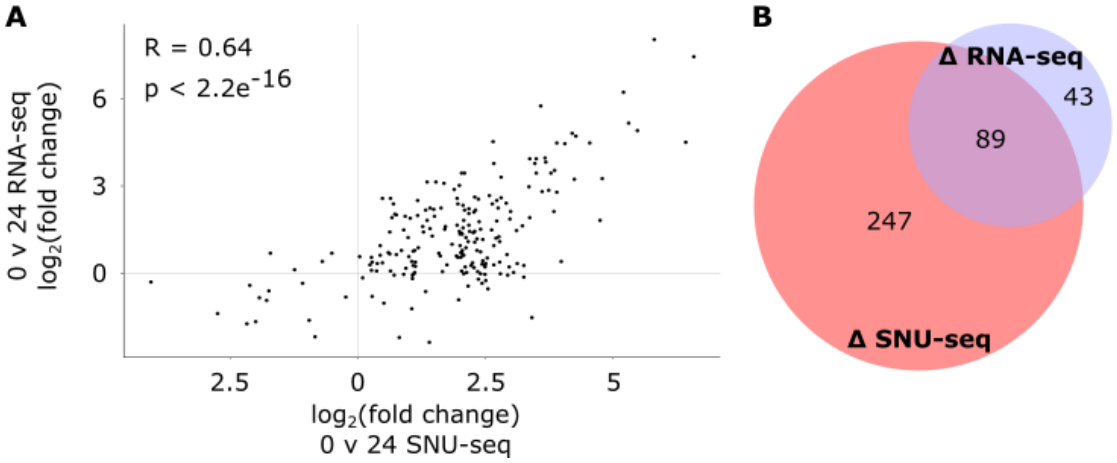

Figure 4.3: Correlation of IFNγ-induced SNU-seq genes versus RNA-seq genes.
A Correlation plot comparing RNA-seq data to SNU-seq data. Only genes common to both datasets that display a significant change in IFNγ treated cells compared to untreated cells in either dataset are shown. **B** Venn diagram showing overlaps between significant changes in gene expression as measured by SNU-seq versus RNA-seq.

highly stable RNA present at high levels in untreated cells may mask any increases in transcript levels despite an increase in transcription. All of the above may result in the inconsistencies seen between the RNA-seq and SNU-seq datasets.

4.2.1.2.3 SNU-seq identifies a shift from STAT to IRF binding motifs over 24 hrs of IFNγ treatments

SNU-seq reveals distinct subsets of transcriptional changes; early, intermediate and late as well as transiently transcribed and sustained genes (Fig:4.2A). 89/198 ($\sim$45%) that are differentially regulated either from 30 min or 2 hrs of IFNγ treatment maintain their altered expression until 24 hrs of treatment. The majority of genes ($\sim$55%) have a burst of transcriptional change which is lost or no longer significant by 24 hrs of treatment. To determine whether specific TFs were involved in either the timings of differential expression, or whether transcription changes were sustained, motif analysis was performed on multiple gene groups; significant genes after 0.5,

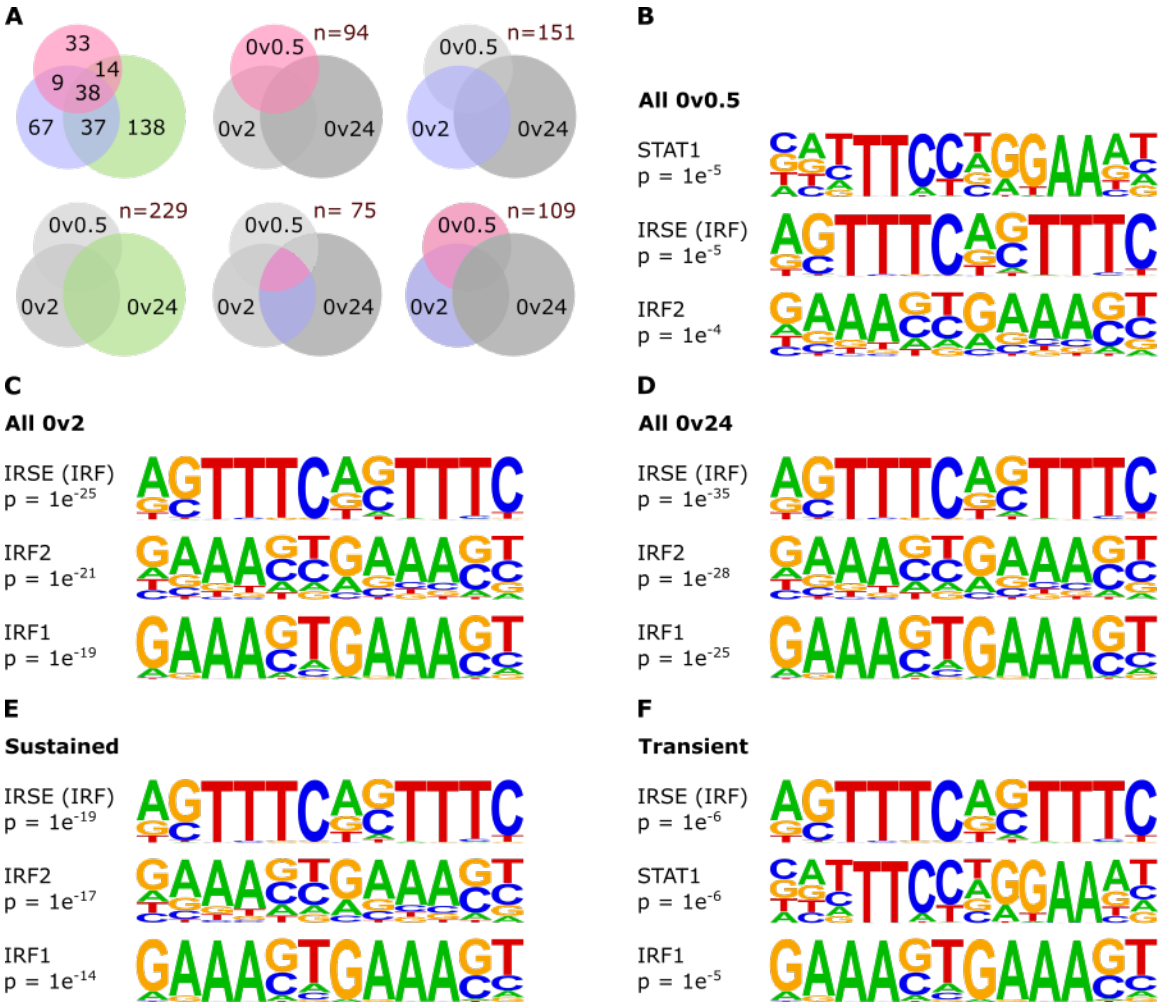

Figure 4.4: Motif analysis of different SNU-seq gene subsets.
A A key to which genes are analysed in the following sub-figures. The top left Venn diagram shows overlaps between significant changes in gene expression as measured by SNU-seq (n=3) for each condition; untreated vs 0.5 hrs (pink), 2 hrs (blue) or 24 hrs (green) of IFNγ treatments. Coloured regions in the remaining Venn charts represent the genes used in each analysis, with the total number of genes including shown above each Venn chart. **B-F** Homer motif analysis identifying enriched known motifs within a 2kb region surrounding the promoter of each gene input. The analysis is performed on all significant untreated vs 0.5 hrs treated (**B**), untreated vs 2 hrs treated (**C**), untreated vs 24 hrs treated (**D**), sustained differential transcription (**E**) and transient differential transcription (**F**) genes. The top three ranked motifs are shown for each subset.

2 or 24 hrs IFNγ treatment, genes differentially transcribed at 0.5 and/or 2 hrs of treatment which lose significance by 24 hrs and genes that become and remain differentially expressed throughout the treatment course (Fig:4.4A). The top three ranked motifs for each group of genes analysed were very similar, all containing a combination of an IRSE (an IRF protein binding motif), IRF1, IRF2 or STAT1 binding motif (Fig:4.4B-F). Given that STAT1 and IRF1 are the main drivers of IFNγ signalling, the enrichment of these motifs was unsurprising. IRF1 and IRF2 directly compete for the same DNA binding sites, with IRF2 being a negative regulator of the IFNγ response [Harada et al., 1989]. Thus the enrichment of either IRF1 or IRF2 is often concurrent with the other. Other IRF and STAT TF binding motifs were also significant in at least one gene group, namely IRF3, IRF8, STAT3, STAT4 and STAT5.

STAT1 is the most enriched motif within the early response genes (untreated vs 0.5 hrs IFNγ treatments, Fig:4.4B). As seen previously, IRF1 protein is only first identified by WB at 2 hrs of IFNγ treatment (Fig:3.1A, Section 3.2.1.1). Therefore, despite an enrichment of an IRSE motif in the early response genes, IRF1 probably is not involved in their differential expression. As the IFNγ timecourse progresses, IRF binding sites dominate over STAT binding sites (Fig:4.4C & D). STAT1 binding motifs remain significantly enriched in the 2 hrs and 24 hrs IFNγ-induced genes but with a comparably low significance of p=1e^{-8} and p=1e^{-3} respectively. pSTAT1 protein is still present at high levels in Hep3B cells up to 24 hrs of IFNγ treatment (Fig:3.1A, Section 3.2.1.1). IRF1 is known to redirect pSTAT1 to alternate sites which may explain the shift towards IRF enriched binding motifs at the later timepoints (Fig:4.5).

The sustained genes are predominantly enriched with IRF binding motifs whereas STAT1 binding motifs are amongst the highest enriched in the transiently expressed genes (Fig:4.4E & F). This could suggest that IFNγ-induced transcription of these

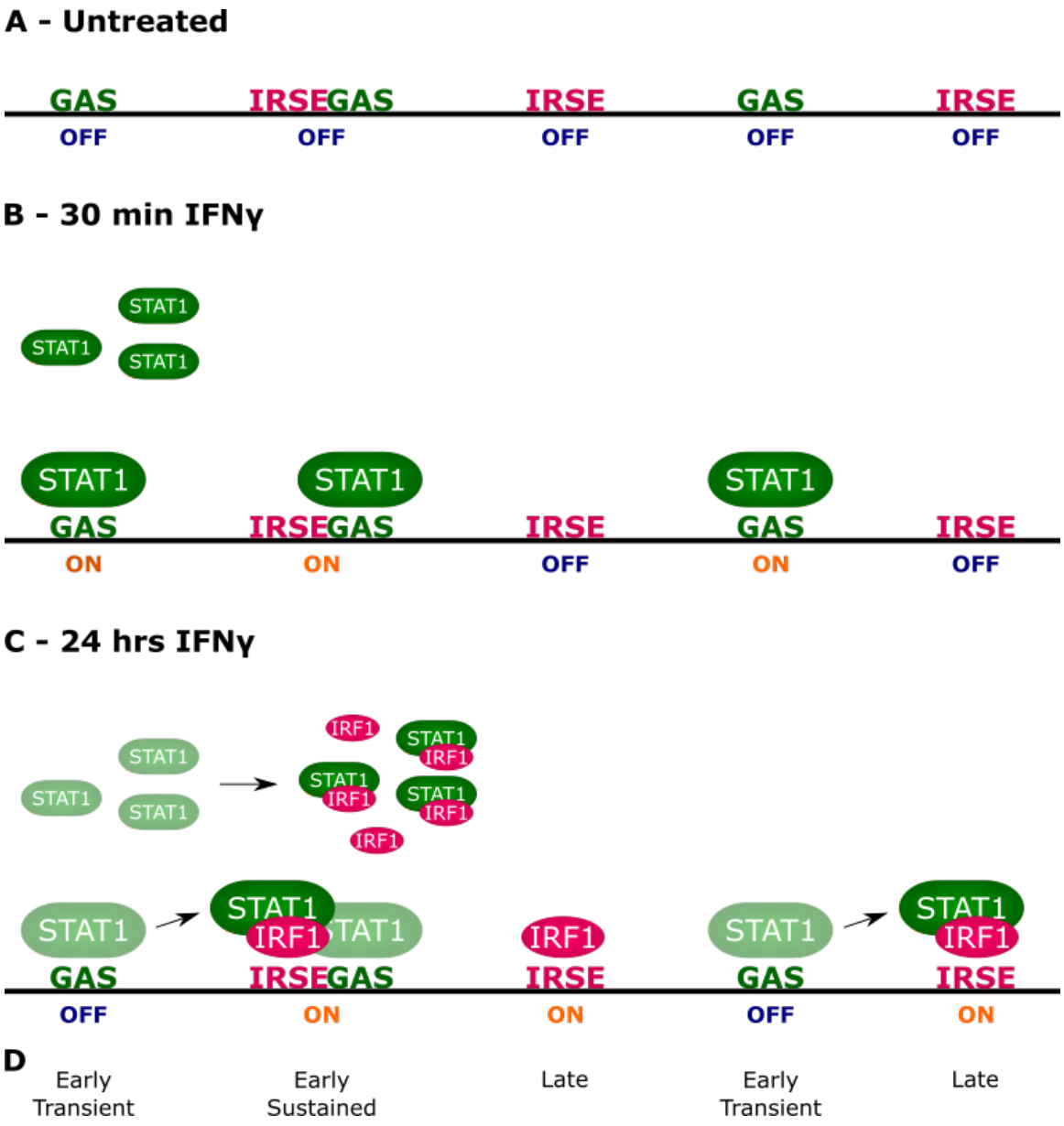

Figure 4.5: Model: STAT1 and IRF1 dictate early and late IFNγ-induced activation respectively.
A In untreated cells pSTAT1 and IRF1 TFs are not present in the nucleus and thus do not bind DNA. Genes/enhancers regulated by these TFs are inactive. **B** After short induction by IFNγ, STAT1 becomes activated and binds to GAS elements. Binding of STAT1 induces these elements. **C** After long induction by IFNγ, IRF1 is expressed. IRF1 interacts with STAT1 and binds IRSE motifs, alone or in combination with STAT1. IRF1 binding sites dictate activation of late genes/enhancers. **D** Examples of different classes of genes/enhancers. Early: Elements containing a GAS motif. Late: Elements with an IRSE motif, but lacking a GAS motif. Sustained: Elements containing an IRSE motif. Transient: Elements containing a GAS motif but lacking an IRSE motif.

genes is lost due to the redirected binding of STAT1 away from their promoter (Fig:4.5). However, as STAT1 can be redirected by IRF1 and binding motifs for this TF are also enriched in these transient genes it is unlikely that this is the case. Instead, the high quantity of early genes included in this analysis likely skews the result towards a more enriched STAT1 motif.

To better determine whether more TFs were involved in IFNγ-induced transcriptional changes within these genes, the full lists of enriched motifs were examined, ignoring IRF and STAT binding elements. The only other significantly enriched binding motifs were for NFκB, PRDM1, ZNF264 and NFATC1. PRDM1 was unexpressed in both the RNA-seq and SNU-seq data in all conditions tested within Hep3B cells and therefore is highly unlikely to play a role in altering the transcription of these genes. Its binding motif is similar to the IRSE binding motif which may explain its enrichment. The other three TFs are constitutively expressed in Hep3B cells at a transcriptional and RNA level and were unaffected by IFNγ treatments. NFκB and ZNF264 binding motifs are both enriched in untreated vs 2 hrs IFNγ treatment ($p=1e^{-5}$ and $p=1e^{-3}$ respectively) and sustained genes ($p=1e^{-4}$ and $p=1e^{-3}$), and NFκB binding sites are also enriched in untreated vs 24 hrs IFNγ treatments ($p=1e^{-3}$). Although these are less significantly enriched than IRF binding sites, they may play a role in altering the transcription of late genes and sustaining this expression. Not much is known about the zinc finger protein, ZNF264, but NFκB has previously been linked with IFNγ signalling. NFκB is usually maintained in an inactive state in the cytoplasm by inhibitory IκB proteins. Studies have found that IFN signalling, including IFNγ, leads to the activation of NFκB which in turn contributes to the upregulation of IFNγ-stimulated genes [Pfeffer, 2011, Thapa et al., 2011]. The enrichment of these motifs in later stages of the IFNγ timecourse suggests that this may also be the case in Hep3B cells. NFATC1 (Nuclear Factor of Activated T Cells), a TF that is evolutionarily related

to the Rel subunits of NFκB, is only enriched in the transient gene group (p=1e^{-3}). These TFs may determine whether expression is sustained or short-lived. However, given the low significance of motif enrichment, it seems likely that other factors are involved.

4.2.1.3 H3K4me3 does not appear to be required for IFNγ-induced transcription

4.2.1.3.1 Changes in H3K4me3 are induced after long IFNγ treatments

Levels of tri-methylation at lysine 4 on histone 3 (H3K4me3) show strong correlations to transcription and has thus become known as an active histone mark [Santos-Rosa et al., 2002]. Its distribution around the TSS of active genes is widely conserved from yeast to humans. Due to this, its deposition was assumed to be instructive for gene transcription. However, contradictory evidence has sparked debate in the field as to whether this epigenetic modification is instructive, a downstream consequence, or bares no association to transcription [Howe et al., 2017]. Indeed, partial loss of the mark does not massively alter transcription in yeast and vice versa [Murray et al., 2019]. Upon induced gene expression, H3K4me3 has been found to have a delayed deposition, peaking after gene expression has increased in multiple organisms including yeast and mice [Howe et al., 2017]. Given the ability of IFNγ to induce expression of hundreds of genes, it provides a good model to study modes of transcriptional induction in human cells.

To this end, genome-wide changes in H3K4me3 were assessed upon 0.5, 2 or 24 hrs of IFNγ treatment in Hep3B cells. The first significant changes were seen after 2 hrs of treatment, occurring at four loci including the IRF1 and IRF9 promoters (Fig:4.6). These four changes remain significant at 24 hrs and an additional 146 differential H3K4me3 peaks were seen at this timepoint, of which only seven showed decreases in the epigenetic mark (Fig:4.6B).

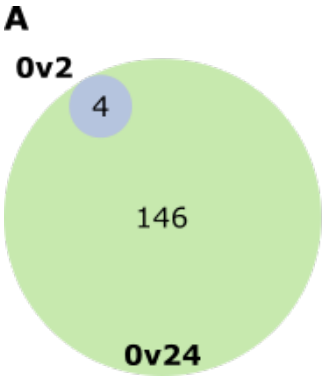

B

	# of genes	
	↑	↓
0v0.5	0	0
0v2	4	0
0v24	143	7

Figure 4.6: IFNγ-induces H3K4me3 after long treatments.
A Venn diagram showing overlaps between significant changes in gene expression as measured by SNU-seq (n=3) for each condition; untreated vs 0.5 hrs (pink), 2 hrs (blue) or 24 hrs (green) of IFNγ treatments. **B** Summary of the number of upregulated or downregulated H3K4me3 peaks per condition; untreated vs 0.5 hrs, 2 hrs or 24 hrs of IFNγ treatment.

4.2.1.3.2 H3K4me3 changes do not correlate with transcriptional changes

The numbers of differential H3K4me3 seen were similar to the number of upregulated and downregulated genes from the RNA-seq data (Fig:4.1B), although more differences were identified in the earlier timepoints in the RNA-seq analysis. To see how well these IFNγ-induced changes correlated with each other, H3K4me3 peaks were first assigned to overlapping genes. Genes showing a significant change in either RNA or H3K4me3 levels upon IFNγ treatments were used to identify correlations between the two datasets. These genes showed a moderate positive correlation between induced changes in H3K4me3 and RNA levels after 24 hrs of IFNγ treatment compared to untreated cells (Fig:4.7A). A similar analysis was performed between the H3K4me3 ChIPmentation and SNU-seq datasets. In contrast, these two datasets show virtually no correlation between IFNγ-induced transcription and H3K4me3 levels after 24 hrs of IFNγ treatment (Fig:4.7B). Less than one-third of significant IFNγ-induced gene expression changes had a corresponding significant differential H3K4me3 peak and over 50% of differential H3K4me3 peaks displayed no altered transcription

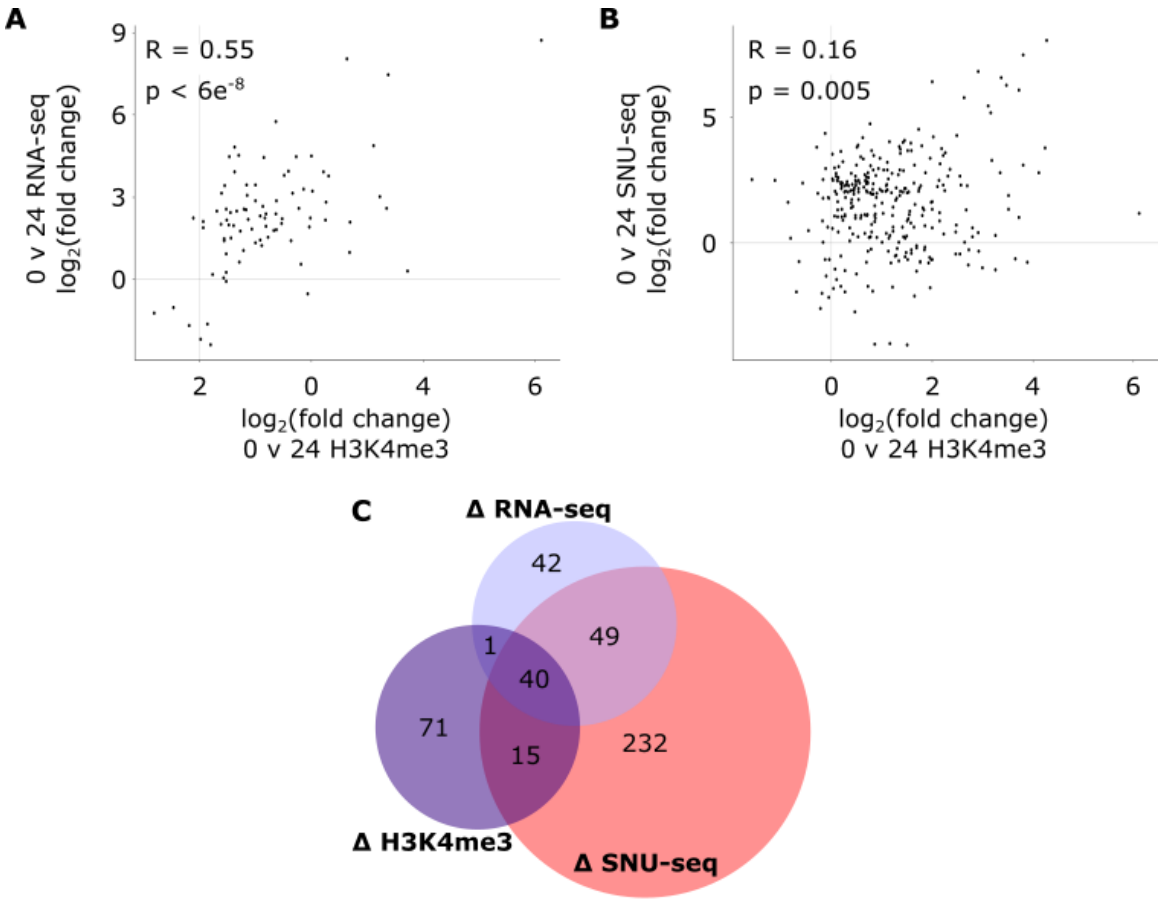

Figure 4.7: IFNγ-induced H3K4me3 changes show little correlation to transcriptional changes.
A-B Correlation plots comparing H3K4me3 $\log_2$(Fold Change) after 24 hrs of IFNγ treatment to RNA-seq (**A**) or SNU-seq $\log_2$(Fold Change) (**B**). Only genes common to both datasets that display a significant change in IFNγ treated cells compared to untreated cells in either dataset are shown. **C** Venn diagram showing overlaps between significant changes in H3K4me3 versus gene expression, measured by SNU-seq and RNA-seq.

or transcript levels (Fig:4.7C). This data, therefore, supports that there may be no association between H3K4me3 and transcription, at least when stress-induced.

No significant differences in H3K4me3 levels were observed at just 0.5 hrs of IFNγ treatment, despite the large numbers of transcriptional changes found at this timepoint (Fig:4.2 & 4.6). To examine this in more detail, I visualised the tracks of some early induced genes (Fig:4.8). Here, the significant increase in transcription is obvious, with large amounts of pink SNU-seq signal, representing transcription at 0.5 hrs of IFNγ treatment. In contrast, most H3K4me3 signal increases after 2 or 24 hrs of IFNγ treatment respectively, thus showing a delay in H3K4me3 deposition after transcription has already been initiated. Contrary to this, large significant increases in H3K27ac are immediately seen at 0.5 hrs of IFNγ treatment demonstrating that the delay in H3K4me3 deposition is not due to an impediment in the ChIPmentation technique. Altogether these data suggest that levels of H3K4me3 does not correlate with stress-induced transcription and deposition of H3K4me3 is not required to induce transcription.

Sharp peaks of both SNU-seq signal and RNA-seq signal could be seen within intronic regions approximately 2kb and 4kb into the UBE2L6 and NLRC5 genes respectively (Fig:4.8, see *). As this peak corresponded to induced H3K27ac in UBE2L6, the possibility of eRNA at this site was considered. eRNA transcription is not linked to H3K4me3 deposition and could explain the lack of correlation between transcription and trimethylation at these loci. However, on closer inspection, the peaks at both genes aligned to poly(A) sequences and could represent an alternate poly(A) site. As the intronic RNA peak at NLRC5 does not associate with H3K27ac it is unlikely that they represent eRNAs.

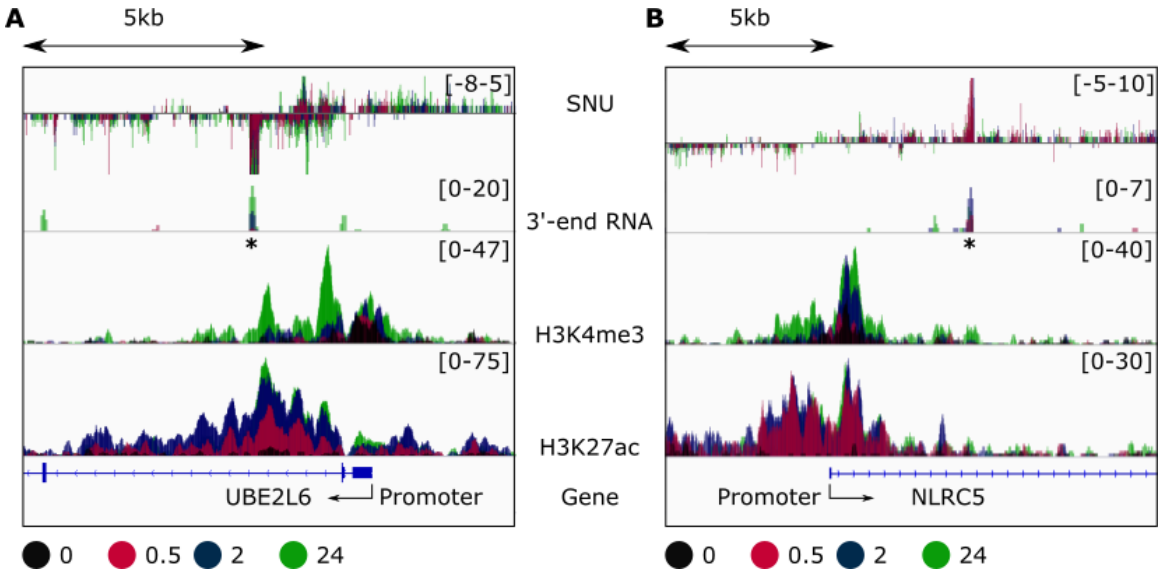

Figure 4.8: Examples of IFNγ-induced transcriptional and H3K4me3 upregulation.
A-B Transcriptional and ChIPmentation data surrounding the UBE2L6 (**A**) or NLRC5 (**B**) promoter. From top to bottom are tracks of strand-specific SNU-seq, RNA-seq, H3K4me3 and H3K27ac for each treatment sample (n=2-3), with the untreated sample in black, and 0.5, 2 and 24 hrs of IFNγ treatment in pink, navy and green respectively. All tracks are spike-in normalised. * denotes a sharp peak in 3'-end RNA-seq and SNU-seq data.

4.2.2 IFNγ dramatically modifies the enhancer landscape in Hep3B cells

4.2.2.1 SNU-seq identifies IFNγ-induced ncRNA transcriptional changes

4.2.2.1.1 Analysing transcriptional changes at annotated enhancers

As seen previously, IFNγ induces the expression of hundreds of genes particularly enriched for STAT or IRF binding motifs, suggesting a role of these TFs in IFNγ-induced gene regulation. A second level of gene regulation, on top of TF binding to the gene promoter, includes the activity of enhancers. As formerly mentioned, enhancer activity tends to correlate with H3K4me1, H3K27ac and bidirectional enhancer RNA (eRNA) transcription (Fig:1.10). eRNA, as a form of ncRNA, is very short-lived, thus making it difficult to detect in standard RNA-seq methods. SNU-seq, given

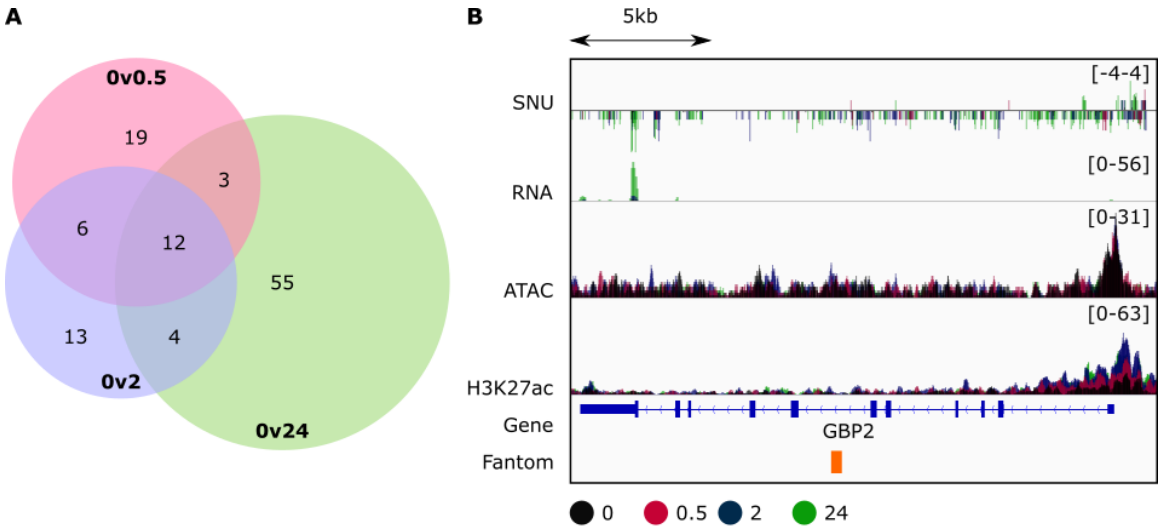

Figure 4.9: Low numbers of transcriptional changes are seen at annotated enhancers.
A Venn diagram showing IFNγ-induced transcriptional changes within a 5kb window surrounding Fantom enhancers for each condition; untreated vs 0.5 hrs (pink), 2 hrs (blue) or 24 hrs (green) of IFNγ treatments. **B** A ~20kb stretch of the GBP2 locus showing strand-specific SNU-seq, RNA-seq, DNA accessibility and ChIP profiles of H3K27ac data for each treatment sample (n=2-3), with the untreated sample in black, and 0.5, 2 and 24 hrs of IFNγ treatment in pink, navy and green respectively. All tracks are spike-in normalised except ATAC-seq which is normalised based on sequencing depth. The annotated Fantom5 enhancer is represented by the orange bar.

its short exposure with 4-thiouridine, is optimised to detect these transient RNAs at single-nucleotide resolution. I, therefore, predicted that SNU-seq would identify IFNγ-induced changes in transcription within the enhancer landscape on top of coding transcriptional changes. To this end, SNU-seq reads were counted within a 5kb window surrounding the public enhancer annotations from the Fantom5 human enhancer database [Lizio et al., 2019]. DESeq2 was used comparing untreated cells to each length of IFNγ treatment to determine differentially transcribed enhancers. Using this method, 112 differentially transcribed enhancers were identified, with the majority of significant changes being identified after 24 hrs of IFNγ treatments (Fig:4.9A).

SNU-seq detects transcription spanning the entire gene, including both exons and

introns. Annotated enhancers situated within the gene body may show differential transcription not due to activation/inactivation of the enhancer element, but due to up-/down-regulation of the gene in which the enhancer resides. As seen in Fig:4.9B, GBP2 shows increased transcription, further validated by increased transcript levels measured by 3'-end RNA-seq. An enhancer present in the Fantom5 enhancer dataset is located within the 6th intron of this gene. This enhancer is recognised as differentially transcribed due to the increase in GBP2 transcription. The lack of a hypersensitive site, H3K27ac and bidirectional transcription suggest that this is not an active enhancer in Hep3B cells under the conditions tested. More situations like this may be present within the 112 differently transcribed enhancers making it difficult to interpret these results.

4.2.2.1.2 Using ATAC-seq peaks to identify novel enhancer elements in Hep3B cells

An alternate method to identify differential activation of regulatory elements was, therefore, sought. Transcriptional initiation requires the assembly of the PIC and subsequent release of RNA polymerase. DNA must be accessible for the transcriptional machinery to assemble and thus a peak of ATAC-seq signal is expected for transcription initiation, both at gene promoters and enhancers [Catarino and Stark, 2018]. Accordingly, ATAC-seq peaks identified in one or more conditions within Hep3B cells were combined and SNU-seq reads were counted within a 5kb window surrounding these peaks. Again differential analysis was performed to determine transcriptional changes upon IFNγ treatments. Although, as in Fig:4.9B, differential gene transcription coincidentally across an intergenic ATAC-seq peak would be recorded as a differentially transcribed ATAC-seq peak, the presence of an accessible DNA site makes it more likely that these sites are regulatory elements.

Astonishingly, this method identified 863 loci with differential transcription

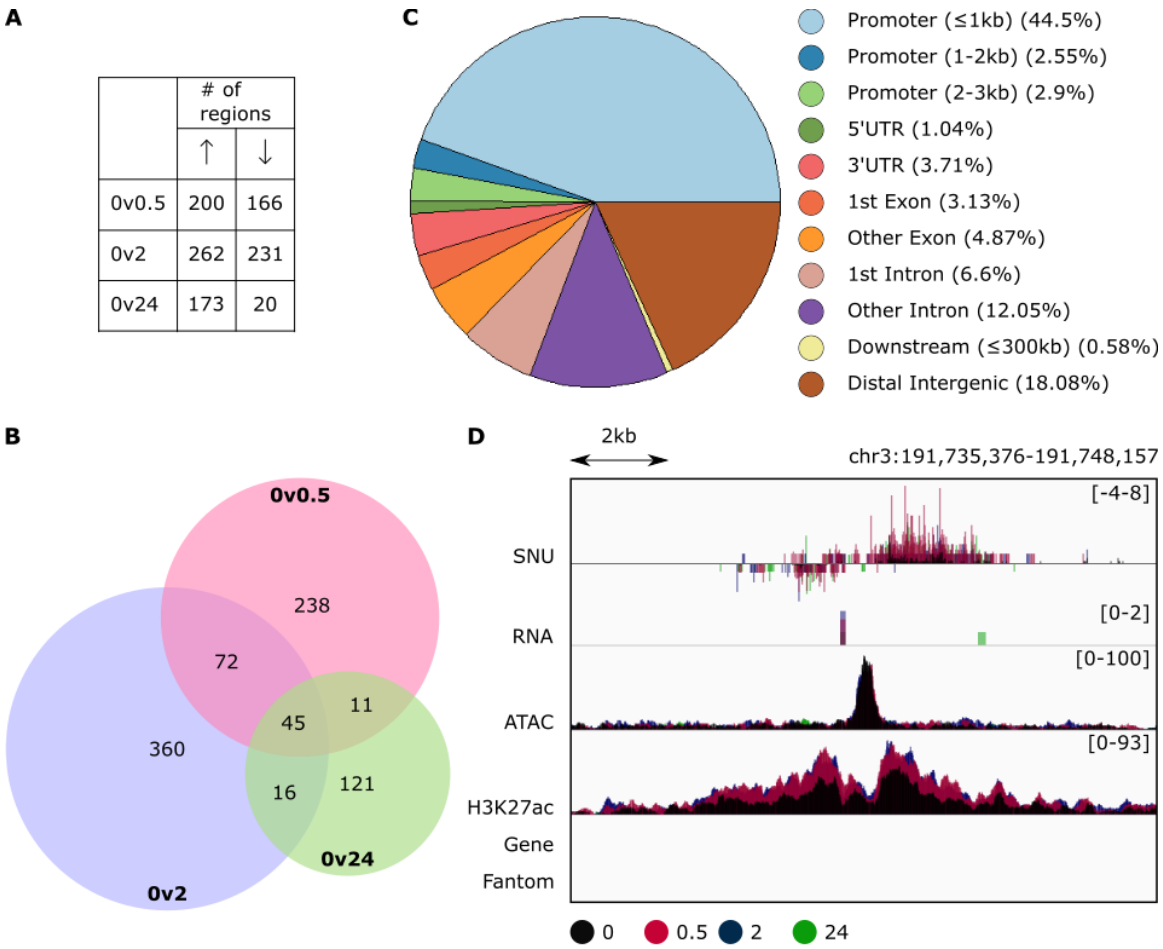

Figure 4.10: SNU-seq identifies IFNγ-induced changes in the enhancer landscape.
A Summary of the numbers of differential transcription within a 5kb window of an ATAC-seq peak per condition; untreated vs 0.5 hrs, 2 hrs or 24 hrs of IFNγ treatment. **B** Venn diagram showing IFNγ-induced transcriptional changes within a 5kb window surrounding ATAC-seq for each condition; untreated vs 0.5 hrs (pink), 2 hrs (blue) or 24 hrs (green) of IFNγ treatments. **C** Distributions of the differential transcription as annotated by ChIPseeker. **D** A ∼12kb stretch of chr3 showing strand-specific SNU-seq, RNA-seq, DNA accessibility and ChIP profiles of H3K27ac data for each treatment sample (n=2-3), with the untreated sample in black, and 0.5, 2 and 24 hrs of IFNγ treatment in pink, navy and green respectively. All tracks are spike-in normalised except ATAC-seq which is normalised based on sequencing depth. Note the lack of annotated Fantom5 enhancers.

(Fig:4.10A & B). These 800+ changes include both differential gene expression and altered activity of regulatory elements. As 336 gene transcriptional changes were previously found in section 4.2.1.2 (Fig:4.2), one may estimate that over 500 transcriptional changes are not involved in coding RNA expression. To better predict the proportion of transcriptional changes potentially involved in the activity of regulatory elements, the distribution of each change in relation to gene elements was analysed using ChIPseeker (Fig:4.10C) [Yu et al., 2015]. 49.95% of altered transcription loci were found within 3kb of a gene promoter. This leaves 432 loci (50.05% of 863) containing a non-promoter ATAC-seq peak and differential transcription upon IFNγ treatments. This suggests that IFNγ induces widespread changes to the enhancer landscape.

An example of a regulatory element, present on chromosome 3, induced by IFNγ treatment is shown in Fig:4.10D. In untreated cells, a large peak of DNA accessibility and moderate levels of H3K27ac can be seen. Small levels of transcription, primarily on the plus strand, is found, suggesting low activity of this enhancer. After just 30 min of IFNγ treatment, more H3K27ac is deposited and a big increase in bidirectional transcriptional occurs, implying an increased activity of the enhancer. Interestingly, no enhancers are present at this locus in the Fantom5 enhancer database indicating that this analysis method can identify novel enhancers in this cell line.

4.2.2.1.3 IFNγ induces bursts of transcription, likely directed by STAT and IRF TFs

Unlike the differential analysis on the annotated Fantom5 enhancers, where most changes occur at 24 hrs of treatment, most transcriptional changes surrounding ATAC-seq peaks occur by 0.5 and 2 hrs of IFNγ treatments (4.9A & 4.10A & B). What's more, only a small proportion of changes are sustained with longer treatments of IFNγ. The minimal overlap between SNU-seq changes at each timepoint taken

demonstrates continual transcriptional landscape remodelling across the genome as IFNγ signalling progresses. pSTAT1 is the most likely candidate as the driver of transcriptional changes within 0.5 hrs of IFNγ treatment as IRF1 is only observed as protein in Hep3B cells from 2 hrs of IFNγ treatment (Fig:3.1A, Section 3.2.1.1). Indeed, motif analysis on all differential SNU-seq signal surrounding an ATAC-seq peak finds the STAT1 binding motif as the most significantly enriched ($p=1e^{-10}$) (Fig:4.11). This remains the most significantly enriched motif at sites of altered transcription by 2 hrs of IFNγ treatments ($p=1e^{-5}$). IRSE motifs begin to be significantly enriched by 2 hrs at sites of increased transcription. By 24 hrs IRSE motifs overtake STAT1 motifs as the most significantly enriched at sites of altered transcription with $p=1e^{-26}$. Again this demonstrates the shift of the IFNγ response from STAT1 to IRF1 mediation and could signify the redistribution of pSTAT1 to IRF binding sites. Early binding of pSTAT1 to DNA followed by its relocation to other loci could explain the short burst of transcriptional change which isn't sustained (Fig:4.5). Additionally, negative feedback loops could be at play.

Both RNA-seq and SNU-seq revealed that IFNγ is associated with predominantly upregulated gene expression at each timepoint analysed. One would hypothesise that the majority of enhancer elements would also, therefore, show increased activity. Contrary to this, the intergenic SNU-seq analysis at 0.5 and 2 hrs of IFNγ treatment found that almost 50% of changes were downregulations of transcription. Interestingly, the only significantly enriched motif present in the 166 loci showing decreased transcription after 0.5 hrs of IFNγ treatment was for CTCF binding, although this was only a minor enrichment with a p-value of $1e^{-4}$ (Fig:4.11). This perhaps indicates that IFNγ may additionally alter the insulator landscape, in addition to enhancers, to regulate gene expression. This will further be discussed in section 4.2.2.4. CTCF, more recently, has been found at gene promoters and has been implicated in enhancer-promoter contacts [Ren et al., 2017]. Therefore

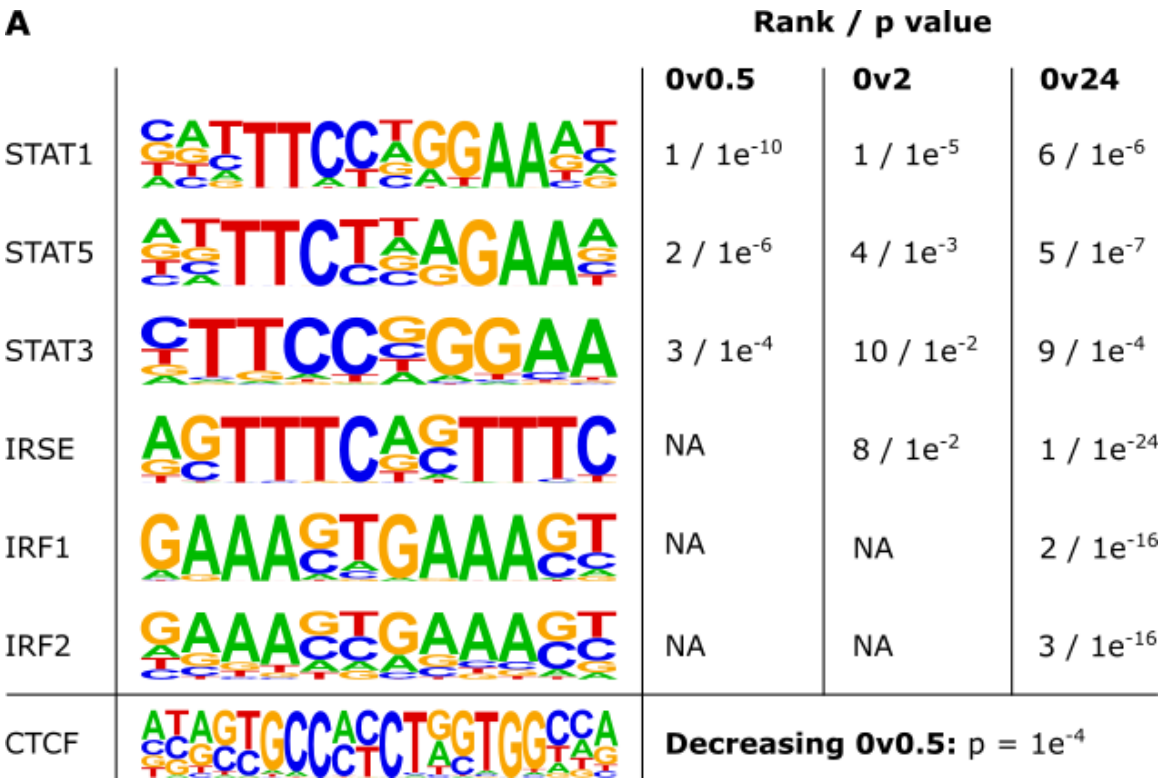

Figure 4.11: Transcriptional changes at peaks of accessibility are enriched for STAT1 and IRF1 binding motifs.
A Homer motif analysis identifying enriched known motifs at ATAC-seq peaks with differential transcription. The analysis is performed on all significant differential peaks identified in untreated vs 0.5 hrs, 2 hrs or 24 hrs of IFNγ treatments. The enrichment rank and p-value are shown for highly ranked motifs for each condition. Additionally, the only significant binding motif, CTCF, enriched at peaks showing decreased transcription is shown.

these transcriptional decreases at CTCF binding motifs may represent decreased transcription at these enhancer-promoter loops. No known motif was enriched at loci whose transcription had decreased after 2 hrs of IFNγ treatment.

Altogether, SNU-seq identifies large numbers of transcriptional changes genome-wide upon treatment with IFNγ, including both coding and non-coding transcription. At each timepoint tested, different loci showed altered transcription. These were sometimes sustained over the IFNγ timecourse but often displayed transient expression perhaps due to a shift from STAT1 binding motifs towards IRF binding motifs. This transient expression reveals a dynamic enhancer landscape as IFNγ

signalling progresses.

4.2.2.2 IFNγ induces distinct phases of *de novo* H3K27 acetylation over 24 hrs

4.2.2.2.1 Thousands of H3K27ac peaks are upregulated by IFNγ treatments

Acetylation of histone 3 lysine 27 (H3K27ac) is a marker of active promoters and enhancers. Indeed, H3K27ac was found to discriminate between active or poised H3K4me1 containing enhancers, with the presence of H3K27ac correlating to more active enhancers [Creyghton et al., 2010]. Thus, analysing genome-wide changes in H3K27ac would further elucidate how IFNγ treatments affect the enhancer landscape in Hep3B cells. Remarkably, IFNγ treatments resulted in 2,744 differential peaks at the three timepoints tested; 0.5, 2 and 24 hrs (Fig:4.12A & B). This is over 3x the number of differential SNU-seq signals detected. What's more, unlike the intergenic SNU-seq data, the vast majority of differential H3K27ac peaks show increases in signal upon IFNγ treatments, with H3K27ac decreasing at only approximately 2% of differential peaks. 77% of differential peaks did not have a peak present in the untreated samples, thus over three-quarters of IFNγ-induced acetylation is deposited at *de novo* loci. Examples of IFNγ-induced *de novo* acetylation can be seen in Fig: 4.8.

IFNγ induces distinct subsets of differential H3K27ac (Fig:4.12B). Only 14% of peaks showing differential acetylation by 0.5 hrs or 2 hrs of IFNγ treatment sustain this change after 24 hrs of treatment. Instead, most of these early differential peaks are lost whilst over 1000 changes are made at unique loci between 2-24 hrs of IFNγ treatment. The loss of most early IFNγ-induced increases demonstrates rapid turnover of the modification.

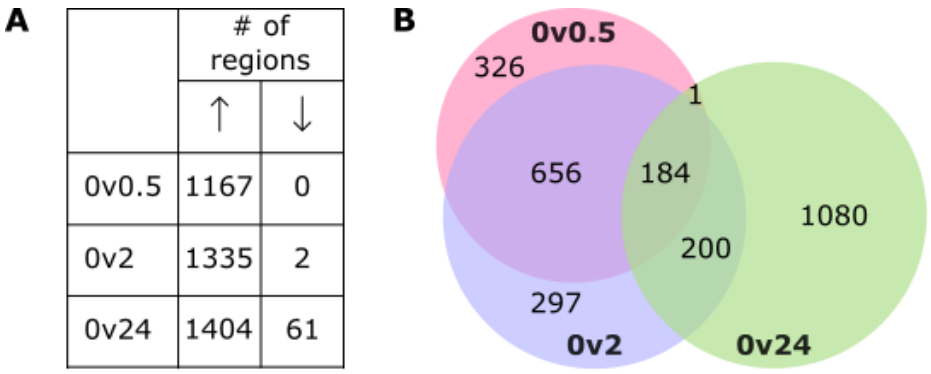

Figure 4.12: IFNγ-induces phases of histone acetylation within 24 hrs of treatment.
A Summary of the numbers of differential H3K27ac peaks per condition; untreated vs 0.5 hrs, 2 hrs or 24 hrs of IFNγ treatment. **B** Venn diagram showing IFNγ-induced H3K27ac changes for each condition; untreated vs 0.5 hrs (pink), 2 hrs (blue) or 24 hrs (green) of IFNγ treatments.

4.2.2.2.2 Motif enrichment identifies a shift from STAT to IRF binding sites at IFNγ-induced differential H3K27ac peaks

As seen previously, as the duration of IFNγ treatment increases, there is a shift from high enrichment of STAT binding motifs to IRF binding motifs at sites of differential acetylation (Fig:4.13). After 0.5 hrs of treatment, STAT binding motifs dominate with IRF binding motifs only slightly or not enriched. By 2 hrs STAT binding motifs are still the most significantly enriched, perhaps explaining the large overlap in IFNγ-induced differential H3K27ac peaks at 0.5 hrs and 2 hrs (Fig:4.12 & 4.13). IRF binding motifs begin to become more significantly enriched after 2 hrs of IFNγ treatment, ranking within the top 10 enriched motifs. Finally, after 24 hrs of IFNγ treatments, IRF binding motifs become extremely enriched with p-values less than $1e^{-500}$. In contrast, the significance of STAT motif enrichments is substantially lower. This demonstrates two distinct phases of IFNγ-induced H3K27ac deposition, early changes likely mediated by STAT TFs followed by late changes mediated by IRF TFs. Indeed, transient genes were significantly enriched for STAT motifs, with

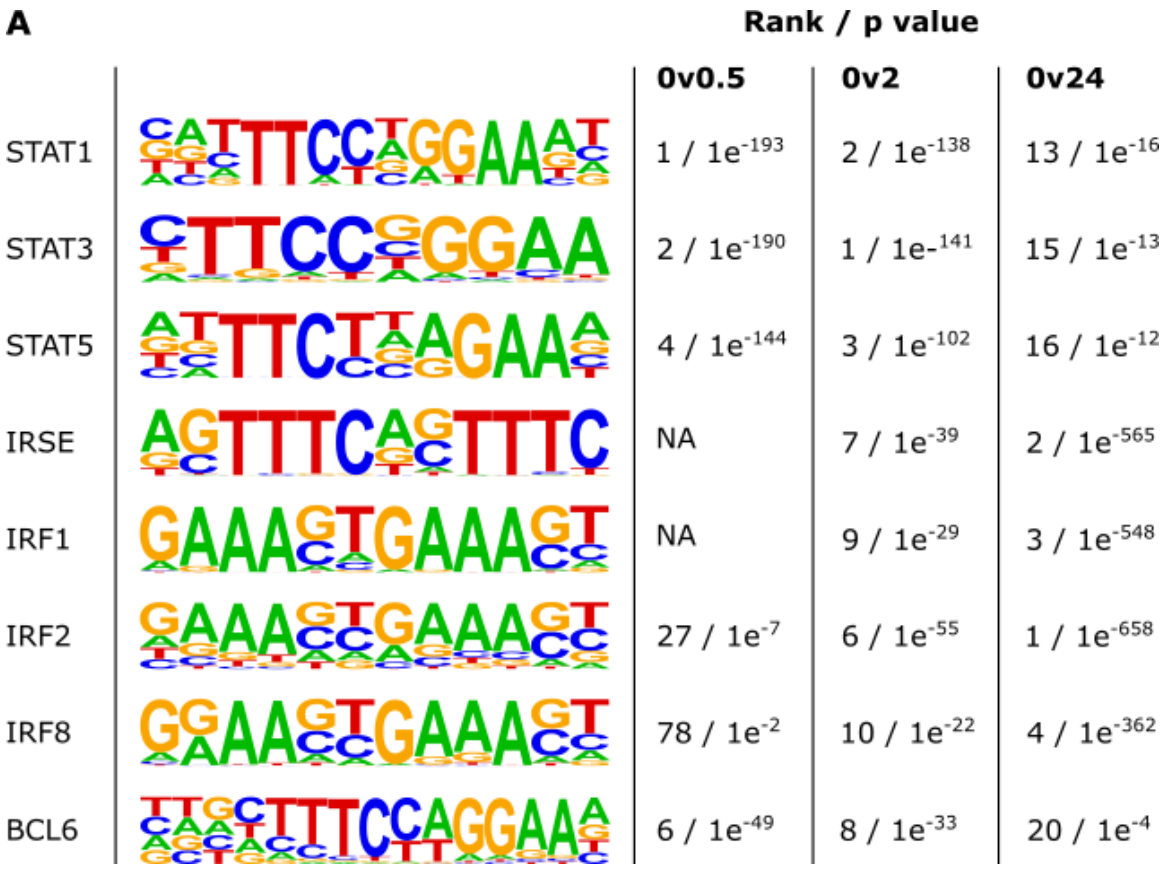

Figure 4.13: Differential peaks of H3K27ac show enrichments in STAT and IRF binding motifs.
A Homer motif analysis identifying enriched known motifs at peaks of H3K27ac. The analysis is performed on all significant differential peaks identified in untreated vs 0.5 hrs, 2 hrs or 24 hrs of IFNγ treatments. The enrichment rank and p-value is shown for highly ranked motifs for each condition.

no significant enrichment of an IRF1 binding motif, whilst sustained genes were significantly associated with IRF motifs (modelled in Fig:4.5).

Both STAT1 and IRF1 have been found to associate with the H3K27ac writers CBP and p300 [Zhang et al., 1996, Ramsauer et al., 2007, Leung et al., 2019]. However, IRF1's association with these acetylases may be due to its corecruitment of STAT1. It is therefore possible that binding of STAT1 results in *de novo* writing of H3K27ac and that this increase in H3K27ac is only sustained so long as STAT1 remains bound (Fig:4.14). The redistribution of STAT1 away from these

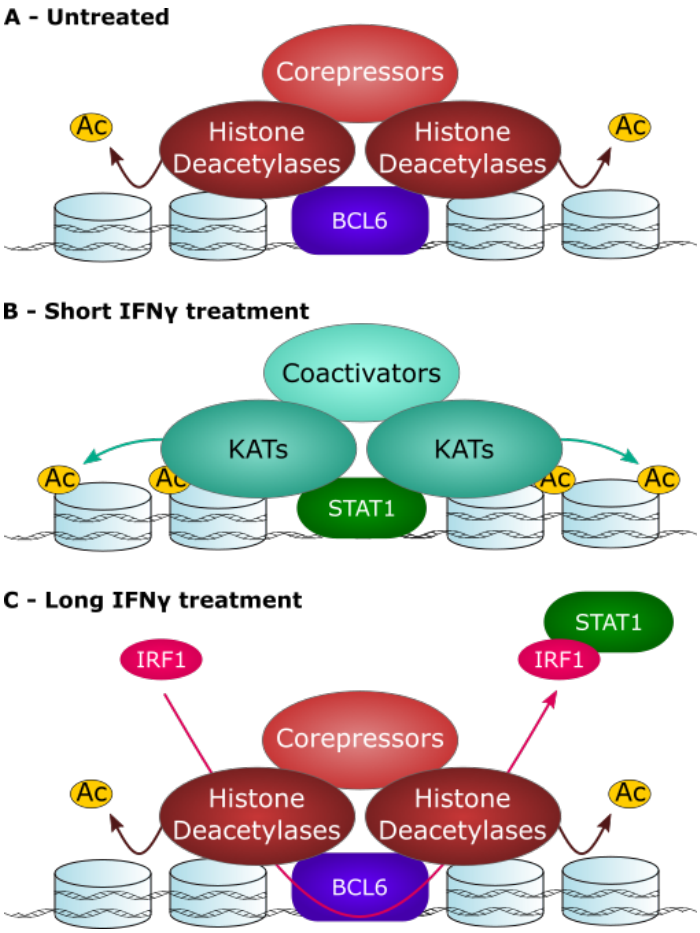

Figure 4.14: Model: Transient histone acetylation is dictated by STAT1 redirection.
A In untreated cells BCL6 maintains histones in a deacetylated state by recruiting histone deacetylases. **B** Short treatments of IFNγ activates STAT1. STAT1 binds regions of DNA and recruits KATs which in turn acetylates histones. **C** Long IFNγ treatments upregulate IRF1. IRF1 interacts with STAT1 and redirects its binding to other loci. Bound BCL6 recruits histone deacetylases which rapidly erases the STAT1-mediated histone acetylation.

sites, mediated by IRF TFs, would then lead to this modification being erased or the histones turned over at these early loci, whilst it is instead deposited at the redistributed STAT1 sites. Accordingly, this would lead to the shift of differential H3K27ac sites seen after early and late IFNγ treatments.

Notably, binding motifs for BCL6, a transcriptional repressor, are significantly enriched in all conditions analysed, albeit to a lesser extent than STAT or IRF TFs (Fig:4.13). Its enrichment is highest within differential H3K27ac peaks after 0.5 hrs of IFNγ treatment ($p=1e^{-49}$) and this enrichment decreases as the treatment progresses ($p=1e^{-33}$ and $p=1e^{-4}$ for 2 hrs and 24 hrs respectively). Furthermore, BCL6 is significantly enriched in transient H3K27ac peaks (peaks differentially regulated at 0.5 hrs and 2 hrs but not at 24 hrs) but is not significantly enriched (q value < 0.05) in sustained peaks (peaks differentially regulated at 0.5 hrs and 2 hrs that remain differentially regulated at 24 hrs). BCL6 functions as a transcriptional repressor by recruiting corepressors and histone deacetylases [Melnick et al., 2002]. Hence its enrichment, especially at the earlier timepoints, could provide a mechanism of erasing the recently deposited acetylation, thus explaining how it is not sustained throughout the timecourse (Fig:4.14). BCL6 is transcriptionally upregulated, as measured by SNU-seq, at every IFNγ treatment timepoint tested, although bizarrely, this is not reflected by a significant upregulation of BCL6 transcript levels, as measured by RNA-seq. Therefore it is difficult to speculate whether BCL6 could be permanently bound to these loci, if IFNγ treatment induces its recruitment or if it is upregulated by IFNγ resulting in increased binding.

4.2.2.2.3 IFNγ-induced changes in H3K27ac bare little correlation to transcriptional changes

H3K27ac is a prominent mark found at both promoter and enhancer elements and has been found to positively correlate with transcription [Wang et al., 2008]. To

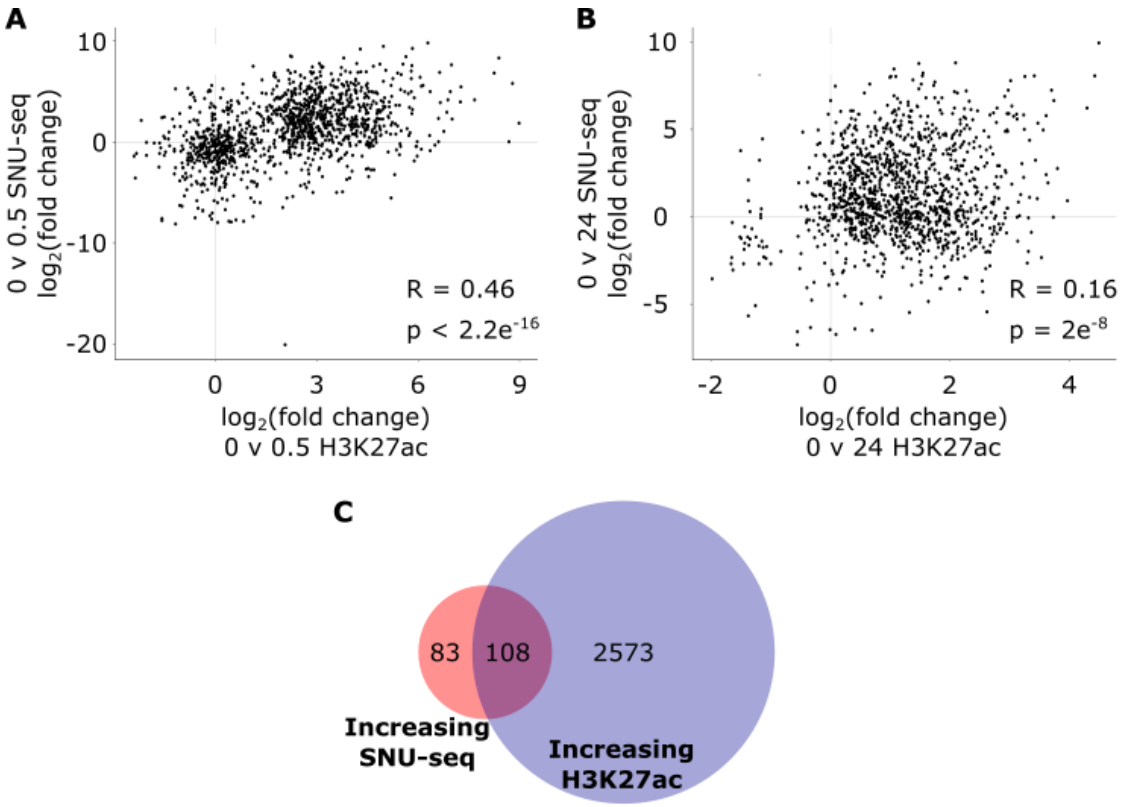

Figure 4.15: IFNγ-induced differential acetylation is uncoupled to transcription.
A-B Correlation scatter plots comparing H3K27ac to SNU-seq $\log_2$(Fold Change) after 0.5 hrs (**A**) or 24 hrs (**B**) of IFNγ treatment. SNU-seq reads within a 2kb window surrounding H3K27ac peaks were counted and significant changes determined by DESeq2. Only peaks displaying a significant change in IFNγ treated cells compared to untreated cells in either dataset at any timepoint analysed are shown. **C** Venn diagram showing overlaps between significant IFNγ-induced increases in transcription versus increases in H3K27ac.

determine if this positive correlation between acetylation and transcription was seen in IFNγ-induced Hep3B cells, induced changes in each dataset were compared. To enable comparison of the data at both genes and regulatory elements, SNU-seq reads within a 2kb window surrounding H3K27ac peaks were counted and significantly induced changes after 0.5 hrs, 2 hrs or 24 hrs were identified using DESeq2. Peaks with a significant change in either dataset at any timepoint tested were used for correlation analysis. Interestingly, although a moderate positive correlation could be seen between the $\log_2$(fold change) of H3K27ac and SNU-seq signal after 0.5 hrs of

IFNγ treatment, there was virtually no correlation between the two after 24 hrs of IFNγ treatment (Fig:4.15A & B). Furthermore, only 57% of significantly increasing transcription was accompanied by a significant increased in H3K27ac (Fig:4.15C). This suggests that the two are not always connected, with an increase/decrease in acetylation not always coupled with an analogous change in transcription.

4.2.2.2.4 A large proportion of IFNγ-induced H3K27ac changes are intergenic

To ascertain the proportion of IFNγ-induced acetylation changes occurring at promoters versus enhancers, ChIPseeker was used to annotate the distributions of differential H3K27ac peaks (Fig:4.16). Only approximately 17% of changes were found within 3kb of a promoter. Acetylation often spreads from the gene promoter in an active gene. To allow for this, if the 5'-UTR, 1^{st} exon and 1^{st} intron are also included, the proportion of changes occurring at or near promoters equates to roughly 30%. Therefore the majority of IFNγ-induced differential H3K27ac does not occur near a gene promoter, indicating that IFNγ induces more changes at regulatory elements than at genes.

The distribution of all H3K27ac peaks found in any condition tested was additionally analysed (Fig:4.16). The distributions of all acetylation peaks and differential peaks were fairly similar. $\sim$20% of all identified H3K27ac peaks were present within 3kb of a promoter, increasing to $\sim$36% if including 5'-UTRs and the 1^{st} exon and intron. Thus the fraction of IFNγ-induced acetylation changes near promoters is marginally smaller than seen in all acetylation peaks, again supporting that IFNγ slightly favours the induction of H3K27ac changes at regulatory elements over promoters.

Collectively, IFNγ induces substantially more changes in peaks of H3K27ac than gene expression or non-coding transcriptional changes. Augmented by the small

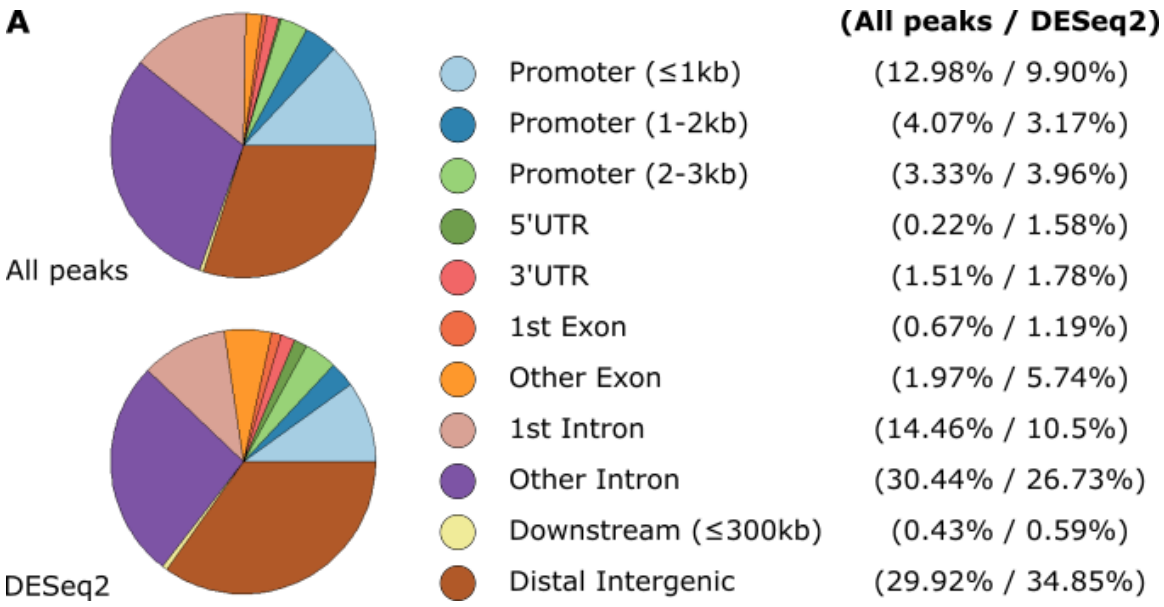

Figure 4.16: IFNγ induces intergenic changes in histone acetylation.
A Pie charts showing the distributions of all (top) or differential (bottom) H3K27ac peaks as annotated by ChIPseeker.

fraction of changes occurring near promoter elements, this indicates that IFNγ signalling affects a larger number of enhancers than genes. This altered enhancer landscape may consequently have a role in altering gene expression required to fulfil the IFNγ response, in addition to priming cells to other immune signals. IFNγ-induced H3K27ac deposition occurs in at least two distinct phases within 24 hrs of signalling. As with gene expression, motif analysis implies that these subsets are regulated by STAT TFs and IRF TFs in the early and very late responses respectively.

4.2.2.3 IFNγ treatments induce thousands of changes in DNA accessibility

4.2.2.3.1 Differential ATAC-seq peaks form after long IFNγ treatments

Commonly, enhancers are distinguished by numerous factors including, but not limited to, DNA accessibility, H3K27ac, H3K4me1 and transcription [Catarino and Stark, 2018]. Having already discussed acetylation and transcriptional

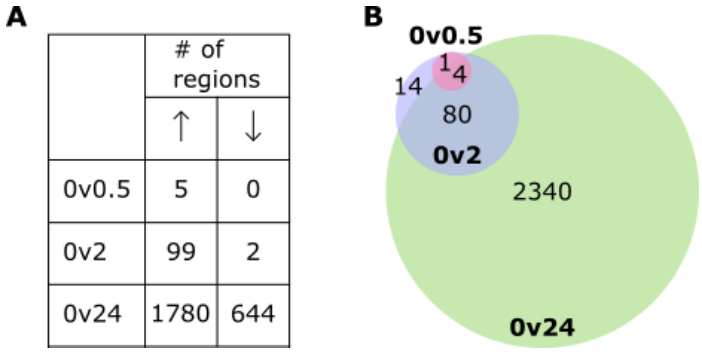

Figure 4.17: IFNγ induces late changes in histone accessibility.
A Summary of the numbers of differential ATAC-seq peaks per condition; untreated vs 0.5 hrs, 2 hrs or 24 hrs of IFNγ treatment. **B** Venn diagram showing IFNγ-induced ATAC-seq changes for each condition; untreated vs 0.5 hrs (pink), 2 hrs (blue) or 24 hrs (green) of IFNγ treatments.

changes in the previous section, I next sought to investigate how DNA accessibility is affected by IFNγ signalling. To this end, DESeq2 was used to identify significant changes in ATAC-seq peaks.

Thousands of differential ATAC-seq peaks were identified over the 24 hr IFNγ timecourse (Fig:4.17A & B). Again this demonstrates the immense impact IFNγ signalling imparts on a cancer cell line's chromatin. Unlike the intergenic SNU-seq and H3K27ac data, virtually all accessibility changes occur at 24 hrs of IFNγ treatment. Early changes in ATAC-seq signal are mostly sustained throughout the remainder of the IFNγ timecourse. Therefore it seems that the dynamics of open chromatin is slower and more durable than histone acetylation and transcription. As open chromatin is bound by several factors, it is likely that the energy required to displace these factors add to the durability of open chromatin.

Interestingly, 85% of increases already have a peak of accessibility in the untreated datasets, indicating that very few accessible regions are formed *de novo*. This suggests that the majority of enhancers/promoters with the ability to be activated have already been predetermined within the cell line. Increased transcription at these elements, caused by their IFNγ-induced activation would, in turn, lead to a higher histone

turnover. The delay in differential ATAC-seq peaks, only becoming significant after 24 hrs of IFNγ treatment (Fig:4.17A & B), could be due to the already high levels of accessibility seen in the untreated samples, thus making significance harder to achieve.

4.2.2.3.2 IFNγ-induced ATAC-seq changes are enriched for IRF binding motifs

Unsurprisingly, given that most significant changes occur late in the IFNγ response, increasing ATAC-seq signals are highly enriched for IRF motifs, with the IRF1 binding motif enriched with a p-value of $1e^{-1571}$ (Fig:4.18). In comparison, the STAT1 motif was very lowly enriched with a p-value of $1e^{-13}$, and thus is unlikely to be involved in this chromatin remodelling. IRF1 may be able to drive increased accessibility directly. It could also modulate this indirectly through increased histone turnover due to sustained elevated transcription, or by recruitment of TFs and chromatin remodellers.

Approximately one-quarter of significant changes show decreases in accessibility (Fig:4.17A). Motif analysis surrounding these decreasing peaks identified a motif enrichment for the TEAD family of TFs, key effectors of the Hippo signalling pathway (Fig:4.18) [Santucci et al., 2015]. IFNγ treatment activates the expression of GBP-1. It has previously been found that this protein binds and inhibits the TEAD TF family which results in suppression of proliferation [Unterer et al., 2018]. The enriched TEAD motifs within decreasing ATAC-seq peaks suggest that IFNγ signalling in Hep3B cells may act to diminish Hippo signalling, once again demonstrating crosstalk between IFNγ and other signalling pathways.

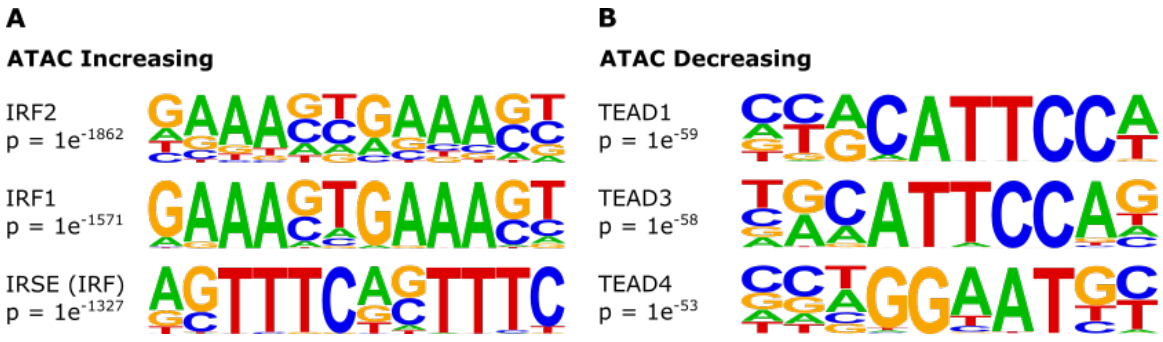

Figure 4.18: Motif enrichment analysis of increasing and decreasing differential ATAC-seq peaks.
A-B Homer motif analysis identifying enriched known motifs at peaks of IFNγ-induced increasing (**A**) or decreasing (**B**) ATAC-seq peaks. The p-value for the top three ranked motifs is shown for each condition.

4.2.2.3.3 ChIPseeker reveals most IFNγ-induced changes in accessibility are intergenic

Peaks of DNA accessibility are found at promoters, enhancers, insulators and topologically associating domain (TAD) boundaries. Histone displacement is required at these sites to allow factors to bind, enabling the regulatory or architectural function. To determine the distribution of differential ATAC-seq peaks across the genome, ChIPseeker was performed on all peaks as well as IFNγ-induced differential peaks (Fig:4.19). Over half of all ATAC-seq peaks identified in Hep3B cells were located at promoters. In sharp comparison, only $\sim$5% of differential accessibility was identified at a promoter. Instead, most changes occur within distal intergenic regions or introns. This indicates that IFNγ signalling dramatically alters non-coding regions of the genome. Given the high numbers of intergenic acetylation and transcriptional changes seen in the previous sections, this data further supports the ability of IFNγ to dramatically alter the enhancer landscape of a cell. Furthermore, the numbers of differential intergenic signals compared to promoter signals suggests that IFNγ regulates more enhancers than genes.

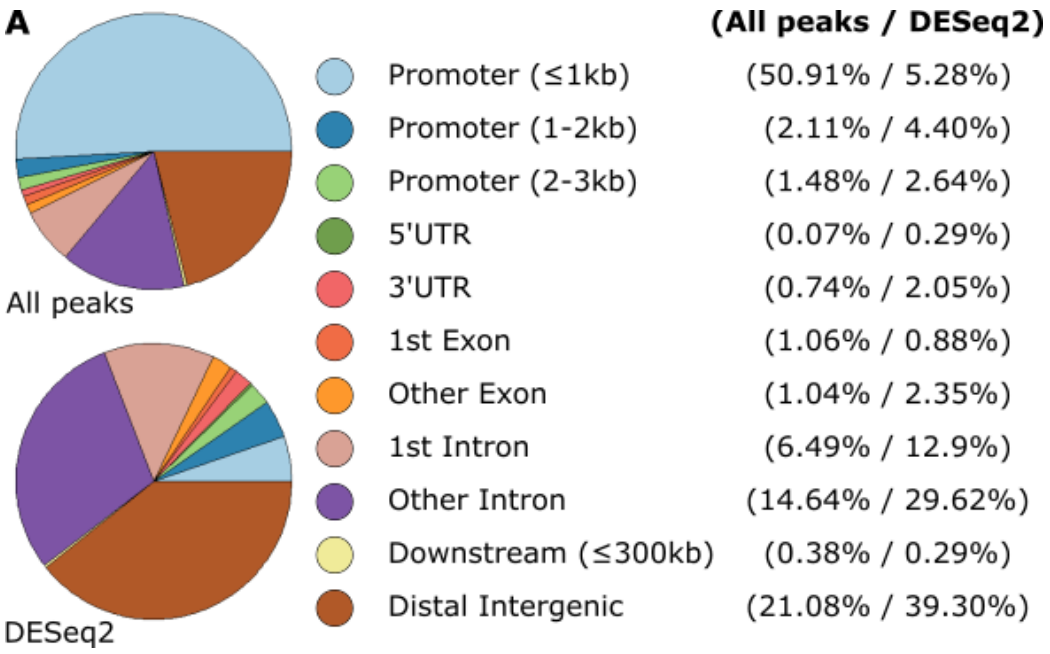

Figure 4.19: Differential ATAC-seq peaks are predominantly found within intergenic regions.
A Pie charts showing the distributions of all (top) or differential (bottom) ATAC-seq peaks as annotated by ChIPseeker.

4.2.2.4 IFNγ signalling has little effect on CTCF binding

Aforementioned in the previous section, regions of open chromatin are commonly present at promoters, enhancers, insulators and at higher-order chromatin structure boundaries. Very few IFNγ-induced ATAC-seq changes occurred at promoters and it is reasonable to assume a large proportion of changes are found at enhancer elements, given the large number of differential intergenic transcription and histone acetylation (Fig:4.10, 4.16 & 4.19). However, the effects of IFNγ on insulators and TAD boundaries have not yet been considered. DNA accessibility, in addition to CTCF binding, is commonly associated with both insulator elements and TAD boundaries [Szabo et al., 2019, Klein and Hainer, 2020].

When analysing motif enrichment at ATAC-seq peaks with significantly decreased transcription, CTCF binding motifs were significantly enriched (Section 4.2.2.1).

Additionally, the CTCF motif is enriched in peaks of significantly decreasing ATAC-seq signal. This suggested activity of insulators and/or TAD boundaries could be affected by IFNγ treatments. Conversely, bidirectional transcription has been observed at CTCF binding sites and CTCF has also been found at enhancers and promoters, suggesting an alternative function of CTCF in gene regulation [Melgar et al., 2011, Ren et al., 2017]. Thus, the enrichment of CTCF binding motifs at sites of IFNγ-induced transcriptional or ATAC-seq changes may represent changes in promoter:enhancer activity, as opposed to insulators or TAD boundaries. However, the p-values for both of these enrichments are relatively low, with p-values of $1e^{-4}$ and $1e^{-3}$ respectively.

Genomic CTCF distributions in untreated and treated cells were identified using ChIPmentation and differential binding was analysed using DESeq2. No changes in CTCF binding was found in the 0.5 hrs and 2 hrs IFNγ treatment groups and only 20 significant changes were identified after 24 hrs. Thus IFNγ has virtually no impact on CTCF binding within Hep3B cells, up to 24 hrs of treatment. It, therefore, seems unlikely that IFNγ signalling dramatically alters the insulator environment or TAD boundaries. TAD boundaries have been found to be relatively stable within a cell line and thus are unlikely to be affected by a stress response, such as IFNγ signalling [Dixon et al., 2012]. However, one cannot rule out that the higher-order chromatin structure within the cell could be changing and this could provide a mechanism to regulate insulators and/or TAD boundaries, independently of CTCF binding.

4.2.3 IFNγ treatments increase enhancer-promoter interactions

As previously demonstrated, IFNγ signalling leads to extensive remodelling of both the promoter and enhancer landscape within Hep3B cells. An active enhancer must be in close 3D proximity to its subjugated promoter to activate gene expression.

Whether a loop between a promoter:enhancer is preformed, or is induced under stress conditions is not well understood. More specifically, the extent to which the higher-order chromatin structure is regulated by IFNγ remains mostly unknown.

As discussed in Sections 3.2.4 & 3.2.8, we have seen two examples of IFNγ-induced gene expression. IRF1 becomes upregulated after just 30 min of IFNγ treatment (Fig:3.12, Section 3.2.3.3). An enhancer element 5kb upstream of the promoter becomes heavily activated at the same time point. Remarkably, within 30 min of treatment, there is a significant increase in interaction between IRF1's promoter and enhancer element. This significance is sustained after 2 hrs of IFNγ treatment (Fig:3.14, Section 3.2.4), thus demonstrating the ability of IFNγ to induce changes in higher-order chromatin structure.

Alternatively, IFNγ treatments induce expression of PD-L1 after 2 hrs of treatment (Fig:3.18). Capture-C experiments examining interactions to the PD-L1 promoter found no significant changes in interaction frequency across the entire genome, exemplifying that differential gene loops are not necessary for every IFNγ-induced gene (Fig:3.25).

4.2.3.1 The STAT1 promoter and enhancer show activating modifications upon IFNγ treatments

To examine whether the gene loop alteration seen at the IRF1 locus was a solitary phenomenon, Capture-C was performed from another vantage point; the promoter of STAT1. Transcription of STAT1 is significantly induced from 30 min of IFNγ treatment, with its transcript levels significantly upregulated by 2 hrs (Fig:4.20). The promoter shows the expected activating signals; increases in bidirectional transcription, H3K27ac and H3K4me3. The latter only increases significantly after 24 hrs IFNγ treatment, again highlighting the uncoupled nature of H3K4me3 and transcription discussed in section 4.2.1.3. The accessibility of the promoter also

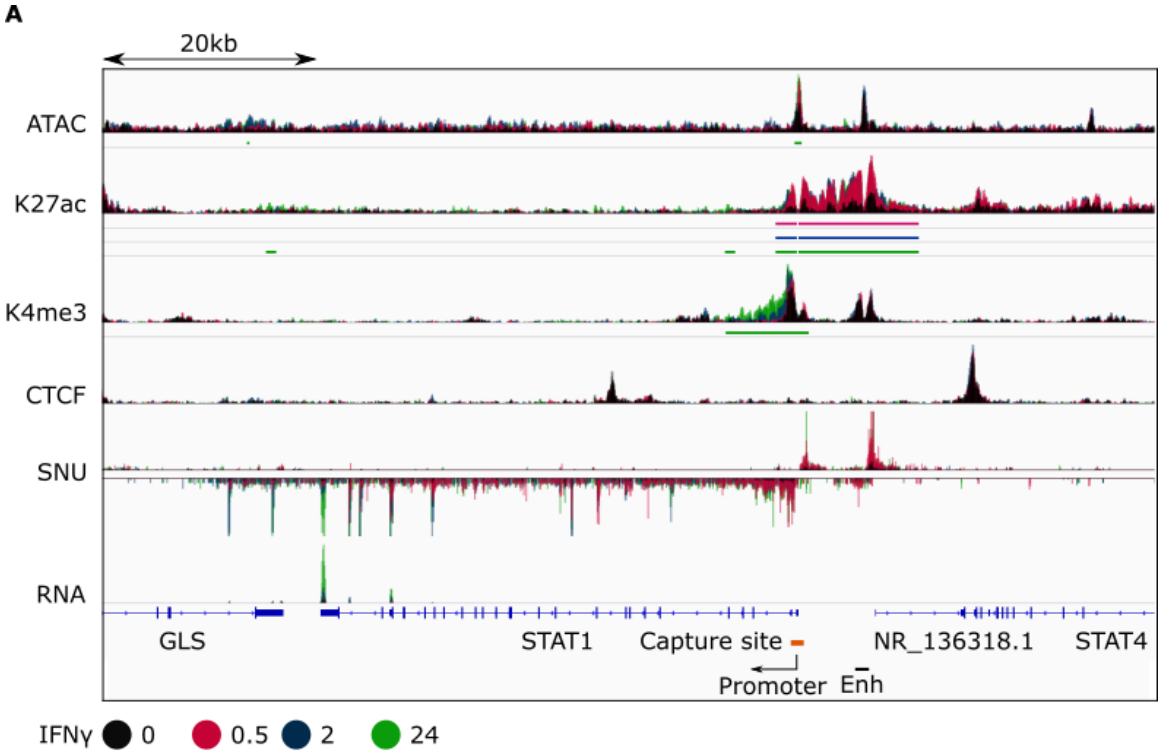

Figure 4.20: STAT1 is regulated by IFNγ via an upstream enhancer element.
A A 200kb stretch of the STAT1 locus showing DNA accessibility, ChIP profiles of H3K27ac, H3K4me3 and CTCF, strand-specific SNU-seq data and 3'-RNA-seq data for each treatment sample (n=2-3). All tracks are spike-in normalised except ATAC-seq and CTCF which are normalised based on sequencing depth. Each track shows the untreated sample in black, and 0.5, 2 and 24 hrs of IFNγ treatment in pink, navy and green respectively. Significant changes ($q<0.05$) for ATAC-seq, H3K4me3, H3K27ac and CTCF are represented by bars below the corresponding track. The colour of the bar denotes which timepoint shows a significant difference compared to the untreated sample, with pink, navy and green representing 0.5, 2 and 24 hrs respectively. The capture site used in Capture-C is denoted by the orange bar.

mildly, but significantly, increases after 24 hrs of IFNγ treatment. All in all, giving the profile of a highly active promoter.

Approximately 6kb upstream of STAT1, an element showing enhancer-like characteristics becomes activated after 30 min of IFNγ treatments (Fig:4.20). The enhancer element, marked by a stable peak of accessibility, demonstrates huge increases in acetylation and bidirectional transcription. The element appears to align with the promoter of NR_136318.1, an uncharacterised ncRNA. However, upon closer inspection, this element actually resides 1kb upstream of the NR_136318.1 promoter (Fig:4.20 & 4.21). This could be due to an incorrect annotation of the TSS. Conversely, as transcription of this enhancer element does not appear to continue across the entire ncRNA gene, it is likely to be independent of the ncRNA. Given the proximity and transcriptional coordination, one would predict that this enhancer is involved in the regulation of STAT1 expression.

4.2.3.2 IRF1 and STAT1 bind to the STAT1 promoter and enhancer elements

As in section 3.2.9, macrophage ChIP-seq and ATAC-seq data from the Ivashkiv lab was used to identify IRF1 and STAT1 binding to the STAT1 locus (Fig:4.21). Upon IFNγ treatments, increases in Pol II can be observed, signifying an increase in STAT1 expression in macrophages. Aligning to that seen in Hep3B cells, the macrophage data reveals a peak of accessibility just upstream of NR_136318.1. STAT1 protein binds to this enhancer element and marginally to the STAT1 promoter in untreated cells, whilst no IRF1 binding is detected. 24 hrs of IFNγ signalling results in increased STAT1 binding and induced IRF1 binding to both the promoter and enhancer. Combining both the macrophage and Hep3B cell data, it would appear that both elements are regulated by STAT1 and IRF1 and are activated simultaneously; transcription and acetylation are significantly upregulated after 30 min of treatment.

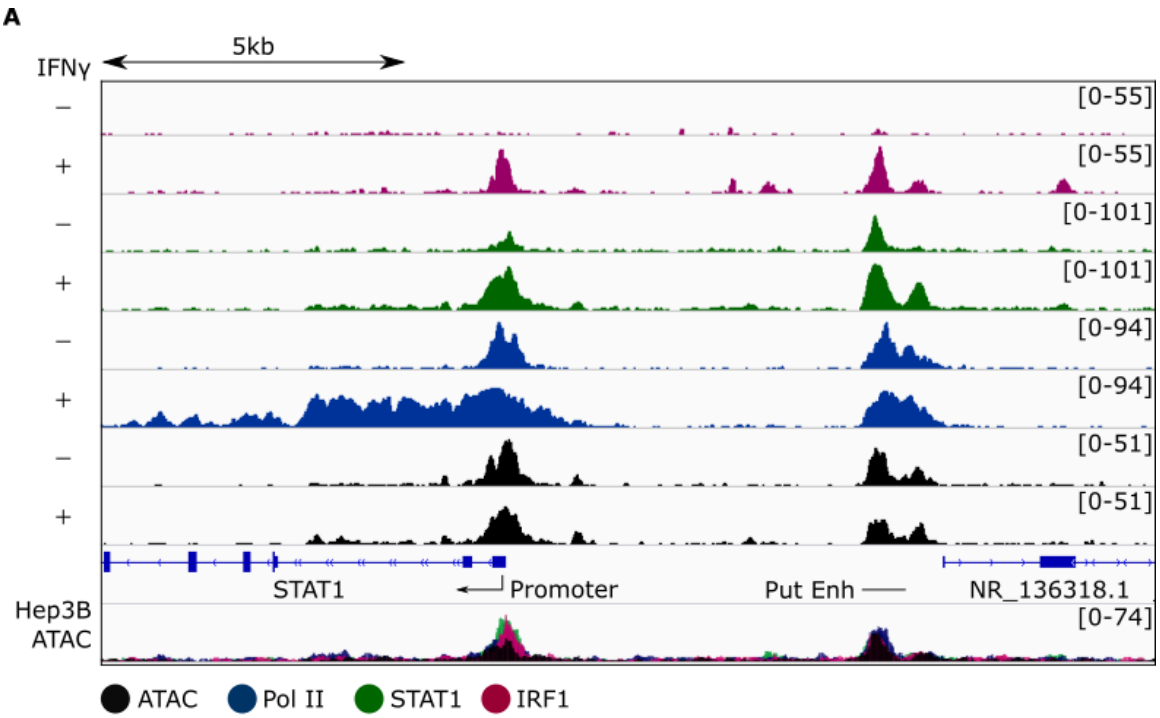

Figure 4.21: Both STAT1 and IRF1 bind to the STAT1 promoter and upstream enhancer element.
A A 20kb stretch of the STAT1 locus, showing published macrophage data (upper tracks) and Hep3B ATAC-seq data (bottom track). The upper tracks (top to bottom) show published macrophage ChIP-seq profiles of IRF1 (pink), STAT1 (green) and Pol II (dark blue) as well as ATAC-seq data (black).

This further cements the notion that this upstream regulatory element is involved in IFNγ-induced STAT1 upregulation.

4.2.3.3 IFNγ treatments significantly upregulate STAT1 promoter:enhancer interactions

To confirm this regulatory element as STAT1's enhancer, and to test inducibility of higher-order chromatin structure by IFNγ treatment, Capture-C was performed on the STAT1 promoter (Fig:4.20, orange bar denotes capture site). In the untreated sample, there is a small interaction to the upstream putative enhancer site (Fig:4.22). This gene loop is observed at every timepoint tested. The STAT1 promoter showed

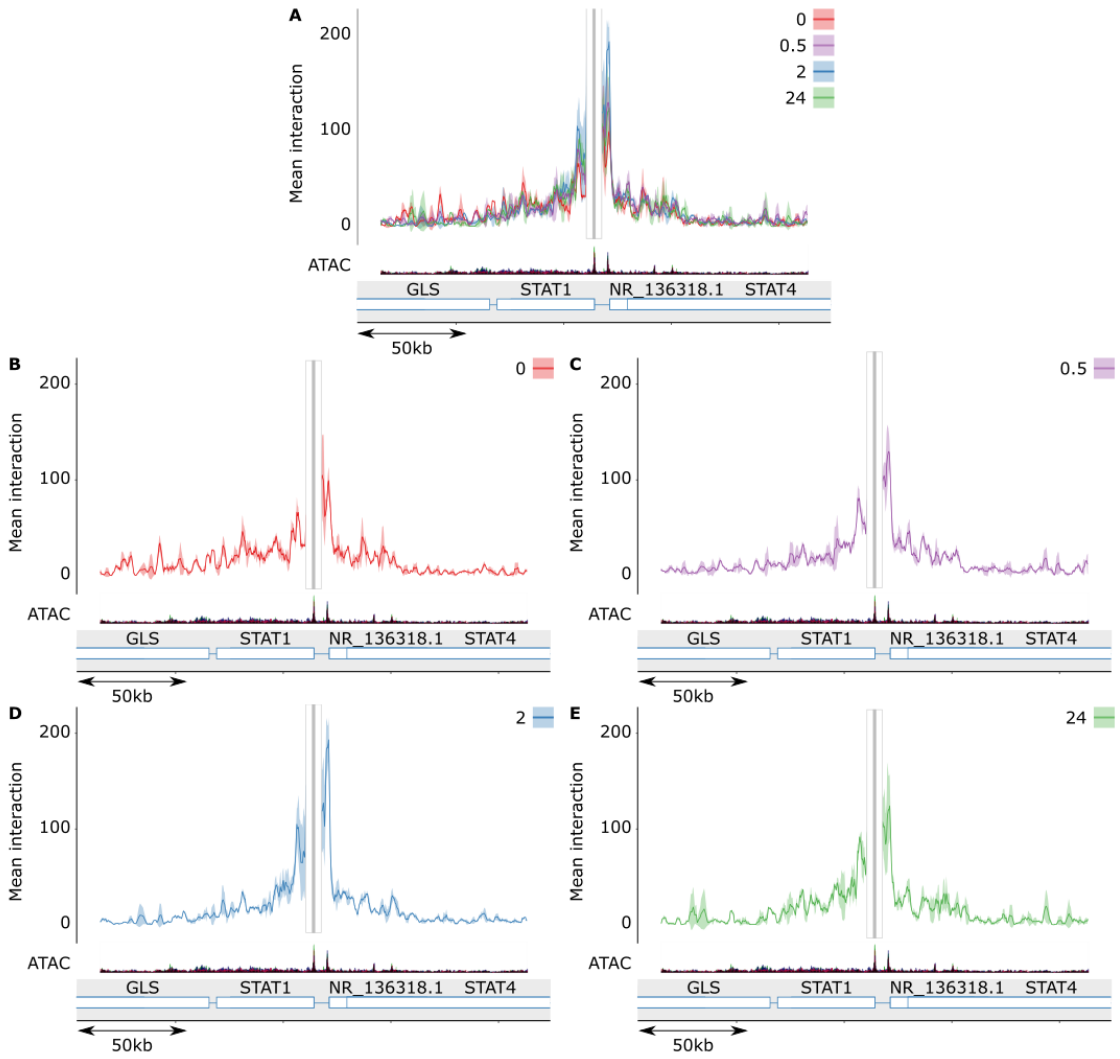

Figure 4.22: The STAT1 promoter loops to the downstream putative enhancer.
Normalised Capture-C data showing the mean and standard deviation of reads for the STAT1 promoter for all samples (**A**), untreated (**B**), 0.5 hrs (**C**), 2 hrs (**D**) or 24 hrs (**E**) IFNγ treated samples (n=2). Reads were normalised based on number of *cis* reads per 100,000 reads. The data is smoothed based on mean reads within a 2000bp window. ATAC-seq data is shown below the Capture-C data.

very little interaction with other regions of the genome.

After just 30 min of IFNγ treatment, the time taken to significantly upregulate STAT1 transcription, there is a significant increase in the interaction of the upstream enhancer element to the STAT1 promoter (Fig:4.22 & 4.23A). The percentage of *cis* reads over total reads (*cis* + *trans* reads) remains fairly constant in each sample, representing similar library qualities in each and indicating that these changes are real (Fig:4.23B). This promoter:enhancer interaction is increased in every IFNγ treatment timepoint tested, as can be seen in Fig:4.22. However, the increase is not significant at 2 and 24 hrs of treatment compared to the untreated samples.

The IRF1 and STAT1 promoters show differential promoter:enhancer contacts induced by IFNγ treatments. In both cases these changes are rapid, occurring after just 30 min of treatment. IRF1 protein is not observed in Hep3B cells until 2 hrs of IFNγ treatment (Fig:3.1, Section 3.2.1.1), thus, the probable TF involved in driving this change is pSTAT1.

Given that two out of three promoters analysed show differential genome interactions, it seems likely that these changes additionally occur elsewhere in the genome. The model of IFNγ-induced activation of IRF1, depicted in Fig:3.17, is likely a general mode of action of IFNγ-induced promoter/enhancer activation, applying to multiple genes. The extent to which IFNγ regulates higher-order chromatin structure requires further investigation. Nonetheless, it is clear that IFNγ regulates copious enhancers in addition to the interactions of these enhancers to their corresponding promoters, the result of which is tightly regulated, dynamic, differential gene expression.

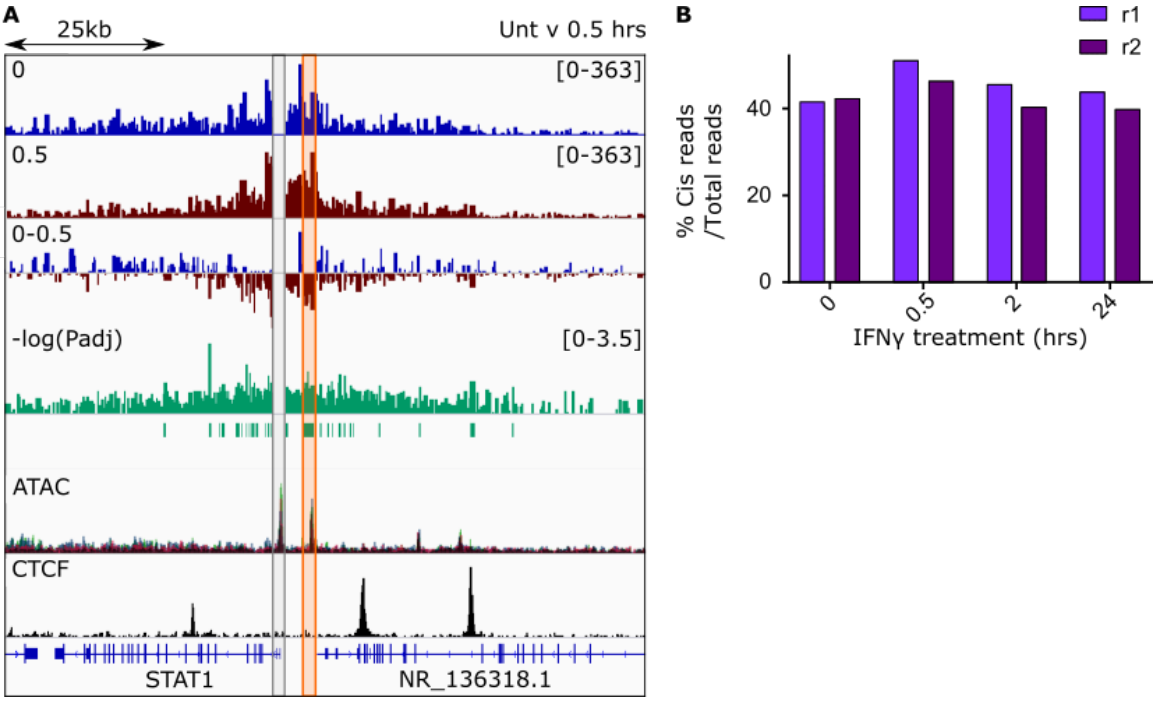

Figure 4.23: IFNγ-induces significant changes in STAT1's promoter:enhancer interactions.
A Untreated vs 0.5 hrs IFNγ treated Capture-C data for the STAT1 promoter. Reads are counted per NlaIII digested fragment. The top two tracks show *cis*-normalised mean data for the untreated and treated samples in blue and red respectively. The 3^{rd} track is subtracted treated sample from untreated sample, with blue and red corresponding to more signal in the untreated or treated sample respectively. In green is the -$\log_{10}$(Padj) value from the DESeq2 results, with bars showing significant (Padj<0.05) differential reads between the untreated and treated NlaIII digested fragment. Normalised ATAC and CTCF tracks are shown. The position of the STAT1 probe is highlighted in grey and the putative STAT1 enhancer element highlighted in orange. **B** Bar chart showing the percent of *cis* reads over the total reads for each Capture-C sample and repeat for STAT1. Similar ratios indicate similar library qualities.

4.3 Discussion

In this chapter I analyse genome-wide effects of IFNγ treatments on the transcriptional, epigenetic and enhancer landscapes within a hepatocellular carcinoma cell line. To this end, I find that IFNγ induces multiple layers of regulation on gene expression, activating promoters and regulatory elements as well as inducing changes in higher-order chromatin structure, resulting in increased interactions between promoters and their constituent enhancers.

4.3.1 An uncoupling between transcription, transcript levels and epigenetic marks

This chapter used multiple techniques to assess transcript levels, nascent transcription and epigenetic marks upon induced cellular stress (IFNγ treatments), allowing the study of the interplay between these factors to gain an understanding of how differential gene expression is achieved. Surprisingly, these factors did not correlate as much as one would expect, and many examples of their uncoupled nature can be seen within the data.

4.3.1.1 Transcription and transcript levels

Firstly, an increase in nascent transcription would, in theory, result in increased transcript levels. Indeed, the correlation between differential RNA-seq data and SNU-seq data was discovered to be significantly positive. However, not all increases in transcription resulted in an increased transcript level and vice versa. This is further demonstrated as IFNγ induced 336 differentially transcribed genes but only 132 genes had significantly different transcript levels. Only 89 genes overlapped between the two datasets. Additionally, there were instances of increased transcription corresponding to no change or decreases in transcript levels, and the same in reverse.

Many mechanisms exist to regulate transcript levels. Every part of transcription is regulated, including initiation, elongation and termination [Porrua and Libri, 2015]. Following this, transcripts are post-transcriptionally modified which may indirectly affect their degradation rates [Guhaniyogi and Brewer, 2001, Boo and Kim, 2020]. Thus, the lack of correlation between transcription levels and transcript abundance could be caused by different rates of transcription termination or an altered RNA transcript stability leading to differential transcript turnover.

Another cause of the discrepancies may be explained by limitations within the RNA-seq and SNU-seq techniques themselves. Although differentially expressed genes are easily determined, it is difficult to define an expressed or highly expressed gene. Increases in transcription at a gene with already high transcript levels may cause differences in transcript levels to be masked and be insignificant. Additionally, as many enhancers reside within genes, differential transcription at these enhancers may result in a false positive within the SNU-seq data; a gene may be regarded as differentially transcribed due to altered transcription within the gene, despite this transcription not being associated with transcription of the gene itself.

Altogether, IFNγ-induced differential transcription and transcripts quantities revealed a general positive correlation. Examples of disparities may have been caused by altered regulation of transcripts or potential limitations within the techniques used.

4.3.1.2 H3K4me3 and RNA expression

Numerous papers state that H3K4me3 is an activating histone modification that correlates strongly with transcription. This is due to the findings that many promoters of highly active genes show high levels of H3K4me3 [Santos-Rosa et al., 2002, Bernstein et al., 2005]. Thus it was proposed that H3K4me3 is required for transcription. Recently, however, this statement is becoming highly debated

and contradictory evidence now leads one to question whether the mark is instructive, a consequence or bears no relation to transcription [Howe et al., 2017, Murray et al., 2019].

Treating Hep3B cells with IFNγ resulted in the differential regulation of over 300 genes. These rapid stress-induced transcriptional changes provided a good system in which to investigate the link between histone modification and gene expression. As both SNU-seq and 3'-end RNA-seq were performed, this allowed a comparison of H3K4me3 to transcript levels in addition to the process of transcription itself.

By looking at individual early induced gene loci, we saw cases where transcription was first induced by IFNγ treatments, but the deposition of H3K4me3 was delayed. A small amount of H3K4me3 was present in the untreated sample in both examples and so it can't be ruled out that some H3K4me3 was required for transcription. Similarly, these delays in the deposition of trimethylation following gene induction have been seen in yeast and mice [Howe et al., 2017]. I demonstrated that IFNγ-induced transcription showed almost no correlation to induced differential H3K4me3 signals. Together this indicates that levels of H3K4me3 do not instruct the level of transcription. The lack of correlation additionally suggests that increased transcription does not result in increased writing of the H3K4me3 mark, further demonstrated by the lack of overlaps between significant transcription and H3K4me3 IFNγ-induced changes.

Interestingly, IFNγ-induced differential H3K4me3 signals correlated more positively with transcript levels. The lack of correlation to transcription suggests no association between transcription initiation and elongation, however, by correlating with transcript levels, could indicate a role in transcriptional termination or RNA stability. Indeed H3K4me3 has been linked to promoting Nrd-1 dependent termination [Terzi et al., 2011], in addition to being linked to RNA splicing, both of which play a role in RNA stability [Howe et al., 2017]. However, recent papers find

H3K4me3 has no effect on RNA stability [Murray et al., 2019]. Thus further research must be performed to ascertain whether H3K4me3 regulates transcript levels or vice versa.

4.3.1.3 H3K27ac and transcription

H3K27ac is a second histone modification that has been correlated to promoter and, additionally, enhancer activity [Wang et al., 2008, Creyghton et al., 2010]. Studies have found links between H3K27ac and eRNA production, with loss of acetylation resulting in a reduction of enhancer transcription and, consequently, activity [Arnold et al., 2020]. Histone acetylation results in weaker histone:DNA contacts, allowing transcriptional machinery to bind to the DNA, thus providing a more transcriptionally permissive environment. TFs involved in IFNγ signalling, namely STAT1 and IRF1, associate with H3K27ac writers, CBP and p300 [Zhang et al., 1996, Ramsauer et al., 2007, Leung et al., 2019]. Therefore unsurprisingly, analysing H3K27ac deposition over an IFNγ treatment timecourse revealed thousands of differential acetylation sites, with only a small proportion of changes occurring at gene promoters. It was decided to correlate H3K27ac changes with the SNU-seq data, as this captures both coding and non-coding transcription, unlike 3'-end RNA-seq.

After 30 min of IFNγ treatment, H3K27ac and transcription showed a slight positive correlation, but this matured to no correlation by 24 hrs of IFNγ treatments. The analysis revealed numerous cases of increasing transcription with decreased or no change in H3K27ac signal and vice versa. This strongly suggests that the two features are uncoupled; an increase of one does not necessarily result in the increase of the other.

Published data found that H3K27ac distinguishes active enhancers from poised enhancers containing H3K4me1 but lacking the acetylation mark

[Creyghton et al., 2010]. The uncoupled nature between acetylation and transcription observed in this study suggests that deposition of H3K27ac may further prime an enhancer/promoter, without fully activating it. In this scenario, enhancer/promoter elements become acetylated, resulting in a more transcriptionally facilitative environment but transcription initiation remains blocked (Fig:4.24). Thus, these 'silent' acetylation changes lack additional signals needed for transcription. This could explain circumstances of IFNγ-induced H3K27ac deposition without corresponding changes in transcription. This phenomenon has previously been observed in macrophages [Qiao et al., 2013]. Similarly, a recent paper found H3K27ac and eRNA production at an enhancer to be separate events, with eRNA production providing a better prediction of enhancer activity [Tyssowski et al., 2018].

Building from this hypothesis, IFNγ treatments may provide the signal that was previously lacking at already acetylated loci. This would then activate transcription, corresponding to activation of the enhancer/promoter, without further increasing levels of H3K27ac. Indeed transcription of enhancers correlates strongly with their activity [Catarino and Stark, 2018]. This would provide an explanation as to how differential transcription is not always coupled to differential H3K27ac. Further analysis would need to be performed to determine how many significantly increasing SNU-seq signals have constitutive high levels of H3K27ac throughout the IFNγ timecourse. Alternatively, situations may arise where transcription is inhibited, whilst peaks of H3K27ac remain, returning the enhancer/promoter into a primed state, or a primed but transcriptionally inactive enhancer/promoter loses its acetylation.

Other possibilities explaining the disassociated nature between transcription and H3K27ac likely exist. Higher levels of transcription correlate with increased histone turnover [Dion et al., 2007], which may, in turn, result in decreased histone acetylation. Negative feedback loops are imperative to IFNγ signalling to prevent aberrant inflammation. Histone deacetylases are likely recruited to

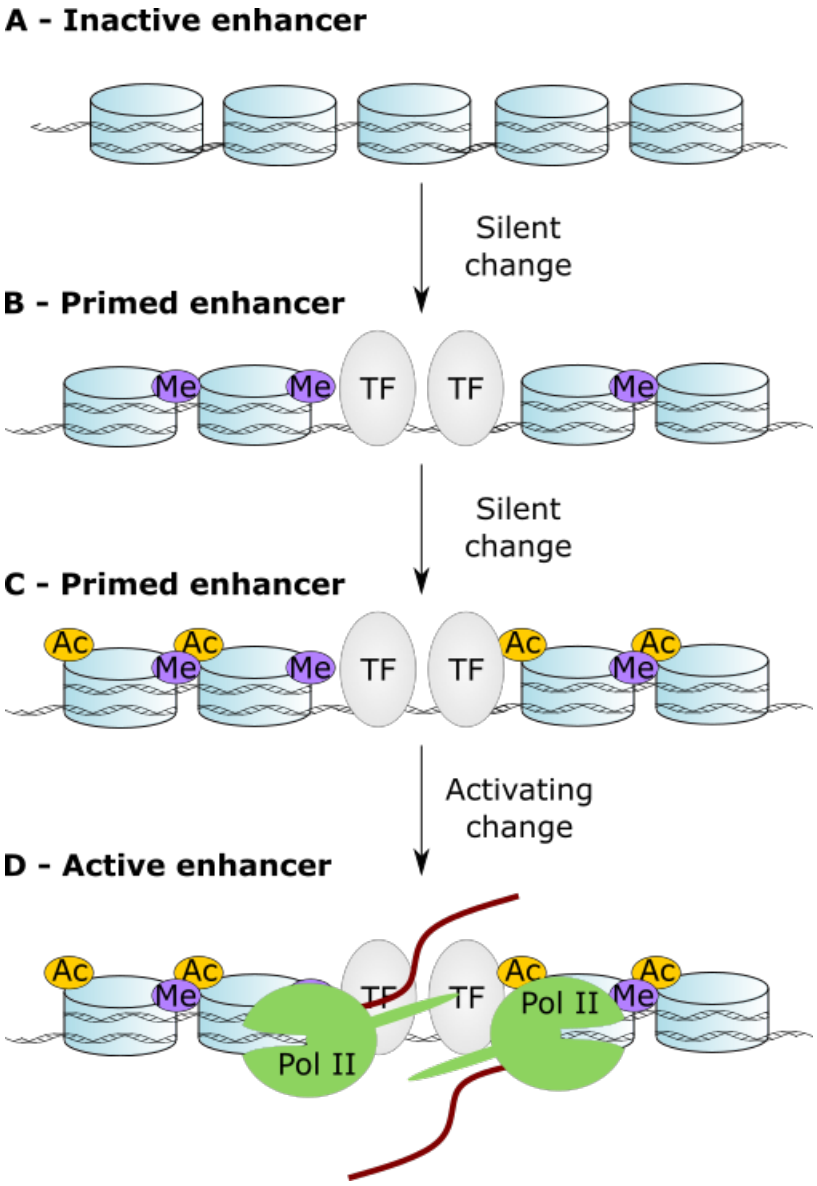

Figure 4.24: Model: Steps resulting in the activation of an enhancer.
A A completely inactive enhancer. The DNA is inaccessible. **B** TF binding to the enhancer maintains an accessible region of DNA. Histones are monomethylated on H3K4, but the enhancer lacks acetylation and bidirectional transcription. This enhancer is primed but not active. **C** Activating signals from **B** are still present, but now histones surrounding the enhancer become heavily acetylated. Bidirectional transcription is still not occurring and the enhancer remains in a further primed, but inactive state. **D** The enhancer becomes fully activated. All active marks from **C** are present, but bidirectional transcription has additionally been induced.
Steps involved in inducing the enhancer up to stage **C** are silent changes; they prime the enhancer without inducing its activity. Each step from **A** to **C** requires further signals to activate the enhancer. A new signal may further prime the enhancer, or fully activate it by inducing multiple steps simultaneously. Additional steps are likely to exist.

sites of increased acetylation to reduce transcription. Indeed the BCL6 motif, a transcriptional repressor that functions by recruiting corepressors and histone deacetylases [Melnick et al., 2002], was found to be enriched at peaks of differential acetylation. Although H3K27ac would be erased, this presumably would not affect already elongating Pol II. Thus a short delay between loss of acetylation and transcription may exist, affecting correlations.

Recently, the requirement for both H3K4me1 and H3K27ac at active enhancers has been questioned, and instances of enhancer activation without these modifications have been identified [Pradeepa et al., 2016, Catarino and Stark, 2018]. This further complicates our understanding of enhancer activity and requires additional research to distinguish between sufficient and necessary activating enhancer marks.

4.3.2 IFNγ dynamically induces transcriptional and epigenetic changes

4.3.2.1 STAT1 and IRF1 mediate the early and late IFNγ response respectively

STAT1 and IRF1 are known key drivers of the IFNγ signalling response. The binding of IFNγ to its receptor rapidly leads to phosphorylation and subsequent activation of STAT1. Activation of this TF results in the differential regulation of IFNγ early induced genes within 30 min of IFNγ signalling, including IRF1. Together with STATs, these early induced genes modulate the full complement of IFNγ-stimulated genes [Platanias, 2005]. In this thesis, cells were monitored at three timepoints; 0.5, 2 and 24 hrs of IFNγ treatment. This time frame enabled the capture of both the early and late IFNγ response.

3'-end RNA-seq and ATAC-seq identified differential regulation almost entirely within two phases; early induced (0.5 and 2 hrs) and late induced changes (24 hrs),

with the majority of differential regulation present in the later. Whilst many early induced changes were maintained throughout the treatment course, a proportion of early IFNγ-induced upregulated signals were lost by 24 hrs of signalling, emphasising the presence of negative feedback loops.

Motif analysis of all datasets primarily identified a shift in motif enrichment from the STAT family to the IRF family of transcription factors. This insinuates pSTAT1 and IRF1 as the main drivers of the early and late response respectively in Hep3B cells, consistent with published data (modelled in Fig:4.5) [Platanias, 2005]. IRFs have been found to interact with STAT1 and redirect it binding properties [Ostuni et al., 2013, Langlais et al., 2016, Abou El Hassan et al., 2017]. This could explain the reduction of enriched STAT1 motifs in the later time points tested, despite levels of pSTAT1 in Hep3B cells remaining high throughout the timecourse.

4.3.2.2 IFNγ treatments induce both transient and sustained changes over 24 hrs

The transcriptional and H3K27ac data reveal that the two distinct phases aren't as well defined as thought. Here, a different subset of promoters and enhancers were activated at every time point examined, revealing at least three distinct phases of IFNγ signalling. These responses will be depicted in this section as early, intermediate and late responses for 0.5, 2 and 24 hrs respectively. Moreover, a large fraction of changes were transient and not sustained into the following tested time point.

The removal of STAT1, by IRF1, from its native binding site may cause the changes in transcription and acetylation to be lost, resulting in the short-lived changes seen in these datasets (modelled in Fig:4.14). STAT1 recruits histone acetylases [Ramsauer et al., 2007]. Upon redistribution of STAT1, these histone acetylases are likely also diverted, and thus no longer sustain the increase in acetylation. Removal of acetylation may, in turn, switch off transcription. BCL6, found to be enriched within

IFNγ upregulated acetylation peaks, may modulate removal of the acetylation mark by recruitment of deacetylases (Fig:4.14) [Melnick et al., 2002]. This model would facilitate early and brief activation of promoters and enhancers, before activation of an alternative subset of genes/enhancers in the late IFNγ response. Altogether this provides a negative feedback loop, enabling fleeting alterations in acetylation and transcription, preventing aberrant IFNγ signalling.

4.3.2.3 IFNγ signalling cannot be divided exclusively into an early and late response

The presence of an intermediate response suggests the process can't be completely explained by a simple shift from STAT to IRF driven changes. This intermediate response was particularly obvious in the SNU-seq data, where transcriptional changes found after 2 hrs of IFNγ treatments were not identified at other timepoints. This phenomenon was seen, to a lesser extent, in the H3K27ac data. One explanation could be that minor deviations in a DNA motif effects TF binding affinities, thus affecting their binding dynamics. Imperfect motifs could delay the binding of STAT1, due to its preference to another motif, thus delaying the promotion of transcription and acetylation at these loci.

A second cause of this intermediate response could be due to the complex integration of other signals. Motifs were enriched for multiple members of the STAT and IRF families at each timepoint. STAT3 was commonly enriched at early/intermediate timepoints. Both STAT3 and pSTAT3 was expressed in untreated Hep3B cells. Therefore it is unlikely that this TF independently modulates the IFNγ response. However, pSTAT3 has been found to dimerise with pSTAT1 and together they may coordinate an altered response [Delgoffe and Vignali, 2013]. IFNγ upregulated the expression of other IRF TFs, in addition to IRF1. Whilst IRF1 mRNA was upregulated within 30 min, significant upregulation of IRF8 and IRF7

was first identified at 2 and 24 hrs respectively, likely causing a delay in the regulation of their governed genes. IFNγ regulates other signalling molecules, altering gene/enhancer expression through other pathways. For example, IFNγ signalling has been found to activate NFκB whilst inhibiting the TEAD family of proteins [Pfeffer, 2011, Thapa et al., 2011, Unterer et al., 2018], both of which regulate the expression of numerous genes. Enrichment of DNA binding motifs for these TFs at sites of IFNγ-induced differential signals suggests their involvement in gene regulation in Hep3B cells.

Altogether it appears that the shift from STAT1 to IRF1 administrating the IFNγ response is more complex, with the enhancer and transcriptional landscapes dynamically changing throughout 24 hrs of treatment. The combinations of multiple signals likely push and pull the response in particular directions, adding multiple levels of positive and negative feedback, resulting in either transient or sustained regulation. This thesis only analysed up to 24 hrs of IFNγ treatments, but the expression phenotype may evolve further with longer treatments.

4.3.2.4 Transcriptional memory and sustained gene expression

Studies have shown that removal of IFNγ treatments causes epigenetic and transcriptional changes to be lost [Siwek et al., 2020], revealing the reversibility of IFNγ signalling. Upon re-administration of IFNγ, a larger and more rapid response can be seen, a process termed transcriptional memory [Siwek et al., 2020]. Transcriptional memory describes the phenomenon whereby re-administration of a stimulus results in enhanced expression of a subset of genes, due to priming of these genes during their initial exposure. This has been observed in multiple organisms ranging from yeast to humans [Kamada et al., 2018, Bheda et al., 2020, Siwek et al., 2020]. The features maintaining memory remain obscure. Recent papers find epigenetic features, such as histone occupancy and histone variants,

to be implicated by accelerating the recruitment of Pol II upon the second stimulus [Kamada et al., 2018, Bheda et al., 2020]. However, another paper found maintenance of chromatin features to be short-lived. Instead, they suggest cohesin plays a key role in establishing transcriptional memory [Siwek et al., 2020].

It would be interesting to study whether the pattern of gene/enhancer activation is identical upon re-induction by IFNγ for 24 hrs. Would a second treatment with IFNγ induce an early, intermediate and late response with similar kinetics? One might predict that transcriptional memory only occurs in genes that were activated and sustained throughout the initial IFNγ treatment, as activating features are already lost within the 24 hrs of initial treatment in transiently expressed genes. This could be determined during a second IFNγ treatment on Hep3B cells.

Given the association of cohesin to transcriptional memory, perhaps establishing gene loops may enable more rapid recruitment of Pol II upon re-administration of IFNγ, conferring memory [Siwek et al., 2020]. None of the three promoters examined in this thesis; PD-L1, IRF1 and STAT1, demonstrated a sustained significant increase in interactions to an enhancer element and did not display IFNγ-induced transcriptional memory in HeLa cells [Siwek et al., 2020]. Thus, to investigate a potential role of higher-order chromatin structure, Capture-C should be performed at genes undergoing transcriptional memory.

4.3.3 IFNγ regulates more regulatory elements than it does genes

4.3.3.1 Thousands of IFNγ-induced epigenetic changes occur in non-coding regions

This study identified less than 400 genes with IFNγ-induced differential transcript or transcription levels respectively. Remarkably, IFNγ treatments stimulated thousands

of differential H3K27ac and ATAC-seq peaks genome-wide. In both datasets, less than 20% of these changes were present within 3kb of a gene promoter. Unlike accessible DNA regions, which form sharp, narrow peaks at a gene promoter, H3K27ac may spread into the gene body, especially into the first exon and intron. However, more than 60% of both ATAC-seq and H3K27ac changes were found in intergenic regions or introns (excluding the first intron). Thus, it appears that a large proportion of IFNγ-induced epigenetic differences were not caused by, or did not instruct, differential activation of a promoter. Instead, this suggests that IFNγ regulates significantly more enhancers than it does genes.

Commonly, due to the nature of H3K27ac deposition, multiple defined peaks are present at promoters and enhancers: In Hep3B cells, three peaks of differential acetylation surrounded the PD-L1 promoter and four and three peaks were present across the IRF1 and STAT1 promoter and enhancer loci respectively. Therefore the numbers of differential H3K27ac peaks do not reflect the exact numbers of differently regulated loci. Nevertheless, one would expect similar numbers of altered peaks at promoters and enhancers. As the distribution of differential acetylation signals favoured non-coding regions as opposed to promoter regions, the data still supports that IFNγ regulates the acetylation of more enhancers than promoters. This is reinforced by the large numbers of differential ATAC-seq peaks not at promoters. Finally, a comparison between the distributions of all H3K27ac/ATAC-seq peaks identified in any condition versus differential peaks found the IFNγ-induced changes were skewed towards non-coding genomic regions, albeit very minorly in the case of acetylation. This further endorses that IFNγ modulates more regulatory elements than genes.

4.3.3.2 Predicting the effect of IFNγ treatments on enhancer activity

Transcription of eRNA at an enhancer positively correlates with transcription of its target promoter, and thus correlates with enhancer activity [Andersson et al., 2014, Catarino and Stark, 2018]. Recently it has been argued that eRNA production provides a better indication of enhancer activity than H3K27ac levels [Tyssowski et al., 2018]. This property has been used to predict connections between enhancers and target promoters [Fishilevich et al., 2017]. As follows, enhancer transcription was investigated in Hep3B cells using SNU-seq to sensitively capture transient non-coding RNAs.

To identify IFNγ-induced transcription at enhancers, changes in SNU-seq data were examined within publicly available annotated enhancer databases. This method only discovered approximately 100 differentially transcribed enhancers. Furthermore, some enhancers were incorrectly identified as regulated by IFNγ: Certain enhancers residing within a gene reflected a change in gene expression as opposed to enhancer activation. Instead, a novel method to identify differential enhancer transcription was sought.

H3K4me1 is a modification commonly found at enhancers, although recent studies have found that it isn't necessary for enhancer activity [Catarino and Stark, 2018]. Performing H3K4me1 ChIP-seq would help identify enhancers within Hep3B cells. However, antibodies against H3K4me1 are notoriously substandard. Despite attempting H3K4me1 ChIP-seq using multiple different H3K4me1 antibodies, the quality of data obtained did not meet the standards I required and hence was not used.

One of the few unquestioned necessary enhancer features is the presence of accessible DNA, required for binding of TFs and promoter:enhancer interactions [Catarino and Stark, 2018]. Therefore, reads within a 5kb window of an ATAC-seq peak were counted, and differential analysis was performed using DESeq2.

This method identified novel enhancers specific to IFNγ treated Hep3B cells, not established in public enhancer databases.

ATAC-seq peaks are present at both promoters and enhancers. Analysing distributions of differentially transcribed accessible peaks found that approximately 50% were present within 3kb of a promoter, suggesting that half of the differentially transcribed peaks were changes in gene expression. This equates to 427 promoters with IFNγ-induced altered activity, an increase from the 336 differentially expressed genes identified. The cause of this discrepancy may be due to the stages of transcription regulation. An increase in transcription initiation may be enriched when analysing a 5kb window surrounding the gene promoter, but without successful elongation, differential transcription of the gene may not be significant. Promoters have also been found to act as enhancer elements, termed ePromoters [Engreitz et al., 2016, Dao et al., 2017, Diao et al., 2017]. Again this could result in increased transcription tightly surrounding the promoter but not into the gene body. Constitutive reads found in the gene body in each treatment group may reduce the significance of changes only occurring near the promoter, thus not identifying altered transcription of the gene. Lastly, IFNγ could alter TF binding at promoters, affecting accessibility, without altering transcription at this promoter.

50% of differentially transcribed ATAC-seq peaks were not within 3kb of a promoter and may represent the differential activity of regulatory elements, namely enhancers. Given the positive correlations found between transcription and enhancer activity, this suggests similar numbers of enhancers and promoters may be differentially activated by IFNγ treatments [Andersson et al., 2014, Catarino and Stark, 2018]. One enhancer can regulate multiple promoters, and multiple enhancers can regulate a single promoter [Sanyal et al., 2012]. Although both of these cases may be true in IFNγ-induced promoter:enhancer activation, the overall ratio appears to be 1:1. However, as

previously discussed, IFNγ treatment regulates more enhancers than genes, at least in terms of H3K27ac and accessibility. Despite an increase in acetylation, many of these enhancers remain quiescent, emphasised by the lack of transcription. This then raises the question, why does IFNγ regulate more enhancers than genes?

4.3.3.3 IFNγ induces silent acetylation deposition at enhancers, priming them for activation

This study raises a hypothesis to address the above question. As discussed in section 4.3.1.3, acetylation may further prime an enhancer element without resulting in full activation of the enhancer (modelled in Fig:4.24). These silent changes lack additional signals to recruit the full transcriptional machinery and/or the target promoter to the enhancer, blocking its activation. This would enable other signalling molecules, both intracellular and extracellular, to provide other components required for complete activation, thus allowing the integration of multiple signals to fine-tune the enhancer landscape of a cell, resulting in a specific gene expression phenotype. Under different signals, a particular subset of enhancers would be differentially activated, leading to an altered gene expression landscape (modelled in Fig:4.25). In the context of a tumour microenvironment, the immense and complex signals present would dictate the outcome of IFNγ signalling, making the effect of IFNγ signalling in a tumour microenvironment context dependent, as witnessed in the literature. Concluding the above, I hypothesise that IFNγ regulates thousands of enhancers, most of which remain redundant, to enable the amalgamation of signals present to instruct the response.

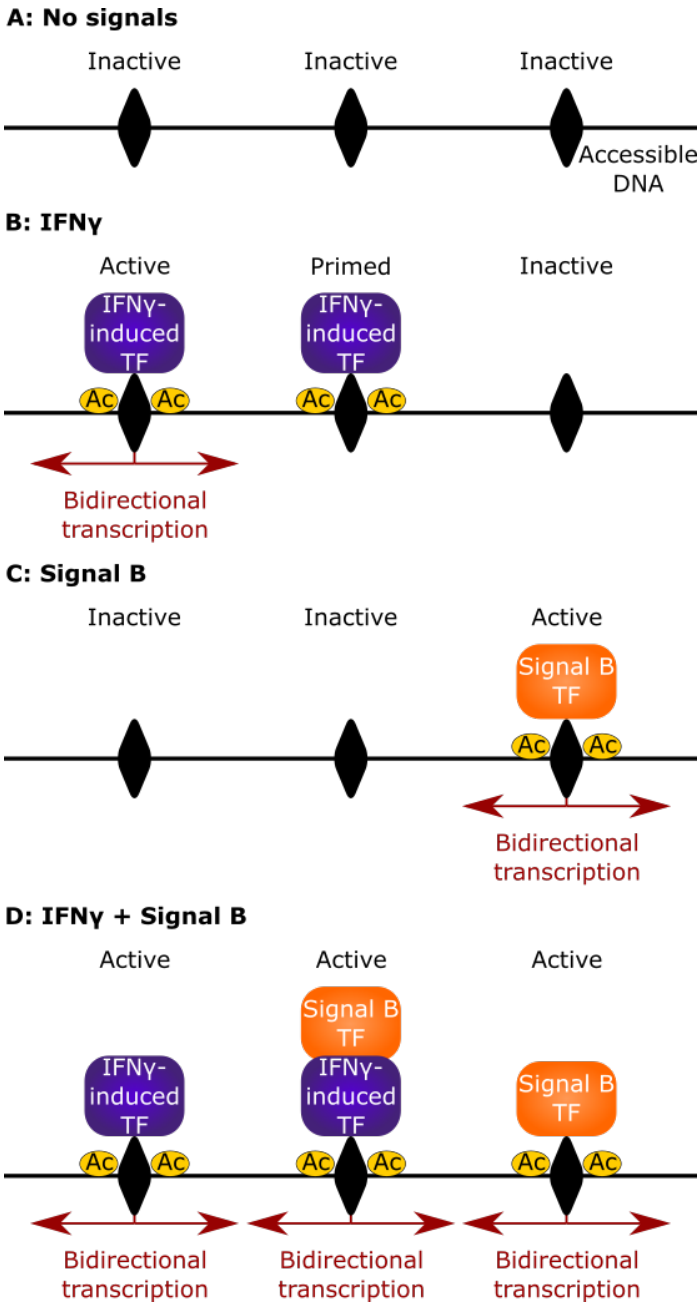

Figure 4.25: Model: IFNγ treatments prime enhancers enabling their activation in the presence of additional signals.
Signal B represents any signal able to synergize with IFNγ. **A** IFNγ and Signal B are not present. IFNγ- and Signal B-dependent enhancers are inactive. **B** In the presence of IFNγ, IFNγ-induced TFs fully activate a subset of enhancers. Another subset of enhancers become primed with acetylation but aren't fully activated. **C** Signal B activates a subset of enhancers, independent of IFNγ signals. **D** Both IFNγ and Signal B are present. Enhancers activated in **B** and **C** are still activated by each signal. Also, enhancers primed by IFNγ-induced TFs become fully activated by Signal B-induced TFs. The two signals synergize to activate a different subset of enhancers, resulting in a different cellular phenotype.

4.3.4 Higher-order chromatin structure as a further form of IFNγ-mediated gene regulation

IFNγ treatments stimulated significantly increased promoter:enhancer interactions within just 30 min of treatment. This highlights that stress responses can induce changes in higher-order chromatin structure, something that has been seldom researched previously. Out of three promoters tested, two promoters (IRF1 and STAT1) showed differential DNA looping to their enhancer elements. It is highly probable that IFNγ modulates higher-order chromatin structure at other gene promoters, thus providing an additional layer of regulation.

4.3.4.1 STAT1 is a likely candidate regulating IFNγ-induced changes in higher-order chromatin structure

pSTAT1 was upregulated within 10 min of IFNγ treatment, whilst IRF1 protein was first observed at 2 hrs of treatment (Fig:3.1). Therefore, given the kinetics of these differential interactions, it is likely that pSTAT1, rather than IRF1, directly or indirectly regulated these IFNγ-induced gene loops. The binding of TFs, such as pSTAT1, may directly bridge together a promoter and enhancer in spatial proximity. Alternatively, studies demonstrated that diminishing eRNA transcripts reduced DNA interactions [Pnueli et al., 2015, Liang et al., 2016]. The impact of eRNA transcripts, or the process of transcription itself, on gene loops requires further research. STAT1 recruits chromatin remodelers, TFs and cofactors, including histone acetylases, to sites of DNA binding to create a transcriptionally permissive environment and thus may indirectly stimulate promoter:enhancer interactions via eRNA transcripts/transcription (Fig:3.17) [Christova et al., 2007, Ramsauer et al., 2007, Qiao et al., 2013]. More research is needed to identify the features necessary and sufficient for promoter:enhancer

interactions.

Although both IRF1 and STAT1 promoters showed increased interactions to their enhancer elements at late IFNγ treatment timepoints versus untreated cells, these increasing interactions had lost significance. As seen with transcription and epigenetic marks, this could suggest negative feedback loops are activated to reduce these interactions, preventing aberrant IFNγ signalling. If STAT1 was critical to IFNγ-mediated differential interactions, redistribution of STAT1 at later timepoints may weaken the interaction. Otherwise, variability in the data may impair the significance of the increased interactions. More repeats of the Capture-C experiment should be performed to access this.

4.3.4.2 Explaining the increases in promoter:enhancer interactions

The increased promoter:enhancer interactions observed could be caused by two scenarios that are not mutually exclusive; the promoter becomes proximal to the enhancer within more individual cells, or the promoter forms stronger/closer interactions to the enhancer within the population of cells. One restriction fragment can only bind to two loci within a single cell during a conformation capture experiment, making single-cell conformation capture experiments extremely challenging. The scope of available experiments cannot currently distinguish between the two scenarios above. Single-cell population studies of IFNγ induced gene expression found that IFNγ stimulated genes were not expressed in all cells of the population, but rather, more cells within the population expressed the gene [Siwek et al., 2020]. This suggests that higher-order chromatin structure may follow this pattern, with more cells in a population forming the interaction, however, further experiments would be required to test this.

4.3.4.3 Potential promoter:enhancer interactions may be predetermined within a specific cell

Although thousands of differential ATAC-seq peaks were observed in Hep3B cells, very few IFNγ-induced increases in DNA accessibility was formed *de novo*. Sites of accessible DNA are features of promoters, enhancers, insulators and anchors of DNA contacts. The lack of newly formed accessible regions implies that DNA loops and regulatory elements are predetermined within a cell line. Indeed, many lineage determining TFs bind *cis* regulatory elements, modulating their accessibility and may correspondingly govern the potential enhancer landscape in a differentiated cell [Senft et al., 2018]. Thus, IFNγ signalling may impart specific gene expression programmes within a particular cell line, depending on the regulatory element and higher-order chromatin structure available, as predisposed by DNA accessibility. This could explain why different cell types within the same tumour microenvironment may respond differently to the same signals.

Altogether, this chapter has found multiple layers of IFNγ-stimulated regulation within Hep3B cells. IFNγ dramatically altered the enhancer landscape, modifying thousands of regulatory elements, without necessarily changing their activity. This could enable the integration of additional signalling pathways to alter gene expression. Furthermore, IFNγ treatments modified promoter:enhancer interactions. Given that an enhancer must be in close 3D proximity to its target promoter to promote transcription, this provides another mechanism to coordinate enhancer activity and gene expression. By using multiple tiers of regulation, IFNγ is able to fine-tune gene expression and the overall cellular phenotype in a context dependant and cell-type specific manner.

Chapter 5

Final discussions, conclusions and future directions

This thesis analysed the effect of IFNγ signalling on a cancer cell line, Hep3B, with respect to transcriptional, epigenetic and enhancer landscapes. The first half analysed mechanisms behind IFNγ-induced PD-L1 expression, a ligand commonly overexpressed in cancers, and IRF1, the major TF involved in promoting IFNγ-induced PD-L1 transcription. It aimed to expand knowledge on induced upregulation of PD-L1, adding to the body of research involved in improving PD-L1-based immunotherapies.

The second half of this thesis broadly investigated the genome-wide effects of IFNγ treatments. The overall objective intended to better elucidate how IFNγ signalling can have varied influences on cancer cells in a cell-type specific and context dependent manner.

5.1 Unconventional regulation of PD-L1

5.1.1 Summary

Studying expression of IRF1 upon treatment with IFNγ revealed a 'text-book' gene activation mechanism. IFNγ rapidly induced a promoter:enhancer interaction, accompanied by activating marks and bidirectional transcription at both elements (Fig:3.17). These changes overlapped pSTAT1 binding motifs and pSTAT1 was found to bind to these sites upon IFNγ treatments in other cell lines. These data aligned with previously published data, suggesting that pSTAT1 activates the IRF1 promoter and enhancer. This work additionally contributes evidence of interaction between the promoter and enhancer and reveals that promoter:enhancer contacts can be significantly upregulated by stress responses, in this case, IFNγ signalling.

Activation of PD-L1 was expected to progress similarly to that seen at IRF1. Instead, multiple potential regulatory mechanisms were identified, all of which were unorthodox. The project, analysing PD-L1's regulatory elements and DNA loops, stemmed from preliminary data from Oxford BioDynamics PLC (OBD). OBD analysed higher-order chromatin structure in patients that responded, or did not respond, to PD-L1-based immunotherapies. Their findings classified particular DNA loops enriched in either patient category. Among these, differential loops from the PD-L1 promoter itself, in addition to loops at IFNγ-stimulated genes, were identified. Therefore, we hypothesised that higher-order chromatin structure and regulatory elements were likely involved in PD-L1 expression and that IFNγ signalling appeared to have a significant role, thus, building the foundations of this research project.

Interestingly, IFNγ treatments did not induce changes in DNA loops at the PD-L1 locus in Hep3B cells. Other cell lines, namely Hek293, were unable to upregulate PD-L1 transcription despite the expression of IRF1. Together, it is possible that

established higher-order chromatin structure in particular cell lines predetermines whether the cell activates PD-L1 transcription upon IFNγ stimulation. Virtually all identified interactions with the PD-L1 promoter were found at two loci; the PLGRKT promoter, and a region approximately 150kb downstream of PD-L1. IFNγ treatments may promote ePromoter activity of the constitutively active PLGRKT promoter, possibly driven by IRF1 and/or pSTAT1. Motifs for both were found at more than one of the promoters, and they were found to bind one or both of these promoters in other cell lines. This would provide evidence for a newly described, unusual gene activation mechanism, whereby promoters use enhancer activity to activate surrounding genes (Fig:3.29). However, knocking out the PLGRKT promoter had no effect on IFNγ-induced PD-L1 expression, arguing against ePromoter activity at this neighbouring gene.

Alternatively, the interacting region downstream of PD-L1 was also bound by IRF1 in macrophage cell lines upon IFNγ treatments. This region contained features atypical to traditional enhancers, CTCF binding and unidirectional transcription, and may play a role in IFNγ-induced upregulation of PD-L1 (Fig:3.31). Cells containing a deletion at this downstream region were still able to upregulate PD-L1 expression suggesting that this interaction is dispensable for upregulation of PD-L1. However, the cell line studied was heterozygous for this deletion and the WT DNA present may be sufficient for the induction of PD-L1.

The final proposed mechanism describes the sufficiency of PD-L1's proximal promoter to promote IFNγ-induced upregulation of transcription. Here, binding of IRF1 to proximal promoter regions would be sufficient to recruit all TFs and cofactors necessary for complete PIC assembly, initiation and elongation. This unorthodox process would demonstrate that promoter:enhancer interactions are unnecessary for gene expression at high levels (Fig:3.28). Only two loci were identified to interact with the PD-L1 promoter. IFNγ treatments still upregulated PD-L1 in cell lines containing

deletions at either of these regions, although neither cell line was homozygous for the deletion. This supports the PD-L1 promoter as self-sufficient for IFNγ-induced upregulation of PD-L1.

The mechanisms described above, if proven as regulatory elements of PD-L1, would diversify our knowledge of promoter/enhancer elements. It would be likely that other genes are regulated by analogous mechanisms and thus would help identify currently undiscovered regulatory elements, significantly developing the field.

5.1.2 Future directions

IFNγ treatment did not induce PD-L1 expression in all cell types studied. A variety of cancer types are able to upregulate PD-L1, but it is unknown what changes in a cancer cell to enable this expression. The inducibility of PD-L1 by IFNγ treatments should be compared in a range of cell lines. A variety of features alone or in combination may predetermine the sensitivity of a cell to IFNγ. Expression of particular TFs can be examined using western blots, and ChIP-qPCR can be used to assess their binding to the PD-L1 promoter. lncRNA expression can be evaluated using SNU-seq. ATAC-seq and Capture-C can be used to analyse higher-order chromatin structure, and potential regulatory elements involved. Also, epigenetic modifications, including DNA methylation, should be assessed across the PD-L1 locus in multiple cell types. Differences between cells may help elucidate the necessary characteristics required for IFNγ-induced PD-L1 expression. This information could be used as biomarkers for early diagnostics and may identify cancer treatment targets.

Identification of PD-L1's IFNγ-dependent regulatory elements, if any exist, has not yet been confirmed. Interactions between the promoter and two DNA loci could first be validated by performing Capture-C from the putative enhancer viewpoint. Repeats of the CRISPR-Cas9 experiment should be performed to obtain homozygous KOs of the regions of interest. These KOs can be used to investigate the effect of these

regions on IFNγ-induced PD-L1 expression at both the transcriptional and protein level. If either interaction is deemed necessary for activation of PD-L1, the activation requirements of these regulatory elements should be determined.

If these interactions are irrelevant to IFNγ-induced PD-L1 expression, as the preliminary KO experiments suggest, it is likely that the proximal promoter of PD-L1 is sufficient for activation. Proving this negative result, that no distinct regulatory element is required, remains difficult. Deleting regions of the promoter would almost certainly affect PD-L1 expression even if a regulatory element existed. Performing a luciferase assay, including particular regions of the PD-L1 promoter, may demonstrate the role of these promoter regions in gene activation, but would not disprove that further regulatory elements are involved. Therefore, disproving the involvement of any potential enhancer element in IFNγ-induced PD-L1 regulation may be the best way to tackle this challenge.

If any of these unconventional gene activation mechanisms are established (Fig:3.28, 3.29 & 3.31), other genes using the same mechanism should be sought. Screening a number of promoters using Capture-C, and complementing these results with genome-wide transcriptional and epigenetic data, may identify a number of genes using similar regulatory processes. This would validate the presence of these unorthodox mechanisms, whilst transforming our current understanding of gene expression.

5.2 How is IFNγ signalling cell-type specific and context dependent?

5.2.1 Summary

IFNγ modulated gene expression through multiple modes of regulation, altering the transcriptional and enhancer landscape, in addition to increasing promoter:enhancer contacts. Whilst some changes were sustained throughout 24 hrs of treatment, other alterations were transient and rapidly reversed (Fig:4.5 & 4.14). More regulatory elements were affected than genes, despite a large proportion of these changes being silent, i.e. not affecting the activity of the enhancer element (Fig:4.24).

This thesis proposes that IFNγ treatments prime a diverse set of enhancers. Certain potential regulatory elements and higher-order chromatin structures appear to be predetermined by the specific cell line as very few ATAC-seq peaks were formed *de novo* upon IFNγ treatments. The presence of other stimuli, extracellular or intracellular, may provide other signals that could complete activation of the IFNγ-primed enhancer elements (Fig:4.25). Thus allowing the precise gene expression phenotype to be both cell-type specific and context dependent. This would enable individual cancers to integrate a myriad of signals, fine-tuning the outcome of IFNγ signalling in the tumour microenvironment.

IFNγ has been implicated in both anti- and pro-tumour functions, but which effect does it have in Hep3B cells? IFNγ promotes anti-tumour effects on a tumour cell by increasing its antigenicity. Indeed, IFNγ treatments in Hep3B cells upregulated the expression of MHCI subunits and proteins involved in antigen processing pathways such as TAP1. Additionally, IFNγ upregulated complement proteins, which may serve to activate the immune system against the tumour. Other cytokines promoting anti-tumour immune responses were also upregulated. Genes involved in inhibiting

cell growth and promoting apoptosis, such as GADD45B and TNFRSF21, were induced upon IFNγ treatments. Thus, it appears that many anti-tumour responses are activated in Hep3B cells.

Some pro-tumour genes were induced in Hep3B cells; non-classical MHC genes such as HLA-E were upregulated and have been found to reduce cytotoxic killing of the cell. Despite this example, the overwhelming response within this HCC cell line seems to promote clearance of the tumour. The exception to this is the upregulation of the PD-L1 ligand, which overrides many of the aforementioned signals to inhibit the immune system. It is possible that the presence of this ligand in the tumour microenvironment is sufficient to enable tumour growth. One may speculate that using an immunotherapy targeting PD-L1 against this specific HCC would restore the overruling anti-tumour function of IFNγ.

5.2.2 Future directions

A major finding in this thesis is that IFNγ is able to induce changes in higher-order chromatin structure. Having only assessed higher-order chromatin structure at three IFNγ-stimulated genes, the extent to which differential promoter:enhancer loops occur remains unknown. Capture-C could be used to analyse promoter interactions for a diverse set of early and late, sustained and transiently IFNγ-induced genes. Identifying which genes show differential interactions and analysing corresponding changes in ncRNA transcription, epigenetic marks and enriched motif analyses may hint at features necessary to induce promoter:enhancer looping. Further research could then investigate how differential higher-order chromatin structure can be induced in response to a stress signal, such as IFNγ signalling.

This thesis hypothesises that IFNγ primes a magnitude of predetermined enhancer elements as a mechanism to integrate signals from a tumour microenvironment. Experiments examining the enhancer landscape following IFNγ treatments should

be performed with a combination of other signals commonly present at a tumour, such as TNFα. If IFNγ+TNFα, or other signalling combinations, activate a subset of enhancers not activated by either cytokine independently, this would support the hypothesis.

5.3 Concluding remarks

The outcome of IFNγ signalling in a tumour microenvironment is complex and difficult to predict. Whilst having a customary role of priming the immune system to suppress harmful cells, including cancerous cells, a contradictory function is often observed. One dominant pro-tumour activity of IFNγ signalling is its ability to upregulate PD-L1 in a wide range of cell types.

This thesis investigated the regulation of IFNγ-induced PD-L1 expression within a tumour cell line, Hep3B. Surprisingly, a conventional enhancer element targeting the PD-L1 promoter was not identified. Instead, the evidence presented in this work suggests that PD-L1 is regulated completely within its proximal promoter, or regulated by either an ePromoter, a regulatory element with atypical features, or both.

More generally, IFNγ regulates gene expression by altering the activity of enhancers, as well as inducing changes in higher-order chromatin structure. Many induced epigenetic changes are silent and do not result in gene activation. Instead of being coincidental, this may provide a mechanism to integrate other signalling responses, enabling an altered phenotype depending on the signals present in the tumour microenvironment.

Bibliography

[Abou El Hassan et al., 2017] Abou El Hassan, M., Huang, K., Eswara, M. B., Xu, Z., Yu, T., Aubry, A., Ni, Z., Livne-bar, I., Sangwan, M., Ahmad, M., and Bremner, R. (2017). Properties of STAT1 and IRF1 enhancers and the influence of SNPs. *BMC Molecular Biology*, 18(1).

[Abou El Hassan et al., 2018] Abou El Hassan, M., Huang, K., Xu, Z., Yu, T., and Bremner, R. (2018). Frequent IRF1 Binding at Remote Elements without Histone Modification. *Journal of Biological Chemistry*, page jbc.RA118.002889.

[Agata et al., 1996] Agata, Y., Kawasaki, A., Nishimura, H., Ishida, Y., Tsubata, T., Yagita, H., and Honjo, T. (1996). Expression of the PD-1 antigen on the surface of stimulated mouse T and B lymphocytes. *International immunology*, 8(5):765–72.

[Aithal et al., 2018] Aithal, A., Rauth, S., Kshirsagar, P., Shah, A., Lakshmanan, I., Junker, W. M., Jain, M., Ponnusamy, M. P., and Batra, S. K. (2018). MUC16 as a novel target for cancer therapy.

[Akhtar et al., 2009] Akhtar, M. S., Heidemann, M., Tietjen, J. R., Zhang, D. W., Chapman, R. D., Eick, D., and Ansari, A. Z. (2009). TFIIH Kinase Places Bivalent Marks on the Carboxy-Terminal Domain of RNA Polymerase II. *Molecular Cell*, 34(3):387–393.

[Alsaab et al., 2017] Alsaab, H. O., Sau, S., Alzhrani, R., Tatiparti, K., Bhise, K., Kashaw, S. K., and Iyer, A. K. (2017). PD-1 and PD-L1 Checkpoint Signaling Inhibition for Cancer Immunotherapy: Mechanism, Combinations, and Clinical Outcome. *Frontiers in pharmacology*, 8:561.

[Andersson et al., 2014] Andersson, R., Gebhard, C., Miguel-Escalada, I., Hoof, I., Bornholdt, J., Boyd, M., Chen, Y., Zhao, X., Schmidl, C., Suzuki, T., Ntini, E., Arner, E., Valen, E., Li, K., Schwarzfischer, L., Glatz, D., Raithel, J., Lilje, B., Rapin, N., Bagger, F. O., Jørgensen, M., Andersen, P. R., Bertin, N., Rackham, O., Burroughs, A. M., Baillie, J. K., Ishizu, Y., Shimizu, Y., Furuhata, E., Maeda, S., Negishi, Y., Mungall, C. J., Meehan, T. F., Lassmann, T., Itoh, M., Kawaji, H., Kondo, N., Kawai, J., Lennartsson, A., Daub, C. O., Heutink, P., Hume, D. A., Jensen, T. H., Suzuki, H., Hayashizaki, Y., Müller, F., Forrest, A. R., Carninci, P., Rehli, M., and Sandelin, A. (2014). An atlas of active enhancers across human cell types and tissues. *Nature*, 507(7493):455–461.

[Ansari and Hampsey, 2005] Ansari, A. and Hampsey, M. (2005). A role for the CPF 3' -end processing machinery in RNAP II-dependent gene looping. *Genes and Development*, 19(24):2969–2978.

[Ansell et al., 2015] Ansell, S. M., Lesokhin, A. M., Borrello, I., Halwani, A., Scott, E. C., Gutierrez, M., Schuster, S. J., Millenson, M. M., Cattry, D., Freeman, G. J., Rodig, S. J., Chapuy, B., Ligon, A. H., Zhu, L., Grosso, J. F., Kim, S. Y., Timmerman, J. M., Shipp, M. A., and Armand, P. (2015). PD-1 Blockade with Nivolumab in Relapsed or Refractory Hodgkin's Lymphoma. *New England Journal of Medicine*, 372(4):311–319.

[Arnold et al., 2020] Arnold, P. R., Wells, A. D., and Li, X. C. (2020). Diversity and Emerging Roles of Enhancer RNA in Regulation of Gene Expression and Cell Fate.

[Asgarova et al., 2018] Asgarova, A., Asgarov, K., Godet, Y., Peixoto, P., Nadaradjane, A., Boyer-Guittaut, M., Galaine, J., Guenat, D., Mougey, V., Perrard, J., Pallandre, J. R., Bouard, A., Balland, J., Tirole, C., Adotevi, O., Hendrick, E., Herfs, M., Cartron, P. F., Borg, C., and Hervouet, E. (2018). PD-L1 expression is regulated by both DNA methylation and NF-kB during EMT signaling in non-small cell lung carcinoma. *OncoImmunology*, 7(5).

[Atsaves et al., 2017] Atsaves, V., Tsesmetzis, N., Chioureas, D., Kis, L., Leventaki, V., Drakos, E., Panaretakis, T., Grander, D., Medeiros, L. J., Young, K. H., and Rassidakis, G. Z. (2017). PD-L1 is commonly expressed and transcriptionally regulated by STAT3 and MYC in ALK-negative anaplastic large-cell lymphoma.

[Bae et al., 2018] Bae, J., Hideshima, T., Tai, Y. T., Song, Y., Richardson, P., Raje, N., Munshi, N. C., and Anderson, K. C. (2018). Histone deacetylase (HDAC) inhibitor ACY241 enhances anti-tumor activities of antigen-specific central memory cytotoxic T lymphocytes against multiple myeloma and solid tumors. *Leukemia*, 32(9):1932–1947.

[Bailey et al., 2009] Bailey, T. L., Boden, M., Buske, F. A., Frith, M., Grant, C. E., Clementi, L., Ren, J., Li, W. W., and Noble, W. S. (2009). MEME SUITE: tools for motif discovery and searching. *Nucleic acids research*, 37(Web Server issue):W202–8.

[Bannister and Kouzarides, 2011] Bannister, A. J. and Kouzarides, T. (2011). Regulation of chromatin by histone modifications.

[Bardhan et al., 2016] Bardhan, K., Anagnostou, T., and Boussiotis, V. A. (2016). The PD1: PD-L1/2 pathway from discovery to clinical implementation.

[Barrat et al., 2019] Barrat, F. J., Crow, M. K., and Ivashkiv, L. B. (2019). Interferon target-gene expression and epigenomic signatures in health and disease.

[Barski et al., 2007] Barski, A., Cuddapah, S., Cui, K., Roh, T. Y., Schones, D. E., Wang, Z., Wei, G., Chepelev, I., and Zhao, K. (2007). High-Resolution Profiling of Histone Methylations in the Human Genome. *Cell*, 129(4):823–837.

[Barsoum et al., 2014] Barsoum, I. B., Smallwood, C. A., Siemens, D. R., and Graham, C. H. (2014). A mechanism of hypoxia-mediated escape from adaptive immunity in cancer cells. *Cancer Research*, 74(3):665–674.

[Bateman et al., 2012] Bateman, J. R., Johnson, J. E., and Locke, M. N. (2012). Comparing enhancer action in cis and in trans. *Genetics*, 191(4):1143–1155.

[Bazhin et al., 2018] Bazhin, A. V., von Ahn, K., Fritz, J., Werner, J., and Karakhanova, S. (2018). Interferon-α Up-Regulates the Expression of PD-L1 Molecules on Immune Cells Through STAT3 and p38 Signaling. *Frontiers in immunology*, 9:2129.

[Beatty and Paterson, 2000] Beatty, G. L. and Paterson, Y. (2000). IFN-γ Can Promote Tumor Evasion of the Immune System In Vivo by Down-Regulating Cellular Levels of an Endogenous Tumor Antigen. *The Journal of Immunology*, 165(10):5502–5508.

[Belkina and Denis, 2012] Belkina, A. C. and Denis, G. V. (2012). BET domain co-regulators in obesity, inflammation and cancer.

[Benci et al., 2016] Benci, J. L., Xu, B., Qiu, Y., Wu, T. J., Dada, H., Twyman-Saint Victor, C., Cucolo, L., Lee, D. S., Pauken, K. E., Huang, A. C., Gangadhar, T. C., Amaravadi, R. K., Schuchter, L. M., Feldman, M. D., Ishwaran, H., Vonderheide, R. H., Maity, A., Wherry, E. J., and Minn, A. J. (2016). Tumor Interferon Signaling Regulates a Multigenic Resistance Program to Immune Checkpoint Blockade. *Cell*, 167(6):1540–1554.e12.

[Bennett et al., 2003] Bennett, F., Luxenberg, D., Ling, V., Wang, I.-M., Marquette, K., Lowe, D., Khan, N., Veldman, G., Jacobs, K. A., Valge-Archer, V. E., Collins, M., and Carreno, B. M. (2003). Program Death-1 Engagement Upon TCR Activation Has Distinct Effects on Costimulation and Cytokine-Driven Proliferation: Attenuation of ICOS, IL-4, and IL-21, But Not CD28, IL-7, and IL-15 Responses. *The Journal of Immunology*, 170(2):711–718.

[Berghoff et al., 2017] Berghoff, A. S., Kiesel, B., Widhalm, G., Wilhelm, D., Rajky, O., Kurscheid, S., Kresl, P., Wöhrer, A., Marosi, C., Hegi, M. E., and Preusser, M. (2017). Correlation of immune phenotype with IDH mutation in diffuse glioma. *Neuro-Oncology*, 19(11):1460–1468.

[Bernstein et al., 2005] Bernstein, B. E., Kamal, M., Lindblad-Toh, K., Bekiranov, S., Bailey, D. K., Huebert, D. J., McMahon, S., Karlsson, E. K., Kulbokas, E. J., Gingeras, T. R., Schreiber, S. L., and Lander, E. S. (2005). Genomic maps and comparative analysis of histone modifications in human and mouse. *Cell*, 120(2):169–181.

[Bheda et al., 2020] Bheda, P., Aguilar-Gómez, D., Becker, N. B., Becker, J., Stavrou, E., Kukhtevich, I., Höfer, T., Maerkl, S., Charvin, G., Marr, C., Kirmizis, A., and Schneider, R. (2020). Single-Cell Tracing Dissects Regulation of Maintenance and Inheritance of Transcriptional Reinduction Memory. *Molecular Cell*, 78(5):915–925.e7.

[Bolger et al., 2014] Bolger, A. M., Lohse, M., and Usadel, B. (2014). Trimmomatic: A flexible trimmer for Illumina sequence data. *Bioinformatics*, 30(15):2114–2120.

[Boo and Kim, 2020] Boo, S. H. and Kim, Y. K. (2020). The emerging role of RNA modifications in the regulation of mRNA stability.

[Booth et al., 2017] Booth, L., Roberts, J. L., Poklepovic, A., Kirkwood, J., and Dent, P. (2017). HDAC inhibitors enhance the immunotherapy response of melanoma cells. *Oncotarget*, 8(47):83155–83170.

[Borggrefe and Yue, 2011] Borggrefe, T. and Yue, X. (2011). Interactions between subunits of the Mediator complex with gene-specific transcription factors.

[Borghaei et al., 2015] Borghaei, H., Paz-Ares, L., Horn, L., Spigel, D. R., Steins, M., Ready, N. E., Chow, L. Q., Vokes, E. E., Felip, E., Holgado, E., Barlesi, F., Kohlhäufl, M., Arrieta, O., Burgio, M. A., Fayette, J., Lena, H., Poddubskaya, E., Gerber, D. E., Gettinger, S. N., Rudin, C. M., Rizvi, N., Crinò, L., Blumenschein, G. R., Antonia, S. J., Dorange, C., Harbison, C. T., Graf Finckenstein, F., and Brahmer, J. R. (2015). Nivolumab versus Docetaxel in Advanced Nonsquamous Non–Small-Cell Lung Cancer. *New England Journal of Medicine*, 373(17):1627–1639.

[Bose et al., 2017] Bose, D. A., Donahue, G., Reinberg, D., Shiekhattar, R., Bonasio, R., and Berger, S. L. (2017). RNA Binding to CBP Stimulates Histone Acetylation and Transcription. *Cell*, 168(1-2):135–149.e22.

[Bray et al., 2018] Bray, F., Ferlay, J., Soerjomataram, I., Siegel, R. L., Torre, L. A., and Jemal, A. (2018). Global cancer statistics 2018: GLOBOCAN estimates of incidence and mortality worldwide for 36 cancers in 185 countries. *CA: A Cancer Journal for Clinicians*, 68(6):394–424.

[Briere et al., 2018] Briere, D., Sudhakar, N., Woods, D. M., Hallin, J., Engstrom, L. D., Aranda, R., Chiang, H., Sodré, A. L., Olson, P., Weber, J. S., and Christensen, J. G. (2018). The class I/IV HDAC inhibitor mocetinostat increases tumor antigen presentation, decreases immune suppressive cell types and augments checkpoint inhibitor therapy. *Cancer Immunology, Immunotherapy*, 67(3):381–392.

[Brody et al., 2009] Brody, J. R., Costantino, C. L., Berger, A. C., Sato, T., Lisanti, M. P., Yeo, C. J., Emmons, R. V., and Witkiewicz, A. K. (2009). Expression of indoleamine 2,3-dioxygenase in metastatic malignant melanoma recruits regulatory T cells to avoid immune detection and affects survival. *Cell Cycle*, 8(12):1930–1934.

[Bu et al., 2017] Bu, L. L., Yu, G. T., Wu, L., Mao, L., Deng, W. W., Liu, J. F., Kulkarni, A. B., Zhang, W. F., Zhang, L., and Sun, Z. J. (2017). STAT3 Induces Immunosuppression by Upregulating PD-1/PD-L1 in HNSCC. *Journal of Dental Research*, 96(9):1027–1034.

[Budczies et al., 2016] Budczies, J., Bockmayr, M., Denkert, C., Klauschen, F., Gröschel, S., Darb-Esfahani, S., Pfarr, N., Leichsenring, J., Onozato, M. L., Lennerz, J. K., Dietel, M., Fröhling, S., Schirmacher, P., Iafrate, A. J., Weichert, W., and Stenzinger, A. (2016). Pan-cancer analysis of copy number changes in programmed death-ligand 1 (PD-L1, CD274) - associations with gene expression, mutational load, and survival. *Genes, Chromosomes and Cancer*, 55(8):626–639.

[Buenrostro et al., 2015] Buenrostro, J. D., Wu, B., Chang, H. Y., and Greenleaf, W. J. (2015). ATAC-seq: A Method for Assaying Chromatin Accessibility Genome-Wide. *Current protocols in molecular biology*, 109:21.29.1–9.

[Bullock et al., 2019] Bullock, B. L., Kimball, A. K., Poczobutt, J. M., Neuwelt, A. J., Li, H. Y., Johnson, A. M., Kwak, J. W., Kleczko, E. K., Kaspar, R. E., Wagner, E. K., Hopp, K., Schenk, E. L., Weiser-Evans, M. C., Clambey, E. T., and Nemenoff, R. A. (2019). Tumor-intrinsic response to IFNy shapes the tumor microenvironment and anti–PD-1 response in NSCLC. *Life Science Alliance*, 2(3):e201900328.

[Buratowski et al., 1989] Buratowski, S., Hahn, S., Guarente, L., and Sharp, P. A. (1989). Five intermediate complexes in transcription initiation by RNA polymerase II. *Cell*, 56(4):549–561.

[Burke and Kadonaga, 1996] Burke, T. W. and Kadonaga, J. T. (1996). Drosophila TFIID binds to a conserved downstream basal promoter element that is present in many TATA-box-deficient promoters. *Genes and Development*, 10(6):711–724.

[Burr et al., 2017] Burr, M. L., Sparbier, C. E., Chan, Y. C., Williamson, J. C., Woods, K., Beavis, P. A., Lam, E. Y., Henderson, M. A., Bell, C. C., Stolzenburg, S., Gilan, O., Bloor, S., Noori, T., Morgens, D. W., Bassik, M. C., Neeson, P. J., Behren, A., Darcy, P. K., Dawson, S. J., Voskoboinik, I., Trapani, J. A., Cebon, J., Lehner, P. J., and Dawson, M. A. (2017). CMTM6 maintains the expression of PD-L1 and regulates anti-Tumour immunity. *Nature*, 549(7670):101–105.

[Butte et al., 2007] Butte, M. J., Keir, M. E., Phamduy, T. B., Sharpe, A. H., and Freeman, G. J. (2007). Programmed Death-1 Ligand 1 Interacts Specifically with the B7-1 Costimulatory Molecule to Inhibit T Cell Responses. *Immunity*, 27(1):111–122.

[Butte et al., 2008] Butte, M. J., Pe∼na-Cruz, V., Kim, M. J., Freeman, G. J., and Sharpe, A. H. (2008). Interaction of human PD-L1 and B7-1. *Molecular Immunology*, 45(13):3567–3572.

[Cairns, 2009] Cairns, B. R. (2009). The logic of chromatin architecture and remodelling at promoters.

[Calderaro et al., 2016] Calderaro, J., Rousseau, B., Amaddeo, G., Mercey, M., Charpy, C., Costentin, C., Luciani, A., Zafrani, E.-S., Laurent, A., Azoulay, D., Lafdil, F., and Pawlotsky, J.-M. (2016). Programmed death ligand 1 expression in hepatocellular carcinoma: Relationship With clinical and pathological features. *Hepatology*, 64(6):2038–2046.

[Calo and Wysocka, 2013] Calo, E. and Wysocka, J. (2013). Modification of Enhancer Chromatin: What, How, and Why? *Molecular Cell*, 49(5):825–837.

[Cao et al., 2011] Cao, Y., Zhang, L., Kamimura, Y., Ritprajak, P., Hashiguchi, M., Hirose, S., and Azuma, M. (2011). B7-H1 overexpression regulates epithelial-mesenchymal transition and accelerates carcinogenesis in skin. *Cancer Research*, 71(4):1235–1243.

[Carow and Rottenberg, 2014] Carow, B. and Rottenberg, M. E. (2014). SOCS3, a major regulator of infection and inflammation.

[Carter et al., 2002] Carter, L. L., Fouser, L. A., Jussif, J., Fitz, L., Deng, B., Wood, C. R., Collins, M., Honjo, T., Freeman, G. J., and Carreno, B. M. (2002). PD-1:PD-L inhibitory pathway affects both CD4+ and CD8+ T cells and is overcome by IL-2. *European Journal of Immunology*, 32(3):634–643.

[Casey et al., 2016] Casey, S. C., Tong, L., Li, Y., Do, R., Walz, S., Fitzgerald, K. N., Gouw, A. M., Baylot, V., Gütgemann, I., Eilers, M., and Felsher, D. W. (2016). MYC regulates the antitumor immune response through CD47 and PD-L1. *Science*, 352(6282):227–231.

[Castro et al., 2018] Castro, F., Cardoso, A. P., Gonçalves, R. M., Serre, K., and Oliveira, M. J. (2018). Interferon-gamma at the crossroads of tumor immune surveillance or evasion.

[Catarino and Stark, 2018] Catarino, R. R. and Stark, A. (2018). Assessing sufficiency and necessity of enhancer activities for gene expression and the mechanisms of transcription activation.

[Cekay et al., 2017] Cekay, M. J., Roesler, S., Frank, T., Knuth, A. K., Eckhardt, I., and Fulda, S. (2017). Smac mimetics and type II interferon synergistically induce necroptosis in various cancer cell lines. *Cancer Letters*, 410:228–237.

[Cha et al., 2018] Cha, J. H., Yang, W. H., Xia, W., Wei, Y., Chan, L. C., Lim, S. O., Li, C. W., Kim, T., Chang, S. S., Lee, H. H., Hsu, J. L., Wang, H. L., Kuo, C. W., Chang, W. C., Hadad, S., Purdie, C. A., McCoy, A. M., Cai, S., Tu, Y., Litton, J. K., Mittendorf, E. A., Moulder, S. L., Symmans, W. F., Thompson, A. M., Piwnica-Worms, H., Chen, C. H., Khoo, K. H., and Hung, M. C. (2018). Metformin Promotes Antitumor Immunity via Endoplasmic-Reticulum-Associated Degradation of PD-L1. *Molecular Cell*, 71(4):606–620.e7.

[Chang et al., 2017] Chang, H., Jung, W., Kim, A., Kim, H. K., Kim, W. B., Kim, J. H., and Kim, B.-h. (2017). Expression and prognostic significance of programmed death protein 1 and programmed death ligand-1, and cytotoxic T lymphocyte-associated molecule-4 in hepatocellular carcinoma. *APMIS*, 125(8):690–698.

[Chen et al., 2018a] Chen, G., Huang, A. C., Zhang, W., Zhang, G., Wu, M., Xu, W., Yu, Z., Yang, J., Wang, B., Sun, H., Xia, H., Man, Q., Zhong, W., Antelo, L. F., Wu, B., Xiong, X., Liu, X., Guan, L., Li, T., Liu, S., Yang, R., Lu, Y., Dong, L., McGettigan, S., Somasundaram, R., Radhakrishnan, R., Mills, G., Lu, Y., Kim, J., Chen, Y. H., Dong, H., Zhao, Y., Karakousis, G. C., Mitchell, T. C., Schuchter, L. M., Herlyn, M., Wherry, E. J., Xu, X., and Guo, W. (2018a). Exosomal PD-L1 contributes to immunosuppression and is associated with anti-PD-1 response. *Nature*, 560(7718):382–386.

[Chen et al., 2018b] Chen, H., Li, C., Peng, X., Zhou, Z., and Weinstein, J. N. (2018b). A Pan-Cancer Analysis of Enhancer Expression in Nearly 9000 Patient Samples Enhancer expression of ∼9,000 tumors Tumors with global enhancer activation. *Cell*, 173:386–399.e12.

[Chen and Ivashkiv, 2010] Chen, J. and Ivashkiv, L. B. (2010). IFN-γ abrogates endotoxin tolerance by facilitating Toll-like receptor-induced chromatin remodeling. *Proceedings of the National Academy of Sciences of the United States of America*, 107(45):19438–19443.

[Chen et al., 2017] Chen, L., Xiong, Y., Li, J., Zheng, X., Zhou, Q., Turner, A., Wu, C., Lu, B., and Jiang, J. (2017). PD-L1 Expression Promotes Epithelial to Mesenchymal Transition in Human Esophageal Cancer. *Cellular Physiology and Biochemistry*, 42(6):2267–2280.

[Cheung et al., 2011] Cheung, A. C., Sainsbury, S., and Cramer, P. (2011). Structural basis of initial RNA polymerase II transcription. *EMBO Journal*, 30(23):4755–4763.

[Chikuma et al., 2009] Chikuma, S., Terawaki, S., Hayashi, T., Nabeshima, R., Yoshida, T., Shibayama, S., Okazaki, T., and Honjo, T. (2009). PD-1-Mediated Suppression of IL-2 Production Induces CD8 + T Cell Anergy In Vivo . *The Journal of Immunology*, 182(11):6682–6689.

[Chin et al., 1996] Chin, Y. E., Kitagawa, M., Su, W. C. S., You, Z. H., Iwamoto, Y., and Fu, X. Y. (1996). Cell growth arrest and induction of cyclin-dependent kinase inhibitor p21WAF1/CIP1 Mediated by STAT1. *Science*, 272(5262):719–722.

[Christova et al., 2007] Christova, R., Jones, T., Wu, P. J., Bolzer, A., Costa-Pereira, A. P., Watling, D., Kerr, I. M., and Sheer, D. (2007). P-STAT1 mediates higher-order chromatin remodelling of the human MHC in response to IFNγ. *Journal of Cell Science*, 120(18):3262–3270.

[Clark et al., 2016] Clark, C. A., Gupta, H. B., Sareddy, G., Pandeswara, S., Lao, S., Yuan, B., Drerup, J. M., Padron, A., Conejo-Garcia, J., Murthy, K., Liu, Y., Turk, M. J., Thedieck, K., Hurez, V., Li, R., Vadlamudi, R., and Curiel, T. J. (2016). Tumor-intrinsic PD-L1 signals regulate cell growth, pathogenesis, and autophagy in ovarian cancer and melanoma. *Cancer Research*, 76(23):6964–6974.

[Cleary et al., 2005] Cleary, M. D., Meiering, C. D., Jan, E., Guymon, R., and Boothroyd, J. C. (2005). Biosynthetic labeling of RNA with uracil phosphoribosyltransferase allows cell-specific microarray analysis of mRNA synthesis and decay. *Nature Biotechnology*, 23(2):232–237.

[Core et al., 2014] Core, L. J., Martins, A. L., Danko, C. G., Waters, C. T., Siepel, A., and Lis, J. T. (2014). Analysis of nascent RNA identifies a unified architecture of initiation regions at mammalian promoters and enhancers. *Nature Genetics*, 46(12):1311–1320.

[Core et al., 2008] Core, L. J., Waterfall, J. J., and Lis, J. T. (2008). Nascent RNA sequencing reveals widespread pausing and divergent initiation at human promoters. *Science*, 322(5909):1845–1848.

[Coughlin et al., 1998] Coughlin, C. M., Salhany, K. E., Gee, M. S., LaTemple, D. C., Kotenko, S., Ma, X. J., Gri, G., Wysocka, M., Kim, J. E., Liu, L., Liao, F., Farber, J. M., Pestka, S., Trinchieri, G., and Lee, W. M. (1998). Tumor cell responses to IFNγ affect tumorigenicity and response to IL- 12 therapy and antiangiogenesis. *Immunity*, 9(1):25–34.

[Creyghton et al., 2010] Creyghton, M. P., Cheng, A. W., Welstead, G. G., Kooistra, T., Carey, B. W., Steine, E. J., Hanna, J., Lodato, M. A., Frampton, G. M., Sharp, P. A., Boyer, L. A., Young, R. A., and Jaenisch, R. (2010). Histone H3K27ac separates active from poised enhancers and predicts developmental state. *Proceedings of the National Academy of Sciences*, 107(50):21931–21936.

[Curiel et al., 2003] Curiel, T. J., Wei, S., Dong, H., Alvarez, X., Cheng, P., Mottram, P., Krzysiek, R., Knutson, K. L., Daniel, B., Zimmermann, M. C., David, O., Burow, M., Gordon, A., Dhurandhar, N., Myers, L., Berggren, R., Hemminki, A., Alvarez, R. D., Emilie, D., Curiel, D. T., Chen, L., and Zou, W. (2003). Blockade of B7-H1 improves myeloid dendritic cell-mediated antitumor immunity. *Nature Medicine*, 9(5):562–567.

[Dao et al., 2017] Dao, L. T. M., Galindo-Albarrán, A. O., Castro-Mondragon, J. A., Andrieu-Soler, C., Medina-Rivera, A., Souaid, C., Charbonnier, G., Griffon, A., Vanhille, L., Stephen, T., Alomairi, J., Martin, D., Torres, M., Fernandez, N., Soler, E., van Helden, J., Puthier, D., and Spicuglia, S. (2017). Genome-wide characterization of mammalian promoters with distal enhancer functions. *Nature Genetics*, 49(7):1073–1081.

[Davies et al., 2015] Davies, J. O., Telenius, J. M., McGowan, S. J., Roberts, N. A., Taylor, S., Higgs, D. R., and Hughes, J. R. (2015). Multiplexed analysis of chromosome conformation at vastly improved sensitivity. *Nature Methods*, 13(1):74–80.

[Delgoffe and Vignali, 2013] Delgoffe, G. M. and Vignali, D. A. (2013). STAT heterodimers in immunity. *JAK-STAT*, 2(1):e23060.

[Derré et al., 2006] Derré, L., Corvaisier, M., Charreau, B., Moreau, A., Godefroy, E., Moreau-Aubry, A., Jotereau, F., and Gervois, N. (2006). Expression and Release of HLA-E by Melanoma Cells and Melanocytes: Potential Impact on the Response of Cytotoxic Effector Cells. *The Journal of Immunology*, 177(5):3100–3107.

[Di Cerbo et al., 2014] Di Cerbo, V., Mohn, F., Ryan, D. P., Montellier, E., Kacem, S., Tropberger, P., Kallis, E., Holzner, M., Hoerner, L., Feldmann, A., Richter, F. M., Bannister, A. J., Mittler, G., Michaelis, J., Khochbin, S., Feil, R., Schuebeler, D., Owen-Hughes, T., Daujat, S., and Schneider, R. (2014). Acetylation of histone H3 at lysine 64 regulates nucleosome dynamics and facilitates transcription. *eLife*, 2014(3).

[Diao et al., 2017] Diao, Y., Fang, R., Li, B., Meng, Z., Yu, J., Qiu, Y., Lin, K. C., Huang, H., Liu, T., Marina, R. J., Jung, I., Shen, Y., Guan, K. L., and Ren, B. (2017). A tiling-deletion-based genetic screen for cis-regulatory element identification in mammalian cells. *Nature Methods*, 14(6):629–635.

[Dion et al., 2007] Dion, M. F., Kaplan, T., Kim, M., Buratowski, S., Friedman, N., and Rando, O. J. (2007). Dynamics of replication-independent histone turnover in budding yeast. *Science*, 315(5817):1405–1408.

[Dixon et al., 2012] Dixon, J. R., Selvaraj, S., Yue, F., Kim, A., Li, Y., Shen, Y., Hu, M., Liu, J. S., and Ren, B. (2012). Topological domains in mammalian genomes identified by analysis of chromatin interactions. *Nature*, 485(7398):376–80.

[Dong et al., 1999] Dong, H., Zhu, G., Tamada, K., and Chen, L. (1999). B7-H1, a third member of the B7 family, co-stimulates T-cell proliferation and interleukin-10 secretion. *Nature Medicine*, 5(12):1365–1369.

[Dunham et al., 2012] Dunham, I., Kundaje, A., Aldred, S. F., Collins, P. J., Davis, C. A., Doyle, F., Epstein, C. B., Frietze, S., Harrow, J., Kaul, R., Khatun, J., Lajoie, B. R., Landt, S. G., Lee, B. K., Pauli, F., Rosenbloom, K. R., Sabo, P., Safi, A., Sanyal, A., Shoresh, N., Simon, J. M., Song, L., Trinklein, N. D., Altshuler, R. C., Birney, E., Brown, J. B., Cheng, C., Djebali, S., Dong, X., Ernst, J., Furey, T. S., Gerstein, M., Giardine, B., Greven, M., Hardison, R. C., Harris, R. S., Herrero, J., Hoffman, M. M., Iyer, S., Kellis, M., Kheradpour, P., Lassmann, T., Li, Q., Lin, X., Marinov, G. K., Merkel, A., Mortazavi, A., Parker, S. C., Reddy, T. E., Rozowsky, J., Schlesinger, F., Thurman, R. E., Wang, J., Ward, L. D., Whitfield, T. W., Wilder, S. P., Wu, W., Xi, H. S., Yip, K. Y., Zhuang, J., Bernstein, B. E., Green, E. D., Gunter, C., Snyder, M., Pazin, M. J., Lowdon, R. F., Dillon, L. A., Adams, L. B., Kelly, C. J., Zhang, J., Wexler, J. R., Good, P. J., Feingold, E. A., Crawford, G. E., Dekker, J., Elnitski, L., Farnham, P. J., Giddings, M. C., Gingeras, T. R., Guigó, R., Hubbard, T. J., Kent, W. J., Lieb, J. D., Margulies, E. H., Myers, R. M., Stamatoyannopoulos, J. A., Tenenbaum, S. A., Weng, Z., White, K. P., Wold, B., Yu, Y., Wrobel, J., Risk, B. A., Gunawardena, H. P., Kuiper, H. C., Maier, C. W., Xie, L., Chen, X., Mikkelsen, T. S., Gillespie, S., Goren, A., Ram, O., Zhang, X., Wang, L., Issner, R., Coyne, M. J., Durham, T., Ku, M., Truong, T., Eaton, M. L., Dobin, A., Tanzer, A., Lagarde, J., Lin, W., Xue, C., Williams, B. A., Zaleski, C., Röder, M., Kokocinski, F., Abdelhamid, R. F., Alioto, T., Antoshechkin, I., Baer, M. T., Batut, P., Bell, I., Bell, K., Chakrabortty, S., Chrast, J., Curado, J., Derrien, T., Drenkow, J., Dumais, E., Dumais, J., Duttagupta, R., Fastuca, M., Fejes-Toth, K., Ferreira, P., Foissac, S., Fullwood, M. J., Gao, H., Gonzalez, D., Gordon, A., Howald, C., Jha, S., Johnson, R., Kapranov, P., King, B., Kingswood, C., Li, G., Luo, O. J., Park, E., Preall, J. B., Presaud, K., Ribeca, P., Robyr, D., Ruan, X., Sammeth, M., Sandhu, K. S., Schaeffer, L., See, L. H., Shahab, A., Skancke, J., Suzuki, A. M., Takahashi, H., Tilgner, H., Trout, D., Walters, N., Wang, H., Hayashizaki, Y., Reymond, A., Antonarakis, S. E., Hannon, G. J., Ruan, Y., Carninci, P., Sloan, C. A., Learned, K., Malladi, V. S., Wong, M. C., Barber, G. P.,

Cline, M. S., Dreszer, T. R., Heitner, S. G., Karolchik, D., Kirkup, V. M., Meyer, L. R., Long, J. C., Maddren, M., Raney, B. J., Grasfeder, L. L., Giresi, P. G., Battenhouse, A., Sheffield, N. C., Showers, K. A., London, D., Bhinge, A. A., Shestak, C., Schaner, M. R., Kim, S. K., Zhang, Z. Z., Mieczkowski, P. A., Mieczkowska, J. O., Liu, Z., McDaniell, R. M., Ni, Y., Rashid, N. U., Kim, M. J., Adar, S., Zhang, Z., Wang, T., Winter, D., Keefe, D., Iyer, V. R., Zheng, M., Wang, P., Gertz, J., Vielmetter, J., Partridge, E. C., Varley, K. E., Gasper, C., Bansal, A., Pepke, S., Jain, P., Amrhein, H., Bowling, K. M., Anaya, M., Cross, M. K., Muratet, M. A., Newberry, K. M., McCue, K., Nesmith, A. S., Fisher-Aylor, K. I., Pusey, B., DeSalvo, G., Parker, S. L., Balasubramanian, S., Davis, N. S., Meadows, S. K., Eggleston, T., Newberry, J. S., Levy, S. E., Absher, D. M., Wong, W. H., Blow, M. J., Visel, A., Pennachio, L. A., Petrykowska, H. M., Abyzov, A., Aken, B., Barrell, D., Barson, G., Berry, A., Bignell, A., Boychenko, V., Bussotti, G., Davidson, C., Despacio-Reyes, G., Diekhans, M., Ezkurdia, I., Frankish, A., Gilbert, J., Gonzalez, J. M., Griffiths, E., Harte, R., Hendrix, D. A., Hunt, T., Jungreis, I., Kay, M., Khurana, E., Leng, J., Lin, M. F., Loveland, J., Lu, Z., Manthravadi, D., Mariotti, M., Mudge, J., Mukherjee, G., Notredame, C., Pei, B., Rodriguez, J. M., Saunders, G., Sboner, A., Searle, S., Sisu, C., Snow, C., Steward, C., Tapanari, E., Tress, M. L., Van Baren, M. J., Washietl, S., Wilming, L., Zadissa, A., Zhang, Z., Brent, M., Haussler, D., Valencia, A., Addleman, N., Alexander, R. P., Auerbach, R. K., Balasubramanian, S., Bettinger, K., Bhardwaj, N., Boyle, A. P., Cao, A. R., Cayting, P., Charos, A., Cheng, Y., Eastman, C., Euskirchen, G., Fleming, J. D., Grubert, F., Habegger, L., Hariharan, M., Harmanci, A., Iyengar, S., Jin, V. X., Karczewski, K. J., Kasowski, M., Lacroute, P., Lam, H., Lamarre-Vincent, N., Lian, J., Lindahl-Allen, M., Min, R., Miotto, B., Monahan, H., Moqtaderi, Z., Mu, X. J., O'Geen, H., Ouyang, Z., Patacsil, D., Raha, D., Ramirez, L., Reed, B., Shi, M., Slifer, T., Witt, H., Wu, L., Xu, X., Yan, K. K., Yang, X., Struhl, K., Weissman, S. M., Penalva, L. O., Karmakar, S., Bhanvadia, R. R., Choudhury, A., Domanus, M., Ma, L., Moran, J., Victorsen, A., Auer, T., Centanin, L., Eichenlaub, M., Gruhl, F., Heermann, S., Hoeckendorf, B., Inoue, D., Kellner, T., Kirchmaier, S., Mueller, C., Reinhardt, R., Schertel, L., Schneider, S., Sinn, R., Wittbrodt, B., Wittbrodt, J., Jain, G., Balasundaram, G., Bates, D. L., Byron, R., Canfi (2012). An integrated encyclopedia of DNA elements in the human genome. *Nature*, 489(7414):57–74.

[Ebine et al., 2018] Ebine, K., Kumar, K., Pham, T. N., Shields, M. A., Collier, K. A., Shang, M., DeCant, B. T., Urrutia, R., Hwang, R. F., Grimaldo, S., Principe, D. R., Grippo, P. J., Bentrem, D. J., and Munshi, H. G. (2018). Interplay between interferon regulatory factor 1 and BRD4 in the regulation of PD-L1 in pancreatic stellate cells. *Scientific Reports*, 8(1):13225.

[Eden et al., 2009] Eden, E., Navon, R., Steinfeld, I., Lipson, D., and Yakhini, Z. (2009). GOrilla: a tool for discovery and visualization of enriched GO terms in ranked gene lists. *BMC Bioinformatics*, 10(1):48.

[El-Khoueiry et al., 2017] El-Khoueiry, A. B., Sangro, B., Yau, T., Crocenzi, T. S., Kudo, M., Hsu, C., Kim, T. Y., Choo, S. P., Trojan, J., Welling, T. H., Meyer, T., Kang, Y. K., Yeo, W., Chopra, A., Anderson, J., dela Cruz, C., Lang, L., Neely, J., Tang, H., Dastani, H. B., and Melero, I. (2017). Nivolumab in patients with advanced hepatocellular carcinoma (CheckMate 040): an open-label, non-comparative, phase 1/2 dose escalation and expansion trial. *The Lancet*, 389(10088):2492–2502.

[Engreitz et al., 2016] Engreitz, J. M., Haines, J. E., Perez, E. M., Munson, G., Chen, J., Kane, M., McDonel, P. E., Guttman, M., and Lander, E. S. (2016). Local regulation of gene expression by lncRNA promoters, transcription and splicing. *Nature*, 539(7629):452–455.

[Finn et al., 2020] Finn, R. S., Ryoo, B. Y., Merle, P., Kudo, M., Bouattour, M., Lim, H. Y., Breder, V., Edeline, J., Chao, Y., Ogasawara, S., Yau, T., Garrido, M., Chan, S. L., Knox, J., Daniele, B., Ebbinghaus, S. W., Chen, E., Siegel, A. B., Zhu, A. X., and Cheng, A. L. (2020). Pembrolizumab As Second-Line Therapy in Patients With Advanced Hepatocellular Carcinoma in KEYNOTE-240: A Randomized, Double-Blind, Phase III Trial. *Journal of clinical oncology : official journal of the American Society of Clinical Oncology*, 38(3):193–202.

[Fishburn et al., 2015] Fishburn, J., Tomko, E., Galburt, E., and Hahn, S. (2015). Double-stranded DNA translocase activity of transcription factor TFIIH and the mechanism of RNA polymerase II open complex formation. *Proceedings of the National Academy of Sciences of the United States of America*, 112(13):3961–3966.

[Fishilevich et al., 2017] Fishilevich, S., Nudel, R., Rappaport, N., Hadar, R., Plaschkes, I., Iny Stein, T., Rosen, N., Kohn, A., Twik, M., Safran, M., Lancet, D., and Cohen, D. (2017). GeneHancer: genome-wide integration of enhancers and target genes in GeneCards. *Database : the journal of biological databases and curation*, 2017(bax028):1–17.

[Freeman et al., 2000] Freeman, G. J., Long, A. J., Iwai, Y., Bourque, K., Chernova, T., Nishimura, H., Fitz, L. J., Malenkovich, N., Okazaki, T., Byrne, M. C., Horton, H. F., Fouser, L., Carter, L., Ling, V., Bowman, M. R., Carreno, B. M., Collins, M., Wood, C. R., and Honjo, T. (2000). Engagement of the PD-1 immunoinhibitory receptor by a novel B7 family member leads to negative regulation of lymphocyte activation. *The Journal of experimental medicine*, 192(7):1027–34.

[Frigola et al., 2012] Frigola, X., Inman, B. A., Krco, C. J., Liu, X., Harrington, S. M., Bulur, P. A., Dietz, A. B., Dong, H., and Kwon, E. D. (2012). Soluble B7-H1: Differences in production between dendritic cells and T cells.

[Frigola et al., 2011] Frigola, X., Inman, B. A., Lohse, C. M., Krco, C. J., Cheville, J. C., Thompson, R. H., Leibovich, B., Blute, M. L., Dong, H., and Kwon, E. D. (2011). Identification of a soluble form of B7-H1 that retains immunosuppressive activity and is associated with aggressive renal cell carcinoma. *Clinical Cancer Research*, 17(7):1915–1923.

[Gajewski and Fitch, 1988] Gajewski, T. F. and Fitch, F. W. (1988). Anti-proliferative effect of IFN-gamma in immune regulation. I. IFN-gamma inhibits the proliferation of Th2 but not Th1 murine helper T lymphocyte clones. *The Journal of Immunology*, 140(12).

[Gao et al., 2016] Gao, J., Shi, L. Z., Zhao, H., Chen, J., Xiong, L., He, Q., Chen, T., Roszik, J., Bernatchez, C., Woodman, S. E., Chen, P.-L., Hwu, P., Allison, J. P., Futreal, A., Wargo, J. A., and Sharma, P. (2016). Loss of IFN-γ Pathway Genes in Tumor Cells as a Mechanism of Resistance to Anti-CTLA-4 Therapy. *Cell*, 167(2):397–404.e9.

[Garcia-Diaz et al., 2017] Garcia-Diaz, A., Shin, D. S., Moreno, B. H., Saco, J., Escuin-Ordinas, H., Rodriguez, G. A., Zaretsky, J. M., Sun, L., Hugo, W., Wang, X., Parisi, G., Saus, C. P., Torrejon, D. Y., Graeber, T. G., Comin-Anduix, B., Hu-Lieskovan, S., Damoiseaux, R., Lo, R. S., and Ribas, A. (2017). Interferon Receptor Signaling Pathways Regulating PD-L1 and PD-L2 Expression. *Cell reports*, 19(6):1189–1201.

[Gato-Canas et al., 2017] Gato-Canas, M., Zuazo, M., Arasanz, H., Iba∼nez-Vea, M., Lorenzo, L., Fernandez-Hinojal, G., Vera, R., Smerdou, C., Martisova, E., Arozarena, I., Wellbrock, C., Llopiz, D., Ruiz, M., Sarobe, P., Breckpot, K., Kochan, G., and Escors, D. (2017). PDL1 Signals through Conserved Sequence Motifs to Overcome Interferon-Mediated Cytotoxicity. *Cell Reports*, 20(8):1818–1829.

[Geng et al., 2006] Geng, H., Zhang, G.-M., Xiao, H., Yuan, Y., Li, D., Zhang, H., Qiu, H., He, Y.-F., and Feng, Z.-H. (2006). HSP70 vaccine in combination with gene therapy with plasmid DNA encoding sPD-1 overcomes immune resistance and suppresses the progression of pulmonary metastatic melanoma. *International Journal of Cancer*, 118(11):2657–2664.

[Gerber et al., 2013] Gerber, S. A., Sedlacek, A. L., Cron, K. R., Murphy, S. P., Frelinger, J. G., and Lord, E. M. (2013). IFN-γ mediates the antitumor effects of radiation therapy in a murine colon tumor. *American Journal of Pathology*, 182(6):2345–2354.

[Glasner et al., 2018] Glasner, A., Levi, A., Enk, J., Isaacson, B., Viukov, S., Orlanski, S., Scope, A., Neuman, T., Enk, C. D., Hanna, J. H., Sexl, V., Jonjic, S., Seliger, B., Zitvogel, L., and Mandelboim, O. (2018). NKp46 Receptor-Mediated Interferon-γ Production by Natural Killer Cells Increases Fibronectin 1 to Alter Tumor Architecture and Control Metastasis. *Immunity*, 48(1):107–119.e4.

[Goltz et al., 2017] Goltz, D., Gevensleben, H., Dietrich, J., and Dietrich, D. (2017). Pd-l1 (CD274) promoter methylation predicts survival in colorectal cancer patients. *OncoImmunology*, 6(1).

[Gong et al., 2019] Gong, B., Kiyotani, K., Sakata, S., Nagano, S., Kumehara, S., Baba, S., Besse, B., Yanagitani, N., Friboulet, L., Nishio, M., Takeuchi, K., Kawamoto, H., Fujita, N., and Katayama, R. (2019). Secreted PD-L1 variants mediate resistance to PD-L1 blockade therapy in non-small cell lung cancer. *Journal of Experimental Medicine*, 216(4):982–1000.

[Gordon et al., 2017] Gordon, S. R., Maute, R. L., Dulken, B. W., Hutter, G., George, B. M., McCracken, M. N., Gupta, R., Tsai, J. M., Sinha, R., Corey, D., Ring, A. M., Connolly, A. J., and Weissman, I. L. (2017). PD-1 expression by tumour-associated macrophages inhibits phagocytosis and tumour immunity. *Nature*, 545(7655):495–499.

[Gowrishankar et al., 2015] Gowrishankar, K., Gunatilake, D., Gallagher, S. J., Tiffen, J., Rizos, H., and Hersey, P. (2015). Inducible but not constitutive expression of PD-L1 in human melanoma cells is dependent on activation of NF-κB. *PLoS ONE*, 10(4).

[Grant et al., 2011] Grant, C., Bailey, T., and Stafford Noble, W. (2011). FIMO: scanning for occurrences of a given motif. *Bioinformatics*, 27(7):1017–1018.

[Green et al., 2010] Green, M. R., Monti, S., Rodig, S. J., Juszczynski, P., Currie, T., O'Donnell, E., Chapuy, B., Takeyama, K., Neuberg, D., Golub, T. R., Kutok, J. L., and Shipp, M. A. (2010). Integrative analysis reveals selective 9p24.1 amplification, increased PD-1 ligand expression, and further induction via JAK2 in nodular sclerosing Hodgkin lymphoma and primary mediastinal large B-cell lymphoma. *Blood*, 116(17):3268–3277.

[Green et al., 2012] Green, M. R., Rodig, S., Juszczynski, P., Ouyang, J., Sinha, P., O'Donnell, E., Neuberg, D., and Shipp, M. A. (2012). Constitutive AP-1 activity and EBV infection induce PD-l1 in Hodgkin lymphomas and posttransplant lymphoproliferative disorders: Implications for targeted therapy. *Clinical Cancer Research*, 18(6):1611–1618.

[Grünberg et al., 2012] Grünberg, S., Warfield, L., and Hahn, S. (2012). Architecture of the RNA polymerase II preinitiation complex and mechanism of ATP-dependent promoter opening. *Nature Structural and Molecular Biology*, 19(8):788–796.

[Guhaniyogi and Brewer, 2001] Guhaniyogi, J. and Brewer, G. (2001). Regulation of mRNA stability in mammalian cells.

[Haberle and Stark, 2018] Haberle, V. and Stark, A. (2018). Eukaryotic core promoters and the functional basis of transcription initiation.

[Hamanishi et al., 2007] Hamanishi, J., Mandai, M., Iwasaki, M., Okazaki, T., Tanaka, Y., Yamaguchi, K., Higuchi, T., Yagi, H., Takakura, K., Minato, N., Honjo, T., and Fujii, S. (2007). Programmed cell death 1 ligand 1 and tumor-infiltrating CD8+ T lymphocytes are prognostic factors of human ovarian cancer. *Proceedings of the National Academy of Sciences*, 104(9):3360–3365.

[Hamdan and Johnsen, 2019] Hamdan, F. H. and Johnsen, S. A. (2019). Perturbing enhancer activity in cancer therapy. *Cancers*, 11(5).

[Hanahan and Weinberg, 2011] Hanahan, D. and Weinberg, R. A. (2011). Hallmarks of cancer: The next generation.

[Hansen et al., 2008] Hansen, K. H., Bracken, A. P., Pasini, D., Dietrich, N., Gehani, S. S., Monrad, A., Rappsilber, J., Lerdrup, M., and Helin, K. (2008). A model for transmission of the H3K27me3 epigenetic mark. *Nature Cell Biology*, 10(11):1291–1300.

[Harada et al., 1989] Harada, H., Fujita, T., Miyamoto, M., Kimura, Y., Maruyama, M., Furia, A., Miyata, T., and Taniguchi, T. (1989). Structurally similar but functionally distinct factors, IRF-1 and IRF-2, bind to the same regulatory elements of IFN and IFN-inducible genes. *Cell*, 58(4):729–739.

[Hartley et al., 2017] Hartley, G., Regan, D., Guth, A., and Dow, S. (2017). Regulation of PD-L1 expression on murine tumor-associated monocytes and macrophages by locally produced TNF-α. *Cancer Immunology, Immunotherapy*, 66(4):523–535.

[Hartley et al., 2018] Hartley, G. P., Chow, L., Ammons, D. T., Wheat, W. H., and Dow, S. W. (2018). Programmedcell death ligand 1 (PD-L1) signaling regulates macrophage proliferation and activation. *Cancer Immunology Research*, 6(10):1260–1273.

[Harvat et al., 1997] Harvat, B. L., Seth, P., and Jetten, A. M. (1997). The role of p27(Kip1) in gamma interferon-mediated growth arrest of mammary epithelial cells and related defects in mammary carcinoma cells. *Oncogene*, 14(17):2111–2122.

[Hassounah et al., 2019] Hassounah, N. B., Malladi, V. S., Huang, Y., Freeman, S. S., Beauchamp, E. M., Koyama, S., Souders, N., Martin, S., Dranoff, G., Wong, K. K., Pedamallu, C. S., Hammerman, P. S., and Akbay, E. A. (2019). Identification and characterization of an alternative cancer-derived PD-L1 splice variant. *Cancer Immunology, Immunotherapy*, 68(3):407–420.

[He et al., 2004] He, X. H., Liu, Y., Xu, L. H., and Zeng, Y. Y. (2004). Cloning and identification of two novel splice variants of human PD-L2. *Acta Biochimica et Biophysica Sinica*, 36(4):284–289.

[HE et al., 2005] HE, X.-h., XU, L.-h., and LIU, Y. (2005). Identification of a novel splice variant of human PD-L1 mRNA encoding an isoform-lacking Igv-like domain1. *Acta Pharmacologica Sinica*, 26(4):462–468.

[Heinz et al., 2010] Heinz, S., Benner, C., Spann, N., Bertolino, E., Lin, Y. C., Laslo, P., Cheng, J. X., Murre, C., Singh, H., and Glass, C. K. (2010). Simple Combinations of Lineage-Determining Transcription Factors Prime cis-Regulatory Elements Required for Macrophage and B Cell Identities. *Molecular Cell*, 38(4):576–589.

[Hino et al., 2010] Hino, R., Kabashima, K., Kato, Y., Yagi, H., Nakamura, M., Honjo, T., Okazaki, T., and Tokura, Y. (2010). Tumor cell expression of programmed cell death-1 ligand 1 is a prognostic factor for malignant melanoma. *Cancer*, 116(7):1757–1766.

[Hirano et al., 2005] Hirano, F., Kaneko, K., Tamura, H., Dong, H., Wang, S., Ichikawa, M., Rietz, C., Flies, D. B., Lau, J. S., Zhu, G., Tamada, K., and Chen, L. (2005). Blockade of B7-H1 and PD-1 by monoclonal antibodies potentiates cancer therapeutic immunity. *Cancer research*, 65(3):1089–96.

[Hogg et al., 2017] Hogg, S. J., Vervoort, S. J., Deswal, S., Ott, C. J., Li, J., Cluse, L. A., Beavis, P. A., Darcy, P. K., Martin, B. P., Spencer, A., Traunbauer, A. K., Sadovnik, I., Bauer, K., Valent, P., Bradner, J. E., Zuber, J., Shortt, J., and Johnstone, R. W. (2017). BET-Bromodomain Inhibitors Engage the Host Immune System and Regulate Expression of the Immune Checkpoint Ligand PD-L1. *Cell Reports*, 18(9):2162–2174.

[Horita et al., 2017] Horita, H., Law, A., Hong, S., and Middleton, K. (2017). Identifying Regulatory Posttranslational Modifications of PD-L1: A Focus on Monoubiquitinaton. *Neoplasia (United States)*, 19(4):346–353.

[Hou et al., 2014] Hou, J., Yu, Z., Xiang, R., Li, C., Wang, L., Chen, S., Li, Q., Chen, M., and Wang, L. (2014). Correlation between infiltration of FOXP3+ regulatory T cells and expression of B7-H1 in the tumor tissues of gastric cancer. *Experimental and Molecular Pathology*, 96(3):284–291.

[Howe et al., 2017] Howe, F. S., Fischl, H., Murray, S. C., and Mellor, J. (2017). Is H3K4me3 instructive for transcription activation? *BioEssays*, 39(1):e201600095.

[Hsu et al., 2018a] Hsu, J. M., Xia, W., Hsu, Y. H., Chan, L. C., Yu, W. H., Cha, J. H., Chen, C. T., Liao, H. W., Kuo, C. W., Khoo, K. H., Hsu, J. L., Li, C. W., Lim, S. O., Chang, S. S., Chen, Y. C., Ren, G. X., and Hung, M. C. (2018a). STT3-dependent PD-L1 accumulation on cancer stem cells promotes immune evasion. *Nature Communications*, 9(1):1–17.

[Hsu et al., 2018b] Hsu, P.-C., Miao, J., Wang, Y.-C., Zhang, W.-Q., Yang, Y.-L., Wang, C.-W., Yang, C.-T., Huang, Z., You, J., Xu, Z., Jablons, D. M., and You, L. (2018b). Inhibition of yes-associated protein down-regulates PD-L1 (CD274) expression in human malignant pleural mesothelioma. *Journal of Cellular and Molecular Medicine*, 22(6):3139–3148.

[Hu et al., 2013] Hu, G., Cui, K., Northrup, D., Liu, C., Wang, C., Tang, Q., Ge, K., Levens, D., Crane-Robinson, C., and Zhao, K. (2013). H2A.Z facilitates access of active and repressive complexes to chromatin in embryonic stem cell self-renewal and differentiation. *Cell Stem Cell*, 12(2):180–192.

[Hu et al., 2017] Hu, Y.-B., Zhang, Q., Li, H.-J., Michot, J. M., Liu, H.-B., Zhan, P., Lv, T.-F., Song, Y., and written on behalf of the AME Academic Lung Cancer Cooperation Group (2017). Evaluation of rare but severe immune related adverse effects in PD-1 and PD-L1 inhibitors in non-small cell lung cancer: a meta-analysis. *Translational Lung Cancer Research*, 6(S1):S8–S20.

[Huang et al., 2013] Huang, H., Liu, H., and Sun, X. (2013). Nucleosome Distribution near the 3' Ends of Genes in the Human Genome. *Bioscience, Biotechnology, and Biochemistry*, 77(10):2051–2055.

[Hughes and Rando, 2014] Hughes, A. L. and Rando, O. J. (2014). Mechanisms Underlying Nucleosome Positioning In Vivo. *Annual Review of Biophysics*, 43(1):41–63.

[Hughes et al., 2014] Hughes, J. R., Roberts, N., Mcgowan, S., Hay, D., Giannoulatou, E., Lynch, M., De Gobbi, M., Taylor, S., Gibbons, R., and Higgs, D. R. (2014). Analysis of hundreds of cis-regulatory landscapes at high resolution in a single, high-throughput experiment. *Nature Genetics*, 46(2):205–212.

[Ishida et al., 1992] Ishida, Y., Agata, Y., Shibahara, K., and Honjo1, T. (1992). Induced expression of PD-1, a novel member of the immunoglobulin gene superfamily, upon programmed cell death. *The EMBO Journal*, 1(1):3887–3895.

[Ivashkiv, 2018] Ivashkiv, L. B. (2018). IFNγ: signalling, epigenetics and roles in immunity, metabolism, disease and cancer immunotherapy.

[Iwai et al., 2002] Iwai, Y., Ishida, M., Tanaka, Y., Okazaki, T., Honjo, T., and Minato, N. (2002). Involvement of PD-L1 on tumor cells in the escape from host immune system and tumor immunotherapy by PD-L1 blockade. *Proceedings of the National Academy of Sciences*, 99(19):12293–12297.

[Jalali et al., 2019] Jalali, S., Price-Troska, T., Bothun, C., Villasboas, J., Kim, H. J., Yang, Z. Z., Novak, A. J., Dong, H., and Ansell, S. M. (2019). Reverse signaling via PD-L1 supports malignant cell growth and survival in classical Hodgkin lymphoma. *Blood Cancer Journal*, 9(22).

[Janse van Rensburg et al., 2018] Janse van Rensburg, H. J., Azad, T., Ling, M., Hao, Y., Snetsinger, B., Khanal, P., Minassian, L. M., Graham, C. H., Rauh, M. J., and Yang, X. (2018). The Hippo pathway component TAZ promotes immune evasion in human cancer through PD-L1. *Cancer Research*, 78(6):1457–1470.

[Jenne and Kubes, 2013] Jenne, C. N. and Kubes, P. (2013). Immune surveillance by the liver.

[Ji et al., 2018] Ji, X., Wang, E., and Tian, F. (2018). MicroRNA-140 suppresses osteosarcoma tumor growth by enhancing anti-tumor immune response and blocking mTOR signaling. *Biochemical and Biophysical Research Communications*, 495(1):1342–1348.

[Jiang et al., 2019] Jiang, X., Wang, J., Deng, X., Xiong, F., Ge, J., Xiang, B., Wu, X., Ma, J., Zhou, M., Li, X., Li, Y., Li, G., Xiong, W., Guo, C., and Zeng, Z. (2019). Role of the tumor microenvironment in PD-L1/PD-1-mediated tumor immune escape.

[Jiang et al., 2013] Jiang, X., Zhou, J., Giobbie-Hurder, A., Wargo, J., and Hodi, F. S. (2013). The activation of MAPK in melanoma cells resistant to BRAF inhibition promotes PD-L1 expression that is reversible by MEK and PI3K inhibition. *Clinical Cancer Research*, 19(3):598–609.

[Jiang and Zhan, 2020] Jiang, Y. and Zhan, H. (2020). Communication between EMT and PD-L1 signaling: New insights into tumor immune evasion.

[Jin et al., 2009] Jin, C., Zang, C., Wei, G., Cui, K., Peng, W., Zhao, K., and Felsenfeld, G. (2009). H3.3/H2A.Z double variant-containing nucleosomes mark 'nucleosome-free regions' of active promoters and other regulatory regions. *Nature Genetics*, 41(8):941–945.

[Juneja et al., 2017] Juneja, V. R., McGuire, K. A., Manguso, R. T., LaFleur, M. W., Collins, N., Nicholas Haining, W., Freeman, G. J., and Sharpe, A. H. (2017). PD-L1 on tumor cells is sufficient for immune evasion in immunogenic tumors and inhibits CD8 T cell cytotoxicity. *Journal of Experimental Medicine*, 214(4):895–904.

[Kagey et al., 2010] Kagey, M. H., Newman, J. J., Bilodeau, S., Zhan, Y., Orlando, D. A., Van Berkum, N. L., Ebmeier, C. C., Goossens, J., Rahl, P. B., Levine, S. S., Taatjes, D. J., Dekker, J., and Young, R. A. (2010). Mediator and cohesin connect gene expression and chromatin architecture. *Nature*, 467(7314):430–435.

[Kamada et al., 2018] Kamada, R., Yang, W., Zhang, Y., Patel, M. C., Yang, Y., Ouda, R., Dey, A., Wakabayashi, Y., Sakaguchi, K., Fujita, T., Tamura, T., Zhu, J., and Ozato, K. (2018). Interferon stimulation creates chromatin marks and establishes transcriptional memory. *Proceedings of the National Academy of Sciences of the United States of America*, 115(39):E9162–E9171.

[Kammertoens et al., 2017] Kammertoens, T., Friese, C., Arina, A., Idel, C., Briesemeister, D., Rothe, M., Ivanov, A., Szymborska, A., Patone, G., Kunz, S., Sommermeyer, D., Engels, B., Leisegang, M., Textor, A., Joerg Fehling, H., Fruttiger, M., Lohoff, M., Herrmann, A., Yu, H., Weichselbaum, R., Uckert, W., Hübner, N., Gerhardt, H., Beule, D., Schreiber, H., and Blankenstein, T. (2017). Tumour ischaemia by interferon-γ resembles physiological blood vessel regression. *Nature*, 545(7652):98–102.

[Kang et al., 2017] Kang, K., Park, S. H., Chen, J., Qiao, Y., Giannopoulou, E., Berg, K., Hanidu, A., Li, J., Nabozny, G., Kang, K., Park-Min, K. H., and Ivashkiv, L. B. (2017). Interferon-y Represses M2 Gene Expression in Human Macrophages by Disassembling Enhancers Bound by the Transcription Factor MAF. *Immunity*, 47(2):235–250.e4.

[Kataoka et al., 2016] Kataoka, K., Shiraishi, Y., Takeda, Y., Sakata, S., Matsumoto, M., Nagano, S., Maeda, T., Nagata, Y., Kitanaka, A., Mizuno, S., Tanaka, H., Chiba, K., Ito, S., Watatani, Y., Kakiuchi, N., Suzuki, H., Yoshizato, T., Yoshida, K., Sanada, M., Itonaga, H., Imaizumi, Y., Totoki, Y., Munakata, W., Nakamura, H., Hama, N., Shide, K., Kubuki, Y., Hidaka, T., Kameda, T., Masuda, K., Minato, N., Kashiwase, K., Izutsu, K., Takaori-Kondo, A., Miyazaki, Y., Takahashi, S., Shibata, T., Kawamoto, H., Akatsuka, Y., Shimoda, K., Takeuchi, K., Seya, T., Miyano, S., and Ogawa, S. (2016). Aberrant PD-L1 expression through 3'-UTR disruption in multiple cancers. *Nature*, 534(7607):402–406.

[Kebede et al., 2017] Kebede, A. F., Nieborak, A., Shahidian, L. Z., Le Gras, S., Richter, F., Gómez, D. A., Baltissen, M. P., Meszaros, G., De Fatima Magliarelli, H., Taudt, A., Margueron, R., Colomé-Tatché, M., Ricci, R., Daujat, S., Vermeulen, M., Mittler, G., and Schneider, R. (2017). Histone propionylation is a mark of active chromatin. *Nature Structural and Molecular Biology*, 24(12):1048–1056.

[Keir et al., 2008] Keir, M. E., Butte, M. J., Freeman, G. J., and Sharpe, A. H. (2008). PD-1 and Its Ligands in Tolerance and Immunity. *Annual Review of Immunology*, 26(1):677–704.

[Kelly and Issa, 2017] Kelly, A. D. and Issa, J. P. J. (2017). The promise of epigenetic therapy: reprogramming the cancer epigenome.

[Kim et al., 2015] Kim, D., Langmead, B., and Salzberg, S. L. (2015). HISAT: A fast spliced aligner with low memory requirements. *Nature Methods*, 12(4):357–360.

[Kim et al., 2019] Kim, D. H., Kim, H. R., Choi, Y. J., Kim, S. Y., Lee, J. E., Sung, K. J., Sung, Y. H., Pack, C. G., kyo Jung, M., Han, B., Kim, K., Kim, W. S., Nam, S. J., Choi, C. M., Yun, M., Lee, J. C., and Rho, J. K. (2019). Exosomal PD-L1 promotes tumor growth through immune escape in non-small cell lung cancer. *Experimental and Molecular Medicine*, 51(8).

[Kim et al., 2018] Kim, M. H., Kim, C. G., Kim, S. K., Shin, S. J., Shin, E. C., Park, S. H., Shin, E. C., and Kim, J. (2018). YAP-induced PD-L1 expression drives immune evasion in BRAFi-resistant melanoma. *Cancer Immunology Research*, 6(3):255–266.

[Kim et al., 2010] Kim, T. K., Hemberg, M., Gray, J. M., Costa, A. M., Bear, D. M., Wu, J., Harmin, D. A., Laptewicz, M., Barbara-Haley, K., Kuersten, S., Markenscoff-Papadimitriou, E., Kuhl, D., Bito, H., Worley, P. F., Kreiman, G., and Greenberg, M. E. (2010). Widespread transcription at neuronal activity-regulated enhancers. *Nature*, 465(7295):182–187.

[Klein and Hainer, 2020] Klein, D. C. and Hainer, S. J. (2020). Genomic methods in profiling DNA accessibility and factor localization. *Chromosome research : an international journal on the molecular, supramolecular and evolutionary aspects of chromosome biology*, 28(1):69–85.

[Kleinovink et al., 2017] Kleinovink, J. W., Marijt, K. A., Schoonderwoerd, M. J., van Hall, T., Ossendorp, F., and Fransen, M. F. (2017). PD-L1 expression on malignant cells is no prerequisite for checkpoint therapy. *OncoImmunology*, 6(4).

[Klemm et al., 2019] Klemm, S. L., Shipony, Z., and Greenleaf, W. J. (2019). Chromatin accessibility and the regulatory epigenome.

[Kobayashi and Van Den Elsen, 2012] Kobayashi, K. S. and Van Den Elsen, P. J. (2012). NLRC5: A key regulator of MHC class I-dependent immune responses.

[Koch et al., 2011] Koch, F., Fenouil, R., Gut, M., Cauchy, P., Albert, T. K., Zacarias-Cabeza, J., Spicuglia, S., De La Chapelle, A. L., Heidemann, M., Hintermair, C., Eick, D., Gut, I., Ferrier, P., and Andrau, J. C. (2011). Transcription initiation platforms and GTF recruitment at tissue-specific enhancers and promoters. *Nature Structural and Molecular Biology*, 18(8):956–963.

[Kondo et al., 2010] Kondo, A., Yamashita, T., Tamura, H., Zhao, W., Tsuji, T., Shimizu, M., Shinya, E., Takahashi, H., Tamada, K., Chen, L., Dan, K., and Ogata, K. (2010). Interferon-γ and tumor necrosis factor-α induce an immunoinhibitory molecule, B7-H1, via nuclear factor-κB activation in blasts in myelodysplastic syndromes. *Blood*, 116(7):1124–1131.

[Konishi et al., 2004] Konishi, J., Yamazaki, K., Azuma, M., Kinoshita, I., Dosaka-Akita, H., and Nishimura, M. (2004). B7-H1 expression on non-small cell lung cancer cells and its relationship with tumor-infiltrating lymphocytes and their PD-1 expression. *Clinical Cancer Research*, 10(15):5094–5100.

[Lagrange et al., 1998] Lagrange, T., Kapanidis, A. N., Tang, H., Reinberg, D., and Ebright, R. H. (1998). New core promoter element in RNA polymerase II-dependent transcription: Sequence-specific DNA binding by transcription factor IIB. *Genes and Development*, 12(1):34–44.

[Lai et al., 2018] Lai, Q., Wang, H., Li, A., Xu, Y., Tang, L., Chen, Q., Zhang, C., Gao, Y., Song, J., and Du, Z. (2018). Decitibine improve the efficiency of anti-PD-1 therapy via activating the response to IFN/PD-L1 signal of lung cancer cells. *Oncogene*, 37(17):2302–2312.

[Langlais et al., 2016] Langlais, D., Barreiro, L. B., and Gros, P. (2016). The macrophage IRF8/IRF1 regulome is required for protection against infections and is associated with chronic inflammation. *Journal of Experimental Medicine*, 213(4):585–603.

[Langmead and Salzberg, 2012] Langmead, B. and Salzberg, S. L. (2012). Fast gapped-read alignment with Bowtie 2. *Nature Methods*, 9(4):357–359.

[Latchman et al., 2001] Latchman, Y., Wood, C. R., Chernova, T., Chaudhary, D., Borde, M., Chernova, I., Iwai, Y., Long, A. J., Brown, J. A., Nunes, R., Greenfield, E. A., Bourque, K., Boussiotis, V. A., Carter, L. L., Carreno, B. M., Malenkovich, N., Nishimura, H., Okazaki, T., Honjo, T., Sharpe, A. H., and Freeman, G. J. (2001). PD-L2 is a second ligand for PD-1 and inhibits T cell activation. *Nature Immunology*, 2(3):261–268.

[Lau et al., 2017] Lau, J., Cheung, J., Navarro, A., Lianoglou, S., Haley, B., Totpal, K., Sanders, L., Koeppen, H., Caplazi, P., McBride, J., Chiu, H., Hong, R., Grogan, J., Javinal, V., Yauch, R., Irving, B., Belvin, M., Mellman, I., Kim, J. M., and Schmidt, M. (2017). Tumour and host cell PD-L1 is required to mediate suppression of anti-tumour immunity in mice. *Nature Communications*, 8(14572).

[Lawrence et al., 2016] Lawrence, M., Daujat, S., and Schneider, R. (2016). Lateral Thinking: How Histone Modifications Regulate Gene Expression.

[Le Poole et al., 2002] Le Poole, I. C., Riker, A. I., Quevedo, M. E., Stennett, L. S., Wang, E., Marincola, F. M., Kast, W. M., Robinson, J. K., and Nickoloff, B. J. (2002). Interferon-γ reduces melanosomal antigen expression and recognition of melanoma cells by cytotoxic T cells. *American Journal of Pathology*, 160(2):521–528.

[Lecis et al., 2019] Lecis, D., Sangaletti, S., Colombo, M. P., and Chiodoni, C. (2019). Immune checkpoint ligand reverse signaling: Looking back to go forward in cancer therapy. *Cancers*, 11(5):624.

[Lee et al., 2004] Lee, C. K., Shibata, Y., Rao, B., Strahl, B. D., and Lieb, J. D. (2004). Evidence for nucleosome depletion at active regulatory regions genome-wide. *Nature Genetics*, 36(8):900–905.

[Lee et al., 2017] Lee, K. S., Lee, K., Yun, S., Moon, S., Park, Y., Han, J. H., Kim, C.-Y., Lee, H. S., and Choe, G. (2017). Prognostic relevance of programmed cell death ligand 1 expression in glioblastoma. *Journal of Neuro-Oncology*, pages 1–9.

[Leung et al., 2019] Leung, Y. T., Maurer, K., Song, L., Convissar, J., and Sullivan, K. E. (2019). Prolactin activates IRF1 and leads to altered balance of histone acetylation: Implications for systemic lupus erythematosus. *Modern Rheumatology*, 30(3):532–543.

[Li et al., 2018] Li, C. W., Lim, S. O., Chung, E. M., Kim, Y. S., Park, A. H., Yao, J., Cha, J. H., Xia, W., Chan, L. C., Kim, T., Chang, S. S., Lee, H. H., Chou, C. K., Liu, Y. L., Yeh, H. C., Perillo, E. P., Dunn, A. K., Kuo, C. W., Khoo, K. H., Hsu, J. L., Wu, Y., Hsu, J. M., Yamaguchi, H., Huang, T. H., Sahin, A. A., Hortobagyi, G. N., Yoo, S. S., and Hung, M. C. (2018). Eradication of Triple-Negative Breast Cancer Cells by Targeting Glycosylated PD-L1. *Cancer Cell*, 33(2):187–201.e10.

[Li et al., 2016] Li, C. W., Lim, S. O., Xia, W., Lee, H. H., Chan, L. C., Kuo, C. W., Khoo, K. H., Chang, S. S., Cha, J. H., Kim, T., Hsu, J. L., Wu, Y., Hsu, J. M., Yamaguchi, H., Ding, Q., Wang, Y., Yao, J., Lee, C. C., Wu, H. J., Sahin, A. A., Allison, J. P., Yu, D., Hortobagyi, G. N., and Hung, M. C. (2016). Glycosylation and stabilization of programmed death ligand-1 suppresses T-cell activity. *Nature Communications*, 7(1):1–11.

[Li et al., 2009] Li, H., Handsaker, B., Wysoker, A., Fennell, T., Ruan, J., Homer, N., Marth, G., Abecasis, G., and Durbin, R. (2009). The Sequence Alignment/Map format and SAMtools. *Bioinformatics*, 25(16):2078–2079.

[Li et al., 2017] Li, N., Wang, J., Zhang, N., Zhuang, M., Zong, Z., Zou, J., Li, G., Wang, X., Zhou, H., Zhang, L., and Shi, Y. (2017). Cross-talk between TNF-α and IFN-γ signaling in induction of B7-H1 expression in hepatocellular carcinoma cells. *Cancer Immunology, Immunotherapy*, 67(2):271–283.

[Li et al., 2012] Li, W., Huang, X., Tong, H., Wang, Y., Zhang, T., Wang, W., Dai, L., Li, T., Lin, S., and Wu, H. (2012). Comparison of the Regulation of β-Catenin Signaling by Type I, Type II and Type III Interferons in Hepatocellular Carcinoma Cells. *PLoS ONE*, 7(10).

[Liang et al., 2016] Liang, J., Zhou, H., Gerdt, C., Tan, M., Colson, T., Kaye, K. M., Kieff, E., and Zhao, B. (2016). Epstein–Barr virus super-enhancer eRNAs are essential for MYC oncogene expression and lymphoblast proliferation. *Proceedings of the National Academy of Sciences*, 113(49):14121–14126.

[Liao et al., 2014] Liao, Y., Smyth, G. K., and Shi, W. (2014). FeatureCounts: An efficient general purpose program for assigning sequence reads to genomic features. *Bioinformatics*, 30(7):923–930.

[Lienlaf et al., 2016] Lienlaf, M., Perez-Villarroel, P., Knox, T., Pabon, M., Sahakian, E., Powers, J., Woan, K. V., Lee, C., Cheng, F., Deng, S., Smalley, K. S., Montecino, M., Kozikowski, A., Pinilla-Ibarz, J., Sarnaik, A., Seto, E., Weber, J., Sotomayor, E. M., and Villagra, A. (2016). Essential role of HDAC6 in the regulation of PD-L1 in melanoma. *Molecular Oncology*, 10(5):735–750.

[Lim et al., 2004] Lim, C. Y., Santoso, B., Boulay, T., Dong, E., Ohler, U., and Kadonaga, J. T. (2004). The MTE, a new core promoter element for transcription by RNA poymerase II. *Genes and Development*, 18(13):1606–1617.

[Lim et al., 2016] Lim, S. O., Li, C. W., Xia, W., Cha, J. H., Chan, L. C., Wu, Y., Chang, S. S., Lin, W. C., Hsu, J. M., Hsu, Y. H., Kim, T., Chang, W. C., Hsu, J. L., Yamaguchi, H., Ding, Q., Wang, Y., Yang, Y., Chen, C. H., Sahin, A. A., Yu, D., Hortobagyi, G. N., and Hung, M. C. (2016). Deubiquitination and Stabilization of PD-L1 by CSN5. *Cancer Cell*, 30(6):925–939.

[Lin et al., 2018] Lin, H., Wei, S., Hurt, E. M., Green, M. D., Zhao, L., Vatan, L., Szeliga, W., Herbst, R., Harms, P. W., Fecher, L. A., Vats, P., Chinnaiyan, A. M., Lao, C. D., Lawrence, T. S., Wicha, M., Hamanishi, J., Mandai, M., Kryczek, I., and Zou, W. (2018). Host expression of PD-L1 determines efficacy of PD-L1 pathway blockade–mediated tumor regression. *Journal of Clinical Investigation*, 128(2):805–815.

[Liu et al., 2017a] Liu, B., Song, Y., and Liu, D. (2017a). Recent development in clinical applications of PD-1 and PD-L1 antibodies for cancer immunotherapy. *Journal of Hematology & Oncology*, 10(1):174.

[Liu et al., 2020] Liu, J., He, D., Cheng, L., Huang, C., Zhang, Y., Rao, X., Kong, Y., Li, C., Zhang, Z., Liu, J., Jones, K., Napier, D., Lee, E. Y., Wang, C., and Liu, X. (2020). p300/CBP inhibition enhances the efficacy of programmed death-ligand 1 blockade treatment in prostate cancer. *Oncogene*, pages 1–13.

[Liu et al., 2017b] Liu, Y., Liang, X., Yin, X., Lv, J., Tang, K., Ma, J., Ji, T., Zhang, H., Dong, W., Jin, X., Chen, D., Li, Y., Zhang, S., Xie, H. Q., Zhao, B., Zhao, T., Lu, J., Hu, Z. W., Cao, X., Qin, F. X. F., and Huang, B. (2017b). Blockade of IDO-kynurenine-AhR metabolic circuitry abrogates IFN-γ-induced immunologic dormancy of tumor-repopulating cells. *Nature Communications*, 8(1):1–15.

[Lizio et al., 2019] Lizio, M., Abugessaisa, I., Noguchi, S., Kondo, A., Hasegawa, A., Hon, C. C., De Hoon, M., Severin, J., Oki, S., Hayashizaki, Y., Carninci, P., Kasukawa, T., and Kawaji, H. (2019). Update of the FANTOM web resource: Expansion to provide additional transcriptome atlases. *Nucleic Acids Research*, 47(D1):D752–D758.

[Love et al., 2014] Love, M. I., Huber, W., and Anders, S. (2014). Moderated estimation of fold change and dispersion for RNA-seq data with DESeq2. *Genome Biology*, 15(12):550.

[Lu et al., 2017] Lu, C., Paschall, A. V., Shi, H., Savage, N., Waller, J. L., Sabbatini, M. E., Oberlies, N. H., Pearce, C., and Liu, K. (2017). The MLL1-H3K4me3 axis-mediated PD-L1 expression and pancreatic cancer immune evasion. *Journal of the National Cancer Institute*, 109(6).

[Lu et al., 2014] Lu, Y., Gu, X., Chen, L., Yao, Z., Song, J., Niu, X., Xiang, R., Cheng, T., Qin, Z., Deng, W., and Li, L. Y. (2014). Interferon-γ produced by tumor-infiltrating NK cells and CD4 + T cells downregulates TNFSF15 expression in vascular endothelial cells. *Angiogenesis*, 17(3):529–540.

[Lv et al., 2015] Lv, N., Gao, Y., Guan, H., Wu, D., Ding, S., Teng, W., and Shan, Z. (2015). Inflammatory mediators, tumor necrosis factor-α and interferon-γ, induce EMT in human PTC cell lines. *Oncology Letters*, 10(4):2591–2597.

[Ma et al., 2020] Ma, H., Chang, H., Yang, W., Lu, Y., Hu, J., and Jin, S. (2020). A novel IFNa-induced long noncoding RNA negatively regulates immunosuppression by interrupting H3K27 acetylation in head and neck squamous cell carcinoma. *Molecular cancer*, 19(1):4.

[Mahoney et al., 2019] Mahoney, K. M., Shukla, S. A., Patsoukis, N., Chaudhri, A., Browne, E. P., Arazi, A., Eisenhaure, T. M., Pendergraft, W. F., Hua, P., Pham, H. C., Bu, X., Zhu, B., Hacohen, N., Fritsch, E. F., Boussiotis, V. A., Wu, C. J., and Freeman, G. J. (2019). A secreted PD-L1 splice variant that covalently dimerizes and mediates immunosuppression. *Cancer Immunology, Immunotherapy*, 68(3):421–432.

[Mancino et al., 2015] Mancino, A., Termanini, A., Barozzi, I., Ghisletti, S., Ostuni, R., Prosperini, E., Ozato, K., and Natoli, G. (2015). A dual cis-regulatory code links IRF8 to constitutive and inducible gene expression in macrophages. *Genes and Development*, 29(4):394–408.

[Manguso et al., 2017] Manguso, R. T., Pope, H. W., Zimmer, M. D., Brown, F. D., Yates, K. B., Miller, B. C., Collins, N. B., Bi, K., LaFleur, M. W., Juneja, V. R., Weiss, S. A., Lo, J., Fisher, D. E., Miao, D., Van Allen, E., Root, D. E., Sharpe, A. H., Doench, J. G., and Haining, W. N. (2017). In vivo CRISPR screening identifies Ptpn2 as a cancer immunotherapy target. *Nature*, 547(7664):413–418.

[Martini et al., 2010] Martini, M., Testi, M. G., Pasetto, M., Picchio, M. C., Innamorati, G., Mazzocco, M., Ugel, S., Cingarlini, S., Bronte, V., Zanovello, P., Krampera, M., Mosna, F., Cestari, T., Riviera, A. P., Brutti, N., Barbieri, O., Matera, L., Tridente, G., Colombatti, M., and Sartoris, S. (2010). IFN-γ-mediated upmodulation of MHC class I expression activates tumor-specific immune response in a mouse model of prostate cancer. *Vaccine*, 28(20):3548–3557.

[Marzec et al., 2008] Marzec, M., Zhang, Q., Goradia, A., Raghunath, P. N., Liu, X., Paessler, M., Hong, Y. W., Wysocka, M., Cheng, M., Ruggeri, B. A., and Wasik, M. A. (2008). Oncogenic kinase NPM/ALK induces through STAT3 expression of immunosuppressive protein CD274 (PD-L1, B7-H1). *Proceedings of the National Academy of Sciences of the United States of America*, 105(52):20852–20857.

[Mataki et al., 2007] Mataki, N., Kikuchi, K., Kawai, T., Higashiyama, M., Okada, Y., Kurihara, C., Hokari, R., Kawaguchi, A., Nagao, S., Kondo, T., Itoh, K., Miyakawa, H., and Miura, S. (2007). Expression of PD-1, PD-L1, and PD-L2 in the liver in autoimmune liver diseases. *American Journal of Gastroenterology*, 102(2):302–312.

[McLoughlin et al., 2003] McLoughlin, R. M., Witowski, J., Robson, R. L., Wilkinson, T. S., Hurst, S. M., Williams, A. S., Williams, J. D., Rose-John, S., Jones, S. A., and Topley, N. (2003). Interplay between IFN-γ and IL-6 signaling governs neutrophil trafficking and apoptosis during acute inflammation. *Journal of Clinical Investigation*, 112(4):598–607.

[Medina-Echeverz et al., 2014] Medina-Echeverz, J., Haile, L. A., Zhao, F., Gamrekelashvili, J., Ma, C., Métais, J. Y., Dunbar, C. E., Kapoor, V., Manns, M. P., Korangy, F., and Greten, T. F. (2014). IFN-γ regulates survival and function of tumor-induced CD11b+Gr-1high myeloid derived suppressor cells by modulating the anti-apoptotic molecule Bcl2a1. *European Journal of Immunology*, 44(8):2457–2467.

[Melgar et al., 2011] Melgar, M. F., Collins, F. S., and Sethupathy, P. (2011). Discovery of active enhancers through bidirectional expression of short transcripts. *Genome Biology*, 12(11):R113.

[Melnick et al., 2002] Melnick, A., Carlile, G., Ahmad, K. F., Kiang, C.-L., Corcoran, C., Bardwell, V., Prive, G. G., and Licht, J. D. (2002). Critical Residues within the BTB Domain of PLZF and Bcl-6 Modulate Interaction with Corepressors. *Molecular and Cellular Biology*, 22(6):1804–1818.

[Messai et al., 2016] Messai, Y., Gad, S., Noman, M. Z., Le Teuff, G., Couve, S., Janji, B., Kammerer, S. F., Rioux-Leclerc, N., Hasmim, M., Ferlicot, S., Baud, V., Mejean, A., Mole, D. R., Richard, S., Eggermont, A. M., Albiges, L., Mami-Chouaib, F., Escudier, B., and Chouaib, S. (2016). Renal Cell Carcinoma Programmed Death-ligand 1, a New Direct Target of Hypoxia-inducible Factor-2 Alpha, is Regulated by von Hippel–Lindau Gene Mutation Status. *European Urology*, 70(4):623–632.

[Mezzadra et al., 2017] Mezzadra, R., Sun, C., Jae, L. T., Gomez-Eerland, R., De Vries, E., Wu, W., Logtenberg, M. E., Slagter, M., Rozeman, E. A., Hofland, I., Broeks, A., Horlings, H. M., Wessels, L. F., Blank, C. U., Xiao, Y., Heck, A. J., Borst, J., Brummelkamp, T. R., and Schumacher, T. N. (2017). Identification of CMTM6 and CMTM4 as PD-L1 protein regulators. *Nature*, 549(7670):106–110.

[Micevic et al., 2019] Micevic, G., Thakral, D., McGeary, M., and Bosenberg, M. W. (2019). PD-L1 methylation regulates PD-L1 expression and is associated with melanoma survival. *Pigment Cell & Melanoma Research*, 32(3):435–440.

[Michel et al., 2017] Michel, M., Demel, C., Zacher, B., Schwalb, B., Krebs, S., Blum, H., Gagneur, J., and Cramer, P. (2017). TT-seq captures enhancer landscapes immediately after T-cell stimulation. *Molecular systems biology*, 13(3):920.

[Mimura et al., 2018] Mimura, K., Teh, J. L., Okayama, H., Shiraishi, K., Kua, L.-F., Koh, V., Smoot, D. T., Ashktorab, H., Oike, T., Suzuki, Y., Fazreen, Z., Asuncion, B. R., Shabbir, A., Yong, W.-P., So, J., Soong, R., and Kono, K. (2018). PD-L1 expression is mainly regulated by interferon gamma associated with JAK-STAT pathway in gastric cancer. *Cancer science*, 109(1):43–53.

[Mo et al., 2018] Mo, X., Zhang, H., Preston, S., Martin, K., Zhou, B., Vadalia, N., Gamero, A. M., Soboloff, J., Tempera, I., and Zaidi, M. R. (2018). Interferon-γ signaling in melanocytes and melanoma cells regulates expression of CTLA-4. *Cancer Research*, 78(2):436–450.

[Moon et al., 2017] Moon, J. W., Kong, S.-K., Kim, B. S., Kim, H. J., Lim, H., Noh, K., Kim, Y., Choi, J.-W., Lee, J.-H., and Kim, Y.-S. (2017). IFNγ induces PD-L1 overexpression by JAK2/STAT1/IRF-1 signaling in EBV-positive gastric carcinoma. *Scientific Reports*, 7(1):17810.

[Morgado et al., 2016] Morgado, M., Sutton, M. N., Simmons, M., Warren, C. R., Lu, Z., Constantinou, P. E., Liu, J., Francis, L. L., Steven Conlan, R., Bast, R. C., and Carson, D. D. (2016). Tumor necrosis factor-α and Interferon-γ stimulate MUC16 (CA125) expression in breast, endometrial and ovarian cancers through NFκB. *Oncotarget*, 7(12):14871–14884.

[Mould et al., 2015] Mould, A. W., Morgan, M. A., Nelson, A. C., Bikoff, E. K., and Robertson, E. J. (2015). Blimp1/Prdm1 Functions in Opposition to Irf1 to Maintain Neonatal Tolerance during Postnatal Intestinal Maturation. *PLoS Genetics*, 11(7).

[Mu et al., 2018] Mu, L., Long, Y., Yang, C., Jin, L., Tao, H., Ge, H., Chang, Y. E., Karachi, A., Kubilis, P. S., De Leon, G., Qi, J., Sayour, E. J., Mitchell, D. A., Lin, Z., and Huang, J. (2018). The IDH1 mutation-induced oncometabolite, 2-hydroxyglutarate, may affect DNA methylation and expression of PD-L1 in gliomas. *Frontiers in Molecular Neuroscience*, 11(82).

[Mullard, 2020] Mullard, A. (2020). FDA approves an inhibitor of a novel 'epigenetic writer'.

[Muro et al., 2016] Muro, K., Chung, H. C., Shankaran, V., Geva, R., Catenacci, D., Gupta, S., Eder, J. P., Golan, T., Le, D. T., Burtness, B., McRee, A. J., Lin, C. C., Pathiraja, K., Lunceford, J., Emancipator, K., Juco, J., Koshiji, M., and Bang, Y. J. (2016). Pembrolizumab for patients with PD-L1-positive advanced gastric cancer (KEYNOTE-012): a multicentre, open-label, phase 1b trial. *The Lancet Oncology*, 17(6):717–726.

[Murray et al., 2019] Murray, S., Lorenz, P., Howe, F., Wouters, M., Brown, T., Xi, S., Fischl, H., Khushaim, W., Rayappu, J. R., Angel, A., and Mellor, J. (2019). H3K4me3 is neither instructive for, nor informed by, transcription. *bioRxiv*, page 709014.

[Nakanishi et al., 2007] Nakanishi, J., Wada, Y., Matsumoto, K., Azuma, M., Kikuchi, K., and Ueda, S. (2007). Overexpression of B7-H1 (PD-L1) significantly associates with tumor grade and postoperative prognosis in human urothelial cancers. *Cancer Immunology, Immunotherapy*, 56(8):1173–1182.

[Nanni et al., 2020] Nanni, L., Ceri, S., and Logie, C. (2020). Spatial patterns of CTCF sites define the anatomy of TADs and their boundaries. *Genome Biology*, 21(1):197.

[Ni et al., 2008] Ni, Z., Hassan, M. A. E., Xu, Z., Yu, T., and Bremner, R. (2008). The chromatin-remodeling enzyme BRG1 coordinates CIITA induction through many interdependent distal enhancers. *Nature Immunology*, 9(7):785–793.

[Nishimura et al., 1999] Nishimura, H., Nose, M., Hiai, H., Minato, N., Honjo, T., Melet, F., Bernstein, A., Law, C., Clark, E., and Shokat, K. (1999). Development of lupus-like autoimmune diseases by disruption of the PD-1 gene encoding an ITIM motif-carrying immunoreceptor. *Immunity*, 11(2):141–51.

[Nishimura et al., 2001] Nishimura, H., Okazaki, T., Tanaka, Y., Nakatani, K., Hara, M., Matsumori, A., Sasayama, S., Mizoguchi, A., Hiai, H., Minato, N., and Honjo, T. (2001). Autoimmune dilated cardiomyopathy in PD-1 receptor-deficient mice. *Science (New York, N.Y.)*, 291(5502):319–322.

[Noguchi et al., 2017] Noguchi, T., Ward, J. P., Gubin, M. M., Arthur, C. D., Lee, S. H., Hundal, J., Selby, M. J., Graziano, R. F., Mardis, E. R., Korman, A. J., and Schreiber, R. D. (2017). Temporally distinct PD-L1 expression by tumor and host cells contributes to immune escape. *Cancer Immunology Research*, 5(2):106–117.

[Noman et al., 2014] Noman, M. Z., Desantis, G., Janji, B., Hasmim, M., Karray, S., Dessen, P., Bronte, V., and Chouaib, S. (2014). PD-L1 is a novel direct target of HIF-1α, and its blockade under hypoxia enhanced: MDSC-mediated T cell activation. *Journal of Experimental Medicine*, 211(5):781–790.

[Nomi et al., 2007] Nomi, T., Sho, M., Akahori, T., Hamada, K., Kubo, A., Kanehiro, H., Nakamura, S., Enomoto, K., Yagita, H., Azuma, M., and Nakajima, Y. (2007). Clinical significance and therapeutic potential of the programmed death-1 ligand/programmed death-1 pathway in human pancreatic cancer. *Clinical Cancer Research*, 13(7):2151–2157.

[Okazaki et al., 2001] Okazaki, T., Maeda, A., Nishimura, H., Kurosaki, T., and Honjo, T. (2001). PD-1 immunoreceptor inhibits B cell receptor-mediated signaling by recruiting src homology 2-domain-containing tyrosine phosphatase 2 to phosphotyrosine. *Proceedings of the National Academy of Sciences of the United States of America*, 98(24):13866–13871.

[O'Neil et al., 2017] O'Neil, B. H., Wallmark, J. M., Lorente, D., Elez, E., Raimbourg, J., Gomez-Roca, C., Ejadi, S., Piha-Paul, S. A., Stein, M. N., Abdul Razak, A. R., Dotti, K., Santoro, A., Cohen, R. B., Gould, M., Saraf, S., Stein, K., and Han, S.-W. (2017). Safety and antitumor activity of the anti–PD-1 antibody pembrolizumab in patients with advanced colorectal carcinoma. *PLOS ONE*, 12(12):e0189848.

[Ostuni et al., 2013] Ostuni, R., Piccolo, V., Barozzi, I., Polletti, S., Termanini, A., Bonifacio, S., Curina, A., Prosperini, E., Ghisletti, S., and Natoli, G. (2013). Latent enhancers activated by stimulation in differentiated cells. *Cell*, 152(1-2):157–171.

[O'Sullivan et al., 2004] O'Sullivan, J. M., Tan-Wong, S. M., Morillon, A., Lee, B., Coles, J., Mellor, J., and Proudfoot, N. J. (2004). Gene loops juxtapose promoters and terminators in yeast. *Nature Genetics*, 36(9):1014–1018.

[Overacre-Delgoffe et al., 2017] Overacre-Delgoffe, A. E., Chikina, M., Dadey, R. E., Yano, H., Brunazzi, E. A., Shayan, G., Horne, W., Moskovitz, J. M., Kolls, J. K., Sander, C., Shuai, Y., Normolle, D. P., Kirkwood, J. M., Ferris, R. L., Delgoffe, G. M., Bruno, T. C., Workman, C. J., and Vignali, D. A. (2017). Interferon-γ Drives Treg Fragility to Promote Anti-tumor Immunity. *Cell*, 169(6):1130–1141.e11.

[Pak-Wittel et al., 2013] Pak-Wittel, M. A., Yang, L., Sojka, D. K., Rivenbark, J. G., and Yokoyama, W. M. (2013). Interferon-γ mediates chemokine-dependent recruitment of natural killer cells during viral infection. *Proceedings of the National Academy of Sciences of the United States of America*, 110(1):E50.

[Park et al., 2010] Park, J. J., Omiya, R., Matsumura, Y., Sakoda, Y., Kuramasu, A., Augustine, M. M., Yao, S., Tsushima, F., Narazaki, H., Anand, S., Liu, Y., Strome, S. E., Chen, L., and Tamada, K. (2010). B7-H1/CD80 interaction is required for the induction and maintenance of peripheral T-cell tolerance. *Blood*, 116(8):1291–1298.

[Parry et al., 2005] Parry, R. V., Chemnitz, J. M., Frauwirth, K. A., Lanfranco, A. R., Braunstein, I., Kobayashi, S. V., Linsley, P. S., Thompson, C. B., and Riley, J. L. (2005). CTLA-4 and PD-1 Receptors Inhibit T-Cell Activation by Distinct Mechanisms. *Molecular and Cellular Biology*, 25(21):9543–9553.

[Parsa et al., 2007] Parsa, A. T., Waldron, J. S., Panner, A., Crane, C. A., Parney, I. F., Barry, J. J., Cachola, K. E., Murray, J. C., Tihan, T., Jensen, M. C., Mischel, P. S., Stokoe, D., and Pieper, R. O. (2007). Loss of tumor suppressor PTEN function increases B7-H1 expression and immunoresistance in glioma. *Nature Medicine*, 13(1):84–88.

[Patel et al., 2017] Patel, S. J., Sanjana, N. E., Kishton, R. J., Eidizadeh, A., Vodnala, S. K., Cam, M., Gartner, J. J., Jia, L., Steinberg, S. M., Yamamoto, T. N., Merchant, A. S., Mehta, G. U., Chichura, A., Shalem, O., Tran, E., Eil, R., Sukumar, M., Guijarro, E. P., Day, C. P., Robbins, P., Feldman, S., Merlino, G., Zhang, F., and Restifo, N. P. (2017). Identification of essential genes for cancer immunotherapy. *Nature*, 548(7669):537–542.

[Patsoukis et al., 2012] Patsoukis, N., Brown, J., Petkova, V., Liu, F., Li, L., and Boussiotis, V. A. (2012). Selective effects of PD-1 on Akt and ras pathways regulate molecular components of the cell cycle and inhibit T cell proliferation. *Science Signaling*, 5(230).

[Pentcheva-Hoang et al., 2007] Pentcheva-Hoang, T., Chen, L., Pardoll, D. M., and Allison, J. P. (2007). Programmed death-1 concentration at the immunological synapse is determined by ligand affinity and availability. *Proceedings of the National Academy of Sciences of the United States of America*, 104(45):17765–17770.

[Pfeffer, 2011] Pfeffer, L. M. (2011). The role of nuclear factor κb in the interferon response.

[Phillips-Cremins and Corces, 2013] Phillips-Cremins, J. E. and Corces, V. G. (2013). Chromatin Insulators: Linking Genome Organization to Cellular Function.

[Phillips-Cremins et al., 2013] Phillips-Cremins, J. E., Sauria, M. E., Sanyal, A., Gerasimova, T. I., Lajoie, B. R., Bell, J. S., Ong, C. T., Hookway, T. A., Guo, C., Sun, Y., Bland, M. J., Wagstaff, W., Dalton, S., McDevitt, T. C., Sen, R., Dekker, J., Taylor, J., and Corces, V. G. (2013). Architectural protein subclasses shape 3D organization of genomes during lineage commitment. *Cell*, 153(6):1281–1295.

[Piccolo et al., 2017] Piccolo, V., Curina, A., Genua, M., Ghisletti, S., Simonatto, M., Sabò, A., Amati, B., Ostuni, R., and Natoli, G. (2017). Opposing macrophage polarization programs show extensive epigenomic and transcriptional cross-talk. *Nature Immunology*, 18(5):530–540.

[Pitroda et al., 2018] Pitroda, S. P., Stack, M. E., Liu, G.-F., Song, S.-S., Chen, L., Liang, H., Parekh, A. D., Huang, X., Roach, P., Posner, M. C., Weichselbaum, R. R., and Khodarev, N. N. (2018). JAK2 Inhibitor SAR302503 Abrogates PD-L1 Expression and Targets Therapy-Resistant Non–small Cell Lung Cancers. *Molecular Cancer Therapeutics*, 17(4):732–739.

[Plaschka et al., 2015] Plaschka, C., Larivière, L., Wenzeck, L., Seizl, M., Hemann, M., Tegunov, D., Petrotchenko, E. V., Borchers, C. H., Baumeister, W., Herzog, F., Villa, E., and Cramer, P. (2015). Architecture of the RNA polymerase II-Mediator core initiation complex. *Nature*, 518(7539):376–380.

[Platanias, 2005] Platanias, L. C. (2005). Mechanisms of type-I- and type-II-interferon-mediated signalling. *Nature Reviews Immunology*, 5(5):375–386.

[Pnueli et al., 2015] Pnueli, L., Rudnizky, S., Yosefzon, Y., and Melamed, P. (2015). RNA transcribed from a distal enhancer is required for activating the chromatin at the promoter of the gonadotropin α-subunit gene. *Proceedings of the National Academy of Sciences*, 112(14):4369–4374.

[Porrua and Libri, 2015] Porrua, O. and Libri, D. (2015). Transcription termination and the control of the transcriptome: Why, where and how to stop.

[Pradeepa et al., 2016] Pradeepa, M. M., Grimes, G. R., Kumar, Y., Olley, G., Taylor, G. C., Schneider, R., and Bickmore, W. A. (2016). Histone H3 globular domain acetylation identifies a new class of enhancers. *Nature Genetics*, 48(6):681–686.

[Prendergast, 2008] Prendergast, G. C. (2008). Immune escape as a fundamental trait of cancer: Focus on IDO.

[Pugh and Tjian, 1991] Pugh, B. F. and Tjian, R. (1991). Transcription from a TATA-less promoter requires a multisubunit TFIID complex. *Genes and Development*, 5(11):1935–1945.

[Qiao et al., 2013] Qiao, Y., Giannopoulou, E. G., Chan, C. H., ho Park, S., Gong, S., Chen, J., Hu, X., Elemento, O., and Ivashkiv, L. B. (2013). Synergistic activation of inflammatory cytokine genes by interferon-γ-induced chromatin remodeling and toll-like receptor signaling. *Immunity*, 39(3):454–469.

[Qiao et al., 2016] Qiao, Y., Kang, K., Giannopoulou, E., Fang, C., and Ivashkiv, L. B. (2016). IFN-γ Induces Histone 3 Lysine 27 Trimethylation in a Small Subset of Promoters to Stably Silence Gene Expression in Human Macrophages. *Cell Reports*, 16(12):3121–3129.

[Qin et al., 2019] Qin, W., Hu, L., Zhang, X., Jiang, S., Li, J., Zhang, Z., and Wang, X. (2019). The Diverse Function of PD-1/PD-L Pathway Beyond Cancer.

[Quinlan and Hall, 2010] Quinlan, A. R. and Hall, I. M. (2010). BEDTools: A flexible suite of utilities for comparing genomic features. *Bioinformatics*, 26(6):841–842.

[Rahnamoun et al., 2018] Rahnamoun, H., Lee, J., Sun, Z., Lu, H., Ramsey, K. M., Komives, E. A., and Lauberth, S. M. (2018). RNAs interact with BRD4 to promote enhanced chromatin engagement and transcription activation. *Nature Structural & Molecular Biology*, 25(8):687–697.

[Ramsauer et al., 2007] Ramsauer, K., Farlik, M., Zupkovitz, G., Seiser, C., Kröger, A., Hauser, H., and Decker, T. (2007). Distinct modes of action applied by transcription factors STAT1 and IRF1 to initiate transcription of the IFN-γ-inducible gbp2 gene. *Proceedings of the National Academy of Sciences of the United States of America*, 104(8):2849–2854.

[Rao et al., 2014] Rao, S. S., Huntley, M. H., Durand, N. C., Stamenova, E. K., Bochkov, I. D., Robinson, J. T., Sanborn, A. L., Machol, I., Omer, A. D., Lander, E. S., and Aiden, E. L. (2014). A 3D map of the human genome at kilobase resolution reveals principles of chromatin looping. *Cell*, 159(7):1665–1680.

[Relation et al., 2018] Relation, T., Yi, T., Guess, A. J., La Perle, K., Otsuru, S., Hasgur, S., Dominici, M., Breuer, C., and Horwitz, E. M. (2018). Intratumoral Delivery of Interferonγ-Secreting Mesenchymal Stromal Cells Repolarizes Tumor-Associated Macrophages and Suppresses Neuroblastoma Proliferation In Vivo. *STEM CELLS*, 36(6):915–924.

[Ren et al., 2017] Ren, G., Jin, W., Cui, K., Rodrigez, J., Hu, G., Zhang, Z., Larson, D. R., and Zhao, K. (2017). CTCF-Mediated Enhancer-Promoter Interaction Is a Critical Regulator of Cell-to-Cell Variation of Gene Expression. *Molecular Cell*, 67(6):1049–1058.e6.

[Robert et al., 2015] Robert, C., Schachter, J., Long, G. V., Arance, A., Grob, J. J., Mortier, L., Daud, A., Carlino, M. S., McNeil, C., Lotem, M., Larkin, J., Lorigan, P., Neyns, B., Blank, C. U., Hamid, O., Mateus, C., Shapira-Frommer, R., Kosh, M., Zhou, H., Ibrahim, N., Ebbinghaus, S., and Ribas, A. (2015). Pembrolizumab versus Ipilimumab in Advanced Melanoma. *New England Journal of Medicine*, 372(26):2521–2532.

[Roemer et al., 2016] Roemer, M. G., Advani, R. H., Ligon, A. H., Natkunam, Y., Redd, R. A., Homer, H., Connelly, C. F., Sun, H. H., Daadi, S. E., Freeman, G. J., Armand, P., Chapuy, B., De Jong, D., Hoppe, R. T., Neuberg, D. S., Rodig, S. J., and Shipp, M. A. (2016). PD-L1 and PD-L2 genetic alterations define classical hodgkin lymphoma and predict outcome. *Journal of Clinical Oncology*, 34(23):2690–2697.

[Rosenwald et al., 2003] Rosenwald, A., Wright, G., Leroy, K., Yu, X., Gaulard, P., Gascoyne, R. D., Chan, W. C., Zhao, T., Haioun, C., Greiner, T. C., Weisenburger, D. D., Lynch, J. C., Vose, J., Armitage, J. O., Smeland, E. B., Kvaloy, S., Holte, H., Delabie, J., Campo, E., Montserrat, E., Lopez-Guillermo, A., Ott, G., Muller-Hermelink, H. K., Connors, J. M., Braziel, R., Grogan, T. M., Fisher, R. I., Miller, T. P., LeBlanc, M., Chiorazzi, M., Zhao, H., Yang, L., Powell, J., Wilson, W. H., Jaffe, E. S., Simon, R., Klausner, R. D., and Staudt, L. M. (2003). Molecular diagnosis of primary mediastinal B cell lymphoma identifies a clinically favorable subgroup of diffuse large B cell lymphoma related to Hodgkin lymphoma. *Journal of Experimental Medicine*, 198(6):851–862.

[Rubin et al., 2017] Rubin, A. J., Barajas, B. C., Furlan-Magaril, M., Lopez-Pajares, V., Mumbach, M. R., Howard, I., Kim, D. S., Boxer, L. D., Cairns, J., Spivakov, M., Wingett, S. W., Shi, M., Zhao, Z., Greenleaf, W. J., Kundaje, A., Snyder, M., Chang, H. Y., Fraser, P., and Khavari, P. A. (2017). Lineage-specific dynamic and pre-established enhancer-promoter contacts cooperate in terminal differentiation. *Nature Genetics*, 49(10):1522–1528.

[Rüegg et al., 1998] Rüegg, C., Yilmaz, A., Bieler, G., Bamat, J., Chaubert, P., and Lejeune, F. J. (1998). Evidence for the involvement of endothelial cell integrin $\alpha V\beta 3$ in the disruption of the tumor vasculature induced by TNF and IFN-γ. *Nature Medicine*, 4(4):408–414.

[Sainsbury et al., 2015] Sainsbury, S., Bernecky, C., and Cramer, P. (2015). Structural basis of transcription initiation by RNA polymerase II.

[Sakabe et al., 2012] Sakabe, N. J., Savic, D., and Nobrega, M. A. (2012). Transcriptional enhancers in development and disease.

[Samson et al., 2018] Samson, A., Scott, K. J., Taggart, D., West, E. J., Wilson, E., Nuovo, G. J., Thomson, S., Corns, R., Mathew, R. K., Fuller, M. J., Kottke, T. J., Thompson, J. M., Ilett, E. J., Cockle, J. V., van Hille, P., Sivakumar, G., Polson, E. S., Turnbull, S. J., Appleton, E. S., Migneco, G., Rose, A. S., Coffey, M. C., Beirne, D. A., Collinson, F. J., Ralph, C., Alan Anthoney, D., Twelves, C. J., Furness, A. J., Quezada, S. A., Wurdak, H., Errington-Mais, F., Pandha, H., Harrington, K. J., Selby, P. J., Vile, R. G., Griffin, S. D., Stead, L. F., Short, S. C., and Melcher, A. A. (2018). Intravenous delivery of oncolytic reovirus to brain tumor patients immunologically primes for subsequent checkpoint blockade. *Science Translational Medicine*, 10(422):eaam7577.

[Sandelin, 2004] Sandelin, A. (2004). JASPAR: an open-access database for eukaryotic transcription factor binding profiles. *Nucleic Acids Research*, 32(90001):91D–94.

[Santos-Rosa et al., 2002] Santos-Rosa, H., Schneider, R., Bannister, A. J., Sherriff, J., Bernstein, B. E., Emre, N. C., Schreiber, S. L., Mellor, J., and Kouzarides, T. (2002). Active genes are tri-methylated at K4 of histone H3. *Nature*, 419(6905):407–411.

[Santucci et al., 2015] Santucci, M., Vignudelli, T., Ferrari, S., Mor, M., Scalvini, L., Bolognesi, M. L., Uliassi, E., and Costi, M. P. (2015). The Hippo Pathway and YAP/TAZ-TEAD Protein-Protein Interaction as Targets for Regenerative Medicine and Cancer Treatment.

[Sanyal et al., 2012] Sanyal, A., Lajoie, B. R., Jain, G., and Dekker, J. (2012). The long-range interaction landscape of gene promoters. *Nature*, 489(7414):109–113.

[Savan et al., 2009] Savan, R., Ravichandran, S., Collins, J. R., Sakai, M., and Young, H. A. (2009). Structural conservation of interferon gamma among vertebrates.

[Schaefer et al., 1995] Schaefer, T. S., Sanders, L. K., and Nathans, D. (1995). Cooperative transcriptional activity of Jun and Stat3β, a short form of Stat3. *Proceedings of the National Academy of Sciences of the United States of America*, 92(20):9097–9101.

[Schmidl et al., 2015] Schmidl, C., Rendeiro, A. F., Sheffield, N. C., and Bock, C. (2015). ChIPmentation: fast, robust, low-input ChIP-seq for histones and transcription factors. *Nature methods*, 12(10):963–965.

[Schmittgen and Livak, 2008] Schmittgen, T. D. and Livak, K. J. (2008). Analyzing real-time PCR data by the comparative CT method. *Nature Protocols*, 3(6):1101–1108.

[Schones et al., 2008] Schones, D. E., Cui, K., Cuddapah, S., Roh, T. Y., Barski, A., Wang, Z., Wei, G., and Zhao, K. (2008). Dynamic Regulation of Nucleosome Positioning in the Human Genome. *Cell*, 132(5):887–898.

[Schwalb et al., 2016] Schwalb, B., Michel, M., Zacher, B., Frühauf, K., Demel, C., Tresch, A., Gagneur, J., and Cramer, P. (2016). TT-seq maps the human transient transcriptome. *Science (New York, N.Y.)*, 352(6290):1225–8.

[Senft et al., 2018] Senft, A. D., Costello, I., King, H. W., Mould, A. W., Bikoff, E. K., and Robertson, E. J. (2018). Combinatorial Smad2/3 Activities Downstream of Nodal Signaling Maintain Embryonic/Extra-Embryonic Cell Identities during Lineage Priming. *Cell Reports*, 24(8):1977–1985.e7.

[Shao et al., 2019] Shao, L., Hou, W., Scharping, N. E., Vendetti, F. P., Srivastava, R., Roy, C. N., Menk, A. V., Wang, Y., Chauvin, J.-M., Karukonda, P., Thorne, S. H., Hornung, V., Zarour, H. M., Bakkenist, C. J., Delgoffe, G. M., and Sarkar, S. N. (2019). IRF1 Inhibits Antitumor Immunity through the Upregulation of PD-L1 in the Tumor Cell. *Cancer Immunology Research*, 7(8):1258–1266.

[Sharpe and Pauken, 2018] Sharpe, A. H. and Pauken, K. E. (2018). The diverse functions of the PD1 inhibitory pathway.

[Shen et al., 2019] Shen, X., Zhang, L., Li, J., Li, Y., Wang, Y., and Xu, Z. X. (2019). Recent findings in the regulation of programmed death ligand 1 expression.

[Shibahara et al., 2018] Shibahara, D., Tanaka, K., Iwama, E., Kubo, N., Ota, K., Azuma, K., Harada, T., Fujita, J., Nakanishi, Y., and Okamoto, I. (2018). Intrinsic and Extrinsic Regulation of PD-L2 Expression in Oncogene-Driven Non–Small Cell Lung Cancer. *Journal of Thoracic Oncology*, 13(7):926–937.

[Shime et al., 2017] Shime, H., Maruyama, A., Yoshida, S., Takeda, Y., Matsumoto, M., and Seya, T. (2017). Toll-like receptor 2 ligand and interferon-γ suppress anti-tumor T cell responses by enhancing the immunosuppressive activity of monocytic myeloid-derived suppressor cells. *OncoImmunology*, 7(1).

[Shin et al., 2017] Shin, D. S., Zaretsky, J. M., Escuin-Ordinas, H., Garcia-Diaz, A., Hu-Lieskovan, S., Kalbasi, A., Grasso, C. S., Hugo, W., Sandoval, S., Torrejon, D. Y., Palaskas, N., Rodriguez, G. A., Parisi, G., Azhdam, A., Chmielowski, B., Cherry, G., Seja, E., Berent-Maoz, B., Shintaku, I. P., Le, D. T., Pardoll, D. M., Diaz, L. A., Tumeh, P. C., Graeber, T. G., Lo, R. S., Comin-Anduix, B., and Ribas, A. (2017). Primary Resistance to PD-1 Blockade Mediated by JAK1/2 Mutations. *Cancer Discovery*, 7(2):188–201.

[Silvennoinen et al., 1993] Silvennoinen, O., Ihle, J. N., Schlessinger, J., and Levy, D. E. (1993). Interferon-induced nuclear signalling by Jak protein tyrosine kinases. *Nature*, 366(6455):583–585.

[Simon et al., 2017] Simon, C. S., Downes, D. J., Gosden, M. E., Telenius, J., Higgs, D. R., Hughes, J. R., Costello, I., Bikoff, E. K., and Robertson, E. J. (2017). Functional characterisation of cis-regulatory elements governing dynamic Eomes expression in the early mouse embryo. *Development (Cambridge)*, 144(7):1249–1260.

[Siwek et al., 2020] Siwek, W., Tehrani, S. S., Mata, J. F., and Jansen, L. E. (2020). Activation of Clustered IFNγ Target Genes Drives Cohesin-Controlled Transcriptional Memory. *Molecular Cell*, 80(3):396–409.e6.

[Smale and Baltimore, 1989] Smale, S. T. and Baltimore, D. (1989). The "initiator" as a transcription control element. *Cell*, 57(1):103–13.

[Song et al., 2013] Song, M., Chen, D., Lu, B., Wang, C., Zhang, J., Huang, L., Wang, X., Timmons, C. L., Hu, J., Liu, B., Wu, X., Wang, L., Wang, J., and Liu, H. (2013). PTEN Loss Increases PD-L1 Protein Expression and Affects the Correlation between PD-L1 Expression and Clinical Parameters in Colorectal Cancer. *PLoS ONE*, 8(6):e65821.

[Song et al., 2011] Song, M.-Y., Park, S.-H., Nam, H. J., Choi, D.-H., and Sung, Y.-C. (2011). Enhancement of Vaccine-induced Primary and Memory CD8+ T-cell Responses by Soluble PD-1. *Journal of Immunotherapy*, 34(3):297–306.

[Steidl et al., 2011] Steidl, C., Shah, S. P., Woolcock, B. W., Rui, L., Kawahara, M., Farinha, P., Johnson, N. A., Zhao, Y., Telenius, A., Neriah, S. B., McPherson, A., Meissner, B., Okoye, U. C., Diepstra, A., Van Den Berg, A., Sun, M., Leung, G., Jones, S. J., Connors, J. M., Huntsman, D. G., Savage, K. J., Rimsza, L. M., Horsman, D. E., Staudt, L. M., Steidl, U., Marra, M. A., and Gascoyne, R. D. (2011). MHC class II transactivator CIITA is a recurrent gene fusion partner in lymphoid cancers. *Nature*, 471(7338):377–383.

[Street et al., 1997] Street, D., Kaufmann, A. M., Vaughan, A., Fisher, S. G., Hunter, M., Schreckenberger, C., Potkul, R. K., Gissmann, L., and Qiao, L. (1997). Interferon-γ enhances susceptibility of cervical cancer cells to lysis by tumor-specific cytotoxic T cells. *Gynecologic Oncology*, 65(2):265–272.

[Strome et al., 2003] Strome, S. E., Dong, H., Tamura, H., Voss, S. G., Flies, D. B., Tamada, K., Salomao, D., Cheville, J., Hirano, F., Lin, W., Kasperbauer, J. L., Ballman, K. V., and Chen, L. (2003). B7-H1 blockade augments adoptive T-cell immunotherapy for squamous cell carcinoma. *Cancer research*, 63(19):6501–5.

[Sumimoto et al., 2016] Sumimoto, H., Takano, A., Teramoto, K., and Daigo, Y. (2016). RAS-mitogen-activated protein kinase signal is required for enhanced PD-L1 expression in human lung cancers. *PLoS ONE*, 11(11).

[Sunshine and Taube, 2015] Sunshine, J. and Taube, J. M. (2015). PD-1/PD-L1 inhibitors. *Current opinion in pharmacology*, 23:32–8.

[Szabo et al., 2019] Szabo, Q., Bantignies, F., and Cavalli, G. (2019). Principles of genome folding into topologically associating domains.

[Takeda et al., 2017] Takeda, K., Nakayama, M., Hayakawa, Y., Kojima, Y., Ikeda, H., Imai, N., Ogasawara, K., Okumura, K., Thomas, D. M., and Smyth, M. J. (2017). IFN-γ is required for cytotoxic T cell-dependent cancer genome immunoediting. *Nature Communications*, 8(14607).

[Tang et al., 2020] Tang, F., Yang, Z., Tan, Y., and Li, Y. (2020). Super-enhancer function and its application in cancer targeted therapy. *npj Precision Oncology*, 4(1):2.

[Tang et al., 2018] Tang, H., Liang, Y., Anders, R. A., Taube, J. M., Qiu, X., Mulgaonkar, A., Liu, X., Harrington, S. M., Guo, J., Xin, Y., Xiong, Y., Nham, K., Silvers, W., Hao, G., Sun, X., Chen, M., Hannan, R., Qiao, J., Dong, H., Peng, H., and Fu, Y. X. (2018). PD-L1 on host cells is essential for PD-L1 blockade–mediated tumor regression. *Journal of Clinical Investigation*, 128(2):580–588.

[Tao et al., 2017] Tao, L. H., Zhou, X. R., Li, F. C., Chen, Q., Meng, F. Y., Mao, Y., Li, R., Hua, D., Zhang, H. J., Wang, W. P., and Chen, W. C. (2017). A polymorphism in the promoter region of PD-L1 serves as a binding-site for SP1 and is associated with PD-L1 overexpression and increased occurrence of gastric cancer. *Cancer Immunology, Immunotherapy*, 66(3):309–318.

[Taube et al., 2012] Taube, J. M., Anders, R. A., Young, G. D., Xu, H., Sharma, R., McMiller, T. L., Chen, S., Klein, A. P., Pardoll, D. M., Topalian, S. L., and Chen, L. (2012). Colocalization of inflammatory response with B7-H1 expression in human melanocytic lesions supports an adaptive resistance mechanism of immune escape. *Science Translational Medicine*, 4(127):127ra37.

[Taube et al., 2018] Taube, J. M., Galon, J., Sholl, L. M., Rodig, S. J., Cottrell, T. R., Giraldo, N. A., Baras, A. S., Patel, S. S., Anders, R. A., Rimm, D. L., and Cimino-Mathews, A. (2018). Implications of the tumor immune microenvironment for staging and therapeutics. *Modern Pathology*, 31(2):214–234.

[Telenius et al., 2020] Telenius, J. M., Downes, D., Sergeant, M., Oudelaar, A. M., McGowan, S., Kerry, J., Hanssen, L. L. P., Schwessinger, R., Eijsbouts, C. Q., Davies, J. O. J., Taylor, S., and Hughes, J. R. (2020). CaptureCompendium: a comprehensive toolkit for 3C analysis. *bioRxiv*, page 2020.02.17.952572.

[Terracina et al., 2016] Terracina, K. P., Graham, L. J., Payne, K. K., Manjili, M. H., Baek, A., Damle, S. R., and Bear, H. D. (2016). DNA methyltransferase inhibition increases efficacy of adoptive cellular immunotherapy of murine breast cancer. *Cancer Immunology, Immunotherapy*, 65(9):1061–1073.

[Terzi et al., 2011] Terzi, N., Churchman, L. S., Vasiljeva, L., Weissman, J., and Buratowski, S. (2011). H3K4 Trimethylation by Set1 Promotes Efficient Termination by the Nrd1-Nab3-Sen1 Pathway. *Molecular and Cellular Biology*, 31(17):3569–3583.

[Thapa et al., 2011] Thapa, R. J., Basagoudanavar, S. H., Nogusa, S., Irrinki, K., Mallilankaraman, K., Slifker, M. J., Beg, A. A., Madesh, M., and Balachandran, S. (2011). NF-kappaB Protects Cells from Gamma Interferon-Induced RIP1-Dependent Necroptosis. *Molecular and Cellular Biology*, 31(14):2934–2946.

[Thurman et al., 2012] Thurman, R. E., Rynes, E., Humbert, R., Vierstra, J., Maurano, M. T., Haugen, E., Sheffield, N. C., Stergachis, A. B., Wang, H., Vernot, B., Garg, K., John, S., Sandstrom, R., Bates, D., Boatman, L., Canfield, T. K., Diegel, M., Dunn, D., Ebersol, A. K., Frum, T., Giste, E., Johnson, A. K., Johnson, E. M., Kutyavin, T., Lajoie, B., Lee, B. K., Lee, K., London, D., Lotakis, D., Neph, S., Neri, F., Nguyen, E. D., Qu, H., Reynolds, A. P., Roach, V., Safi, A., Sanchez, M. E., Sanyal, A., Shafer, A., Simon, J. M., Song, L., Vong, S., Weaver, M., Yan, Y., Zhang, Z., Zhang, Z., Lenhard, B., Tewari, M., Dorschner, M. O., Hansen, R. S., Navas, P. A., Stamatoyannopoulos, G., Iyer, V. R., Lieb, J. D., Sunyaev, S. R., Akey, J. M., Sabo, P. J., Kaul, R., Furey, T. S., Dekker, J., Crawford, G. E., and Stamatoyannopoulos, J. A. (2012). The accessible chromatin landscape of the human genome. *Nature*, 489(7414):75–82.

[Tsao et al., 2017] Tsao, M.-S., Le Teuff, G., Shepherd, F., Landais, C., Hainaut, P., Filipits, M., Pirker, R., Le Chevalier, T., Graziano, S., Kratze, R., Soria, J.-C., Pignon, J.-P., Seymour, L., and Brambilla, E. (2017). PD-L1 protein expression assessed by immunohistochemistry is neither prognostic nor predictive of benefit from adjuvant chemotherapy in resected non-small cell lung cancer. *Annals of Oncology*, 28(4):882–889.

[Tsuda et al., 2005] Tsuda, M., Matsumoto, K., Inoue, H., Matsumura, M., Nakano, T., Mori, A., Azuma, M., and Nakanishi, Y. (2005). Expression of B7-H1 and B7-DC on the airway epithelium is enhanced by double-stranded RNA. *Biochemical and Biophysical Research Communications*, 330(1):263–270.

[Twa et al., 2014] Twa, D. D., Chan, F. C., Ben-Neriah, S., Woolcock, B. W., Mottok, A., Tan, K. L., Slack, G. W., Gunawardana, J., Lim, R. S., McPherson, A. W., Kridel, R., Telenius, A., Scott, D. W., Savage, K. J., Shah, S. P., Gascoyne, R. D., and Steidl, C. (2014). Genomic rearrangements involving programmed death ligands are recurrent in primary mediastinal large B-cell lymphoma. *Blood*, 123(13):2062–2065.

[Tyssowski et al., 2018] Tyssowski, K. M., DeStefino, N. R., Cho, J. H., Dunn, C. J., Poston, R. G., Carty, C. E., Jones, R. D., Chang, S. M., Romeo, P., Wurzelmann, M. K., Ward, J. M., Andermann, M. L., Saha, R. N., Dudek, S. M., and Gray, J. M. (2018). Different Neuronal Activity Patterns Induce Different Gene Expression Programs. *Neuron*, 98(3):530–546.e11.

[Unterer et al., 2018] Unterer, B., Wiesmann, V., Gunasekaran, M., Sticht, H., Tenkerian, C., Behrens, J., Leone, M., Engel, F. B., Britzen-Laurent, N., Naschberger, E., Wittenberg, T., and Stürzl, M. (2018). IFN-γ-response mediator GBP-1 represses human cell proliferation by inhibiting the Hippo signaling transcription factor TEAD. *Biochemical Journal*, 475(18):2955–2967.

[Viéitez et al., 2020] Viéitez, C., Martínez-Cebrián, G., Solé, C., Böttcher, R., Potel, C. M., Savitski, M. M., Onnebo, S., Fabregat, M., Shilatifard, A., Posas, F., and de Nadal, E. (2020). A genetic analysis reveals novel histone residues required for transcriptional reprogramming upon stress. *Nucleic acids research*, 48(7):3455–3475.

[Vivarelli et al., 2021] Vivarelli, S., Falzone, L., Torino, F., Scandurra, G., Russo, G., Bordonaro, R., Pappalardo, F., Spandidos, D. A., Raciti, G., and Libra, M. (2021). Immune-checkpoint inhibitors from cancer to COVID-19: A promising avenue for the treatment of patients with COVID-19 (Review).

[Waldmann and Schneider, 2013] Waldmann, T. and Schneider, R. (2013). Targeting histone modifications - epigenetics in cancer.

[Wang et al., 2013] Wang, F. Q., Chen, G., Zhu, J. Y., Zhang, W., Ren, J. G., Liu, H., Sun, Z. J., Jia, J., and Zhao, Y. F. (2013). M2-polarised macrophages in infantile haemangiomas: Correlation with promoted angiogenesis. *Journal of Clinical Pathology*, 66(12):1058–1064.

[Wang et al., 2020] Wang, H., Fu, C., Du, J., Wang, H., He, R., Yin, X., Li, H., Li, X., Wang, H., Li, K., Zheng, L., Liu, Z., and Qiu, Y. (2020). Enhanced histone H3 acetylation of the PD-L1 promoter via the COP1/c-Jun/HDAC3 axis is required for PD-L1 expression in drug-resistant cancer cells. *Journal of experimental & clinical cancer research : CR*, 39(1):29.

[Wang et al., 2017a] Wang, H., Yao, H., Li, C., Liang, L., Zhang, Y., Shi, H., Zhou, C., Chen, Y., Fang, J.-Y., and Xu, J. (2017a). PD-L2 expression in colorectal cancer: Independent prognostic effect and targetability by deglycosylation. *OncoImmunology*, 6(7):e1327494.

[Wang et al., 2015] Wang, L., Wang, H., Chen, H., Wang, W. D., Chen, X. Q., Geng, Q. R., Xia, Z. J., and Lu, Y. (2015). Serum levels of soluble programmed death ligand 1 predict treatment response and progression free survival in multiple myeloma. *Oncotarget*, 6(38):41228–41236.

[Wang et al., 2017b] Wang, L.-L., Li, Z.-H., Hu, X.-H., Muyayalo, K. P., Zhang, Y.-H., and Liao, A.-H. (2017b). The roles of the PD-1/PD-L1 pathway at immunologically privileged sites. *American Journal of Reproductive Immunology*, 78(2):e12710.

[Wang et al., 2017c] Wang, P.-F., Chen, Y., Song, S.-Y., Wang, T.-J., Ji, W.-J., Li, S.-W., Liu, N., and Yan, C.-X. (2017c). Immune-Related Adverse Events Associated with Anti-PD-1/PD-L1 Treatment for Malignancies: A Meta-Analysis. *Frontiers in pharmacology*, 8:730.

[Wang et al., 2017d] Wang, Q., Lin, W., Tang, X., Li, S., Guo, L., Lin, Y., and Kwok, H. F. (2017d). The roles of microRNAs in regulating the expression of PD-1/PD-l1 immune checkpoint.

[Wang et al., 2018a] Wang, Q. S., Shen, S. Q., Sun, H. W., Xing, Z. X., and Yang, H. L. (2018a). Interferon-gamma induces autophagy-associated apoptosis through induction of cPLA2-dependent mitochondrial ROS generation in colorectal cancer cells. *Biochemical and Biophysical Research Communications*, 498(4):1058–1065.

[Wang et al., 2012] Wang, W., Sun, J., Li, F., Li, R., Gu, Y., Liu, C., Yang, P., Zhu, M., Chen, L., Tian, W., Zhou, H., Mao, Y., Zhang, L., Jiang, J., Wu, C., Hua, D., Chen, W., Lu, B., Ju, J., and Zhang, X. (2012). A frequent somatic mutation in CD274 3'-UTR leads to protein over-expression in gastric cancer by disrupting miR-570 binding. *Human Mutation*, 33(3):480–484.

[Wang et al., 2017e] Wang, X., Yang, L., Huang, F., Zhang, Q., Liu, S., Ma, L., and You, Z. (2017e). Inflammatory cytokines IL-17 and TNF-α up-regulate PD-L1 expression in human prostate and colon cancer cells. *Immunology Letters*, 184:7–14.

[Wang et al., 2018b] Wang, Y. F., Liu, F., Sherwin, S., Farrelly, M., Yan, X. G., Croft, A., Liu, T., Jin, L., Zhang, X. D., and Jiang, C. C. (2018b). Cooperativity of HOXA5 and STAT3 Is Critical for HDAC8 Inhibition-Mediated Transcriptional Activation of PD-L1 in Human Melanoma Cells. *Journal of Investigative Dermatology*, 138(4):922–932.

[Wang et al., 2006] Wang, Z., Hong, J., Sun, W., Xu, G., Li, N., Chen, X., Liu, A., Xu, L., Sun, B., and Zhang, J. Z. (2006). Role of IFN-γ in induction of Foxp3 and conversion of CD4 +CD25- T cells to CD4+ Tregs. *Journal of Clinical Investigation*, 116(9):2434–2441.

[Wang et al., 2008] Wang, Z., Zang, C., Rosenfeld, J. A., Schones, D. E., Barski, A., Cuddapah, S., Cui, K., Roh, T. Y., Peng, W., Zhang, M. Q., and Zhao, K. (2008). Combinatorial patterns of histone acetylations and methylations in the human genome. *Nature Genetics*, 40(7):897–903.

[Wen et al., 1995] Wen, Z., Zhong, Z., and Darnell, J. E. (1995). Maximal activation of transcription by statl and stat3 requires both tyrosine and serine phosphorylation. *Cell*, 82(2):241–250.

[Wickham, 2016] Wickham, H. (2016). ggplot2: Elegant Graphics for Data Analysis.

[Windbichler et al., 2000] Windbichler, G. H., Hausmaninger, H., Stummvoll, W., Graf, A. H., Kainz, C., Lahodny, J., Denison, U., Müller-Holzner, E., and Marth, C. (2000). Interferon-gamma in the first-line therapy of ovarian cancer: A randomized phase III trial. *British Journal of Cancer*, 82(6):1138–1144.

[Wintterle et al., 2003] Wintterle, S., Schreiner, B., Mitsdoerffer, M., Schneider, D., Chen, L., Meyermann, R., Weller, M., and Wiendl, H. (2003). Expression of the B7-Related Molecule B7-H1 by Glioma Cells: A Potential Mechanism of Immune Paralysis. *Cancer Research*, 63(21):7462–7467.

[Wong et al., 2014] Wong, K. H., Jin, Y., and Struhl, K. (2014). TFIIH Phosphorylation of the Pol II CTD Stimulates Mediator Dissociation from the Preinitiation Complex and Promoter Escape. *Molecular Cell*, 54(4):601–612.

[Woods et al., 2015] Woods, D. M., Sodré, A. L., Villagra, A., Sarnaik, A., Sotomayor, E. M., and Weber, J. (2015). HDAC Inhibition Upregulates PD-1 Ligands in Melanoma and Augments Immunotherapy with PD-1 Blockade. *Cancer immunology research*, 3(12):1375–85.

[Wrangle et al., 2013] Wrangle, J., Wang, W., Koch, A., Easwaran, H., Mohammad, H. P., Vendetti, F., VanCriekinge, W., DeMeyer, T., Du, Z., Parsana, P., Rodgers, K., Yen, R. W., Zahnow, C. A., Taube, J. M., Brahmer, J. R., Tykodi, S. S., Easton, K., Carvajal, R. D., Jones, P. A., Laird, P. W., Weisenberger, D. J., Tsai, S., Juergens, R. A., Topalian, S. L., Rudin, C. M., Brock, M. V., Pardoll, D., and Baylin, S. B. (2013). Alterations of immune response of non-small cell lung cancer with Azacytidine. *Oncotarget*, 4(11):2067–2079.

[Wu et al., 2006] Wu, C., Zhu, Y., Jiang, J., Zhao, J., Zhang, X. G., and Xu, N. (2006). Immunohistochemical localization of programmed death-1 ligand-1 (PD-L1) in gastric carcinoma and its clinical significance. *Acta Histochemica*, 108(1):19–24.

[Xi et al., 2018] Xi, J., Huang, Q., Wang, L., Ma, X., Deng, Q., Kumar, M., Zhou, Z., Li, L., Zeng, Z., Young, K. H., Zhang, M., and Li, Y. (2018). MiR-21 depletion in macrophages promotes tumoricidal polarization and enhances PD-1 immunotherapy. *Oncogene*, 37(23):3151–3165.

[Xiao et al., 2014] Xiao, Y., Yu, S., Zhu, B., Bedoret, D., Bu, X., Duke-Cohan, L. M., Umetsu, D. T., Sharpe, A. H., DeKruyff, R. H., and Freeman, G. J. (2014). RGMb is a novel binding partner for PD-l2 and its engagement with PD-l2 promotes respiratory tolerance. *Journal of Experimental Medicine*, 211(5):943–959.

[Xie et al., 2016] Xie, Q. K., Zhao, Y. J., Pan, T., Lyu, N., Mu, L. W., Li, S. L., Shi, M. D., Zhang, Z. F., Zhou, P. H., and Zhao, M. (2016). Programmed death ligand 1 as an indicator of pre-existing adaptive immune responses in human hepatocellular carcinoma. *OncoImmunology*, 5(7):e1181252.

[Xin Yu et al., 2019] Xin Yu, J., Hodge, J. P., Oliva, C., Neftelinov, S. T., Hubbard-Lucey, V. M., and Tang, J. (2019). Trends in clinical development for PD-1/PD-L1 inhibitors. *Nature Reviews Drug Discovery*.

[Xiong et al., 2019] Xiong, W., Deng, H., Huang, C., Zen, C., Jian, C., Ye, K., Zhong, Z., Zhao, X., and Zhu, L. (2019). MLL3 enhances the transcription of PD-L1 and regulates anti-tumor immunity. *Biochimica et Biophysica Acta (BBA) - Molecular Basis of Disease*, 1865(2):454–463.

[Xu et al., 2019] Xu, Y., Wu, Y., Zhang, S., Ma, P., Jin, X., Wang, Z., Yao, M., Zhang, E., Tao, B., Qin, Y., Chen, H., Liu, A., Chen, M., Xiao, M., Lu, C., Mao, R., and Fan, Y. (2019). A Tumor-Specific Super-Enhancer Drives Immune Evasion by Guiding Synchronous Expression of PD-L1 and PD-L2. *Cell Reports*, 29(11):3435–3447.e4.

[Yamazaki et al., 2002] Yamazaki, T., Akiba, H., Iwai, H., Matsuda, H., Aoki, M., Tanno, Y., Shin, T., Tsuchiya, H., Pardoll, D. M., Okumura, K., Azuma, M., and Yagita, H. (2002). Expression of Programmed Death 1 Ligands by Murine T Cells and APC. *The Journal of Immunology*, 169(10):5538–5545.

[Yan et al., 2020] Yan, Y., Zheng, L., Du, Q., Yan, B., and Geller, D. A. (2020). Interferon regulatory factor 1 (IRF-1) and IRF-2 regulate PD-L1 expression in hepatocellular carcinoma (HCC) cells. *Cancer Immunology, Immunotherapy*, pages 1–13.

[Yang et al., 2019] Yang, Y., Hsu, J. M., Sun, L., Chan, L. C., Li, C. W., Hsu, J. L., Wei, Y., Xia, W., Hou, J., Qiu, Y., and Hung, M. C. (2019). Palmitoylation stabilizes PD-L1 to promote breast tumor growth.

[Yau et al., 2019] Yau, T., Park, J., Finn, R., Cheng, A.-l., Mathurin, P., Edeline, J., Kudo, M., Han, K.-h., Harding, J., Merle, P., Rosmorduc, O., Wyrwicz, L., Schott, E., Choo, S., Kelley, R., Begic, D., Chen, G., Neely, J., Anderson, J., and Sangro, B. (2019). CheckMate 459: A randomized, multi-center phase III study of nivolumab (NIVO) vs sorafenib (SOR) as first-line (1L) treatment in patients (pts) with advanced hepatocellular carcinoma (aHCC). *Non-Colorectal*, 30(5):874–875.

[Yokosuka et al., 2012] Yokosuka, T., Takamatsu, M., Kobayashi-Imanishi, W., Hashimoto-Tane, A., Azuma, M., and Saito, T. (2012). Programmed cell death 1 forms negative costimulatory microclusters that directly inhibit T cell receptor signaling by recruiting phosphatase SHP2. *Journal of Experimental Medicine*, 209(6):1201–1217.

[Youngnak et al., 2003] Youngnak, P., Kozono, Y., Kozono, H., Iwai, H., Otsuki, N., Jin, H., Omura, K., Yagita, H., Pardoll, D. M., Chen, L., and Azuma, M. (2003). Differential binding properties of B7-H1 and B7-DC to programmed death-1. *Biochemical and Biophysical Research Communications*, 307(3):672–677.

[Yu et al., 2015] Yu, G., Wang, L. G., and He, Q. Y. (2015). ChIP seeker: An R/Bioconductor package for ChIP peak annotation, comparison and visualization. *Bioinformatics*, 31(14):2382–2383.

[Yuan et al., 2004] Yuan, Y., He, Y., Wang, X., Zhang, H., Li, D., Feng, Z., and Zhang, G. (2004). Investigation on the effects of soluble Programmed Death-1 (sPD-1) enhancing anti-tumor immune response. *Journal of Huazhong University of Science and Technology - Medical Science*, 24(6):531–534.

[Zaidi, 2019] Zaidi, M. R. (2019). The Interferon-Gamma Paradox in Cancer. *Journal of Interferon and Cytokine Research*, 39(1):30–38.

[Zaretsky et al., 2016] Zaretsky, J. M., Garcia-Diaz, A., Shin, D. S., Escuin-Ordinas, H., Hugo, W., Hu-Lieskovan, S., Torrejon, D. Y., Abril-Rodriguez, G., Sandoval, S., Barthly, L., Saco, J., Homet Moreno, B., Mezzadra, R., Chmielowski, B., Ruchalski, K., Shintaku, I. P., Sanchez, P. J., Puig-Saus, C., Cherry, G., Seja, E., Kong, X., Pang, J., Berent-Maoz, B., Comin-Anduix, B., Graeber, T. G., Tumeh, P. C., Schumacher, T. N., Lo, R. S., and Ribas, A. (2016). Mutations Associated with Acquired Resistance to PD-1 Blockade in Melanoma. *New England Journal of Medicine*, 375(9):819–829.

[Zeng et al., 2011] Zeng, Z., Shi, F., Zhou, L., Zhang, M. N., Chen, Y., Chang, X. J., Lu, Y. Y., Bai, W. L., Qu, J. H., Wang, C. P., Wang, H., Lou, M., Wang, F. S., Lv, J. Y., and Yang, Y. P. (2011). Upregulation of circulating PD-L1/PD-1 is associated with poor post-cryoablation prognosis in patients with HBV-related hepatocellular carcinoma. *PLoS ONE*, 6(9).

[Zerdes et al., 2018] Zerdes, I., Matikas, A., Bergh, J., Rassidakis, G. Z., and Foukakis, T. (2018). Genetic, transcriptional and post-translational regulation of the programmed death protein ligand 1 in cancer: biology and clinical correlations.

[Zhang et al., 2018] Zhang, J., Bu, X., Wang, H., Zhu, Y., Geng, Y., Nihira, N. T., Tan, Y., Ci, Y., Wu, F., Dai, X., Guo, J., Huang, Y. H., Fan, C., Ren, S., Sun, Y., Freeman, G. J., Sicinski, P., and Wei, W. (2018). Cyclin D-CDK4 kinase destabilizes PD-L1 via cullin 3-SPOP to control cancer immune surveillance. *Nature*, 553(7686):91–95.

[Zhang et al., 1996] Zhang, J. J., Vinkemeier, U., Gu, W., Chakravarti, D., Horvath, C. M., and Darnell, J. E. (1996). Two contact regions between Stat1 and CBP/p300 in interferon γ signaling. *Proceedings of the National Academy of Sciences of the United States of America*, 93(26):15092–15096.

[Zhang et al., 2008] Zhang, Y., Liu, T., Meyer, C. A., Eeckhoute, J., Johnson, D. S., Bernstein, B. E., Nussbaum, C., Myers, R. M., Brown, M., Li, W., and Shirley, X. S. (2008). Model-based analysis of ChIP-Seq (MACS). *Genome Biology*, 9(9):R137.

[Zhao et al., 2019] Zhao, L., Duan, Y.-T., Lu, P., Zhang, Z.-J., Zheng, X.-K., Wang, J.-L., and Feng, W.-S. (2019). Epigenetic Targets and their Inhibitors in Cancer Therapy. *Current Topics in Medicinal Chemistry*, 18(28):2395–2419.

[Zhou et al., 2017] Zhou, G., Sprengers, D., Boor, P. P., Doukas, M., Schutz, H., Mancham, S., Pedroza-Gonzalez, A., Polak, W. G., de Jonge, J., Gaspersz, M., Dong, H., Thielemans, K., Pan, Q., IJzermans, J. N., Bruno, M. J., and Kwekkeboom, J. (2017). Antibodies Against Immune Checkpoint Molecules Restore Functions of Tumor-Infiltrating T Cells in Hepatocellular Carcinomas. *Gastroenterology*, 153(4):1107–1119.e10.

[Zhu et al., 2018a] Zhu, A. X., Finn, R. S., Edeline, J., Cattan, S., Ogasawara, S., Palmer, D., Verslype, C., Zagonel, V., Fartoux, L., Vogel, A., Sarker, D., Verset, G., Chan, S. L., Knox, J., Daniele, B., Webber, A. L., Ebbinghaus, S. W., Ma, J., Siegel, A. B., Cheng, A. L., Kudo, M., Alistar, A., Asselah, J., Blanc, J. F., Borbath, I., Cannon, T., Chung, K., Cohn, A., Cosgrove, D. P., Damjanov, N., Gupta, M., Karino, Y., Karwal, M., Kaubisch, A., Kelley, R., Van Laethem, J. L., Larson, T., Lee, J., Li, D., Manhas, A., Manji, G. A., Numata, K., Parsons, B., Paulson, A. S., Pinto, C., Ramirez, R., Ratnam, S., Rizell, M., Rosmorduc, O., Sada, Y., Sasaki, Y., Stal, P. I., Strasser, S., Trojan, J., Vaccaro, G., Van Vlierberghe, H., Weiss, A., Weiss, K. H., and Yamashita, T. (2018a). Pembrolizumab in patients with advanced hepatocellular carcinoma previously treated with sorafenib (KEYNOTE-224): a non-randomised, open-label phase 2 trial. *The Lancet Oncology*, 19(7):940–952.

[Zhu et al., 2018b] Zhu, B., Tang, L., Chen, S., Yin, C., Peng, S., Li, X., Liu, T., Liu, W., Han, C., Stawski, L., Xu, Z.-X., Zhou, G., Chen, X., Gao, X., Goding, C. R., Xu, N., Cui, R., and Cao, P. (2018b). Targeting the upstream transcriptional activator of PD-L1 as an alternative strategy in melanoma therapy. *Oncogene*.

[Zhu et al., 2016] Zhu, H., Bengsch, F., Svoronos, N., Rutkowski, M. R., Bitler, B. G., Allegrezza, M. J., Yokoyama, Y., Kossenkov, A. V., Bradner, J. E., Conejo-Garcia, J. R., and Zhang, R. (2016). BET Bromodomain Inhibition Promotes Anti-tumor Immunity by Suppressing PD-L1 Expression. *Cell Reports*, 16(11):2829–2837.

[Zhu et al., 2014] Zhu, J., Chen, L., Zou, L., Yang, P., Wu, R., Mao, Y., Zhou, H., Li, R., Wang, K., Wang, W., Hua, D., and Zhang, X. (2014). MiR-20b, -21, and -130b inhibit PTEN expression resulting in B7-H1 over-expression in advanced colorectal cancer. *Human Immunology*, 75(4):348–353.

[Zongyi and Xiaowu, 2020] Zongyi, Y. and Xiaowu, L. (2020). Immunotherapy for hepatocellular carcinoma. *Cancer Letters*, 470:8–17.

[Zou et al., 2018] Zou, J., Zhuang, M., Yu, X., Li, N., Mao, R., Wang, Z., Wang, J., Wang, X., Zhou, H., Zhang, L., and Shi, Y. (2018). MYC inhibition increases PD-L1 expression induced by IFN-y in hepatocellular carcinoma cells. *Molecular Immunology*, 101:203–209.